Durham E-Theses

Anthracenediylidene derivatives: control of molecular and supramolecular architecture

Godbert, Nicolas

ANTHRACENEDIYLIDENE DERIVATIVES:

CONTROL OF MOLECULAR AND

SUPRAMOLECULAR ARCHITECTURE

Nicolas GODBERT

Department of Chemistry
University of Durham

A Thesis submitted for the degree of Doctor of Philosophy
at the University of Durham

- 8 MAR 2002

Statement of Copyright

The copyright of this thesis rests with the author. No quotation from it should be published without his written consent and information derived from it should be acknowledged.

Declaration

The work described in this thesis was carried out in the Department of Chemistry at the University of Durham between October 1998 and September 01. All the work was carried out by the author unless otherwise stated, and has not previously been submitted for a degree at this or any other university.

ACKNOWLEDMENTS

Dedicated to

Marie,

Antoine,

Julien,

Clémence,

Camille,

Corentin,

and the future ones !

ABSTRACT

Anthracenediylidene Derivatives: Control of Molecular and Supramolecular Architecture

Nicolas Denis Jean-Michel GODBERT

University of Durham (October 2001)

In the context of new π-donor molecules, extended tetrathiafulvalenes have been widely studies for their use as components of electronically conductive charge-transfer materials. In contrast with the planar π-systems, we have focused our attention on extended tetrathiafulvalenes containing a conjugated anthracenyl spacer (anthracenediylidene derivatives). These TTF derivatives adopt a saddle-shaped conformation in the neutral state and a drastic change of conformation occurs upon oxidation to the dication species. Our main objective was to investigate the molecular and supramolecular architecture of these compounds. At the molecular scale, we synthesised cyclophanes by bridging the preformed anthracene tetrathiafulvalene system and studied their redox properties and crystal packing. We developed the chemistry of anthracenediylidene derivatives in order to direct the supramolecular architecture by secondary interactions (hydrogen-bonding, π-π stacking). Finally, we also investigated the incorporation of anthracenediylidene units inside dendritic structures in order to study the highly charged species formed upon oxidation.

TABLE OF CONTENTS

CHAPTER TWO:

SECONDARY INTERACTIONS: TOWARDS INCREASED SUPRAMOLECULAR ORDER IN THE SOLID STATE.

CHAPTER FIVE:

EXPERIMENTAL DETAILS

APPENDIX ONE:

APPENDIX TWO:

APPENDIX THREE:

Chapter One

INTRODUCTION

&

BIBLIOGRAPHIC BACKGROUND

1.1 Tetrathiafulvalene: Description and Properties.

During the last thirty years, the π-electron donor molecule tetrathiafulvalene (TTF) and its derivatives have been central to the development of organic metals and organic superconductors. It was in 1970 that *Wudl et al.*[1] reported the synthesis of TTF (**1**) for the first time.
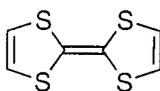
1

TTF is a non-aromatic, planar molecule with 14π electrons. The oxidation of TTF occurs sequentially in two reversible steps, forming first at low potential the radical cation species which can be further oxidised into the dication species ($E_1^{1/2}$=0.34V; $E_2^{1/2}$=0.78V *vs.* Ag/AgCl in acetonitrile (*Figure 1.1*).
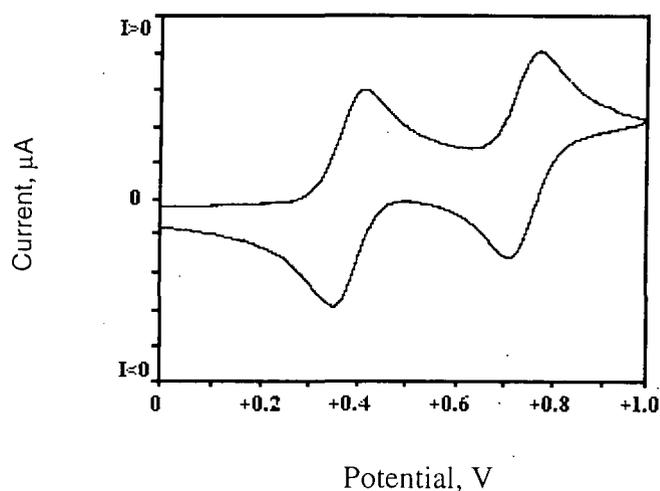
Figure 1.1. Cyclic voltammogram of TTF (**1**) in acetonitrile *vs.* Ag/AgCl.

2

The TTF cation radical and dication species are thermodynamically very stable due to a contribution from 6π electron heteroaromaticity of the 1,3-dithiolium ring (*Figure 1.2*). By treating a carbon tetrachloride solution of TTF with one equivalent of chlorine gas, the formation of a stable purple radical cation can be observed. An excess of chlorine yields the stable yellow dication.

$$E_1{}^{1/2} = +0.34V \qquad E_2{}^{1/2} = +0.71V$$

1 $(7\pi\text{-}7\pi)$ \qquad **1**$^{+\bullet}$ $(6\pi\text{-}7\pi)$ \qquad **1**$^{2+}$ $(6\pi\text{-}6\pi)$

Non-Aromatic \qquad Aromatic Non-Aromatic \qquad Aromatic Aromatic
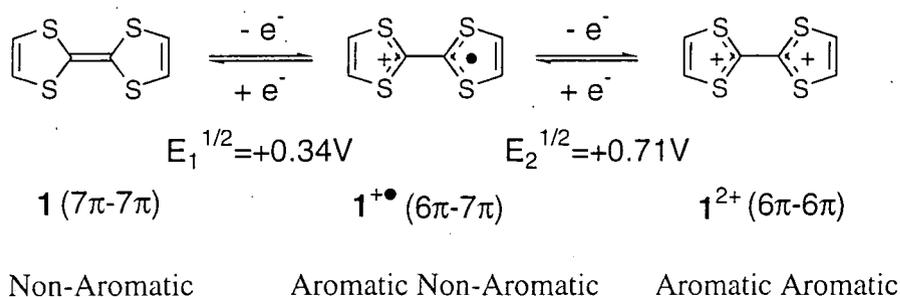
Figure 1.2. Stabilisation of TTF radical cation and dication species.

In 1973, the first "organic metal" tetrathiafulvalene-tetracyano-p-quinodinemethane (TTF-TCNQ) was discovered.[2,3] This crystalline material is composed of segregated stacks of π-donor TTF (**1**) and π-acceptor TCNQ·(**2**). TCNQ can be reduced sequentially in two reversible steps to give first the radical anion and then the dianion. The short interplanar distances which allow significant interactions between π-molecular orbitals of neighbours and a partial charge-transfer from donor to acceptor result in a highly anisotropic conductivity along the stacking axis (*Figure 1.3*). The degree of charge transfer is partial $\delta = 0.59$, calculated by diffuse X-ray scattering techniques and infrared spectroscopy ($\delta = 0$, corresponds to a neutral complex, $\delta = 1$ corresponds to a ionic complex where the charge transfer is total). The conductivity is, therefore, due to the presence of mixed valence species inside the crystalline structure, neutral species of the donor TTF (D), of the

acceptor TCNQ (A), radical cation species of TTF ($D^{+\bullet}$) and radical anion species of TCNQ ($A^{-\bullet}$).
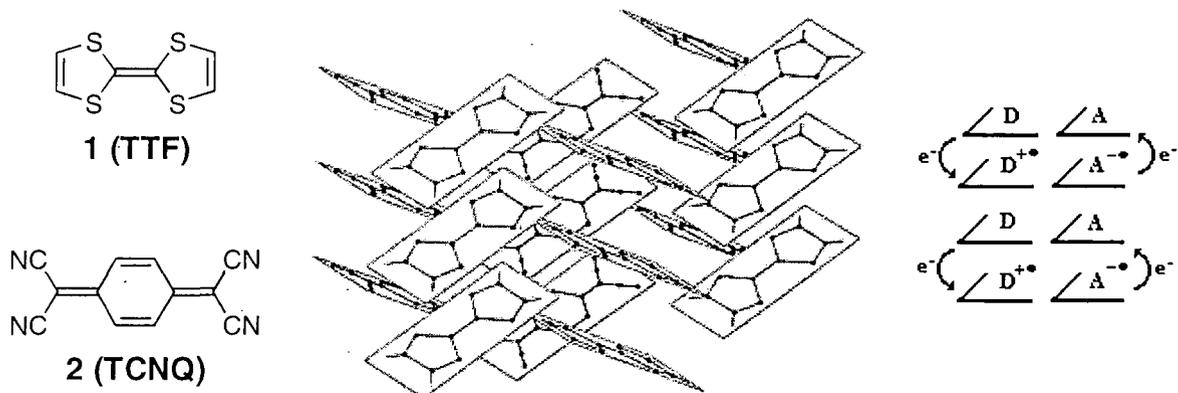
Figure 1.3. X-Ray crystal structure of the first organic metal TTF-TCNQ.

Since the discovery of this organic metal, a large amount of work has been carried out in order to improve the conductivities of salts and charge transfer complexes (CT) of TTF derivatives. However, interest in TTF goes beyond the field of conducting materials to include its role as an important building block in supramolecular chemistry (oligomers, polymers, or dendrimers), crystal engineering (ferromagnets, intramolecular donor-acceptor systems or molecular switches), non linear optics studies (in association with fullerene core and electron-withdrawing substituents), liquid crystalline materials and Langmuir-Blodgett (LB) films. Thus, during the last ten years, many aspects of the synthesis and properties of tetrathiafulvalenes have been reviewed (*Table 1.1*).

Main author	Topic
M.R. Bryce	Recent progress on conducting CT salts.[4]
V. Khodorkovsky	Molecular design of organic conductors.[5]
M.R. Bryce	Increasing dimensionality in the solid state.[6]
G. Schukat	TTF chemistry.[7]
J. Garín	Reactivity of TTF and TseF.[8]
K.B. Simonsen	Functionalization of TTF.[9]
T. Otsubo	TTF dimers.[10]
M. Adam	TTF oligomers.[11]
M.R. Bryce	Macromolecular TTF chemistry.[12]
T. Jørgensen	Supramolecular TTF chemistry.[13]
K.B. Simonsen	Macrocyclic and Supramolecular TTF chemistry.[14]
M.B. Nielsen	Two-and three-dimensional TTF macrocycles.[15]
J. Roncali	Linearly π-extended TTF derivatives.[16]
P. Day	Molecular magnetic semiconductors, metals and superconductors.[17]
M.R. Bryce	TTF as π-donors in intramolecular CT-materials.[18]
M.B. Nielsen	Tetrathiafulvalenes as building blocks in supramolecular chemistry.[19]
M.R. Bryce	Functionalised tetrathiafulvalenes: new applications as versatile π-electron systems in materials chemistry.[20]
L. Ségura	New concepts in tetrathiafulvalene chemistry.[21]

Table 1.1. Recent reviews on specific aspects of TTF.

1.2 Towards Increasing Dimensionality.

A key factor that has challenged many synthetic chemists is an increase in the dimensionality of the material.[6] Several approaches have been extensively considered and can be classified in three categories.

1.2.1 Introduction of Selenium or Tellurium Atoms.

By replacing sulfur atoms of TTF by chalcogens with more diffuse orbitals like selenium or tellurium, the intermolecular π molecular orbital overlap has been improved. Both tetraselenafulvalene (TSF) and tetratellurafulvalene (TTeF) form charge transfer complexes with TCNQ of higher conductivity (800 S cm^{-1} and 1200 S cm^{-1}, respectively) than the complex TTF-TCNQ (500 S cm^{-1}).[22] An illustration of this strategy is the first organic superconductor (TMTSF)$_2$PF$_6$ reported in 1981 by Bechgaard et al.[23] The overlap of selenium π-orbitals along the stacks allows conduction with a band width of ca. 1 eV. (*Figure 1.4*)

3 (TSF)   4 (TTeF)   5 (TMTSF)
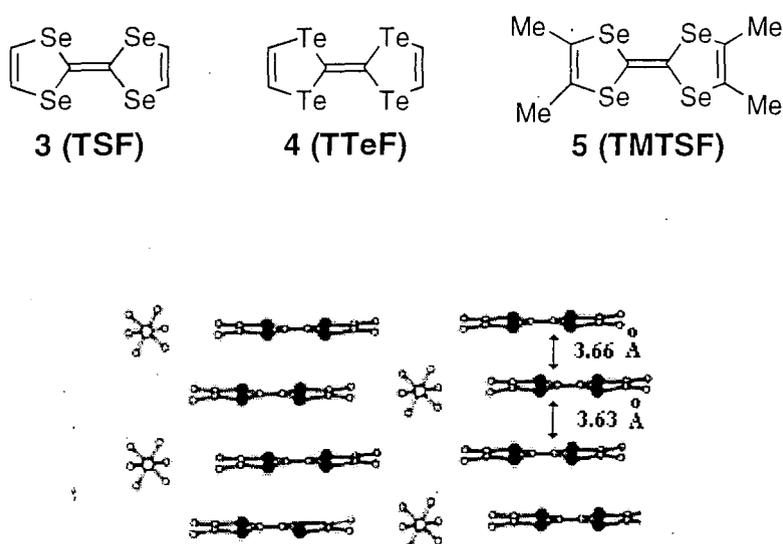
Figure 1.4. X-Ray crystal structure of (TMTSF)$_2$$^{+\bullet}PF_6$$^{-}$.

1.2.2 Addition of Functionality.

The introduction of electron donating substituents such as alkylthio groups raise the highest occupied molecular orbital (HOMO) energy levels of the resultant system. This approach led to the syntheses of salts of BEDT-TTF (**6**), for which a record of superconductivity up to *ca.* 12K at ambient pressure was obtained [*eg.* (BEDT-TTF)$_2$Cu[N(CN)$_2$]Br].[24,25]
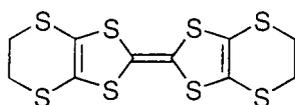
6 (BEDT-TTF)

Also the introduction of other functional groups around the TTF core has been widely studied, mainly for the purpose of increasing crystal order (by π-π-interactions of aryl groups or hydrogen bonds of hydroxyl or amino derivatives for example) and improving the conductivity of obtained salts. The chemistry of TTF is now well developed by adding functional groups before coupling the two 1,3-dithiole units, or after coupling, by lithiation and trapping of the lithiated species of TTF.[8,26]

1.2.3 Spatial Expansion.

The spatial extension of the donor molecule can be achieved by replacing the central double bond by a conjugated spacer, which will stabilize multicationic states (by minimizing Coulombic repulsion between the positively charged 1,3-dithiolium rings), and may also enhance intermolecular and interstack interactions. In this area, a multitude of systems have been studied throughout the last thirty years. Widely studied systems are those which are elongated by conjugated double bonds (**7**, **8**),[27,28] the incorporation of

heterocycles (**9**, **10**),[29-32] and possess larger quinonoidal cores (**11-15**).[33-36] All these π-extended tetrathiafulvalenes present different properties and offer a wide variety of π-donors for the construction of new organic materials.
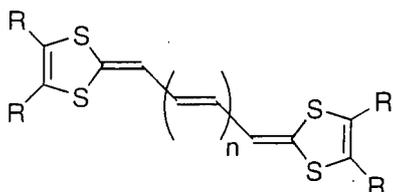
7 R = H, CO$_2$Me, Me, Ph
n = 0,1,2
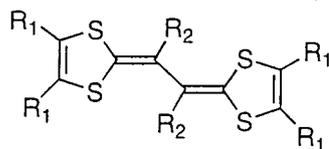
8 R$_1$-R$_1$ = (CH=CH)$_2$, SCH$_2$CH$_2$S
R$_2$ = Me, Ph
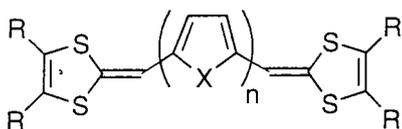
9 R = CO$_2$Me, SMe
X = O, S, Se, NMe
n = 1,2
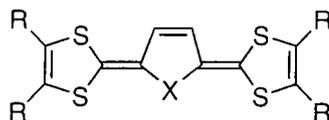
10 R = H, CO$_2$Me, Me, Ph
X = S, Se
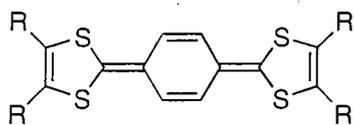
11 R = H
R-R = (CH=CH)$_2$
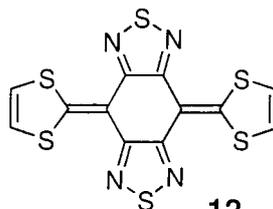
12
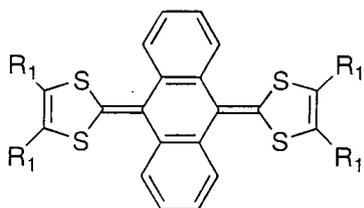
13 R$_1$ = H, Me, SMe
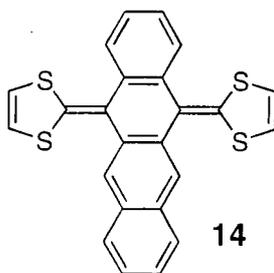
14
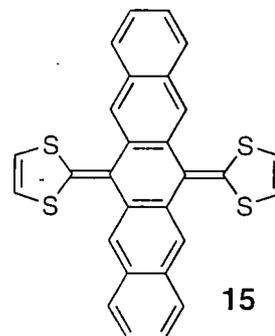
15

A recent strategy for increasing the dimensionality involves the synthesis of non–planar TTF derivatives. To attain efficient intermolecular interactions and optimum stackings to form conducting CT complexes, the general trend was to design planar TTF analogues. However, the study of non-planar TTF derivatives is in constant progress and some CT complexes of them present comparable conductivity to CT complexes derived from related planar molecules.[37] Moreover, upon oxidation a remarkable change of conformation can occur leading to a completely different structure for the charged species compared with its neutral form. It is in this context that 9,10-bis-(1,3-dithiol-2-ylidene)-9,10-dihydroanthracene derivatives (anthracene-TTF or anthracenediylidene derivatives) (**13**) first attracted our attention. Derivatives of **13** have been widely studied in our group due to their unusual redox and structural properties.

1.3 Anthracenediylidene Derivatives.

1.3.1 Synthesis of Anthracene-TTF Derivatives.

The first anthracenediylidene derivative, namely 9,10-bis-(1,3-benzodithiol-2-ylidene)-9,10-dihydroanthracene (**17**) was synthesised by Akiba et al.[38] using a double Horner-Wadsworth-Emmons reaction of the phosphonate ester reagent **16** with anthraquinone in 78% yield (*Scheme 1.1*).
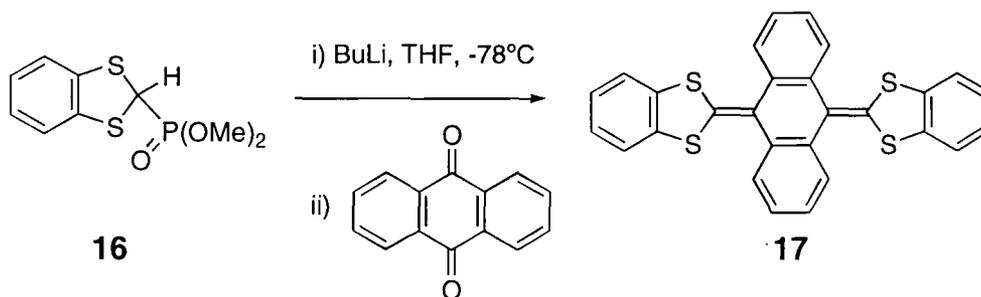
Scheme 1.1. Synthesis of dibenzo-anthracene-TTF (**17**).

Following this scheme, using appropriate phosphonate reagents, symmetrical anthracenediylidene have been synthesised in order to form charge transfer complexes (**18a-c**)[36,39,40] and study the electrochemistry by increasing the solubility of the system (**19, 20**).[41,42]
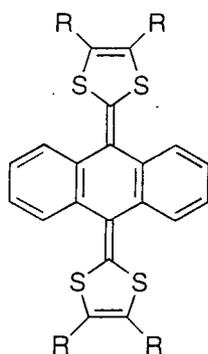
18 a R = H
  b R = Me
  c R = SMe
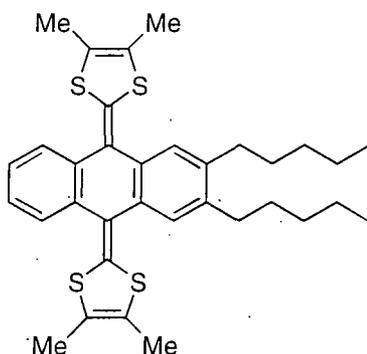
19
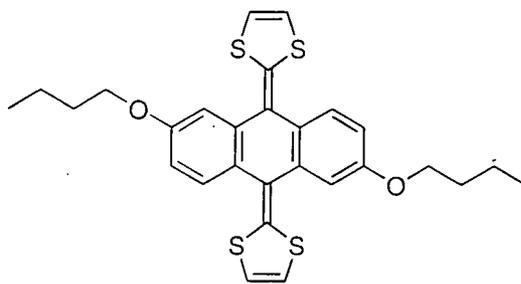
20

Unsymmetrical derivatives have been synthesised following a two step methodology[41,43]. First, the reaction of anthrone (**21**) with 1,3-dithiolium cations (**22a,b**) afforded quinones **23a,b**. A Horner-Wadsworth-Emmons reaction using phosphonates **24a-d** on these quinones, allowed then the formation of unsymmetrical anthracenediylidenes **25a-d** (*Scheme 1.2*).
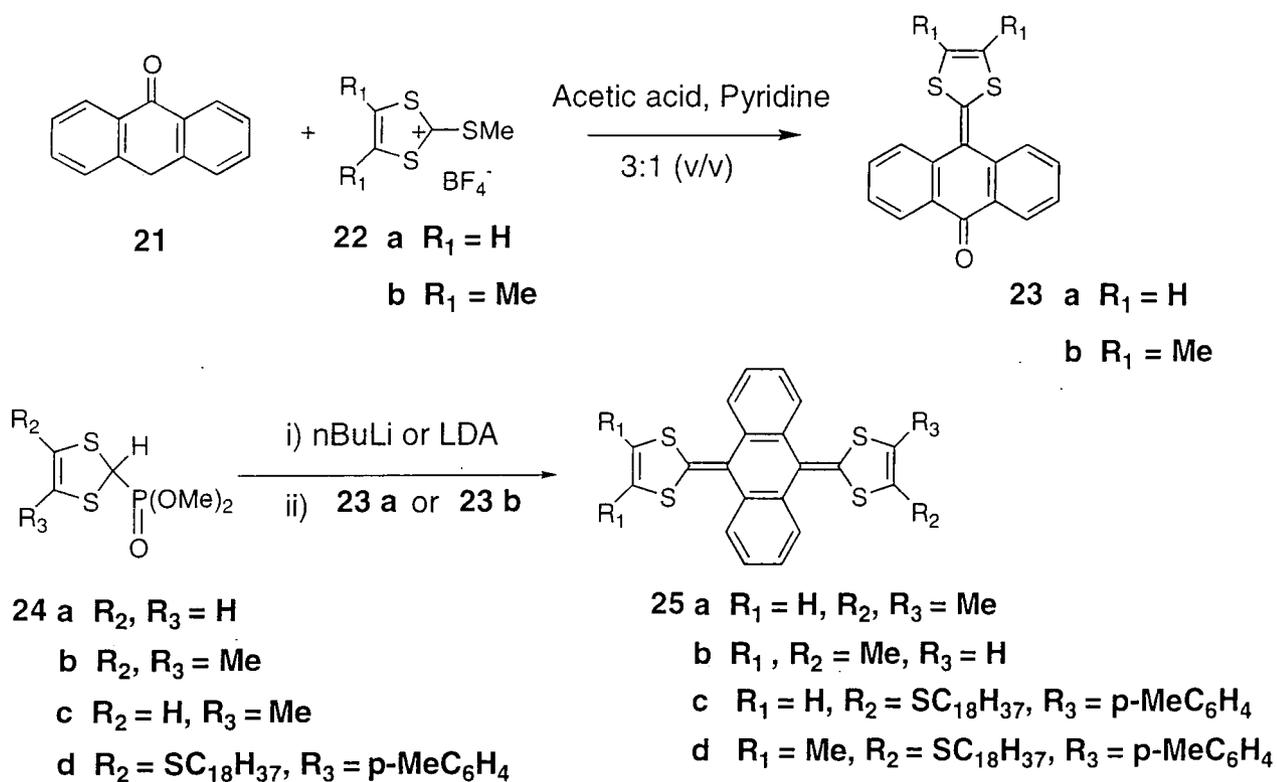
Scheme 1.2. Synthesis of unsymmetrical anthracene-TTF derivatives.

With the aim of using anthracenediylidene systems as building blocks in materials and supramolecular chemistry, functionalisation was performed using lithiation and trapping of the resulting lithiated species with selected electrophiles. To circumvent a problem of precipitation of the lithiated species at low temperature, and to ensure that monolithiation occured, the trimethyl derivative (**25b**) was considered as the best solution[41] (*Scheme 1.3*). Using methylchloroformate as a trapping agent proved to be a very efficient way to obtain the methylester derivative **26** (83% yield). Sulfur insertion followed by addition of benzoyl chloride, gave the thioester derivative **27** (53% yield) which is a convenient precursor of other mono-functionalised derivatives (**30, 31**).
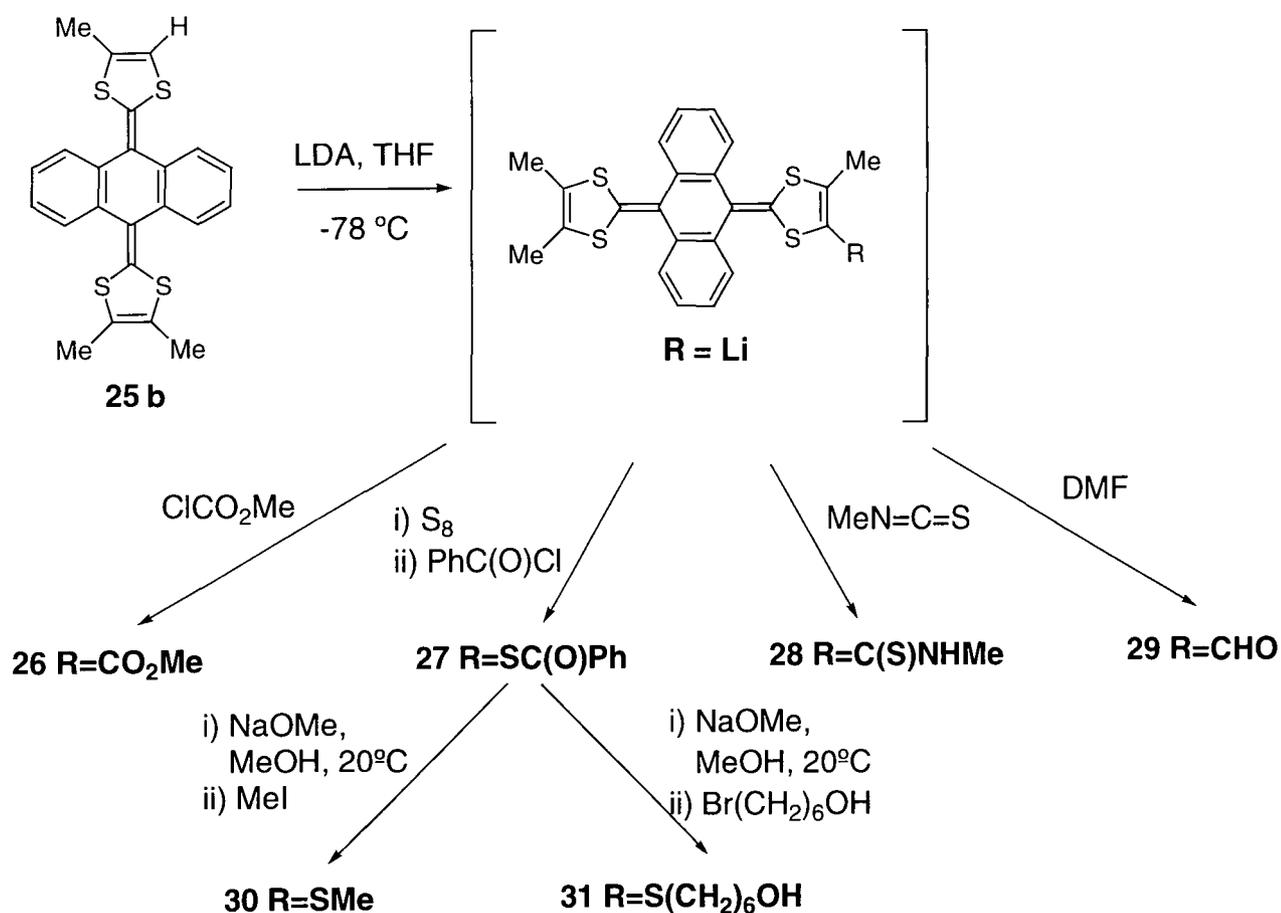
Scheme 1.3. Synthesis of mono-functionalised anthracene-TTF derivatives.

1.3.2 Molecular Structure of Anthracenediylidene System.

1.3.2.1 Neutral State.

The crystal structure of the tetramethyl derivative **18b**, reported by Bryce *et al.* revealed for the first time, the saddle shaped conformation of the anthracene-TTF system[45] (*Figure 1.5a*). The central quinonoid ring is severely distorted into a boat conformation.

Theoretical calculations have been performed on this system by Martín, Ortí *et al.* establishing that steric hindrance between the sulfur atoms and the hydrogen atoms in peri-

positions of the anthraquinoid system causes the molecule to adopt this saddle shaped conformation.[35]

. Thus, derivatives such as **12** in which the repulsive S⋯H contacts are replaced by attractive N⋯S contacts, have been studied by Yamashita *et al* and are completely planar, as expected[44] *(Figure 1.5b)*. Although the conductivity for such compounds is relatively high at room temperature as a single component $(3.7 \times 10^{-3} \text{ S cm}^{-1})$, no organic metals or CT complexes have been reported, probably for solubility reasons.
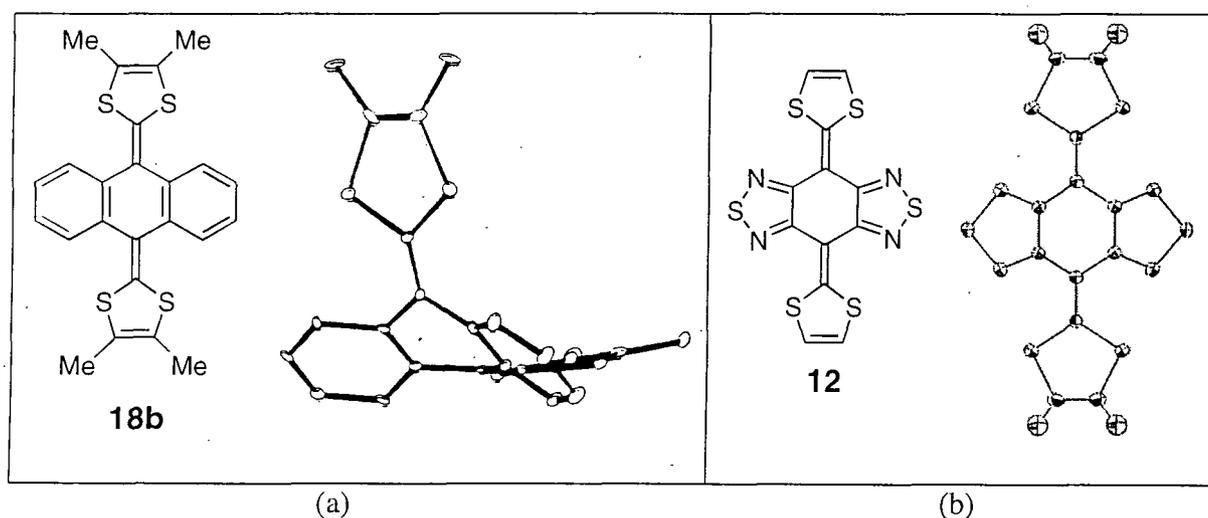
Figure 1.5. X-ray crystal structures of **18b** (a) and **12** (b).

The typical crystal packing of the neutral form of anthracene-TTFs is shown by the methylester derivative **26**, where dimers are formed *(Figure 1.6)*. The 1,3-dithiole moieties contact face to face at the usual van der Waals distances. Solvent molecules can occupy cavities between the pairs. Therefore, the dithiole-dithiole interactions preclude efficient extended stacking in the crystal.[41]
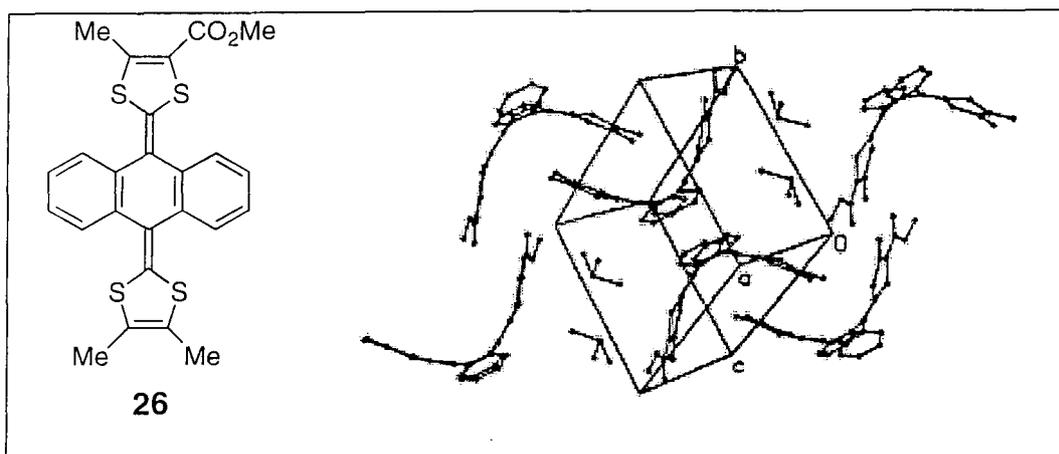
Figure 1.6. Crystal packing of **26** as CDCl₃ solvate.

1.3.2.2 Dicationic State.

The oxidation of anthracenediylidene derivatives occurs in a single two-electron wave leading to the formation of a thermodynamically stable dication (E^{ox} *ca.* 0.3 V *vs.* Ag/AgCl in acetonitrile). During oxidation a dramatic change of conformation of the molecule takes place. The saddle shape of the neutral anthracenediylidene derivative is flattened, the central anthracene ring becomes planar and aromatic whilst the two 1,3-dithiolium rings twist orthogonally to this plane (*Figure 1.7b*).

| (a) | (b) | (c) |
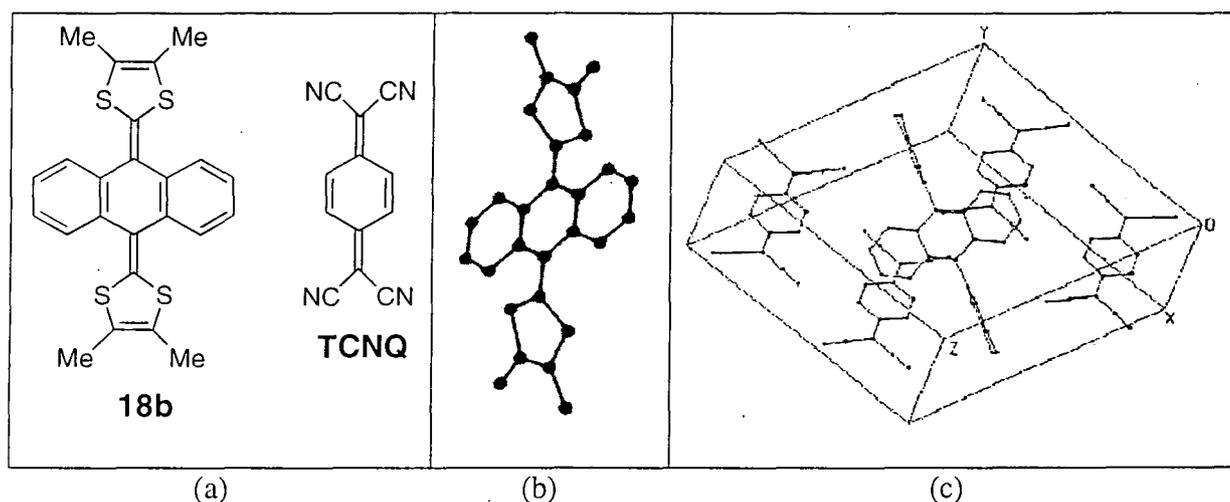
Figure 1.7. Crystal Structure of **18b²⁺** (b) and Crystal packing of 1:4 complex **18b²⁺[(TCNQ)₄]²⁻** •(c).

14

Evidence of the dicationic structure in the solid state was first obtained by X-ray crystallography of the charge transfer complex which formed by mixing the tetramethyl derivative **18b** with TCNQ[45] (*Figure 1.7c*).

The complex of **18b** with TCNQ (ratio 1:4) is highly conductive ($\sigma_{300\ K}$= 60 S cm^{-1}), paramagnetic and was the first semimetallic TCNQ complex formed by a TTF-type donor that adopts such a non planar conformation. Other non planar TTF analogues (**32**) have been recently reported which also show a dramatic change of conformation upon oxidation[27] (*Figure 1.8*). However, the derived cation radical salts with PF$_6^-$ and Au(CN)$_2^-$ have a 1:1 stoichiometry and, therefore, show semiconductivity behaviour (σ_{300K}= 3.10^{-6} S cm^{-1} and σ_{300K}= 10^{-2} S cm^{-1}, respectively).

(a)   (b)
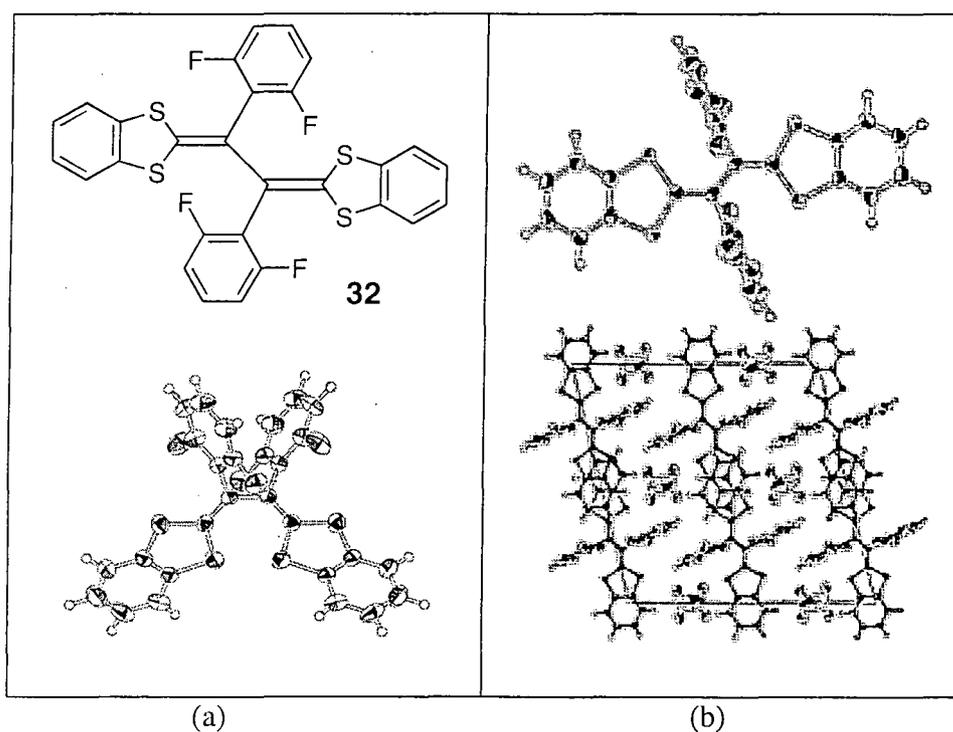
Figure 1.8. Crystal structures of **32** (a) and **32(PF₆)** (b) (top: structure of the donor molecule, bottom: crystal packing of **32(PF₆)**.

1.3.3 Electrochemistry of Anthracene-TTF Derivatives.

1.3.3.1 Cyclic Voltammetry Studies of Anthracenediylidene Derivatives.

The electrochemistry of anthracenediylidene derivatives is influenced by this change of conformation upon oxidation. The characteristic voltammogram obtained for these compounds comprises a single, quasi-reversible two-electron wave (*Figure 1.9a*). The delay observed on the reduction which makes the system quasi-reversible, is correlated to the high stability of the dication species, which are fully aromatic, and also to the change of conformation that the dication species have to undergo to return to their neutral form. This effect is even more pronounced at low temperature, showing a complete irreversibility at −70 °C for compound **19** in DCM.[42]
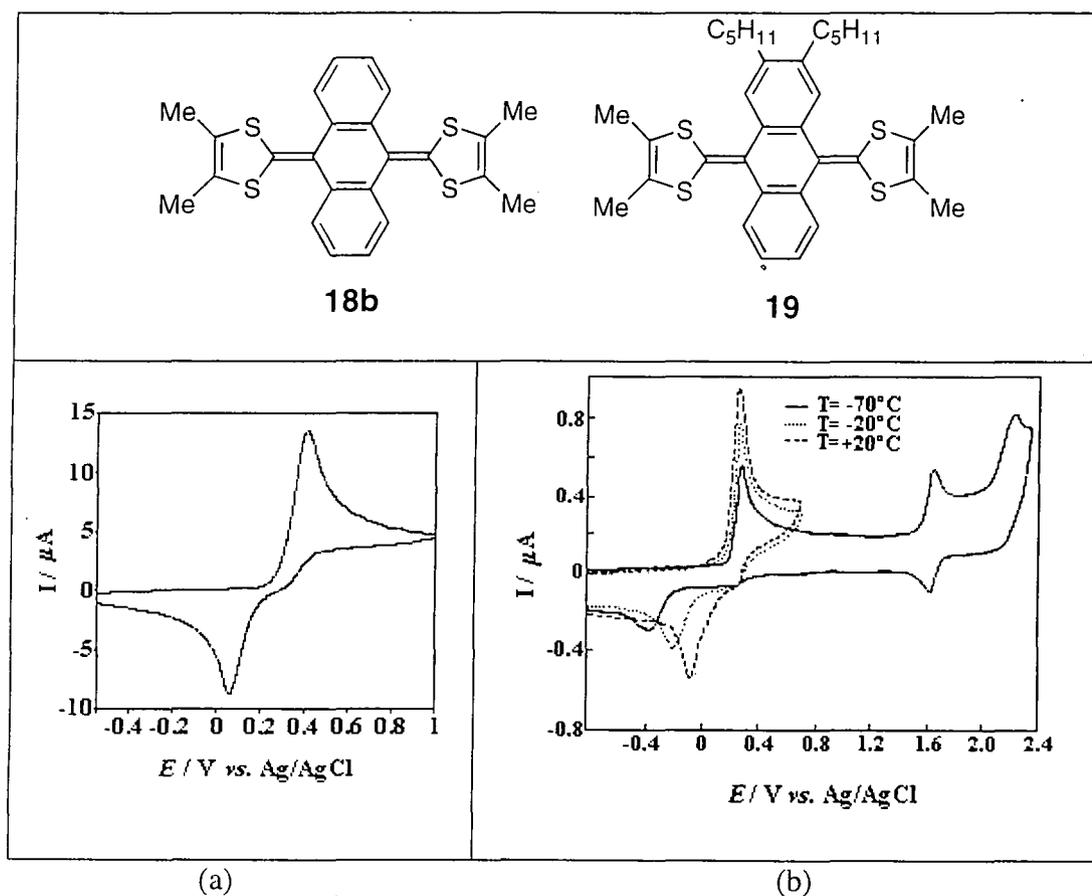
Figure 1.9. Cyclic voltammograms of **18b** (a) and of **19** at various temperature (b).
(Experimental conditions: Pt electrode, in DCM, electrolyte: Bu_4NPF_6 0.1M)

Temperature-dependent studies performed on compound **19** also allowed the observation of a second reversible one-electron wave and a third irreversible one-electron wave, leading to the formation of trication radical species and tetracation species, respectively, corresponding to the oxidation of the anthracene system (*Figure 1.9b*).

As for tetrathiafulvalene[46], oxidation potentials of anthracenediylidene derivatives can be finely tuned by attachment of electron donating or electron withdrawing substituents. The general trend is that an anodically shifted oxidation wave is observed for an electron withdrawing substituent.[41]

1.3.3.2 Radical Cation Form of Anthracene-TTF.

Calculations have been performed on compound **18a**, its radical cation form **18a$^{+\bullet}$** and its dication form **18^{2+}**, in order to explain the electrochemical behaviour of anthracenediylidene derivatives.[47] Oxidation mainly affects the central quinonoid ring and the dithiole units on which the highest occupied molecular orbital (HOMO) (i.e. the orbital from which electrons are removed) is mostly located (*Figure 1.10*).[35]
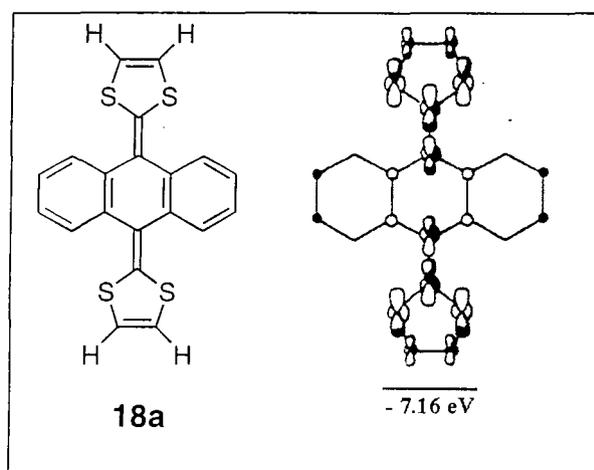
Figure 1.10 Atomic orbital composition and energy of the HOMO of **18a**.

The aromatisation of the anthracene moiety and the dithiole rings during the oxidation process has important consequences for the conformation adopted by the molecule. The radical cation remains significantly distorted from planarity and retains the saddle shaped structure of the neutral form. The dication, comprising three aromatic units (the anthracene moiety and the two dithiolium rings), loses the saddle shape to adopt a planar conformation in which the two dithiolium rings twist perpendicularly to the planar anthracene core, as observed by X-ray analysis[45] (*Figure 1.11*).

Neutral   Radical Cation   Dication
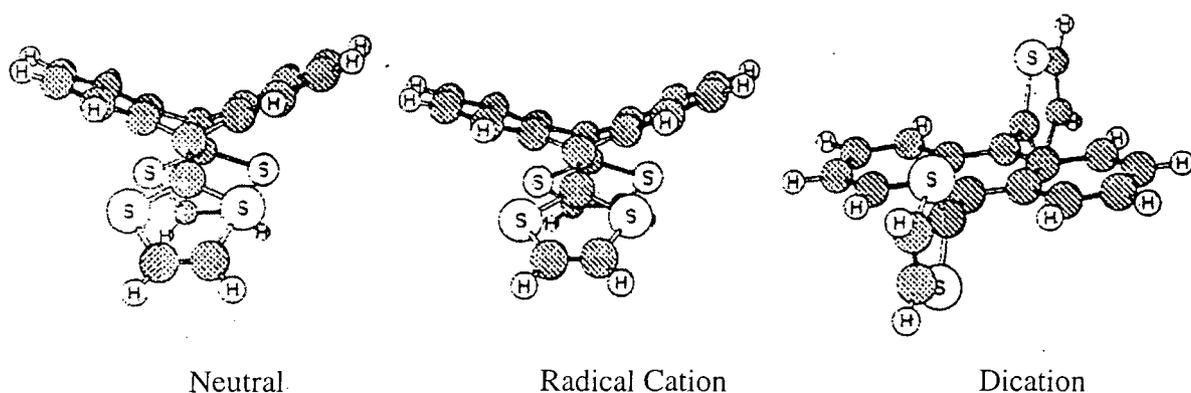
Figure 1.11 Minimum-energy conformation calculated for **18a**, **18a$^{+\bullet}$**, and **18^{2+}**.

This distorted conformation of the radical cation implies its instability with respect to the dication, thus explaining the anodic shift of the first oxidation potential and its coalescence with the second oxidation potential to give the two-electron wave observed by electrochemical studies, which is in contrast to TTF which shows two separated one-electron waves for the radical cation and the dication species.

However, observation of the elusive π-radical cation species of compound **18c** has been achieved by photolytic generation, allowing its characterisation by UV-Vis and Raman spectroscopy.[48] Photolysis of a degassed solution of **18c** led to the formation of the

radical cation species **18c⁺·**, which was shown to disproportionate to give the dication species **18c²⁺**. In aerated solutions, the photodegradation product observed is the ketone **23c** the mechanism of formation of which remains uncertain (*Figure 1.12*).
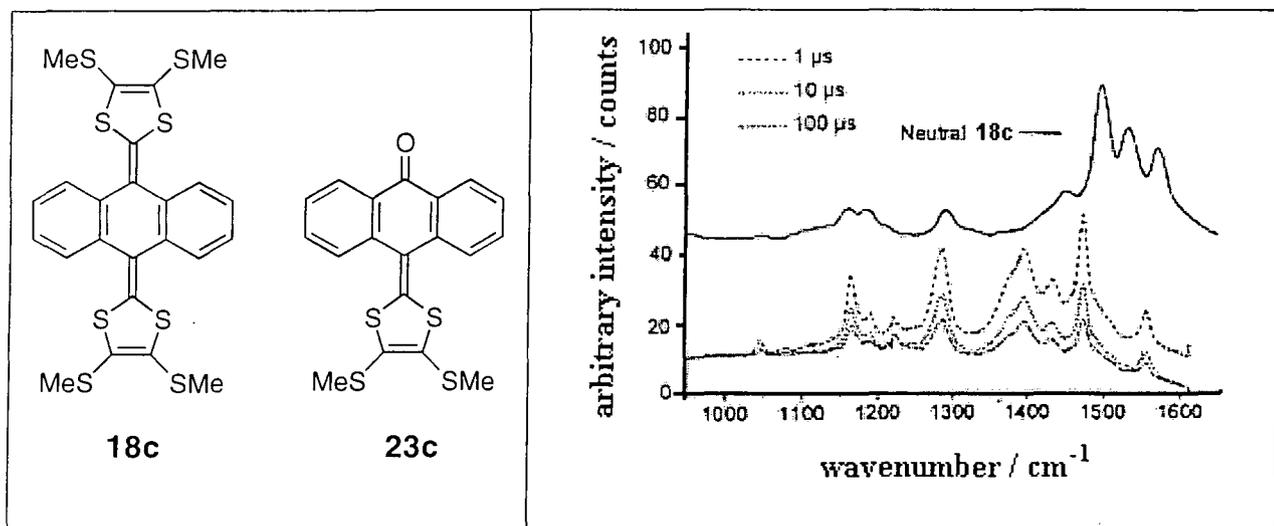
Figure 1.12 Ground state Raman spectrum of **18c** recorded at 630 nm, and time resolved resonance Raman spectrum of **18c⁺·** recorded by using 266 nm pump and 630 nm probe: time delays are indicated.

1.3.3.3 Intramolecular Electronic Interaction Studies.

Several diads containing anthracenediylidene derivatives linked by a σ bond to different donor moieties have been synthesised for the study of intramolecular electronic interactions. Thus, dimeric systems (**33a-c**), donor-donor diads with ferrocenyl moieties (**34, 35a, 36a-c**) or with TTF moieties (**35b, 37a-c**) have been recently reported.
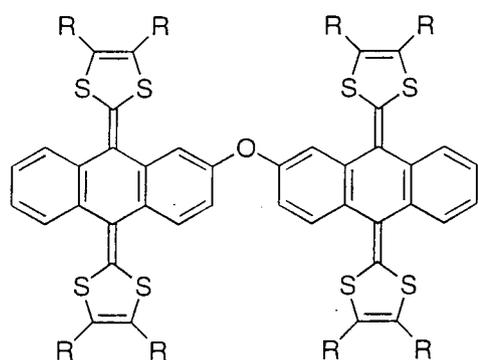
33 a: R = H
 b: R = SCH$_3$
 c: R-R = SCH$_2$CH$_2$S

34

35 a: D=

 b: D=
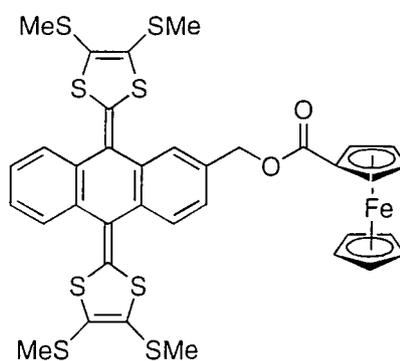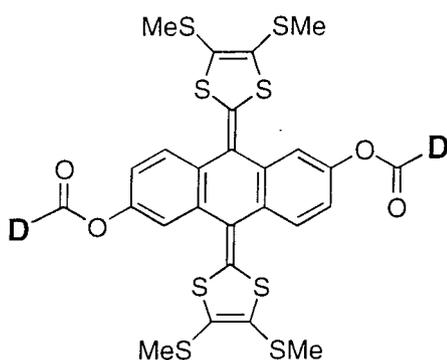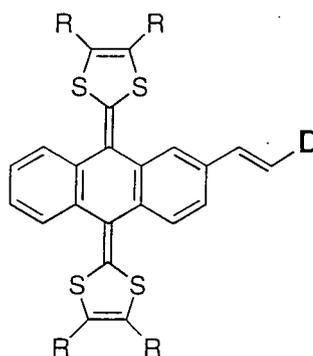
36 D=
a: R = H
b: R = SCH$_3$
c: R-R = SCH$_2$CH$_2$S

37 D=

The electrochemistry of compound **34**[49] is composed of waves from the two redox systems, namely anthracene-TTF and ferrocene. The oxidation of the anthracenediylidene moiety to yield the dication occurs first as the characteristic single, two-electron, quasi-reversible wave (E_1^{ox} = 0.59 V in DCM). The second oxidation of the ferrocene moiety occurs as a clean reversible wave (E_2^{ox} = 0.67 V in DCM) to lead to the formation of the trication species. As expected, since the two redox moieties are not conjugated for this molecule, no intramolecular electronic interactions have been observed, the two redox-moieties acting independently. Similarly, compounds **35a** and **35b**[50] with an ester linkage

20

and compound **33** with an oxygen atom link, display independent redox units. Consequently, compound **33** shows a single four-electron quasi-reversible wave[51], with both anthracenediylidene units being oxidised at the same time under a range of different experimental conditions *eg.* varying temperature, solvent and scan-rate. However, for compounds **36**[52] and **37**[53], in which the connection occurs through a conjugating double bond, intramolecular electronic interactions have been observed by electrochemistry and confirmed by UV-Vis spectroscopic analysis and semiempirical calculations. Therefore, for compound **37**, the oxidation of the ferrocene moiety is delayed (i.e. more difficult) showing an inductive effect from the positively charged dicationic state of the anthracenediylidene moiety.

1.3.3.4 Metal Ion Recognition Properties.

In order to investigate metal recognition properties, Bryce *et al.*[54] recently reported the synthesis of O_4S_2-crown annulated derivatives of the anthracenediylidene system. The unique combination of structural and redox properties of anthracenediylidene derivatives gives to the mono-crown system **38** a high selectivity toward silver and sodium ions. The complexation of the metal ion to the crown unit has been followed by UV/Vis spectroscopy and cyclic voltammetry. In the presence of metal cations, the first oxidation peak (E_1^{ox}) observed for compound **38** is shifted more significantly for silver and sodium ions; while the second oxidation peak $(E_2^{ox}$, due to the anthracene moiety) remained essentially unchanged, consistent with expulsion of the metal cation from the ionophore prior to the second oxidation wave (*Figure 1.13*). Saturation is achieved for *ca.* 10 equivalents of metal ions which makes possible the use of compound **33** as a highly sensitive and efficient voltammetric sensor of silver and sodium ions.
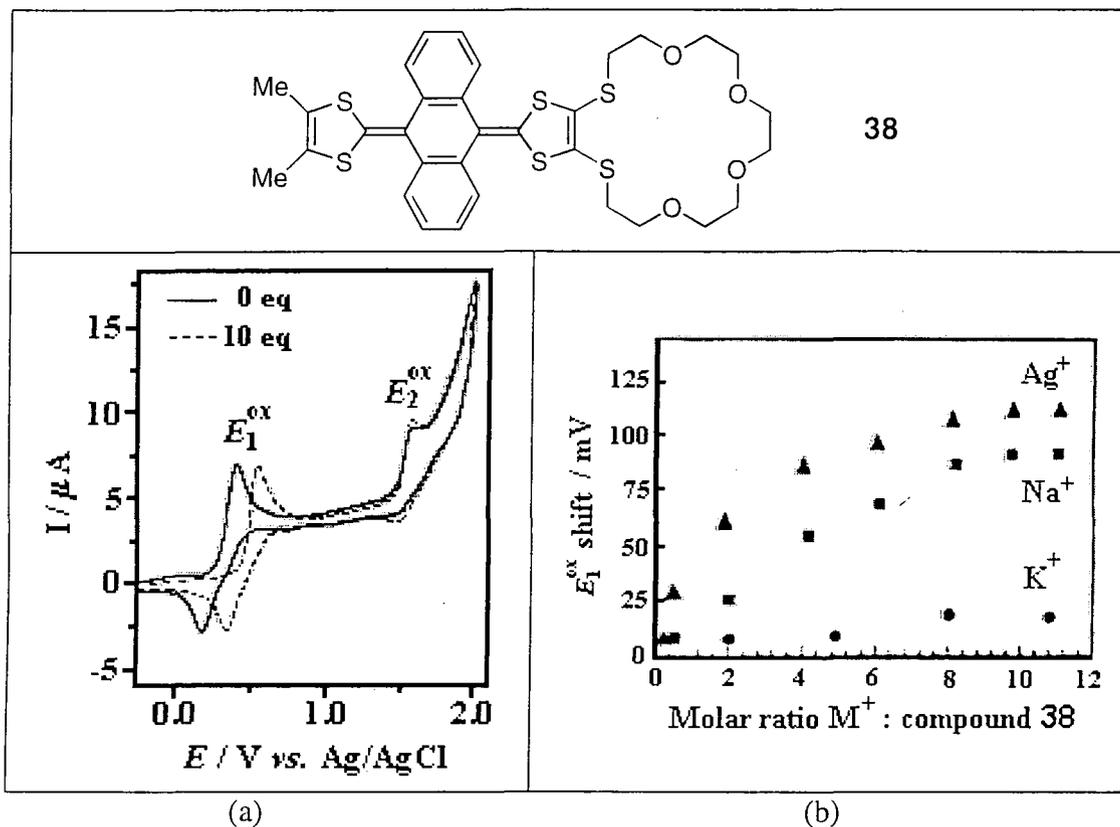
Figure 1.13 Cyclic voltammograms of **38** in the presence of 0 and 10 molar equivalents of $AgCF_3SO_3$ (a), Plot of the shift of the potential E_1^{ox} in the cyclic voltammogram of compound **38** with added equivalents of KCF_3SO_3 (circles), $NaCF_3SO_3$ (squares), and $AgCF_3SO_3$ (triangles) (b).
(Experimental conditions: Pt electrode, in MeCN, electrolyte: Bu_4NPF_6 0.2 M)

1.3.4 Donor-Acceptor Complexes.

In the development of optoelectronic devices, the synthesis of new organic molecules with delocalised π-electron systems bearing both electron donor and electron acceptor moieties within the same molecule has become a very active research area. These donor-acceptor molecules are very attractive for their potential uses in nonlinear optics, molecular electronics, artificial photosynthetic models and solvatochromic effects. Anthracenediylidene derivatives are of a particular interest in this area since the oxidised species are stabilised by aromatisation of the anthracene ring.

High molecular hyperpolarizabilities can be obtained for molecules in which the donor and the acceptor are linked through a π-conjugated spacer allowing an intramolecular charge transfer. Respecting this key factor, in a search of new chromophores, compounds **39a-c** and **40a-c** have been reported as efficient NLO chromophores possessing relatively high second order optical nonlinearity ($\mu\beta_0$ *ca.* 150.10^{-48} esu for **39a-c** and $\mu\beta_0$ *ca.* 300.10^{-48} esu for **40a-c**).[55]

$$39 \quad n=0$$

$$40 \quad n=1$$

a: R=H
b: R=SCH$_3$
c: R-R=SCH$_2$CH$_2$S
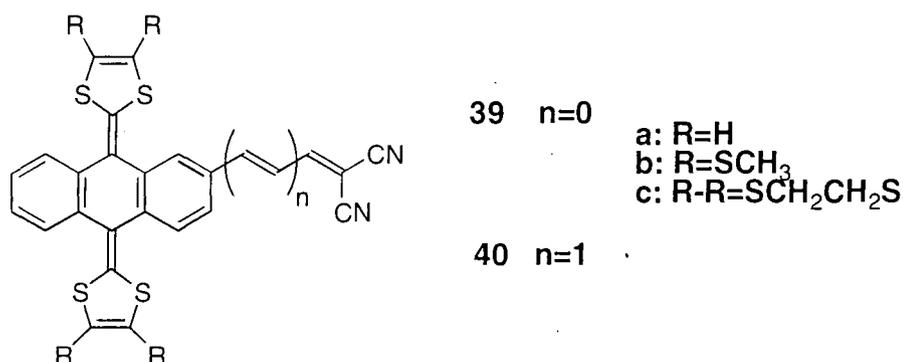
In a search for new compounds exhibiting a long-lived charge separated state, [60]fullerene has been covalently attached to anthracene-TTF derivatives using various linkers, such as pyrrolidine rings (**41, 42, 44**), and cycloaddition using diazo compounds (**43**). These compounds show electroactivity of both the donor and the acceptor moieties exhibiting a two-electron oxidation wave corresponding to the oxidation of the anthracenediylidene moiety, and the four cathodically shifted one-electron reduction waves corresponding to the first four reductions of the C_{60} moiety. Electronic interactions in the solid state were confirmed by magnetic susceptibility (χ_m). Compounds **41a-c** (χ_m *ca.* 2.10^{-3} emu mol-1) show, therefore, paramagnetic behaviour.[56] Photoexcitation of these diads activates an intramolecular electron-transfer from the singlet excited-state of the fullerene moiety to the donor leading to long-lived separated-charged states, characterised as being the radical anion of the C_{60} moiety and the radical cation of the anthracene-TTF (TTFAQ) moiety ($C_{60}^{-\bullet}$–TTFAQ$^{+\bullet}$).[57] The unusual geometry of anthracenediylidene

derivatives has a strong impact on the stabilisation of the charge-separated state, which for these compounds has a relative long life (several hundred nanoseconds in deoxygenated solvent).[58] In addition to the gain of aromaticity of the 1,3-dithiole units, the aromatisation of the anthracene ring occurs upon oxidation leading to larger aromatic stabilisation energy, which seems to be a key feature for obtaining strong stabilisation of photolytically generated radical pairs in C_{60} diads,[59] thus enabling the transformation of the photon energy into chemical energy, paving the way for the use of anthracenediylidene derivatives as appropriate materials for photovoltaic applications.[47]
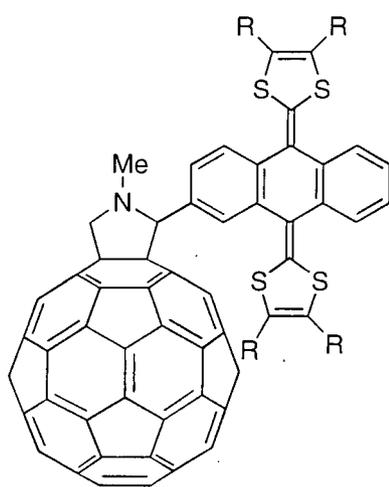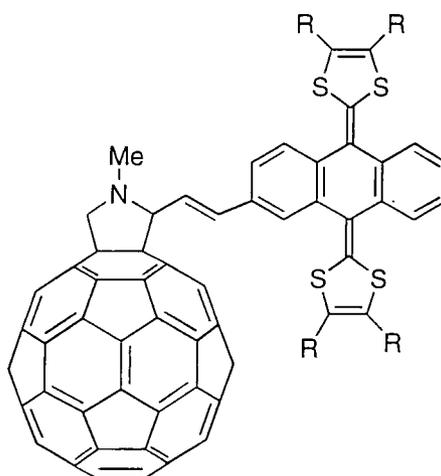
a: R=H
b: R=SCH₃
c: R-R=SCH₂CH₂S

41   42

a: R=H
b: R=SCH₃
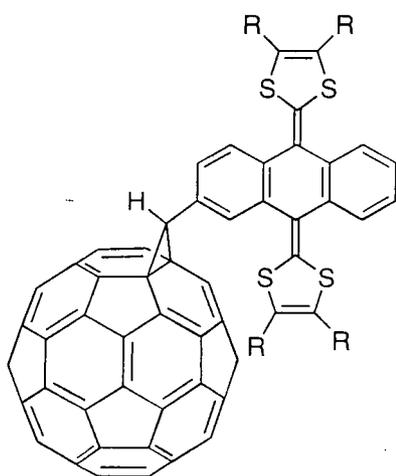
43   44
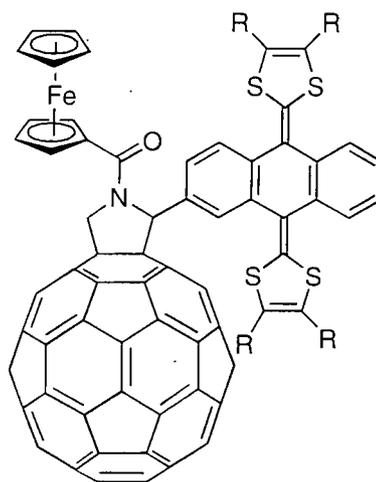
1.4 Conclusion.

Anthracenediylidene derivatives are interesting electron donors which possess an unusual saddle-shaped conformation which imparts special properties to the system. These donors are easily oxidised to the dication species. Upon oxidation, the conformation changes dramatically leading to the loss of the cavity of the neutral structure. Chemical functionalisation is easily performed which allows access to a wide variety of substituted derivatives. We, therefore, decided to investigate the molecular and supramolecular architecture of this class of compounds. At the molecular scale, we targeted the synthesis of cyclophane derivatives by bridging the preformed anthracene tetrathiafulvalene system with a view to studying their redox properties and crystal packing, perhaps even observing the stabilisation of the cation-radical species. We also aimed to develop the chemistry of anthracenediylidene derivatives in order to direct the supramolecular architecture by secondary interactions (π-π stacking, hydrogen-bonding). Finally, we considered it of interest to study the incorporation of anthracenediylidene units into dendritic structures in order to obtain dendrimers which can form highly oxidised states.

1.5 References.

(1)   Wudl, F.; Smith, G. M.; Hufnagel, E. J. *J. Chem. Soc. Chem. Commun.* **1970**, 1453-1454.

(2)   Ferraris, J.; Cowan, D. O.; Walatka, J.; Perlstein, J. H. *J. Am. Chem. Soc.* **1973**, *95*, 948-949.

(3)   Coleman, L. B.; Cohen, M. J.; Sandman, D. J.; Yamagishi, F. G.; Garito, A. F.; Heeger, A. J. *Solid State Commun.* **1973**, *12*, 1125-1126.

(4)   Bryce, M. R. *Chem. Soc. Rev.* **1991**, *20*, 355-371.

(5)   Khodorkovski, V.; Becker, J. Y. In *Organic conductors*; Farges, J.-P., Ed.; Marcel Dekker: New York, 1994, chap 3.

(6)   Bryce, M. R. *J. Mater. Chem.* **1995**, *5*, 1481-1496.

(7)   Schukat, G.; Fanghanel, E. *Sulfur Rep.* **1996**, *18*, 1-22.

(8)   Garín, J. *Adv. Heterocycl. Chem.* **1995**, *62*, 249-304.

(9)   Simonsen, K. B.; Svenstrup, N.; Lau, J.; Simonsen, O.; Mørk, P.; Kristensen, G. J.; Becher, J. *Synthesis* **1996**, 407-418.

(10)   Otsubo, T.; Aso, Y.; Takimiya, K. *Adv. Mater.* **1996**, *8*, 203-211.

(11)   Adam, M.; Müllen, K. *Adv. Mater.* **1994**, *6*, 439-459.

(12)   Bryce, M. R.; Devonport, W.; Goldenberg, L. M.; Wang, C. *Chem. Commun.* **1998**, 945-951.

(13)   Jørgensen, T.; Hansen, T. K.; Becher, J. *Chem. Soc. Rev.* **1994**, *23*, 41-51.

(14)   Simonsen, K. B.; Becher, J. *Synlett* **1997**, 1211-1232.

(15)   Nielsen, M. B.; Becher, J. *Liebigs Ann.* **1997**, *11*, 2177-2187.

(16)   Roncali, J. *J. Mater. Chem.* **1997**, *7*, 2307-2321.

(17)   Day, P.; Kurmoo, M. *J. Mater. Chem.* **1997**, *8*, 1291-1295.

(18)   Bryce, M. R. *Adv. Mater.* **1999**, *11*, 11-23.

(19)   Nielsen, M. B.; Lomholt, C.; Becher, J. *Chem. Soc. Rev.* **2000**, *29*, 153-164.

(20)   Bryce, M. R. *J. Mater. Chem.* **2000**, *10*, 589-598.

(21) Ségura, J. L.; Martín, N. *Angew. Chem., Int. Ed. Engl.* **2001**, *40*, 1973-1409.

(22) Cowan, D. O.; Mays, M. D.; Kistenmacher, T. J.; Poehler, T. O.; Beno, M. A.; Kini, A. M.; Williams, J. M.; Kwok, Y. K.; Carlson, K. D.; Xiao, L.; Novoa, J. J.; Whangbo, M. H. *Mol. Cryst. Liq. Cryst.* **1990**, *181*, 43-58.

(23) Thorup, N.; Rindorf, G.; Soling, H.; Bechgaard, K. *Acta Cryst.* **1981**, *B37*, 1236-1240.

(24) Kini, A. M.; Geiser, U.; Wang, H. H.; Carlson, K. D.; Williams, J. M.; Kwok, W. K.; Vandervoort, K. G.; Thompson, J. E.; Stupka, D. L.; Jung, D.; Whangbo, M. H. *Inorg. Chem.* **1990**, *29*, 2555-2557.

(25) Williams, J. M.; Kini, A. M.; Wang, H. H.; Carlson, K. D.; Geiser, U.; Montgomery, L. K.; Pyrka, G. J.; Watkins, D. M.; Kommers, J. M.; Boryschuk, S. J.; Strieby Crouch, A. V.; Kwock, W. K.; Schirber, J. E.; Overmyer, D. L.; Jung, D.; Whangbo, M. H. *Inorg. Chem.* **1990**, *29*, 3274-3282.

(26) Krief, A. *Tetrahedron* **1986**, *42*, 1209-1252.

(27) Yamashita, Y.; Tomura, M.; Zaman, M. B.; Imaeda, K. *Chem. Commun.* **1998**, 1657-1658.

(28) Sugimoto, T.; Awaji, H.; Sugimoto, I.; Misaki, Y.; Kawase, t.; Yoneda, S.; Yoshida, Z.-I.; Kobayashi, T.; Anzai, H. *Chem. Mater.* **1989**, *1*, 535-547.

(29) Benahmed-Gasmi, A. S.; Frère, P.; Garrigues, B.; Gorgues, A.; Jubault, M.; Carlier, R.; Texier, F. *Tetrahedron Lett.* **1992**, *33*, 6457-6460.

(30) Hansen, T. K.; Lakshmikantham, M. V.; Cava, M. P.; Niziurski-Mann, R. E.; Jensen, F.; Becher, J. *J. Am. Chem. Soc.* **1992**, *114*, 5035-5039.

(31) Takahashi, K.; Nihira, T.; Tomitani, K. *J. Chem. Soc. Chem. Commun.* **1993**, 1617-1619.

(32) Takahashi, K.; Tomitani, K.; Ise, T.; Shirahata, T. *Chem. Lett.* **1995**, 619-620.

(33) Yamashita, Y.; Kobayashi, Y.; Miyashi, T. *Angew. Chem., Int. Ed. Engl.* **1989**, *28*, 1052-1053.

(34) Yamashita, Y.; Miyashi, T. *Chem. Lett.* **1988**, 661-664.

(35) Martín, N.; Sánchez, L.; Seoane, C.; Ortí, E.; Viruela, P. M.; Viruela, R. *J. Org. Chem.* **1998**, *63*, 1268-1279.

(36) Bryce, M. R.; Moore, A. J. *Synth. Met.* **1988**, *27*, B557-B561.

(37) Kato, H.; Kobayashi, T. *Adv. Mater.* **1993**, *5*, 750-751.

(38) Akiba, K.-Y.; Ishikawa, K.; Inamoto, N. *Bull. Chem. Soc. Jpn.* **1978**, *51*, 2674-2683.

(39)   Batsanov, A. S.; Bryce, M. R.; Coffin, M. A.; Green, A.; Hester, R. E.; Howard, J. A. K.; Lednev, I. K.; Martín, N.; Moore, A. J.; Moore, J. N.; Ortí, E.; Sánchez, L.; Savirón, M.; Viruela, P. M.; Viruela, R.; Ye, T.-Q. *Chem. Eur. J.* **1998**, *4*, 2580-2592.

(40)   Bryce, M. R.; Moore, A. J. *Synth. Met.* **1988**, *25*, 203-205.

(41)   Bryce, M. R.; Finn, T.; Moore, A.; Batsanov, A. S.; Howard, J. A. K. *Eur. J. Org. Chem.* **2000**, 51-60.

(42)   Bryce, M. R.; Coffin, M. A.; Hursthouse, M. B.; Karaulov, A. L.; Müllen, K. *Tetrahedron Lett.* **1991**, *32*, 6029-6032.

(43)   Bryce, M.; Moore, A. J.; Lorcy, D.; Dhindsa, A. S.; Robert, A. *J. Chem. Soc. Chem. Commun.* **1990**, 470-472.

(44)   Yamashita, Y.; Tanaka, S.; Imaeda, K.; Inokuchi, H. *Chem. Lett.* **1991**, 1213-1216.

(45)   Bryce, M. R.; Moore, A. J.; Hasan, M.; Ashwell, G. J.; Fraser, A. T.; Clegg, W.; Hursthouse, M. B.; Karaulov, A. I. *Angew. Chem., Int. Ed. Engl.* **1990**, *29*, 1450-1452.

(46)   Moore, A. J.; Bryce, M. R.; Batsanov, A. S.; Cole, J. C.; Howard, J. A. K. *Synthesis* **1995**, *6*, 675-682.

(47)   Martín, N.; Ortí, E. In *Handbook of advanced electronic and photonic materials and devices*; Nalwa, H. S., Ed.; Academic Press: 2001; Vol. 3, p 245-265.

(48)   Jones, A. E.; Christensen, C. A.; Perepichka, D. F.; Batsanov, A. S.; Beeby, A.; Low, P. J.; Bryce, M. R.; Parker, A. W. *Chem. Eur. J.* **2001**, *5*, 973-978.

(49)   Cerrada, E.; Bryce, M. R.; Moore, A. J. *J. Chem. Soc. Perkin Trans. 1* **1993**, 537-538.

(50)   Marshallsay, G. J.; Bryce, M. R. *J. Org. Chem.* **1994**, *59*, 6847-6849.

(51)   Martín, N.; Perez, I.; Sanchez, L.; Seoane, C. *J. Org. Chem.* **1997**, *62*, 870-877.

(52)   Pérez, I.; Liu, S.-G.; Martín, N.; Echegoyen, L. *J. Org. Chem.* **2000**, *65*, 3796-3803.

(53)   Liu, S.-G.; Pérez, I.; Martín, N.; Echegoyen, L. *J. Org. Chem.* **2000**, *65*, 9092-9102.

(54)   Bryce, M. R.; Batsanov, A. S.; Finn, T.; Hansen, T. K.; Moore, A. J.; Howard, J. A. K.; Kamenjicki, M.; Lednev, I. K.; Asher, S. A. *Eur. J. Org. Chem.* **2001**, 933-940.

(55)   Herranz, M. A.; Martín, N.; Sánchez, L.; Garín, J.; Orduna, J.; Alcalá, R.; Villacampa, B.; Sánchez, C. *Tetrahedron* **1998**, *54*, 11651-11658.

(56)   Martín, N.; Pérez, I.; Sánchez, L.; Seoane, C. *J. Org. Chem.* **1997**, *62*, 5690-5695.

(57)   Herranz, M. A.; Illescas, B.; Martín, N. *J. Org. Chem.* **2000**, *65*, 5728-5738.

(58)   Herranz, M. A.; Martín, N.; Sánchez, L.; Seoane, C.; Guldi, D. M. *J. Organomet. Chem.* **2000**, *599*, 2-7.

(59)   Martín, N.; Sánchez, L.; Guldi, D. M. *Chem. Commun.* **2000**, 113-114.

Chapter Two

Secondary Interactions:

Towards Increased Supramolecular

Order in the Solid State.

2.1 Intermolecular Hydrogen Bonding.

As we have already mentioned in the preceding chapter, tetrathiafulvalene (TTF) is a π-electron donor, which readily forms conductive charge transfer salts or organic metals with π-electron acceptors like TCNQ. To increase the conductivity of these materials, organic chemists have synthesised tetrathiafulvalene derivatives bearing different functional groups with the purpose of increasing their intermolecular interactions to gain control over their solid state architecture. Crystal structures of organic solids are governed by a delicate balance between several weak interactions such as electrostatic forces, Van der Waals interactions, hydrogen bonding and π-π stacks.[1] Consequently, changing the strength of one of these interactions can result in a complete change of structure.

2.1.1 Hydrogen-bonded networks in tetrathiafulvalene derivatives.

The first observation of strong hydrogen bonding within the crystal structure of TTF derivatives was realised fortuitously by analysing crystals of BEDT-TTF (**6**) charge-transfer salts containing water molecules [*eg.* $(BEDT\text{-}TTF)_3Cl_2 \cdot 2H_2O)$]. The stacks of BEDT-TTF molecules are connected by hydrogen bonds to $Cl_4(H_2O)_4$ units (*Figure 2.1*). It was the first superconducting hydrate salt to be reported.[2]
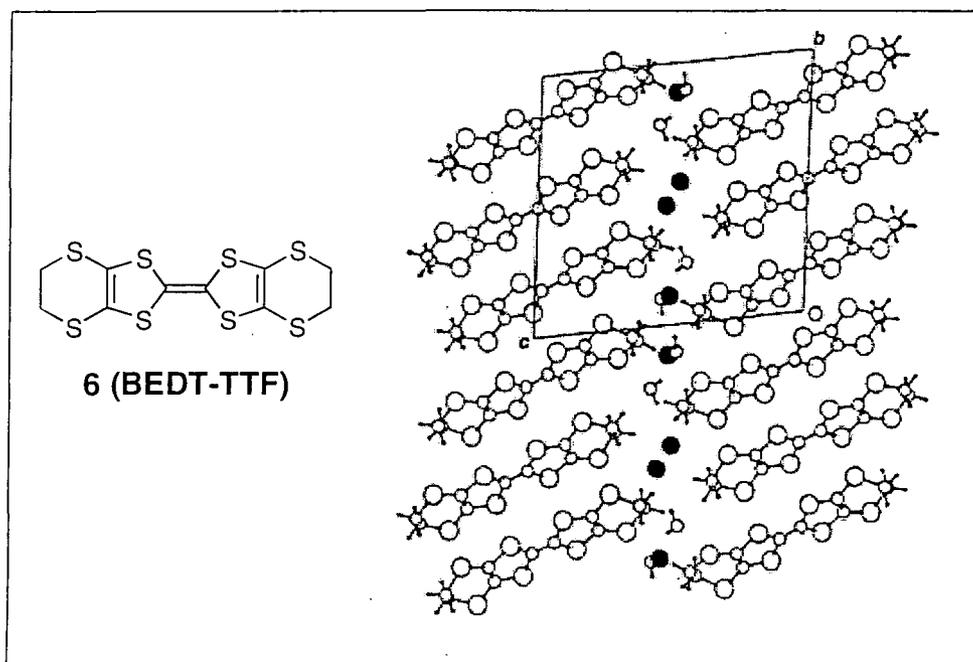
Figure 2.1 Crystal structure of $(BEDT\text{-}TTF)_3Cl_2 \cdot 2H_2O$. (in black: chloride anions)

A wide variety of functionalised TTFs bearing substituents that can participate in intermolecular hydrogen bonding (hydroxy, amido, thioamido, *etc.*) have been synthesised.[3-5] Often, the increase of intermolecular forces results in very low solubility of the molecules, thereby hindering studies on crystal growth. However, hydroxy-functionalised TTF derivatives, such as compounds **45** and **46**[6] have been successfully characterised and present a remarkable network of hydrogen bonding, which, controls together with π-π stacking of the TTF cores, the architecture of their crystal structures (*Figure 2.2*).
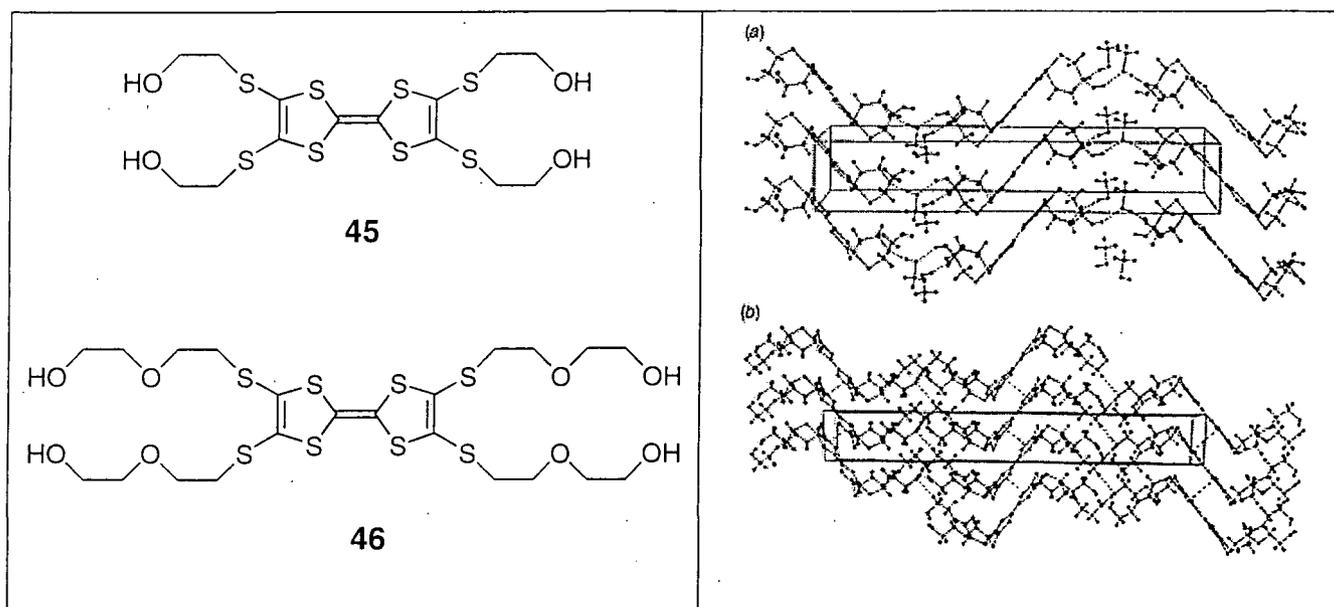
Figure 2.2 Crystal structures of **45** 2MeOH (a), and of **46** (b)

Anthracenediylidene derivatives, as we mentioned in the preceding chapter, possess a saddle shaped conformation in the neutral state. The crystal structures of most of these systems comprises dimers, in which one molecule engulfs the dithiole moiety of another (*Figure 1.6 p.14*). The dithiole-dithiole interaction, which occurs inside these dimers, prevents efficient stacking in the crystal. We recognised that it could be possible to modify the intermolecular interactions by adding to the structure some secondary interactions such as hydrogen bonding by hydroxyl groups. We, therefore, decided to synthesise the mono- and di-hydroxymethyl derivative of the anthracenediylidene system. We also recognised that these functionalised derivatives could be useful building blocks for more elaborate systems, by reactions of the hydroxy group(s).

2.1.2 Hydroxymethyl anthracenediylidene derivative.

2.1.2.1 Synthesis.

Ester **26** was synthesised following the literature procedure[7] from the trimethyl anthracenediylidene derivative **25b** by lithiation followed by trapping of the lithiated species by methyl chloroformate. The synthesis shown in *Scheme 2.1* has been scaled up, with modifications to obtain 20g of **25b**. The problematic step on a large scale is the Horner-Wadsworth-Emmons reaction for which the solubility of the ketones is very important. The reaction needs a rigorously anhydrous media maintained at –78°C during the addition of all the ketone **23b** to the ylide of **24c**; a cannula was used to transfer dropwise the ketone to the reaction mixture under nitrogen. The ketone **23b** was dissolved in hot dry THF, and heating was maintained during the transfer via the cannula, while the reaction mixture containing the phosphonate **24c** dissolved in dry THF with 1.1 equivalent of LDA was maintained at –78°C. Using this procedure, compound **25b** (20 g batch) was obtained in 70% yield.
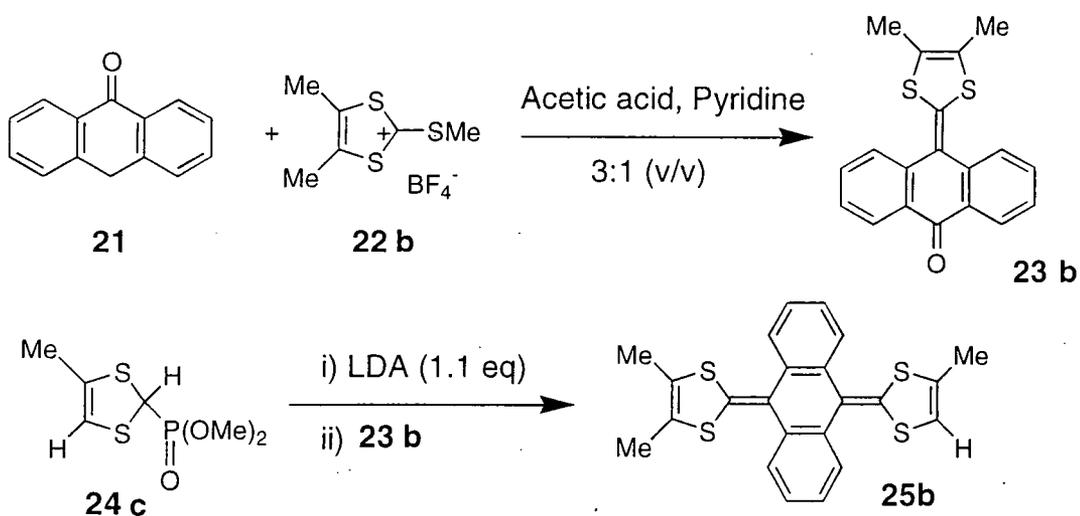
Scheme 2.1 Synthesis of trimethyl-anthracenediylidene derivative **25b**.

The preparation of the hydroxymethyl anthracenediylidene derivative (**47**) was performed by reduction of the corresponding ester (**26**) by lithium aluminium hydride in THF (*Scheme 2.2*) in a very high yield.
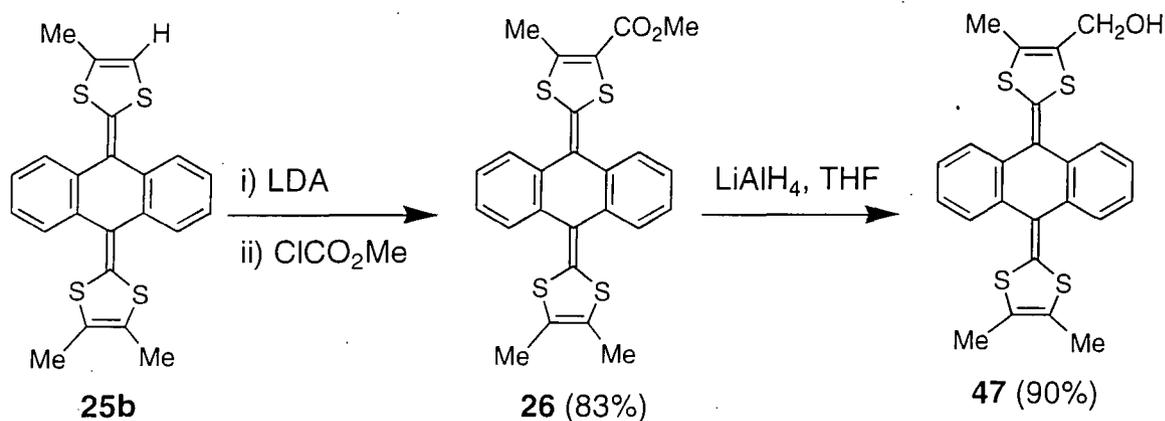
Scheme 2.2 Synthesis of hydroxymethyl anthracenediylidene derivative **47.**

Unfortunately, the lithiation of compound **25b** is not a quantitative reaction. Separation of the starting material and the product **26** was achieved by silica gel chromatography, using DCM/hexanes (1:2 v/v) for the best separation, in which the compounds have low solubility. This solubility problem prevented the scale up of the reaction beyond 5g of **25b**. However, if the alcohol **47** is the desired product, it is possible to circumvent this problem by using the crude product obtained by the lithiation reaction (composed of a mixture of **25b** and **26**) directly in the reduction by lithium aluminium hydride. This second step being almost quantitative, the crude product comprising **25b** and **47**, is easier to purify, by chromatography in pure DCM, in which the compounds are readily soluble. This method allowed the synthesis of 15g of **47** with an overall yield of 70% from **25b**.

2.1.2.2 Dynamic NMR studies.

^{1}H NMR studies performed on **47**, showed a difference in chemical shift for the two protons H_a and H_b in the α-position to the hydroxyl group (*Figure 2.3*). This is observed at 20°C in d_6-DMSO, giving a four-line AB system ($J_{AB} = ca.$ 13 Hz).
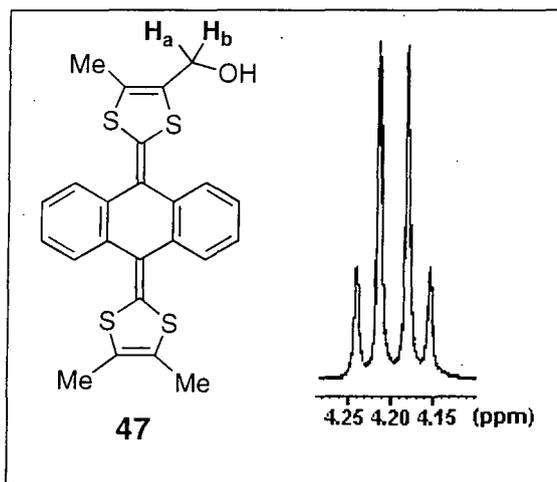
Figure 2.3 ^{1}H NMR spectrum of H_a and H_b of **47** in $(CD_3)_2SO$ at 20°C.

This observation leads to a significant conclusion. The only possibility to observe this four line AB-system is in the case of H_a and H_b being diastereotopic, which directly implies that the molecule is not planar in solution. Therefore, we suggest that the molecule exists as the two conformers A and B, which interconvert slowly (by boat-boat flipping of the central ring) on the NMR timescale at this temperature (*Figure 2.4b*). By increasing the temperature, the interconversion is faster and H_a and H_b are no longer differentiated. At 80°C (*Figure 2.4a*), the four lines have coalesced, the interconversion between form A and form B is fast enough to observe on the NMR timescale for this temperature the average planar conformation via which the two forms are interconverting.
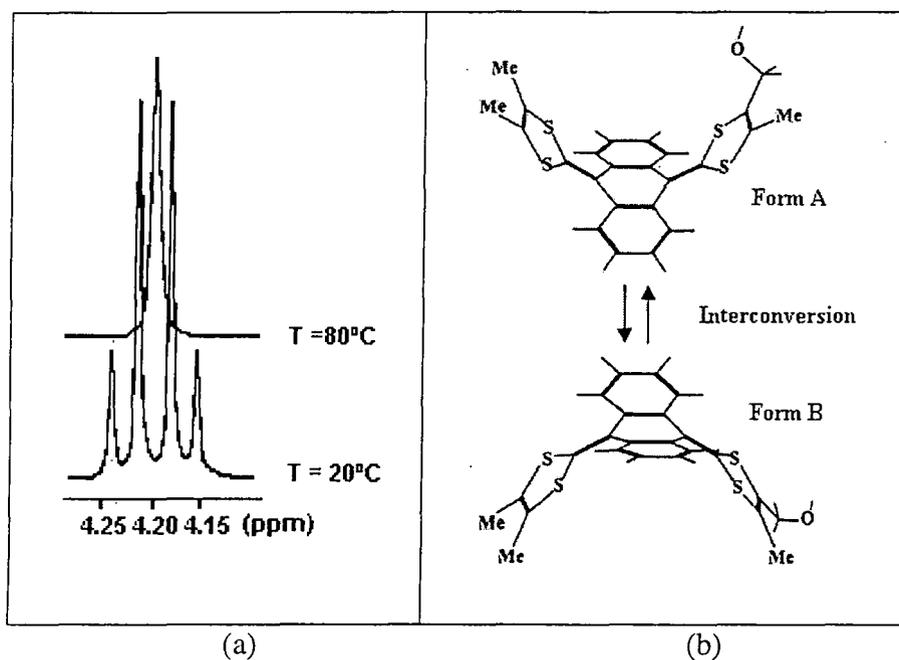
Figure 2.4 (a) ^{1}H NMR spectra of $\mathbf{H_a}$ and $\mathbf{H_b}$ of **47** in $(CD_3)_2SO$ at 20°C and 80°C; (b) Proposed conformations of **47** in solution.

Rate exchange measurements between the two conformations of compound **47** were carried out by Dr P. Hazendonk. Comparing the experimental data for the variation of the chemical shift of the AB system coalescing to the singlet with temperature and simulation of this process, the Eyring relationship gave an activation enthalpy, $\Delta H^{\ddagger} = 75.3$ kJ/mol, and an activation entropy $\Delta S^{\ddagger} = 11.5$ J/mol K. The error in $\Delta S^{\ddagger}$ is too large for reliable interpretation, requiring further studies to reduce the interpolation error in the Eyring plot. This is currently under investigation. (See also Appendix One for more details about the determination of the activation enthalpy $\Delta H^{\ddagger}$ and the activation entropy $\Delta S^{\ddagger}$ of the system).

2.1.2.3 Crystal Structure.

Single crystals of **47** suitable for X-ray analysis were obtained by recrystallisation from dichloromethane/hexanes. Each molecule adopts the characteristic saddle shaped conformation of anthracenediylidene derivatives[7] (See also Chapter One). The packing motif is also similar to that displayed by the precursor methyl ester **26**, constituted by pseudo dimers of molecules, related by an inversion centre and mutually engulfing each other by interactions between the dithiole rings. Hydrogen bonds are present between the dimers but seem not to be strong enough to modify the packing in any significant way (*Figure 2.5*).
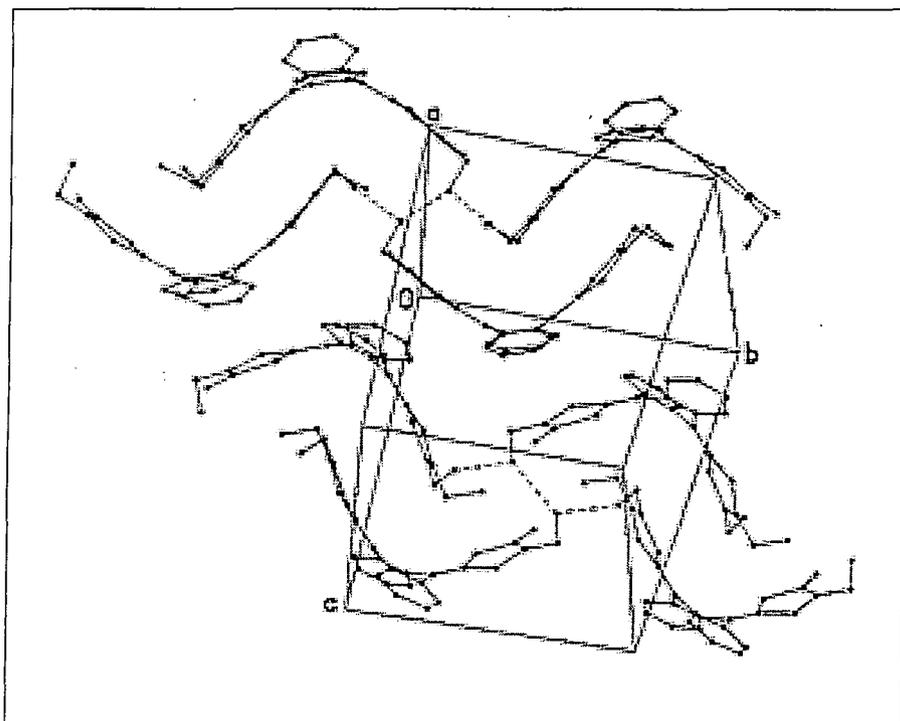
Figure 2.5 Crystal packing of **47** showing possible contacts between disordered O atoms. Hydrogen atoms have been omitted for clarity.

38

2.1.3 Dihydroxymethyl anthracenediylidene derivative.

2.1.3.1 Synthesis.

Following the Scheme used to obtain the monohydroxymethyl derivative **47**, we synthesised the dimethyl derivative **48** as described in the literature.[8] Lithiation of **48** by lithium diisopropylamide (LDA) followed by in situ trapping of the lithiated species with methylchloroformate gave a mixture of the mono-and diester derivatives **49** and **50**. LDA being a strong nucleophilic base cannot be used in excess for this reaction, as it would react with the ester formed. Using independently one or two equivalents of LDA, the mono-ester derivative **49** was always the major product of the reaction with an optimised yield of 32% when using 1.1 equivalent of LDA (*Scheme 2.3*).
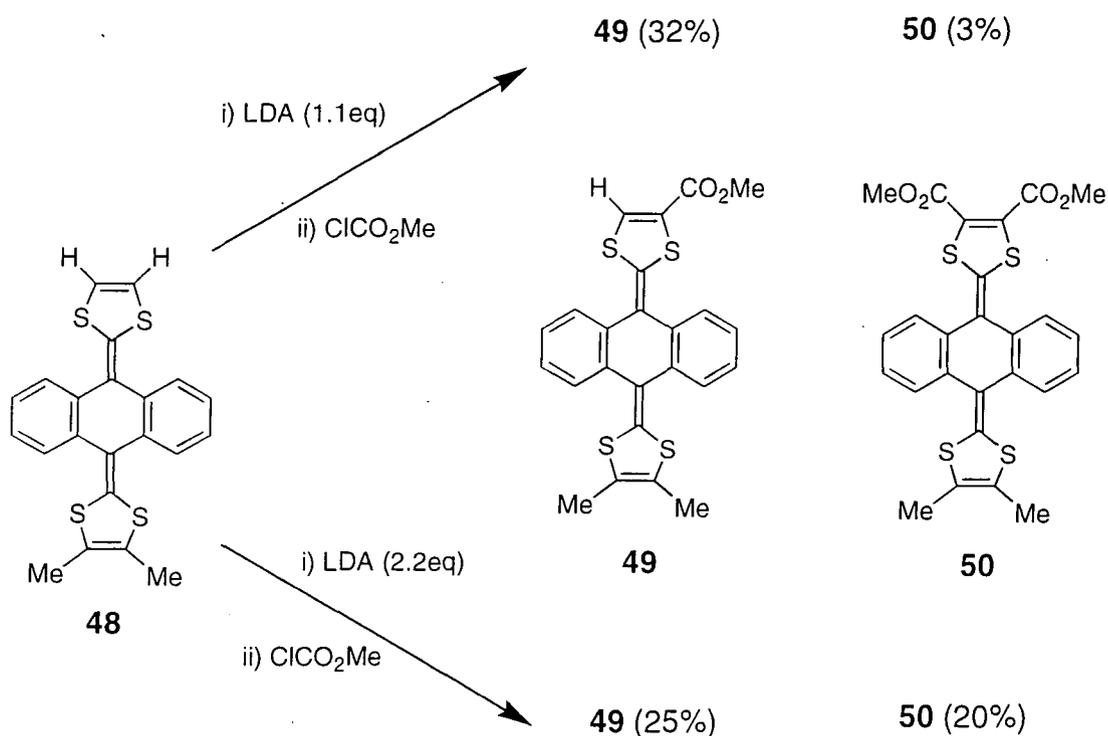
Scheme 2.3 Lithiation of **48** using Lithium diisopropylamide (LDA).

We, therefore, decided to use lithium bis(trimethylsilyl)amide (LHMDS) for the lithiation of **48**. LHMDS is a strong base, equivalent to LDA, but possessing sterically encumbered silyl groups, which decrease the nucleophilicity of the nitrogen atom. Therefore an excess of LHMDS can be used for the lithiation of **48**. Indeed, with 4 equivalents of LHMDS used to form the lithiated species of **48** followed by addition of methylchloroformate, the diester **50** was obtained in an optimised yield of 96% (*Scheme 2.4*).

Reduction of diester **50** was performed using lithium aluminium hydride to yield to the dihydroxymethyl derivative **51** in an almost quantitative yield.
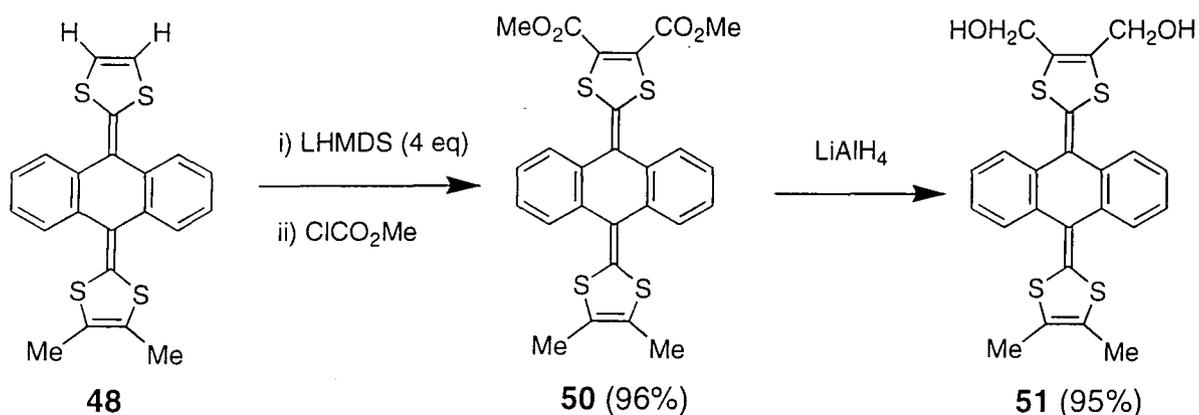
Scheme 2.4 Synthesis of dihydroxymethyl derivative **51**.

2.1.3.2 Crystal Structure.

Single crystals of **51** suitable for X-ray crystallographic studies have been obtained by recrystallisation from dissolution of the compound in dichloromethane and adding methanol. Like the monohydroxymethyl derivative **47**, each molecule adopts the characteristic saddle shaped conformation. The packing motif is also similar, and the presence of the two hydroxyl groups does not modify the structure nor the continuity of the hydrogen bonding chain linking the dimers (*Figure 2.6*). It seems likely that methyl and hydroxymethyl groups form hydrophobic and hydrophilic clusters, respectively, inside the structure directed by the strong dithiole---dithiole ring interactions.
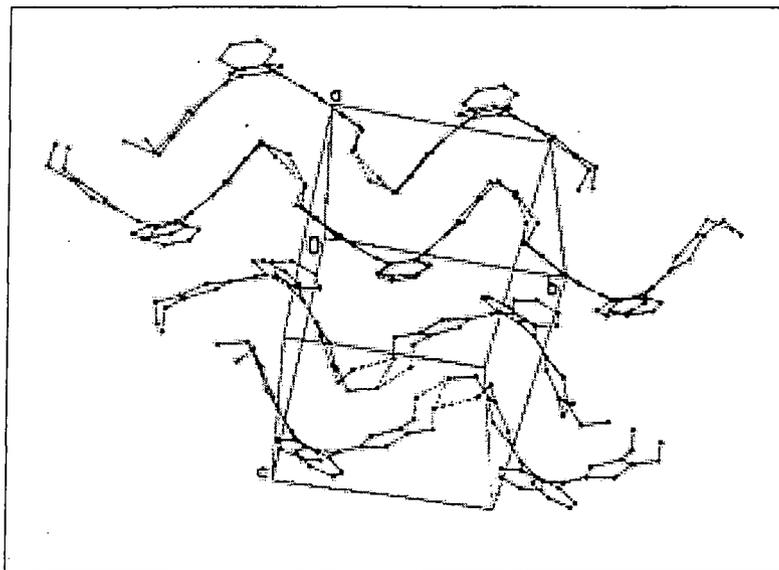
Figure 2.6 Crystal packing of **51** showing possible contacts between disordered O atoms.

2.1.4 Conclusion

We developed the synthesis of the mono and di-hydroxymethyl derivatives of the anthracenediylidene system. The NMR study of the monohydroxymethyl **47** allowed the observation for the first time of the saddle shaped conformation of this class of extended-TTF in solution as observed in X-ray crystallography[9] and predicted by theoretical calculations.[10] Hydrogen bonds are present inside the crystalline structures as expected. Even if the molecules are linked by a chain of hydrogen bonds, RO-H···O(R)-H···O(R)-H, such as exist in the crystals of higher alcohols, the presence of the pseudo-dimeric packing motif prevents its continuity and its order; and, therefore, is evidence of the high stability of this motif. Attempts to synthesise tetrahydroxymethyl derivatives of the system failed, the compounds obtained being insoluble in any solvents. We, therefore, orientated our research towards other secondary interactions such as secondary π-π interactions of aromatic ester derivatives.

2.2 Secondary π-π interactions.

Aromatic interactions are weaker, less well-defined interactions with respect to hydrogen bonds, however, the surface area of intermolecular contact is larger, so van der Waals interactions are much more important and a vast range of different functional groups can be involved.[11]

In order to study secondary π-π interactions, we synthesised a new series of aromatic esters derived from the hydroxymethyl derivative **47**. Esterifications of **47** were performed under N_2 in dichloromethane at room temperature, using triethylamine as catalytic base, and the appropriate acid chloride (*Scheme 2.5*). Reaction of **47** with benzoyl chloride and 2-naphthaloyl chloride gave the corresponding ester derivatives **52** (99% yield) and **53** (67% yield).
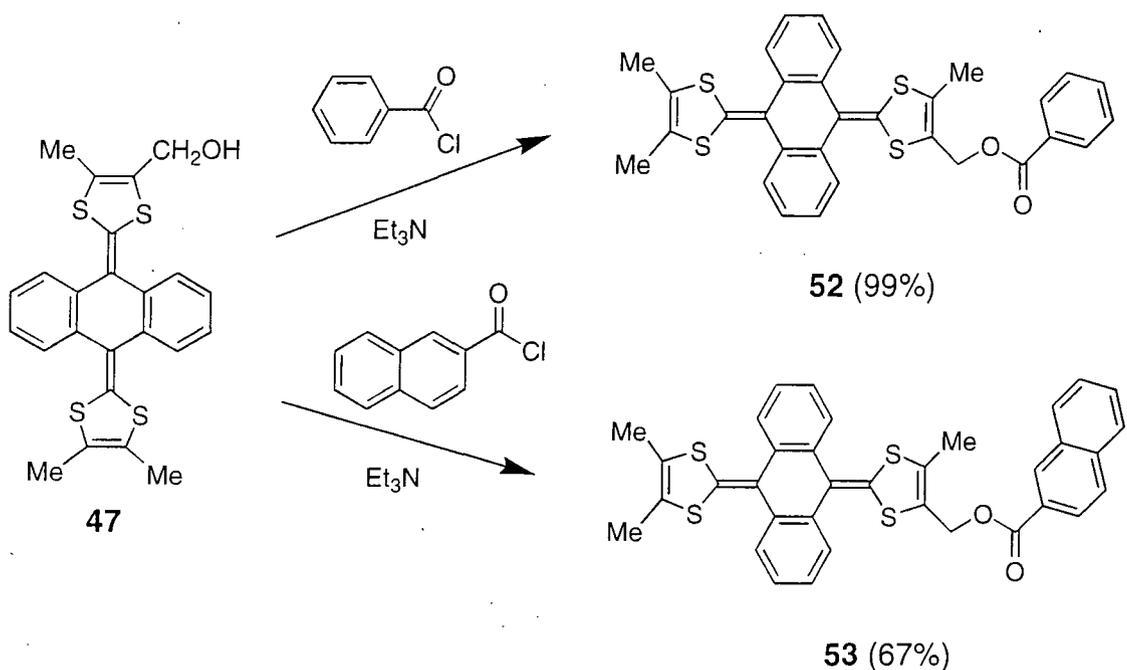
Scheme 2.5 Synthesis of benzoyl ester derivative (**52**) and 2-naphthaloyl ester derivative (**53**).

Both compounds **52** and **53** were recrystallised by dissolution in hot dichloromethane adding hexanes before cooling to room temperature. The crystal structures of **52** and **53**·CH₂Cl₂ (*Figure 2.7*) present the characteristic saddle shaped conformation of anthracenediylidene derivatives.

(a)   (b)
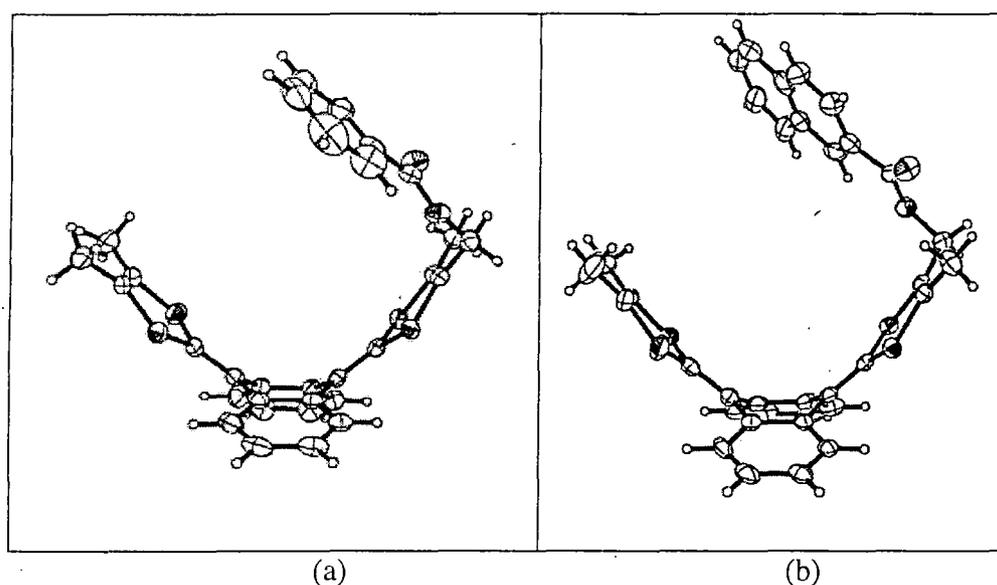
Figure 2.7 Crystal structures of benzoyl ester derivative **52** (a) and 2-naphtaloyl ester derivative **53** (b)

We can notice for the benzoyl ester derivative **52**, the slightly different orientations of the two dithiole rings (*Figure 2.7a*). Moreover, comparing with their precursor **47**, the folding of the saddle increases with the size of the substituents, which can be observed by comparing the angles representative of this structure (φ, δ₁, δ₂, θ) (*Figure 2.8*).

R$_1$= Me, R$_2$=CH$_2$OH : **47**
R$_1$, R$_2$=CO$_2$Me : **50**
R$_1$, R$_2$=CH$_2$OH : **51**
R$_1$= Me, R$_2$=CH$_2$OC(O)Ph : **52**
R$_1$= Me, R$_2$=CH$_2$OC(O)Naph. : **53**

	Dihedral angles (°)					
	47	**50**	**51**	**52**	**53**	
φ	37.3	37.4	37.4	41.4	39.7	38.1
δ$_1$	6.1	16.7	9.0	16.7	11.3	14.9
δ$_2$	9.9	8.7	6.2	9.9	6.3	8.4
θ	89.4	100.2	91.3	89.4	72.9	77.5

φ represents the folding of the anthracenediylidene moiety along C(9)···C(10) vector.

δ$_1$, δ$_2$ represent the folding of the dithiole rings along S(1)···S(2) and S(3)···S(4) vectors, respectively.

θ is the dihedral angle of the outlying planar (S(1)-C(16)-C(17)-S(2)) and (S(3)-C(21)-C(22)-S(4)).

Figure 2.8 Comparative study of the molecular folding of compounds **47**, **50**, **51**, **52**, and **53**.
For compound **53**, two series of data are given, two different molecules existing in its crystal structure.

The packing motif of these ester derivatives is similar to their precursor. Each compound displays pseudo dimers formed by the intermolecular interactions of two dithiole rings, which engulf each other. This motif ensures the most dense packing and to conform to it, molecular folding is increased and twisting can occur, which is the case for the benzoyl ester derivative (**52**) for which the two dithiole rings have slightly different orientations. Contrary to our initial hypothesis, secondary π-π interactions do not occur nor is the dithiole rings interaction broken. There is possible intramolecular charge transfer inside the dimers as the electron-rich dithiole moiety (D) lies in proximity to the electron-poor benzoyl group (A) of the other molecule. The shortest contact between D---A is

45

3.53 Å for **52**, however the donor and acceptor moieties are nearly parallel (interplanar angle 10°) and have anti-orientations, thus limiting their overlap. The crystal structure of **52** thus displays oligomeric stacks of 4 layers ADDA but does not contain infinite stacks (*Figure 2.9*).

(a)   (b)
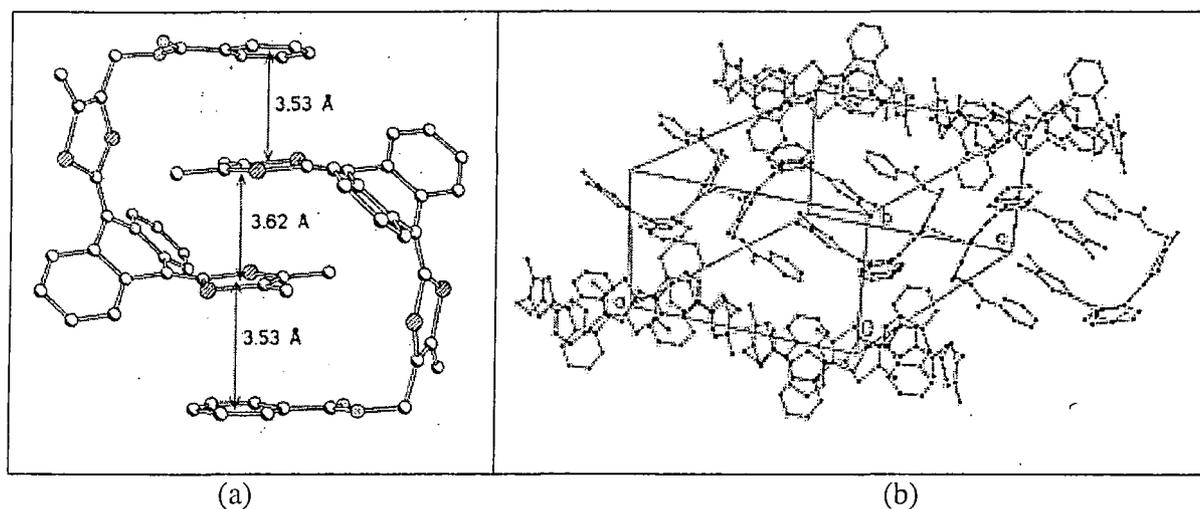
Figure 2.9 Intramolecular charge transfer ADDA (a) and Crystal packing (b) for the benzoyl ester **52** (Hydrogen atoms have been omitted for clarity).

For the naphthaloyl ester derivative **53**, the conditions of intramolecular charge transfer are more favourable. Each naphthaloyl group is sandwiched between two dithiole groups, one belonging to the other molecule of the same dimer and the other belonging to a different dimer. The donor and acceptor moieties are practically parallel (interplanar angles 0.4° and 3.6°), the contacts between them are between 3.41 Å and 3.67 Å, which are close to the sum of the van der Waals' radii (3.61 Å). The crystal structure of **53** thus displays oligomeric stacks of 6 layers DADDAD but does not contain infinite stacks (*Figure 2.10*).

(a)   (b)
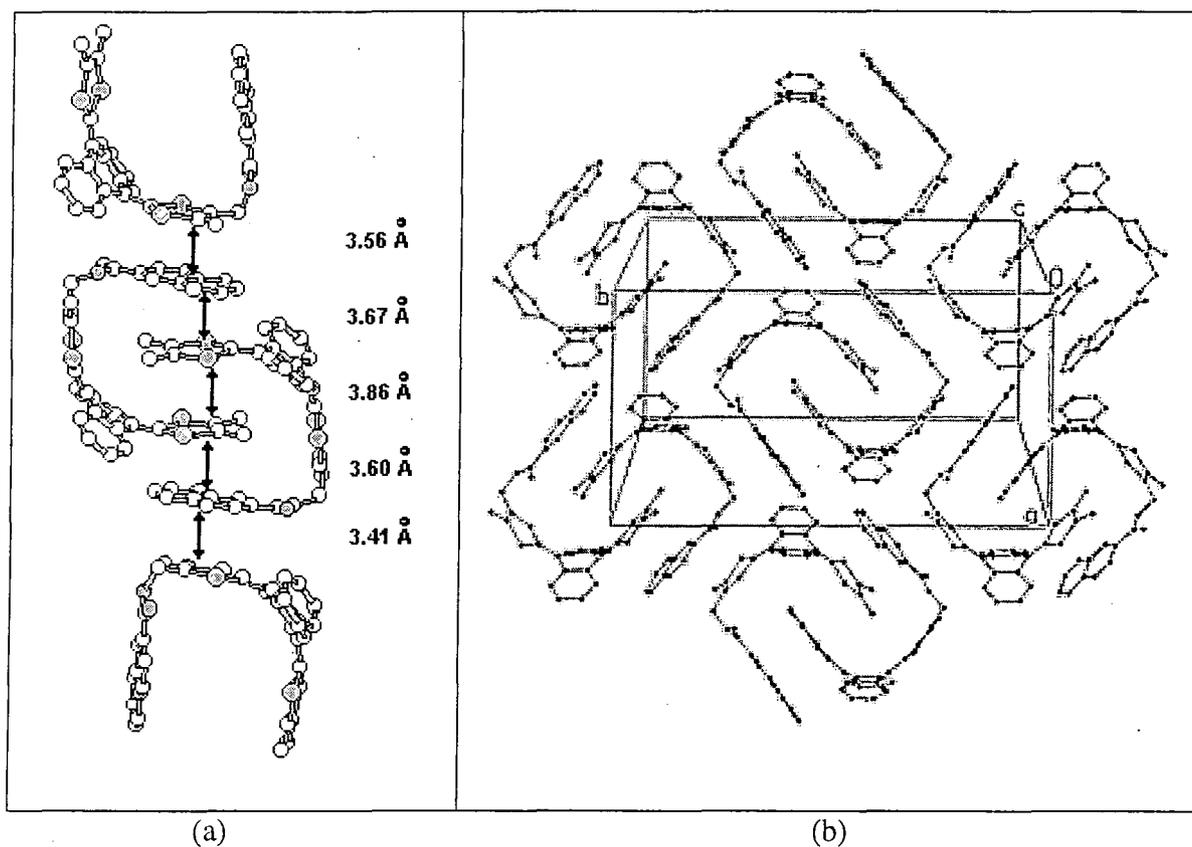
Figure 2.10 Intramolecular charge transfer DADDAD (a) and crystal packing of the naphtaloyl ester **53** (Hydrogen atoms have been omitted for clarity).

In order to increase this interaction between donor and acceptor moieties inside the crystal structure of anthracenediylidene derivatives, we synthesised the ester **54** bearing an anthraquinone acceptor moiety (**55**). (*Scheme 2.6*)
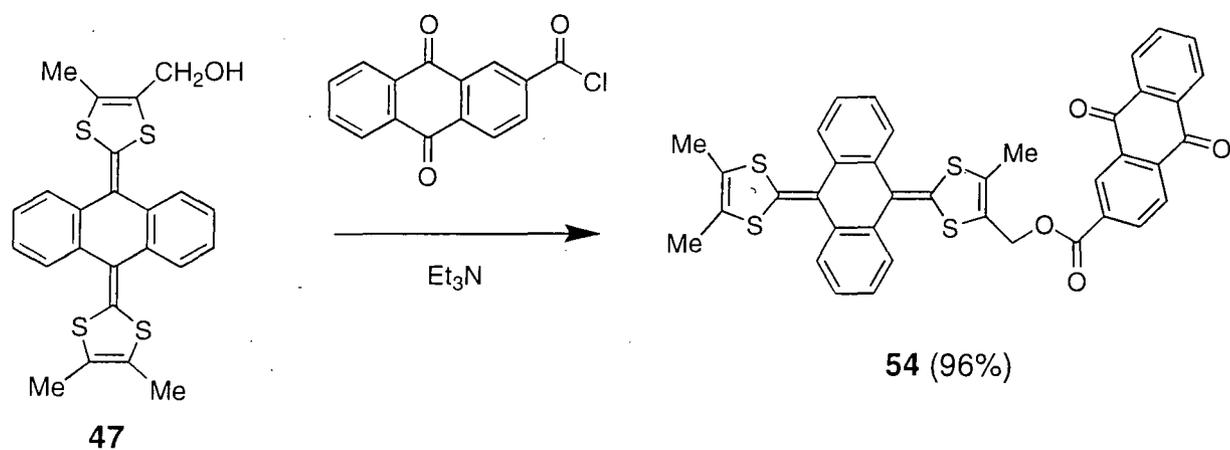
Scheme 2.6 Synthesis of anthraquinoyl ester derivative (**54**).

Recrystallisations in different solvents and mixtures of solvent did not give crystals, which were suitable for X-ray analysis. However, the black-green colour of the crystalline powder of **54** is characteristic of charge transfer interactions in the solid state, which are not present in solution. UV-Vis spectra in solution do not show any characteristic band for charge transfer in solutions (DCM or acetonitrile) for a range of concentrations (10^{-6} to 10^{-4} M) and solutions of **54** are always yellow. However, the UV-Vis spectrum recorded on the solid state, shows the characteristic charge transfer band present at λ_{max} = 550-750 nm (*Figure 2.11*).
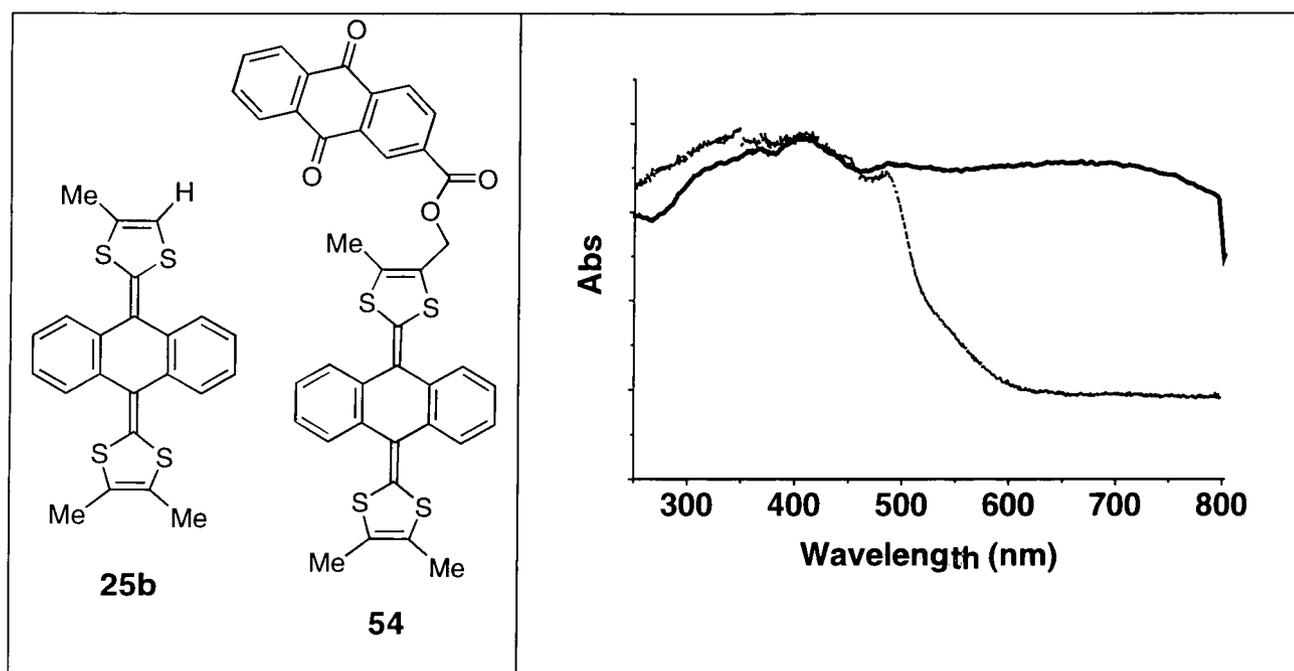
Figure 2.11 UV-Vis spectra on solid state of compounds **25b** (——) and **54** (——).

2.3 Solution Electrochemical Studies.

Solution electrochemical data for the new anthracenediylidene derivatives presented in this chapter are consistent with their substitution patterns (*Table 2.1*). As for TTF derivatives, the general trend is that electron withdrawing substituents result in a positive shift (i.e. more difficult to oxidise) and electron-donating groups in a negative shift (easier to oxidise).

Compound	E_{pa}^{Ox} / V	E_{pc}^{Ox} / V	ΔE / V	
25b	0.40	0.18	0.22	
26	0.51	0.18	0.33	
47	0.39	0.05	0.34	$R_1 = Me; R_2 = H : $ **25b**
48	0.38	0.16	0.22	$R_1 = Me; R_2 = CO_2Me : $ **26**
49	0.52	0.25	0.27	$R_1 = Me; R_2 = CH_2OH : $ **47**
50	0.60	0.29	0.31	$R_1, R_2 = H : $ **48**
51	0.35	0.20	0.15	$R_1 = H; R_2 = CO_2Me : $ **49**
52	0.45	0.14	0.31	$R_1, R_2 = CO_2Me : $ **50**
53	0.46	0.06	0.40	$R_1, R_2 = CH_2OH : $ **51**
54	0.46	0.16	0.30	$R_1 = Me; R_2 = CH_2O_2CPh : $ **52**
29	0.52	0.24	0.28	$R_1 = Me; R_2 = CH_2O_2CNaph : $ **53**

$R_1 = Me; R_2 = CH_2O_2CAnthraquinone : $ **54**

$R_1 = Me; R_2 = CHO : $ **29**

Table 2.1 Cyclic voltammetric data. $\Delta E = E_{pa}^{Ox} - E_{pc}^{Ox}$

E_{pa}^{Ox} is the oxidation peak potential on the first anodic scan;

E_{pc}^{Ox} is the coupled reduction peak potential on the cathodic scan.

[Experimental conditions: Dichloromethane/Acetonitrile (2:1 v/v), Pt electrode, versus Ag/AgCl, electrolyte $Bu_4N^+ClO_4^-$ (0.1M), 20°C, scan rate 100 mV s^{-1}.]

Thus, ester substituents of compounds **26, 49, 50** result in a positive shift of the quasi-reversible, two-electron wave characteristic of the system (*See also Chapter One*). In particular, we can observe the effect of one ester group and the cumulative effect of two ester groups on the system, which respectively increase the oxidation potential by *ca.* 120 mV and 220 mV. Hydroxymethyl groups, being very weak electron donating substituents, result in a small negative shift (*ca.* 10-20 mV), which can be observed by comparing the oxidation potentials of **47** with **25b**. The cumulative effect of two hydroxymethyl groups is seen by comparing the oxidation potentials of **51** with **48** (30 mV). For the esters **52, 53** and **54** (TTFAQ-CH$_2$O$_2$CR), the oxidation potentials are shifted by *ca.* 60 mV which is consistent with the ester functions being further removed from the anthracenediylidene moiety (TTFAQ) than for the previous esters **26, 49** and **50** (TTFAQ-CO$_2$R).

Electrochemical data are really dependent upon the experimental conditions (solvent, nature and concentration of electrolyte, temperature, humidity...) and also depend on the solubility of the compound and its oxidised species, therefore, puzzling unexplained variations in ΔE for compounds **51** (150 mV) and **53** (400 mV) have been observed and might be only due to solubility problems. However, similar unexplained results have already been noted by Martín *et al.* for dimeric compounds of anthracene-TTF derivatives.[12]

The cyclic voltammogram of compound **54** displays clean amphoteric redox behaviour; upon reduction we observe the two one-electron waves of the anthraquinone moiety, and upon oxidation the two-electron wave characteristic of anthracene-TTF derivatives (*Figure 2.12*), and, as expected for non conjugated donor-acceptor compounds (see Chapter One), no interaction between the donor and the acceptor moieties is evident from the CV.
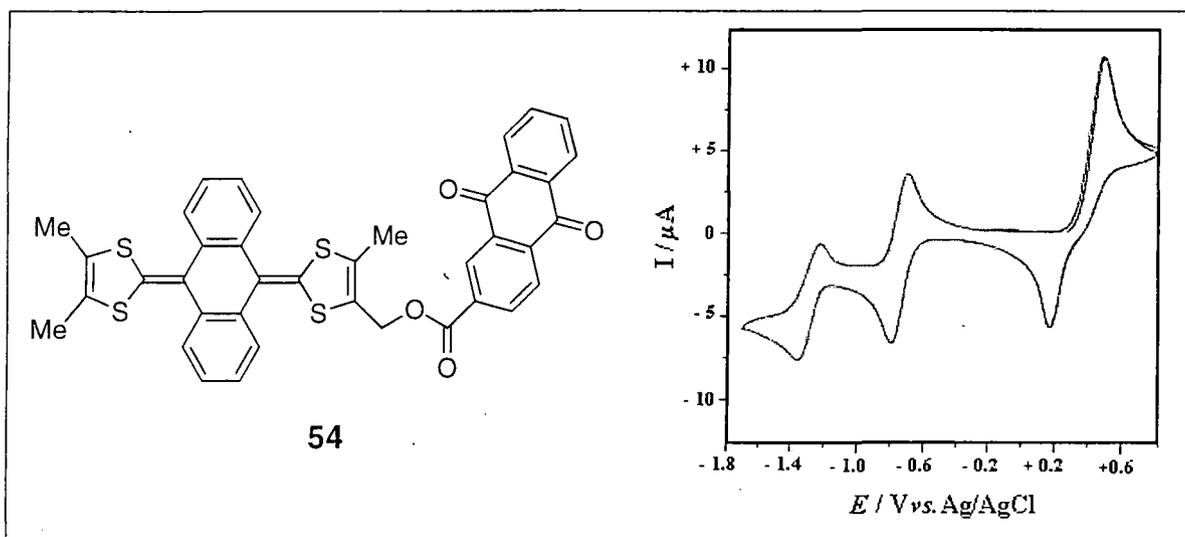
Figure 2.12 Cyclic voltammogram of **54**.
[Experimental conditions: Pt electrode, in DCM/Acetonitrile (2:1), $Bu_4N^+ClO_4^-$ (0.1M), 20°C]

2.4 Conclusion.

Through the synthesis and the study of these new anthracenediylidene derivatives, bearing hydroxyl or ester substituents, we have shown that the anthracenediylidene system possesses a saddle shape conformation in solution and in the solid state in a wide range of derivatives. Moreover, the crystallographic studies suggest a certain flexibility of the structure, the folding increasing with the size of the substituents. In the solid state, the main interaction which predominates, and consequently directs the architecture of the crystal, is the dithiole rings interactions. Therefore, pseudo dimers are formed preventing efficient packing in the crystal. These results led us to consider the possibility of incorporating the anthracenediylidene moiety into cyclophane structures, which would possess interesting solid state structures and also should possess unusual electrochemical properties. The availability in large quantities of the hydroxymethyl derivative **47**, also allows us to consider its incorporation into dendritic macromolecules leading to the synthesis of highly charged redox dendrimers.

2.5 References.

(1)   Desiraju, G. R. *Chem. Commun.* **1997**, 1475-1482.

(2)   Rosseinsky, M. J.; Kurmoo, M.; Talham, D. R.; Day, P.; Chasseau, D.; Watkin, D. *J. Chem. Soc. Chem. Commun.* **1988**, 88-90.

(3)   Li, H.; Zhang, D.; Zhang, B.; Yao, Y.; Xu, W.; Zhu, D.; Wang, Z. *J. Mater. Chem.* **2000**, *10*, 2063-2067.

(4)   Heuzé, K.; Fourmigué, M.; Batail, P. *J. Mater. Chem.* **1999**, *9*, 2373-2379.

(5)   Moore, A. J.; Bryce, M. R.; Batsanov, A. S.; Heaton, J. N.; Lehmann, C. W.; Howard, J. A. K.; Robertson, N.; Underhill, A. E.; Perepichka, I. F. *J. Mater. Chem.* **1998**, *8*, 1541-1550.

(6)   Batsanov, A. S.; Svenstrup, N.; Lau, J.; Becher, J.; Bryce, M. R.; Howard, J. A. K. *J. Chem. Soc. Chem. Commun.* **1995**, 1201-1202.

(7)   Bryce, M. R.; Finn, T.; Moore, A.; Batsanov, A. S.; Howard, J. A. K. *Eur. J. Org. Chem.* **2000**, 51-60.

(8)   Moore, A. J.; Bryce, M. R. *J. Chem. Soc. Perkin Trans. 1* **1991**, 157-168.

(9)   Bryce, M. R.; Moore, A. J.; Hasan, M.; Ashwell, G. J.; Fraser, A. T.; Clegg, W.; Hursthouse, M. B.; Karaulov, A. I. *Angew. Chem., Int. Ed. Engl.* **1990**, *29*, 1450-1452.

(10)   Martín, N.; Sánchez, L.; Seoane, C.; Ortí, E.; Viruela, P. M.; Viruela, R. *J. Org. Chem.* **1998**, *63*, 1268-1279.

(11)   Hunter, C. A.; Lawson, K. R.; Perkins, J.; Urch, C. J. *J. Chem. Soc. Perkin Trans. 2* **2001**, 651-669.

(12)   Martín, N.; Perez, I.; Sanchez, L.; Seoane, C. *J. Org. Chem.* **1997**, *62*, 870-877.

Chapter Three

Redox Active Cyclophanes:

Constraining the

Molecular Architecture.

3.1 Tetrathiafulvalene Cyclophanes.

3.1.1 Synthesis and Characterisation.

The incorporation of tetrathiafulvalene moieties into cyclophane structures was proposed by Staab *et al.* as a possible route to intramolecular charge transfer macrocycles containing both donor and acceptor moieties, with the aim of controlling the crystal structure of derived organic conductors. To illustrate the strategy employed, compounds **56a,b** (tetrathiafulvalenocyclophanes)[1] were synthesised via cyclisation by intramolecular coupling of the bis(1,3-dithiolium tetrafluoroborate) precursors **55a,b** (*Scheme 3.1*). For **57a,b** with a shorter spacer between the two dithiolium rings, intermolecular coupling was observed to yield compounds **58a,b** (tetrathiafulvalenophanes)[2] (*Scheme 3.2*).

55 a n=3
    b n=4

56 a n=3 Cis/Trans (1:1)
    b n=4 Cis only
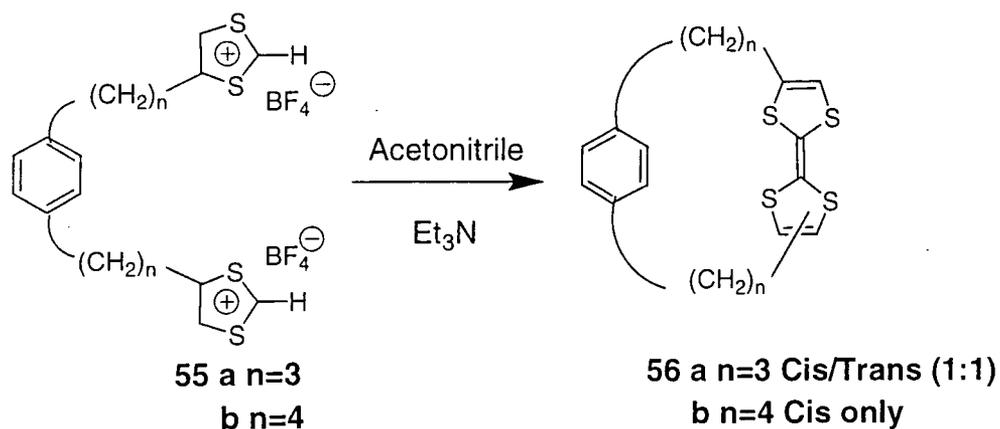
Scheme 3.1 Synthesis of tetrathiafulvalenocyclophanes **56a,b**.
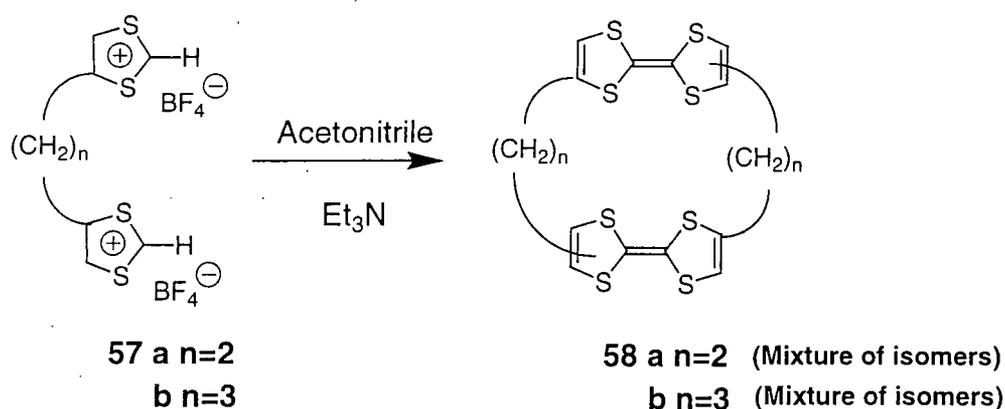
Scheme 3.2 Synthesis of tetrathiafulvalenophanes **58a,b**.

From this first synthesis of cyclophanes containing TTF moieties, we can notice the difficulty of controlling the selectivity of the coupling, which yield to mixtures of cis and trans isomers, which can in some cases be separated by consecutive fractional crystallisations. However, pure isomers are gradually converted into isomeric mixtures. This isomerisation is promoted by traces of acid, as reported by Robert *et al.* based on the isomerisation of compound **59a** (*Scheme 3.3*). The isomerisation of pure trans **59a** into a mixture of cis **59b** and trans **59a** was followed by ^{1}H NMR spectroscopy, *e.g.* in commercially available deuterated chloroform.[3]
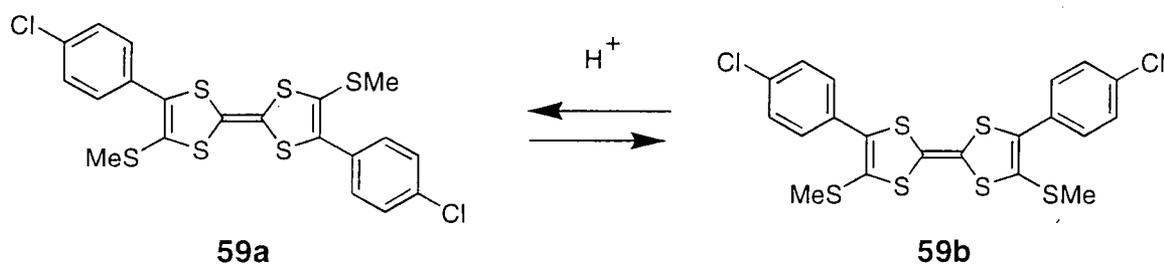
Scheme 3.3 Isomerisation of trans **59a** in acidic media.

Isomerisation of TTF cyclophanes can also occur upon oxidation. This is observed for example, with compounds **60a** and **61a** in the trans configuration.[4] The long bridging chain allowed the synthesis of the trans isomers only. Their oxidised cation radical species, isolated by electrocrystallisation as a salts $(60b^{+\bullet})_2[Re_6S_6Cl_8]^{2-}\cdot 2CH_3CN$ and $(61b)_2^{+\bullet}[Re_6S_5Cl_9]^-$ were analysed by X-ray crystallography confirming their cis configuration (*Figure 3.1*). Cyclic voltammetry data are consistent with an EC mechanism (EC= electron transfer with subsequent chemical reaction) leading to the formation and the observation of cis **60b** and cis **61b** after the second scan.
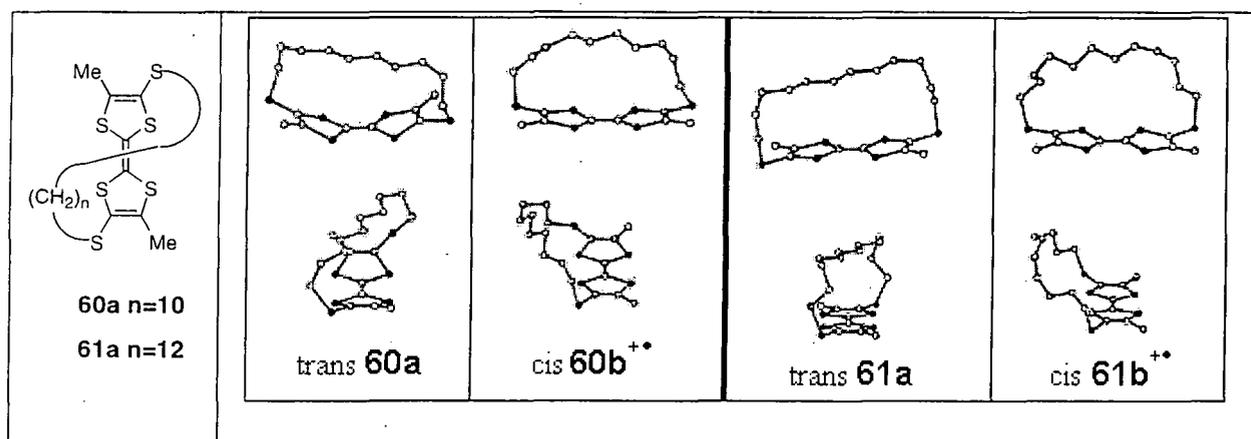
Figure 3.1 Crystal structures of **60a**, **60b⁺•**, **61a** and **61b⁺•**.

Upon oxidation a dimerisation process can also occur. Electrolysis of cyclophane **62a-c** resulted in the formation of the dimer **63a-c** identified for **63b** by X-ray analysis (*Figure 3.2*). Cyclic voltammetry data are also consistent with an EC mechanism. The breakdown of ring strain during the transformation of **62a-c** to **63a-c** can be considered as the driving force for the ring-enlarging dimerisation, even though the exact mechanism of the dimerisation process is unknown.[5]
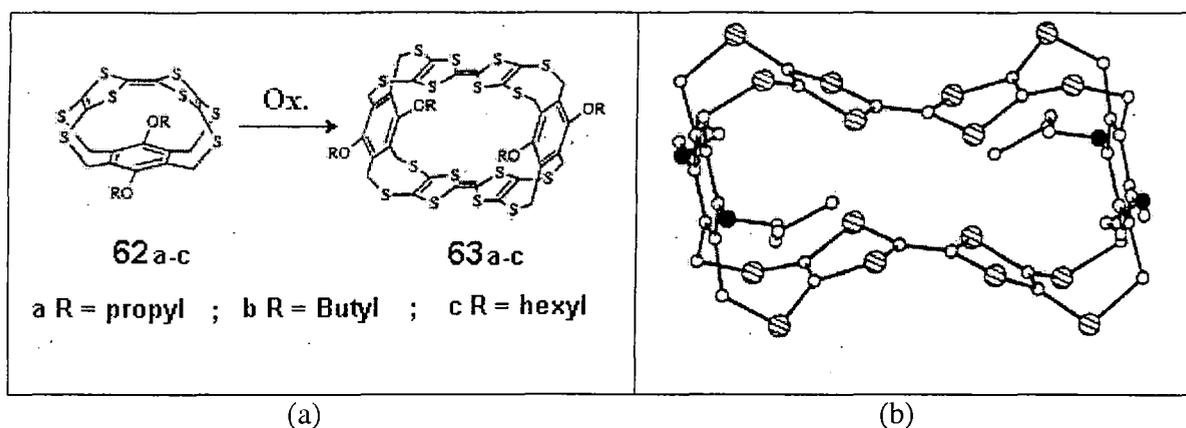
Figure 3.2 Dimerisation of **62a-c** into **63a-c** upon oxidation (a), Crystal structure of **63b** (b).

3.1.2 Electrochemistry of tetrathiafulvalenophanes.

TTF is an electron rich donor, with the HOMO mainly localised on the central $S_2C=CS_2$ moiety. In tetrathiafulvalenophane derivatives, the TTF moiety is often non planar due to steric constraints. Therefore, the folding of the dithiole rings disrupts the extended π-system and enhances this localisation still further. Consequently, the oxidation potentials of strongly distorted bridged TTF derivatives are shifted positively (*i.e.* they are harder to oxidise) compared to their parent planar analogues.

However, in systems containing several TTF units, intramolecular stabilisation of cation radical species can occur. Double-bridge TTF cyclophanes were synthesised by dimeric coupling of the bis-dithiole-2-one **64** followed by decarboxylation leading to the formation of all the possible isomers **65a-d** (*Scheme 3.4*).[6]
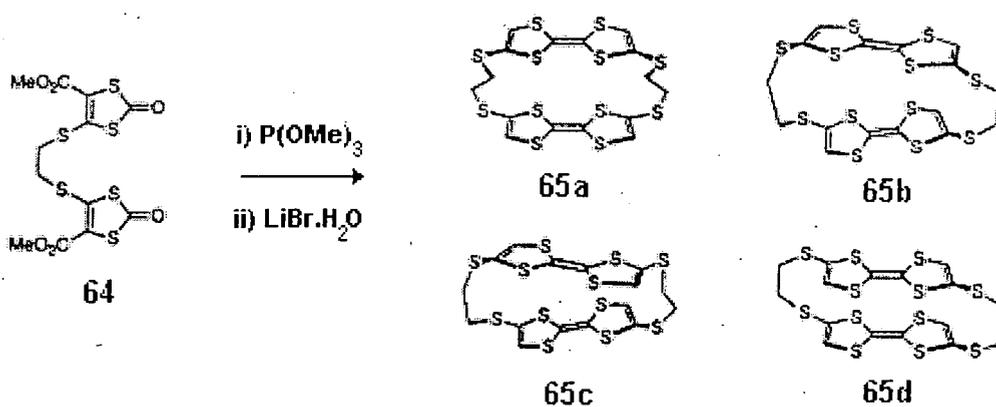
Scheme 3.4 Synthesis of TTF cyclophanes **65a-d**.

Repeated fractional recrystallisations allowed the separation of isomers **65a-c**. These pure isomers were gradually converted into isomeric mixture in solution due to traces amounts of acid. The cyclic voltammetry of the isomer **65b** in benzonitrile showed two reversible one-electron waves ($E_1^{1/2}$ = 0.41 V; $E_2^{1/2}$ = 0.56 V vs. Ag/AgCl) followed by one quasi-reversible two-electron wave ($E_3^{1/2}$ = 0.83 V). In the same conditions, compound **66** used as a non-bridged reference displayed two reversible one-electron waves ($E_1^{1/2}$ = 0.45 V and $E_2^{1/2}$ = 0.80 V).

66
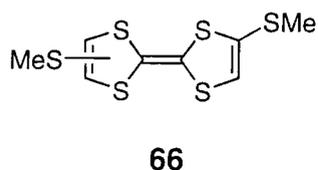
The first oxidation wave of compound **65b** is ascribed to the formation of the cation radical of one TTF unit. The fact that this oxidation occurs at a lower potential than for the non-bridged reference **66**, is good evidence of intramolecular interactions. The cation radical is, therefore, stabilised by the unoxidised TTF unit sharing electron density with the cationic species. The formation of the dicationic species occurs at higher potential due to Coulombic repulsion between the charged TTF units. Electrocrystallisation of **65b** allowed the formation of a radical cation salt of 3:4 donor to anion stoichiometry with

ClO_4^-. X-Ray analysis identified the donor as being **65d** the most compact isomer obtained by isomerisation of the radical cation species of **65b**. Crystal structures of **65d$^{+\bullet}$** and **65d^{2+}** (*Figure 3.3*) provided a clear observation of the intramolecular interaction (interplanar distance of 3.4 Å, sum of van der Waals radii for S$\cdots$S close contact 3.60 Å[7]) and the Coulombic repulsion effect.[8]

(a)   (b)
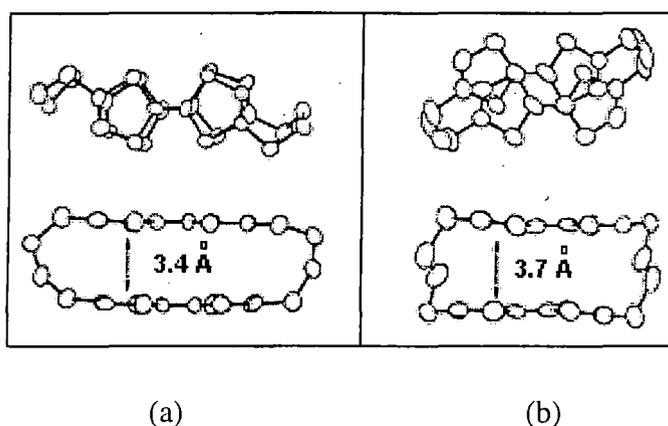
Figure 3.3 Crystal structures of **65d$^{+\bullet}$** (a) and **65d^{2+}** (b).

3.1.3 Conclusion

The incorporation of electroactive components into macrocyclic assemblies is currently a challenge in the field of organic materials chemistry, enabling studies of intramolecular charge transfer. For their unusual electrochemical properties, the design of cyclophanes containing TTF moieties is important for research into new redox components. However, as we noted above, the formation of isomers either during their synthesis or subsequently in the presence of traces of acids or by oxidation raise problems of controlling the final structure of such cyclophanes. Therefore, we decided to investigate the properties of cyclophanes containing anthracenediylidene derivatives, which already present a preformed cavity and for which isomerisation has not been observed.

3.2 Anthracenediylidene Cyclophanes.

3.2.1 First Bridged Extended Tetrathiafulvalene Derivatives.

The first extended tetrathiafulvalene derivatives incorporated in cyclophane structures (**68a,b** and **71**) were reported in 1995 by Lorcy *et al.*[9], synthesised from the bis(2-piperidino-4-alkylthio-1,3-dithiolium) salts **67** (*Scheme 3.5*).
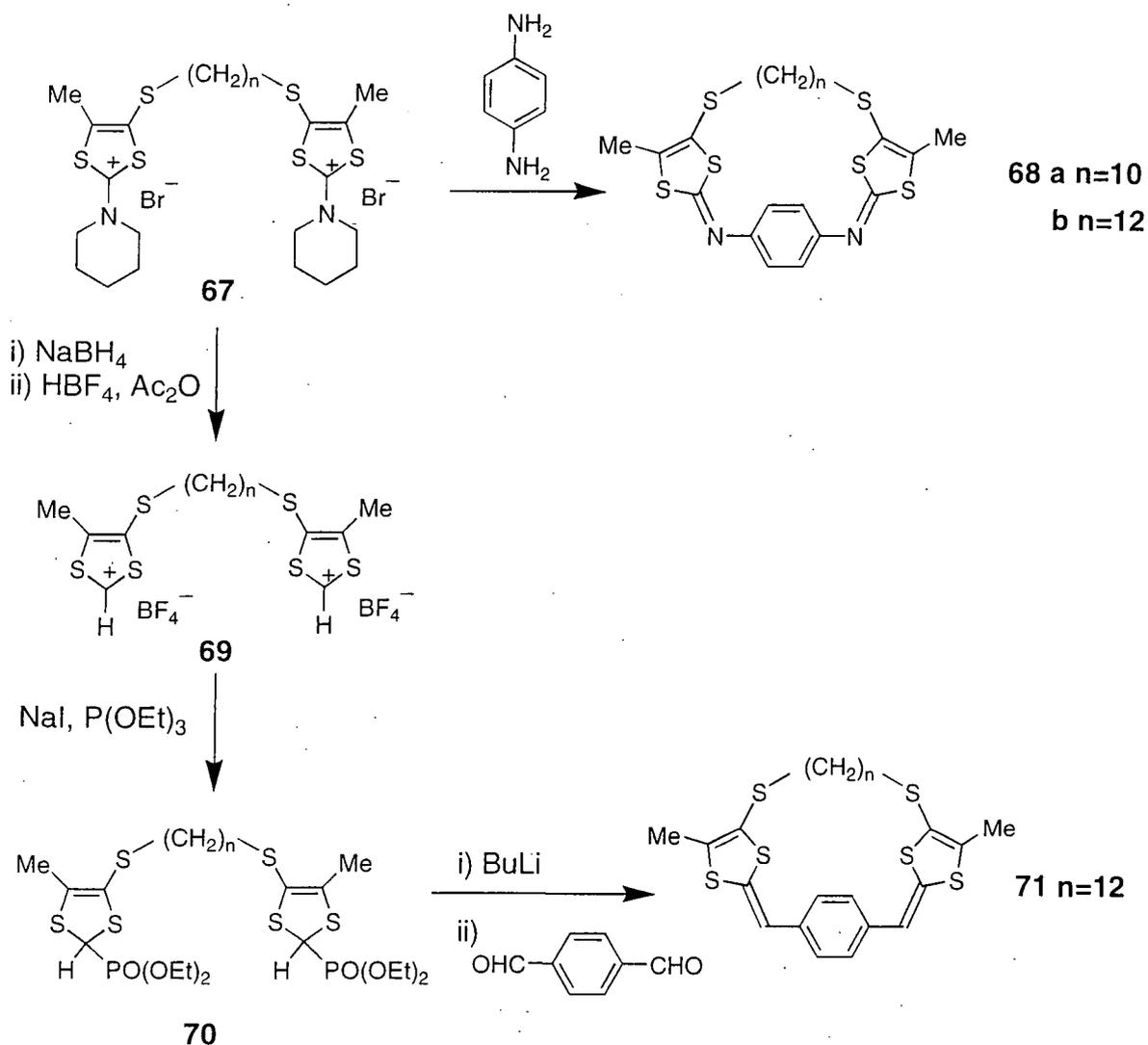
Scheme 3.5 Synthesis of extended tetrathiafulvalenophanes **68a,b** and **71**.

Contrary to the case of TTF cyclophanes for which a long bridging chain allows the formation of trans cyclophanes, the increased spatial extension imposed the cis conformation in compounds **68a,b** and **71**. However, their electrochemical properties are similar to their non-bridged analogues as expected for such long chains.

Recently, Bryce *et al.* investigated the reactivity of shorter chain analogues of compound **70** (**71a,b**) on anthraquinone, to synthesise by a 2-fold Horner-Wadsworth Emmons olefination reaction, the first bridged anthracenediylidene derivatives (**72a,b**)[10] (*Scheme 3.6*).

i) LDA (2.2 eq)

ii) Anthraquinone

71 a n=6
b n=5

72 a n=6
b n=5

Scheme 3.6 Synthesis of anthracenediylidene cyclophanes **72a,b**.

Both compounds **72a** and **72b** gave single crystals suitable for X-ray analysis, which confirmed their cis configurations (*Figure 3.4*).

(a)   (b)

Figure 3.4 Crystal structures of anthracenediylidene cyclophanes **72a** (a) and **72b** (b)

The bridge aggravates the U-bend of the anthracenediylidene system reducing the size of the internal cavity. The dihedral angle between the two dithiole rings is reduced from 77° (non-bridged analogue[11]) to 54° and 46° for the two polymorphic forms obtained for **72a**, and to 35° for **72b**.

The solution electrochemistry of compounds **72a,b** was studied by cyclic voltammetry and differential pulse voltammetry. Both compounds display in acetonitrile an irreversible two-electron oxidation wave (E_1^{ox} = 0.69 V) followed by a second oxidation wave (E_2^{ox} = 1.0 V), which has been attributed to new electrochemical species formed by the decomposition of the oxidised forms of **72a,b**.

We decided, therefore, to investigate a more versatile approach to form anthracenediylidene cyclophanes, with the aim of developing a method, which would allow the incorporation of different bridging spacers. Based on the existence of the saddle shaped conformation of anthracenediylidene derivatives, favourable for intramolecular bridging, we decided to synthesise the dimethylanthracene-TTF derivative **74** and develop its chemistry to build new cyclophane derivatives (*Scheme 3.7*). The overall aim was to study the effect of various spacers on the electrochemical and structural properties of the cyclophanes, perhaps even to stabilise the cation radical species of the anthracenediylidene system.

74

Scheme 3.7 New synthetic strategy towards anthracenediylidene cyclophanes.

3.2.2 New Bridged Anthracenediylidene Derivatives.

3.2.2.1 Synthetic Route.

Compound **74** was synthesised via a 2-fold Horner-Wadsworth Emmons olefination reaction of anthraquinone with the anion of 4-methyl-1,3-dithiole-2-phosphonate **73** prepared beforehand following the literature procedure[12] (*Scheme 3.8*).
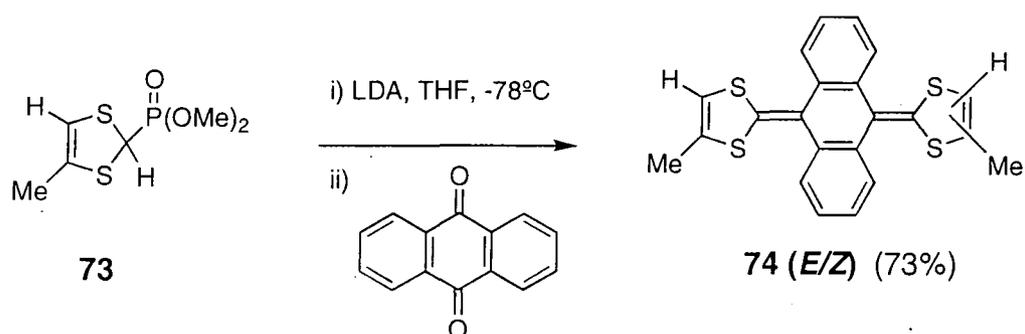
Scheme 3.8 Synthesis of a 50:50 mixture of *E/Z* isomers of **74**.

Compound **74** was obtained in 73% yield as a mixture of inseparable *E/Z* isomers. Deprotonation of **74** using lithium diisopropylamide (LDA) and trapping of the resulting dianion with methylchloroformate afforded diester derivative **(E/Z) 75a** in 61% yield after separation by chromatography from unchanged **74** and monoester derivative **(E/Z) 75b**. Diester **75a** was reduced with lithium aluminium hydride to give the dialcohol derivative **(E/Z) 76** in 82% yield (*Scheme 3.9*).
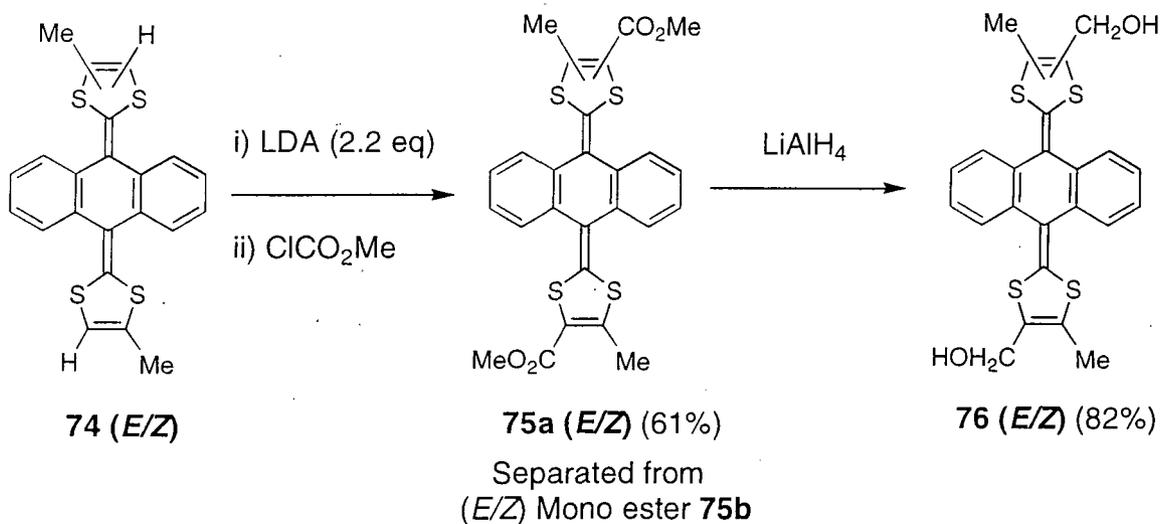
Scheme 3.9 Synthesis of (*E/Z*) dihydroxymethyl derivative **76**.

The dihydroxymethyl derivative **(*E/Z*) 76** was used as the precursor for synthesising new cyclophane derivatives, by diester forming macrocyclisation. We studied the dicarbonyl chloride derivatives **77a-f** to provide a variety of spacer units in the bridging group. Reactions were performed in high dilution conditions in order to favour cyclisation to the detriment of polymerisation, using triethylamine as catalytic base. Thus, cyclophanes **78a** (11% yield), **78b** (8% yield), 78c (14% yield) and **78d** (15% yield) were obtained arising from bridging of the Z isomer of **76** (*Scheme 3.10*), separated by chromatography from intractable material, presumably of oligomeric or polymeric nature.

Me **CH$_2$OH**

77a-d

Et$_3$N

76 (E/Z) (82%)

78 a-d

a

b

c ―Fe―

d

COCl
―COCl

77e

ClOC ― COCl

77f
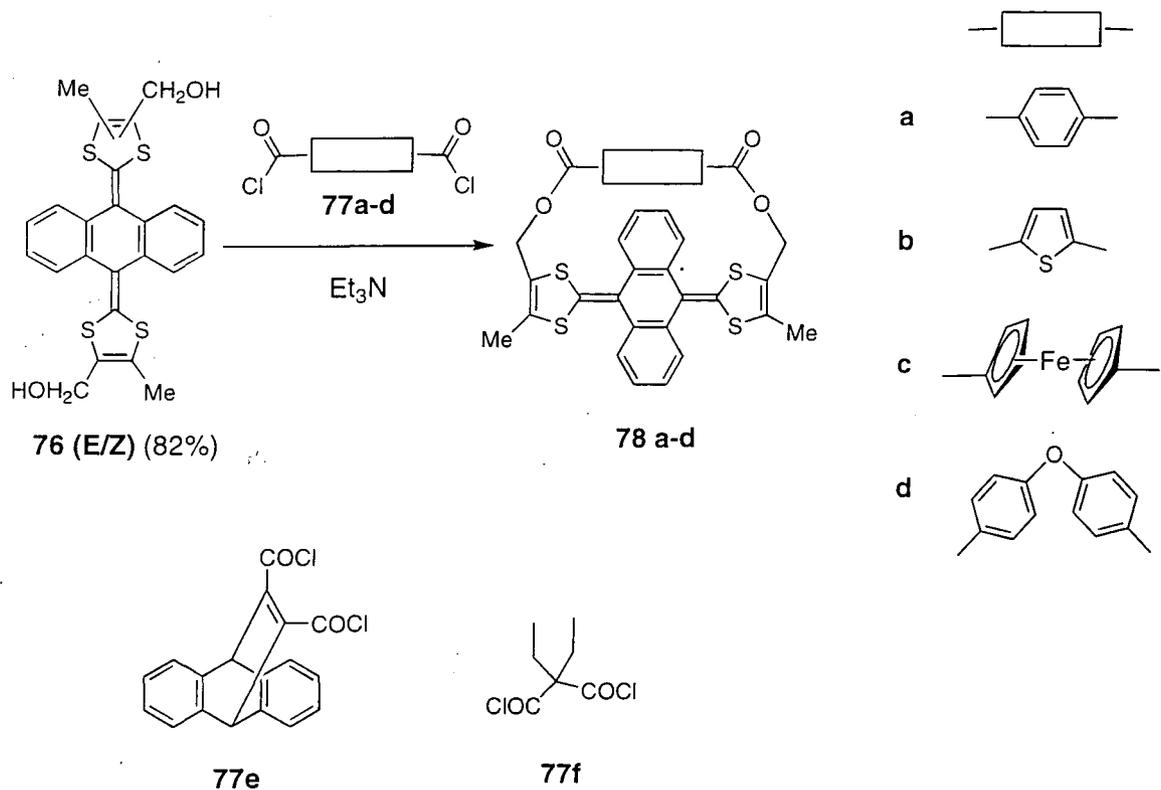
Scheme 3.10 Synthesis of anthracenediylidene cyclophane **78a-d**.

No cyclophane was obtained from the reactions involving **77e** and **77f**, due probably to steric encumbrance and too short distances between the acid chloride functions (*Table 3.1*) compared with the other diacid chlorides used.

	77a	77b	77c	77d	77e	77f		(Z) 76	(E) 76
d_1 (Å)	5.76	5.36	5.91	10.09	3.13	2.56	d_2 (Å)	10.57	10.99
Yield (%)	11	8	14	15	No	No			
(Configuration)	(Z)	(Z)	(Z)	(Z)	reaction	reaction			

Table 3.1 Compared distances (d_1) between carbon atoms of the carbonyl functions of the diacid chlorides **77a-f** and distances (d_2) between the oxygen atoms of the hydroxyl functions of (*Z*) **76** and (*E*) **76**. All distances have been obtained from modelling studies using hyperchem (*See Appendix Two*).

All the cyclophanes **78a-d** were recrystallised from dichloromethane/hexanes forming single crystals suitable for X-ray analysis, which confirmed their cis configuration.

The small difference of the distances between the oxygen atoms of the hydroxyl functions of **(Z) 76** (10.57 Å) and **(E) 76** (10.99 Å) does not explain the puzzling unique formation of the cis configuration of the cyclophanes. On no occasion was the corresponding trans-bridged cyclophane observed.

Initial evidence to support the cyclophane structures **78a-d** came from ^{1}H NMR studies. In particular, the large difference in chemical shift between the two diastereotopic protons H_a and H_b was indicative of the conformational rigidity of their structures *(Table 3.2)*.

	78a	78b	78c	78d	
$\delta\ H_a$ (ppm)	5.70	5.12	4.87	5.37	78 a-d
$\delta\ H_b$ (ppm)	4.43	4.61	4.71	4.65	

Table 3.2 Chemical shift of the diastereotopic protons H_a and H_b. ^{1}H NMR recorded in CDCl$_3$.

A NOESY spectrum (long distance coupling) of the cyclophanes was recorded, identified H_a as being closer to the methyl group *(Figure 3.5)*.
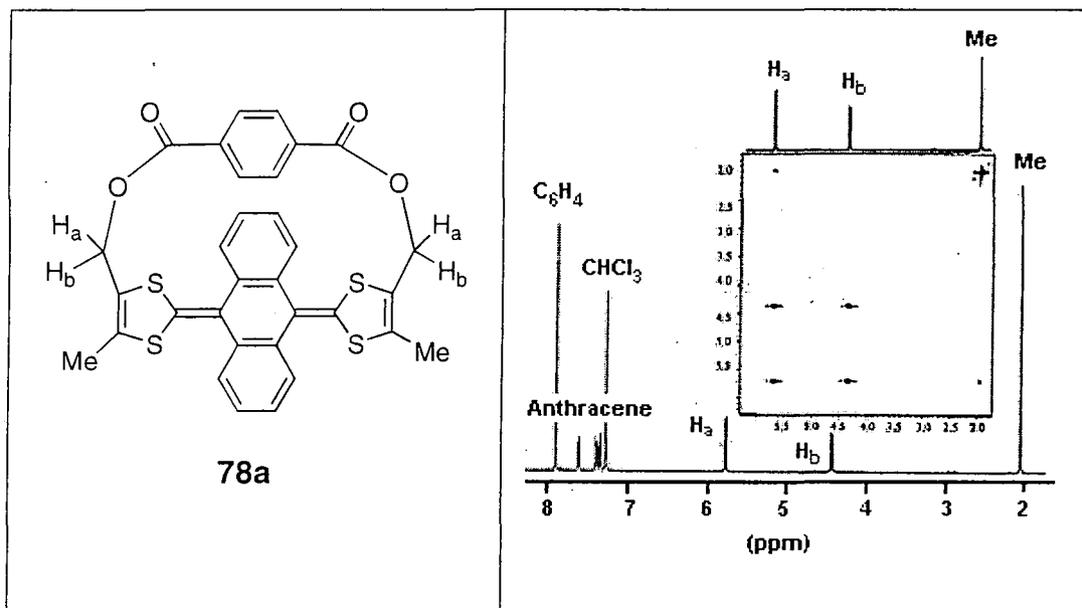
Figure 3.5 NOESY spectrum of cyclophane **78a** recorded in CDCl₃.

3.2.2.2 Molecular Structures of New Cyclophanes.

All cyclophanes **78a-d** have been recrystallised forming single crystals suitable for X-ray analysis. Simultaneously, molecular modelling studies of the cyclophanes have been performed for comparison with the crystal structures (*See Appendix Two for details of these calculations*).

The asymmetric unit of **78a** comprises two molecules of slightly different conformations, forming dimers wherein a methyl group of each molecule is inserted into the intramolecular cavity of another (*Figure 3.6*). In both molecules, the bridging benzene ring suffers a boat like distortion (distortion of the plane formed by the ring of 3°), which clearly indicates the steric strain of these structures (*Figure 3.7*).
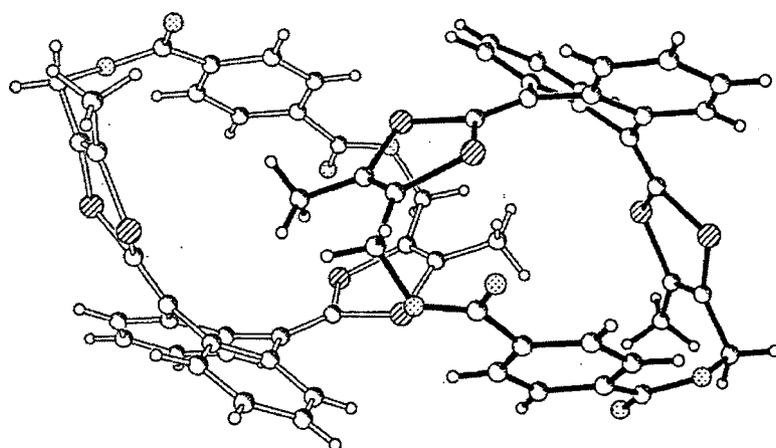
Figure 3.6 Crystal structure of dimers of **78a**.

(a)   (b)
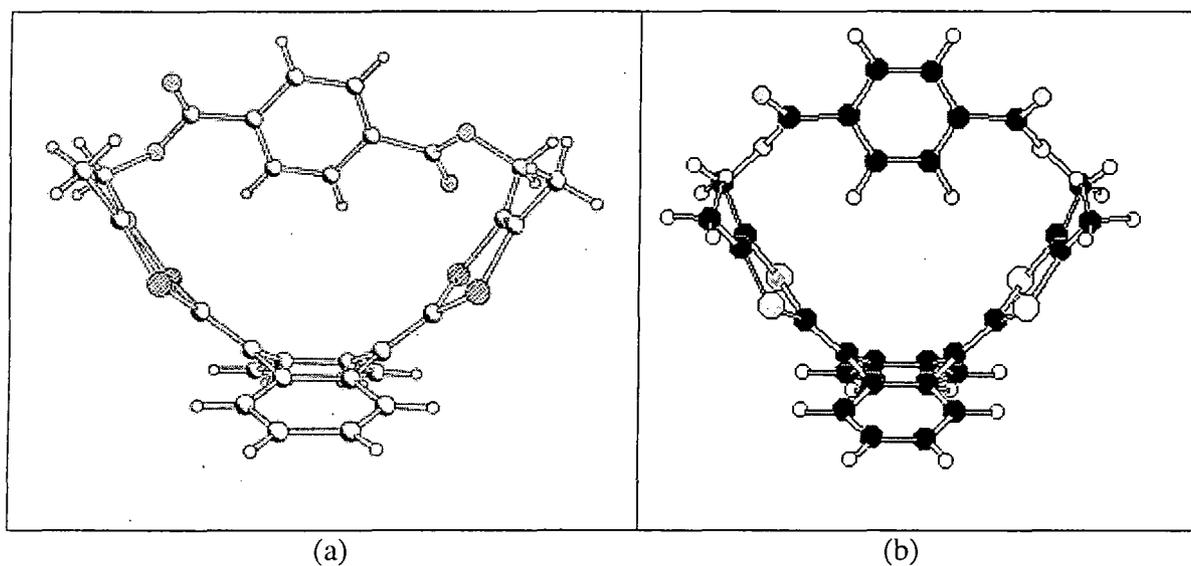
Figure 3.7 Crystal structure (a) and molecular structure obtained by modelling studies (b) of **78a**.

Cyclophane **78b** crystallises as a 1:1 solvate with CH_2Cl_2; the solvent molecule is disordered equally between the two positions. The bridging thiophene ring is planar, the carboxyl groups are inclined to its plane by 6° and 8°. The oxygen atoms of the carbonyl functions adopt a syn orientation with respect to each other and to the sulfur atom of the thiophene ring, resulting in intramolecular noncovalent distances of ca. 2.7 Å (*Figure 3.8*).

(a)   (b)
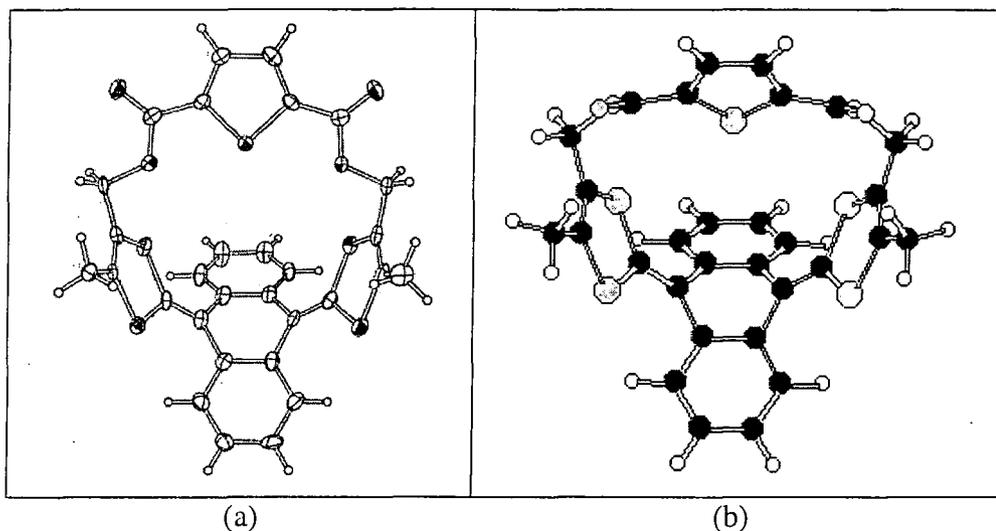
Figure 3.8 Crystal structure (a) and molecular structure obtained by modelling studies (b) of **78b**.

The asymmetric unit of **78c** comprises two molecules, one showing no disorder, while in the other one, the entire ferrocenyl moiety is disordered between two conformations, related by turning the ferrocenyl moiety upside-down. Thus the two conformations are roughly mirror images of each other and either can be identified with the molecule showing no disorder. In all cases, the carboxyl groups are almost coplanar with the cyclopentadienyl rings (*Figure 3.9*).

(a)   (b)
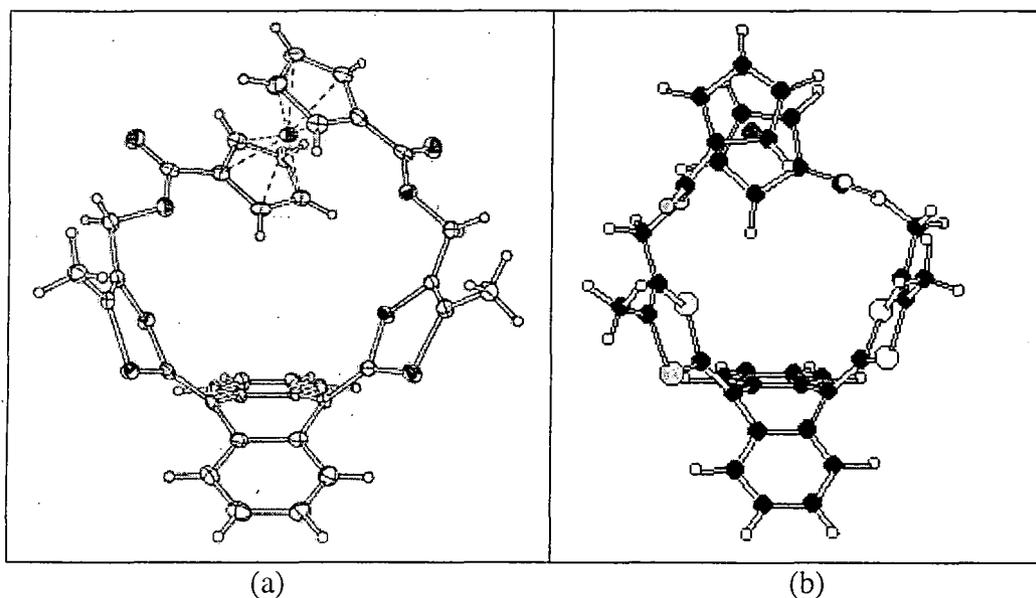
Figure 3.9 Crystal structure (a) and molecular structure obtained by modelling studies (b) of **78c**.

69

Compound **78d** crystallises as a 1:3 solvate with CH_2Cl_2; two molecules of solvent lie inside the molecular cavity of **78d** and are intensely disordered, the third one is situated in the intermolecular space and is ordered. The two bridging benzene rings form a dihedral angle of 73°, while the carboxyl groups at each ring deviate slightly (by 8° and 5°) from the ring plane (Figure 3.10).

| (a) | (b) |
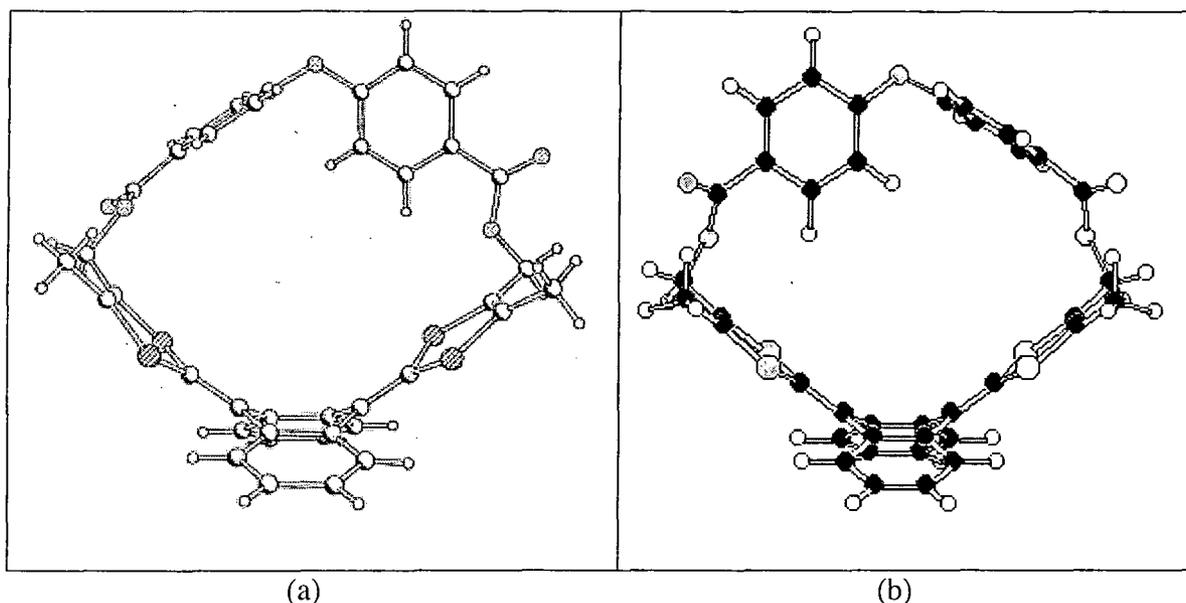
Figure 3.10 Crystal structure (a) and molecular structure obtained by modelling studies (b) of **78d**.

The molecular conformations of **78a-d** are similar to all previous anthracenediylidene derivatives studied. The anthracene moiety is folded along C(9)···C(10) vector by an angle φ (*Table 3.3*); the bis(dithiolene)quinone system is U-shaped through folding of both dithiole rings by the angles δ_1 and δ_2 along S(1)···S(2) and S(3)···S(4) vectors respectively; giving to the structure its saddle shaped conformation. A measure of the overall bending is given by the dihedral angle θ between the S(1)C(16)C(17)S(2) and S(3)C(21)C(22)S(4) planes, which shows a direct linear correlation with the length of the bridge, as defined by the intramolecular distances O(1)···O(2) (d_1) and C(18)···C(23) (d_2).

The bridges in all the compounds are flexible, so the actual molecular conformation is a compromise between steric demands of the bridge and the saddle moiety, strongly influenced by the crystal packing. Comparing the data obtained from the crystal structures with those obtained by molecular modelling, the influence of intermolecular interactions in the solid state can be seen by the slightly different conformations. Calculations have been realised in vacuum, whilst in the solid state the presence of solvent molecules (**78b** and **78d**) or interactions between molecules forming dimers (**78a**) can occur affecting the shape of the overall structure. However, molecular modelling appears to be an useful tool for visualising the molecular conformation, especially in the cases when crystals have not been obtained ((*E*) **76**, **76**$^{2+}$, **78a**$^{2+}$, **78b**$^{2+}$). The flexibility of the structures is manifest in the crystals by the presence of different molecules inside the asymmetric unit (**78a** and **78c**) which differ by their bending angles (φ and θ). Nonbridged anthracenediylidene derivatives display a θ of 73-101°, hence only the bridges with d_2 smaller than 9.5 Å can be said to increase the U-bend, which is not the case for the longest bridge **78d**. It is noteworthy that the overall folding represented by the angle φ is not affected systematically by the length of the bridges. The dithiole ring folding (δ_1 and δ_2) generally increases with the shortening of the bridge, but the correlation is poor, as other degrees of conformational freedom also contribute to the accumulated U-bend.

Crystallisations under iodine vapours of all the bridged derivatives (**78a-d**) have been performed but only in the case of **78d** were crystals of **78d**$^{2+}$**(I_3^-)$_2$·(CH$_2$Cl$_2$)$_{2.25}$** suitable for X-ray analysis obtained (*Figure 3.11*). The asymmetric unit of the triiodide salt of **78d** comprises 2.25 molecules of dichloromethane. One independent solvent molecule fits into the intramolecular cavity and is ordered, one occupies an intermolecular cavity and

displays chaotic disorder (approximated by three orientations), and another is disordered around an inversion centre and has a nonstoichiometric occupancy (estimated as 0.25 per asymmetric unit). The **78d^{2+}** dication shows a drastic change of conformation and bond lengths compared to the neutral molecule, similar to those observed for nonbridged systems (*Cf. Chapter One*). Both dithiolium rings are planar with the bonding pattern indicative of one positive charge on each, while the anthracene moiety is essentially aromatic. However, the bridge imposes significant distortions. Nonbridged dications have rigorously planar anthracene moieties and the dithiolium rings are coplanar to each other and nearly perpendicular to the latter. In **78d^{2+}**, the anthracene moiety displays a small folding of 6°. Both dithiolium rings deviate by ca. 20° from the normality to the anthracene moiety and form a dihedral angle of 163° between them. The conformation of the bridge is basically the same as in the neutral **78d**, the benzene rings forming a dihedral angle of 74°; its overall length increases by 6 or 7%.

(a)   (b)
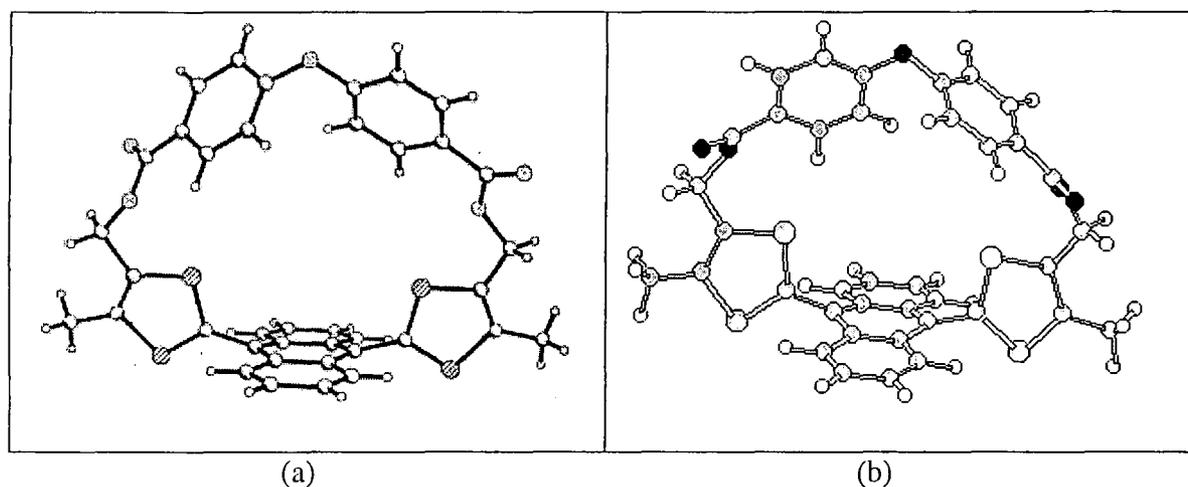
Figure 3.11 Crystal structure (a) and molecular structure obtained by modelling studies (b) of **78d^{2+}**.

In order to visualise the effect of shorter bridges on the molecular structures of the dicationic state, molecular modelling has been performed on **78a^{2+}** and **78b^{2+}** (*Figure 3.12*). Their molecular conformations are similar to their neutral analogues. Contrary to the dication of **78d**, no dramatic change of conformation between the neutral and oxidised states is observed. For both molecules, the saddle shape is still present although less pronounced. The two dithiolium rings are both twisted by 70.8° for **78a^{2+}** and 68.6 ° for **78b^{2+}** (compared to 90° for nonbridged derivatives), the bridge preventing them twisting perpendicularly to the anthracene moiety, and they form a dihedral angle (θ) between each other of 47.6° and 57.7° for the two compounds respectively, which for **78b** is very close to its neutral form (58.8°). For both compounds, the folding of the anthracene moiety is less pronounced but still present (φ equal to 25.5° and 27° for **78a^{2+}** and **78b^{2+}** respectively). The short bridges seem to prevent the system undergoing a change of conformation keeping the dication structures close to their neutral forms (*Table 3.3*).

(a)   (b)
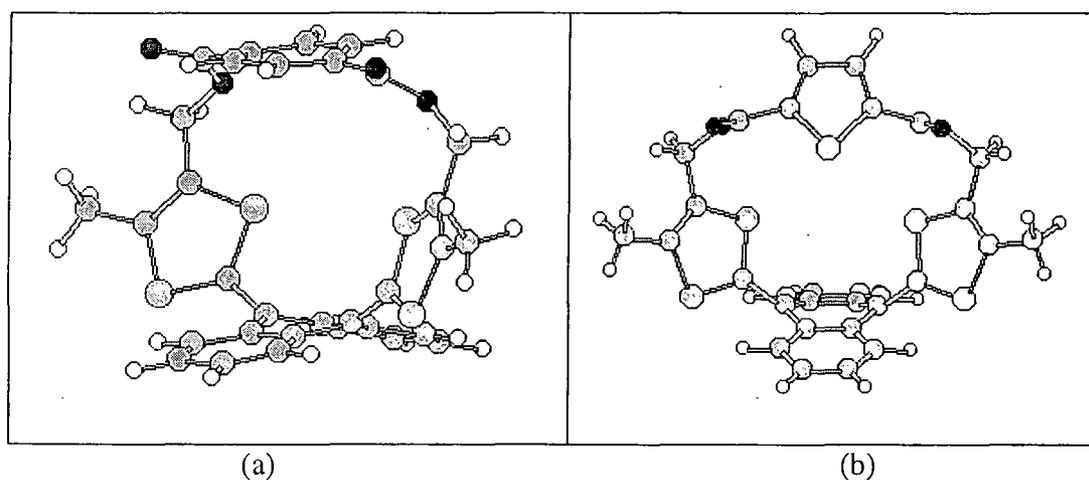
Figure 3.12 Molecular structures obtained by modelling studies of **78a^{2+}** and **78b^{2+}**.

	Crystal Structure						Molecular Modelling					
	$\varphi(°)$	$\delta_1(°)$	$\delta_2(°)$	$\theta(°)$	$d_1(Å)$	$d_2(Å)$	$\varphi(°)$	$\delta_1(°)$	$\delta_2(°)$	$\theta(°)$	$d_1(Å)$	$d_2(Å)$
(E)76	—	—	—	—	—	—	40.8	3.4	3.4	100.4	10.51	10.89
78a	39.2 (35.3)	15.6 (16.0)	15.0 (16.1)	71.4 (67.0)	7.13 (7.11)	9.34 (9.32)	42.9	13.4	13.4	68.3	7.04	9.08
78b	39.4	23.8	19.4	46.7	5.41	8.01	43.8	16	16.1	58.8	6.26	8.48
78c	33.8 (36.2)	23.0 (23.9)	12.3 (17.4)	58.9 (44.3)	6.03 (5.67)	8.40 (7.91)	46.6	18.7	18.7	49.9	5.87	7.72
78d	37.5	11.3	3.1	95.0	8.98	10.60	40.2	4.7	4.3	100.3	9.62	10.93
(E)76^{2+}	—	—	—	—	—	—	0	0	0	180	13.15	12.58
78a^{2+}	—	—	—	—	—	—	25.5	5.3	5.3	47.6	6.68	8.94
78b^{2+}	—	—	—	—	—	—	27.0	6.7	6.7	57.7	8.71	6.42
78d^{2+}	6	0	0	163	9.55	11.35	14.3	1.2	1.5	170.1	9.74	11.27

φ is the folding along the C(9)···C(10) vector.
δ_1 is the folding along S(1)···S(2) vector. δ_2 is the folding along S(3)···S(4) vector.
θ is the dihedral angle between the S(1)C(16)C(17)S(2) and S(3)C(21)C(22)S(4) planes.
d_1 is the intramolecular O(1)···O(2) distance. d_2 is the intramolecular C(18)···C(23) distance.
NB: For 78a and 78c two different molecules are present in their crystal structures.
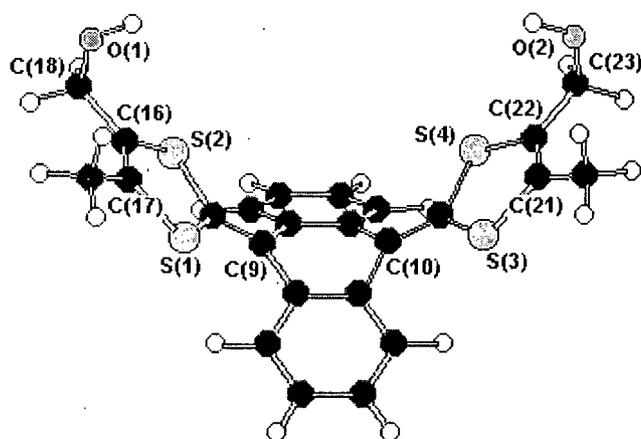
Molecular Modelling of (E) 76.
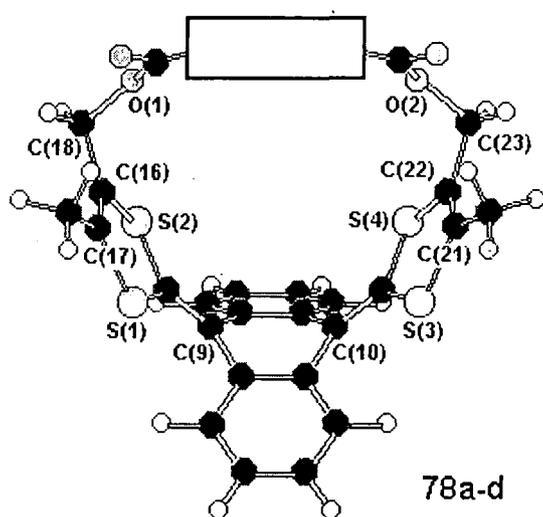
78a-d
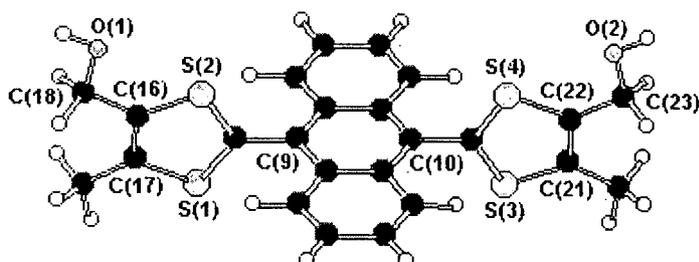
Molecular Modelling of (E) 76^{2+}

Table 3.3 Dihedral angles and intramolecular distances in the crystal structure and calculated from modelling studies (*See Appendix Two*) for compounds 76, 78a-d, 76^{2+}, 78a^{2+}, 78b^{2+} and 78d^{2+}.

3.2.2.2 Electrochemical Studies.

In order to study the electrochemical behaviour of the cyclophanes, cyclic voltammetry studies have been performed on all the bridged systems (**78a-d**) and compared with the redox properties of the model non-bridged compound **52** (see also Chapter Two), and the precursors of the bridged systems (**74, 75a-b** and **76**). The results obtained reveal some very interesting trends (Table 3.4).
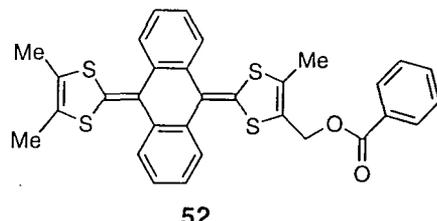
	E_{pa}^{Ox} / V	E_{pc}^{Ox} / V	ΔE / V	
52	0.41 (2e)	0.12	0.29	
(E/Z) 74	0.36 (2e)	0.13	0.23	
(E/Z) 75a	0.61 (2e)	0.26	0.35	
(E/Z) 75b	0.53 (2e)	0.22	0.31	
(E/Z) 76	0.36 (2e)	0.08	0.28	
78a	0.70 (2e)	0.63	0.07	
78b	0.70 (2e)	0.66	0.04	
78c	0.72 (2e) / 1.08 (1e)	0.96 / 0.60	0.12 / 0.12	
78d	0.47 (2e)	0.28	0.19	
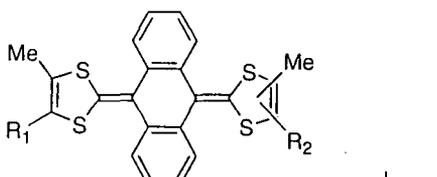
$R_1, R_2 = H$ **(E/Z) 74**
$R_1, R_2 = CO_2Me$ **(E/Z) 75a**
$R_1 = H, R_2 = CO_2Me$ **(E/Z) 75b**
$R_1, R_2 = CH_2OH$ **(E/Z) 76**

Table 3.4 Cyclic voltammetric data. $\Delta E = E_{pa}^{Ox} - E_{pc}^{Ox}$

E_{pa}^{Ox} is the oxidation peak potential on the first anodic scan;

E_{pc}^{Ox} is the coupled reduction peak potential on the cathodic scan.

(Experimental conditions: Acetonitrile, Pt electrode, versus Ag/AgCl, electrolyte $Bu_4N^+PF_6^-$ (0.1M), 20°C, scan rate 100 mV s^{-1}.)

Comparing the non-bridged systems **74-76**, a notable feature, as we discussed in *Chapter Two*, is that the electron withdrawing ester substituents result in a significant positive shift of the quasi-reversible two-electron redox wave, which is consistent with mesomeric conjugation (170 mV for **75b** bearing one ester function and 250 mV for **75a** bearing two ester functions compare to the unsubstituted precursor **74**).

Comparing the bridged systems **78a-d** with the model compound **52**, the oxidation potential (E^{ox}_{pa}) is raised significantly (by ca. 300 mV) for **78a-c** but only slightly (by 60 mV) for **78d**. This is consistent with the shorter bridges of **78a-c** hindering the marked conformational change, which accompanies oxidation to the dication. As we observed previously by molecular modelling for **78a^{2+}** and **78b^{2+}**, their molecular structures are expected to be close to the structure of their neutral forms, the saddle shaped conformation being still present. Another striking feature of these data is a sequential reduction in the value of ΔE, which corresponds to an increased reversibility of the oxidation process as the bridge is progressively shortened. ΔE is reduced to only 70 and 40 mV for compounds **78a** and **78b**, respectively, compared to the typical values of quasi-reversibility in the range 230-350 mV for non-bridged derivatives (*Table 3.4*). This reflects the reduced stability of the twisted dication structure within the steric constraints of the smaller cyclophanes. Moreover, the stability of the dicationic species for non-bridged compounds is increased by the gain in aromaticity of the planar anthracene moiety, which is not the case for the smaller cyclophanes; as we observed by molecular modelling of **78a** and **78b**, the anthracene moiety being still folded. This feature is, therefore, less pronounced for **78d**, which displays redox behaviour close to the nonbridged model **52**, consistent with the molecular structure of the dicationic species **78d^{2+}** which is closer to the dicationic structure of nonbridged derivatives (*Figure 3.13*).

76
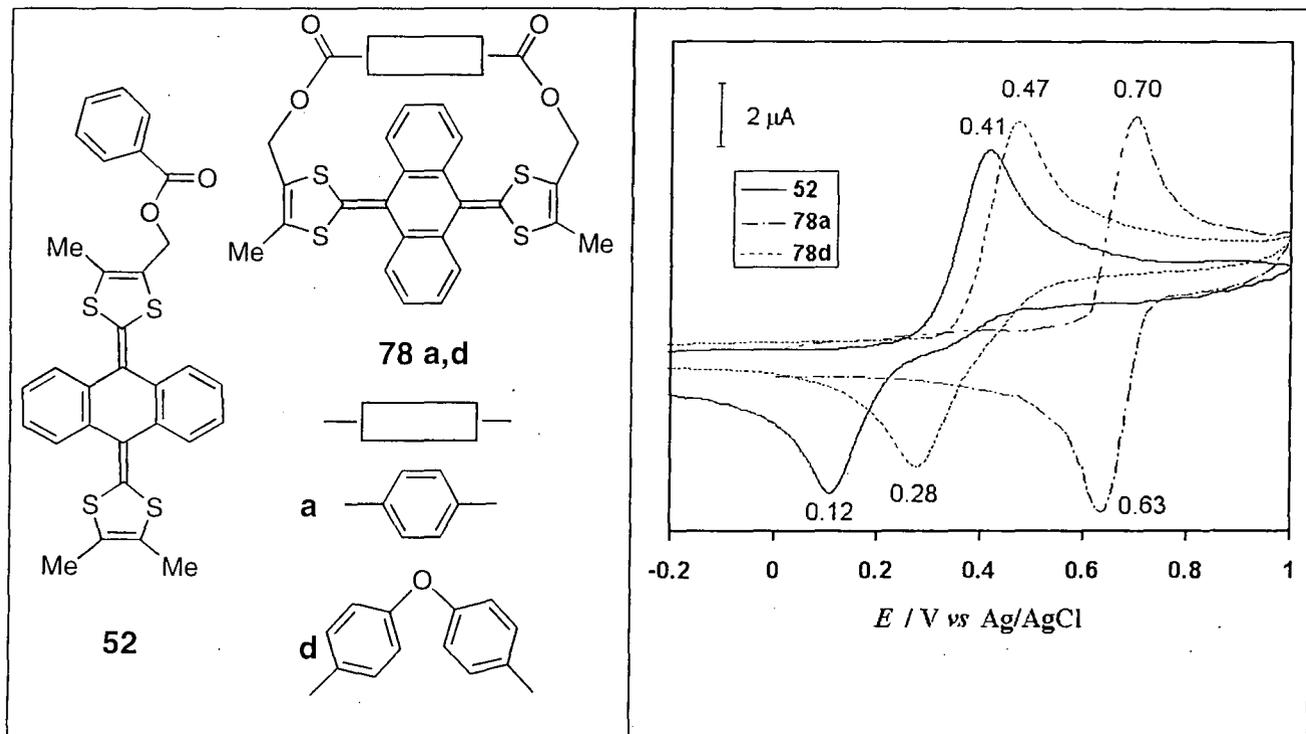
Figure 3.13 Cyclic voltammograms of **52, 78a, 78d** (under the conditions stated in *Table 3.4*)

The cyclic voltammetry of the ferrocenyl bridge **78c** reveals an additional, quasi-reversible, one-electron oxidation wave at E^{ox}_{pa} 1.08 V, arising from the ferrocene/ferrocenium redox couple, which also corresponds to the formation of the **78c^{3+}** species (*Figure 3.14*). The smaller current associated with this second wave is also consistent with the primary oxidation wave of these cyclophanes being a two electron process, which has been also confirmed by ^{1}H NMR studies of the oxidised species (*Figure 3.15*). The positive shift for the ferrocene oxidation wave in **78c,** compared to standard diester derivatives of ferrocene (**79**, $E^{1/2}$ 0.972V *vs* Ag/AgCl in CH_2Cl_2)[13] is explained by intramolecular Coulombic repulsion between the ferrocenium and the dithiolium cations, together with steric constraints of the bridge.
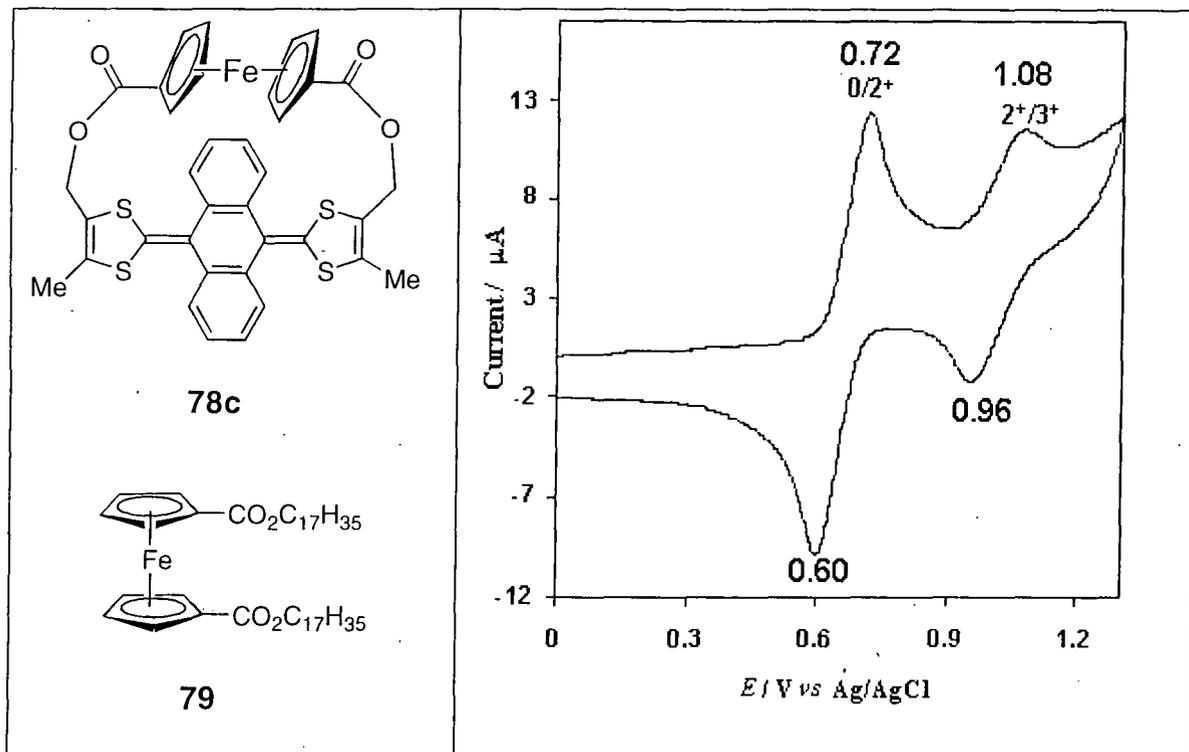
Figure 3.14 Cyclic voltammogram of **78c** (under the conditions stated in *Table 3.4*).

In order to provide additional evidence that the oxidation of all the bridged systems gave their corresponding dication species, to the exclusion of the formation of cation radical species, as was clearly suggested by the electrochemical studies, ^{1}H NMR spectra of the oxidised species have been recorded. For example, ^{1}H NMR spectra of **78a** in CD$_3$CN before and after addition of iodine (*Figure 3.15*), resulted in a clean change in the spectrum consistent with complete conversion to the dication salt **78a^{2+}(I$_3^-$)$_2$** (No broadening was observed which would imply the presence of radicals). New peaks are present at δ5.86 (4H) and 2.93 (6H, Me), replacing those at 4.70 (2H, H$_a$), 5.64 (2H, H$_b$) and 2.07 (6H, Me) obtained for **78a** in CD$_3$CN. This deshielding effect is characteristic of the positive charge on each dithiolium ring. Protons H$_a$ and H$_b$ are no longer differentiable in the spectrum of the oxidised **78a^{2+}**, consistent with a twist of the dithiole rings

occurring during oxidation which places these two protons in the similar magnetic environment, in a more symmetrical position at a distance more analogous to the methyl group, compared with the neutral form where H_a is pointing towards the inside of the cavity, nearer to the methyl group than H_b pointing outside the cavity (*Figure 3.15* and also *Figure 3.5*).

(a)   (b)
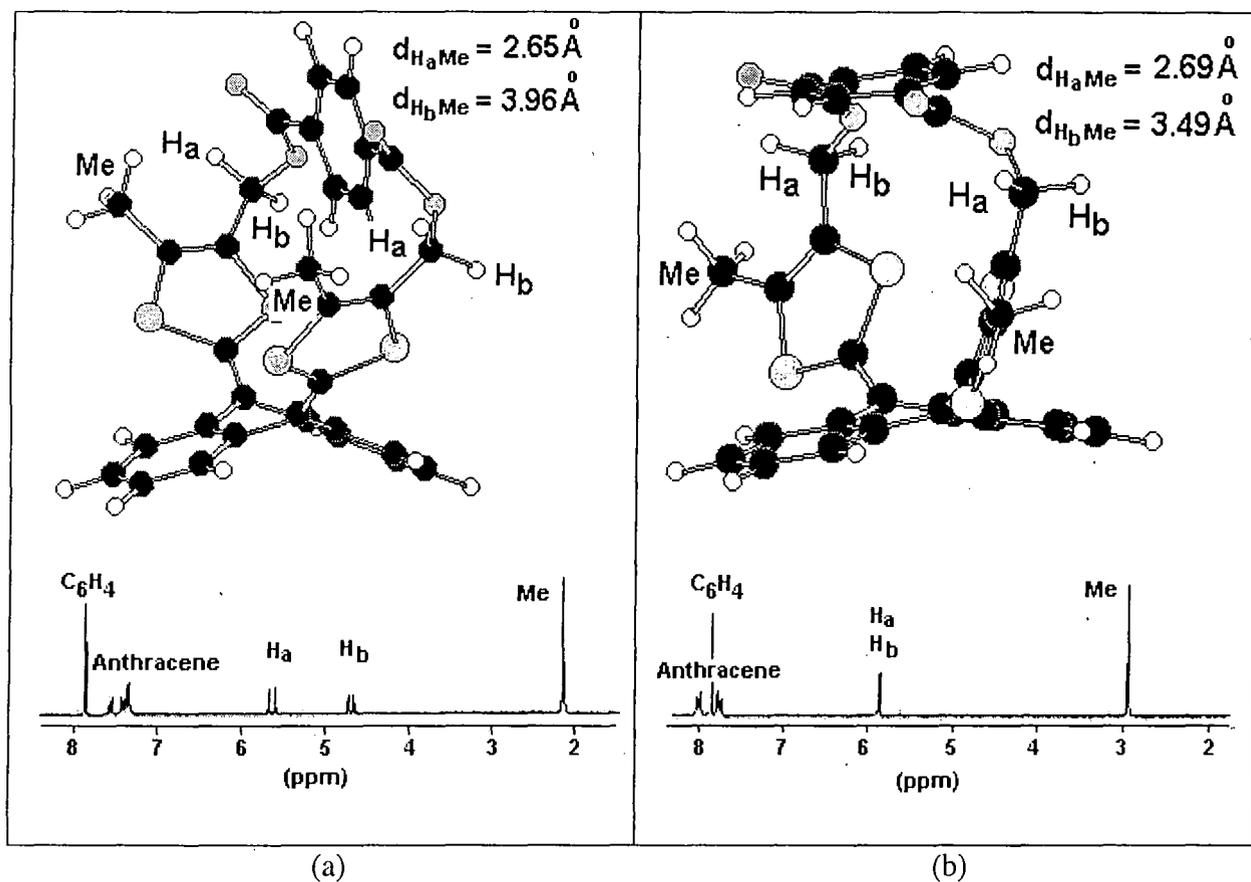
Figure 3.15 Molecular modellings and ^1H NMR spectra in d_3-acetonitrile for **78a** (a) and **78a^{2+}** (b). Residual solvent peaks (at δ 1.93 ppm for acetonitrile and at δ 2.15 ppm for water) have been removed for more clarity.

3.3 Conclusion.

Anthracenediylidene derivatives are outstanding compounds, which exhibit a saddle shaped conformation thus presenting a semi cavity. We have developed a new strategy based on the flexibility of this conformation, which has allowed the synthesis of new cyclophanes by bridging the preformed structure. Therefore, this strategy enables the use of different bridging spacers. Consequently, the size of the inner cavity can be controlled and the redox properties of the resulting cyclophanes can be finely tuned. The redox properties of the bridged systems are unique and depend on the size of the bridge used. Nevertheless, this single bridging is not sufficient to stabilise the radical cation, which has not been observed throughout this study. Even for the smallest bridged system (thienyl bridge **78b**), the structure still possess enough freedom to twist during oxidation which seems to be the key factor in the formation of the dication (theoretical studies, as we discuss in *Chapter One*, having postulated that the radical cation conformation would be very close to the neutral structure). However, this study has paved the way to the synthesis of new cyclophanes including doubly-bridged systems[†], which should exhibit remarkable redox properties and opened the door to the study of redox-controlled molecular recognition within related cyclophane cavities.

[†] During the writing of this thesis, the first doubly-bridged derivative has been synthesised in our group by C.A. Christensen and both the cation radical and dication states are observed in cyclic voltammetry experiments.

3.4 References

(1)   Staab, H. A.; Ippen, J.; Tao-pen, C.; Krieger, C.; Starker, B. *Angew. Chem., Int. Ed. Engl.* **1980**, *19*, 66-67.

(2)   Ippen, J.; Tao-pen, C.; Starker, B.; Schweitzer, D.; Staab, H. A. *Angew. Chem., Int. Ed. Engl.* **1980**, *19*, 67-68.

(3)   Souizi, A.; Robert, A.; Batail, P.; Ouahab, L. *J. Org. Chem.* **1987**, *52*, 1610-1611.

(4)   Boubekeur, K.; Lenoir, C.; Batail, P.; Carlier, R.; Tallec, A.; Le Paillard, M. P.; Lorcy, D.; Robert, A. *Angew. Chem., Int. Ed. Engl.* **1994**, *33*, 1379-1381.

(5)   Adam, M.; Enkelmann, V.; Räder, H.-J.; Röhrich, J.; Müllen, K. *Angew. Chem., Int. Ed. Engl.* **1992**, *31*, 309-310.

(6)   Takimiya, K.; Aso, Y.; Ogura, F.; Otsubo, T. *Chem. Lett.* **1995**, 735-736.

(7)   Rowland, R. S.; Taylor, R. *J. Phys. Chem.* **1996**, *100*, 7384-7391.

(8)   Otsubo, T.; Aso, Y.; Takimiya, K. *Adv. Mater.* **1996**, *8*, 203-211.

(9)   Hascoat, P.; Lorcy, D.; Robert, A.; Boubekeur, K.; Batail, P.; Carlier, R.; Tallec, A. *J. Chem. Soc. Chem. Commun.* **1995**, 1229-1230.

(10)   Finn, T.; Bryce, M. R.; Batsanov, A. S.; Howard, J. A. K. *Chem. Commun.* **1999**, 1835-1836.

(11)   Batsanov, A. S.; Bryce, M. R.; Coffin, M. A.; Green, A.; Hester, R. E.; Howard, J. A. K.; Lednev, I. K.; Martín, N.; Moore, A. J.; Moore, J. N.; Ortí, E.; Sánchez, L.; Savirón, M.; Viruela, P. M.; Viruela, R.; Ye, T.-Q. *Chem. Eur. J.* **1998**, *4*, 2580-2592.

(12)   Bryce, M. R.; Finn, T.; Moore, A.; Batsanov, A. S.; Howard, J. A. K. *Eur. J. Org. Chem.* **2000**, 51-60.

(13)   Medina, J. C.; Gay, I.; Chen, Z.; Echegoyen, L.; Gokel, G. W. *J. Am. Chem. Soc.* **1991**, *113*, 365-366.

Chapter Four

Dendritic Macromolecules:

Towards Supramolecular Architecture.

4.1 Redox-Active Dendrimers.

Dendrimers are a relatively new class of macromolecule. These materials comprise a multifunctionalised core, from which radiate repeating layers of monomers with a branch occurring at each monomer unit (*Figure 4.1*). Dendrimers attract considerable attention for their well-defined, three-dimensional frameworks in which functional groups can be placed in predetermined positions thereby imparting special properties to the molecules.
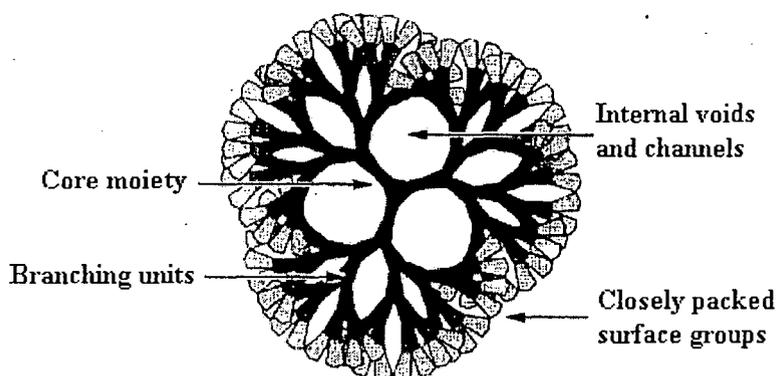
Figure 4.1. A fifth generation dendritic structure.

The interest in dendrimers has blooming over the last decade; thus, partial aspects of the synthesis and properties of dendrimers have been reviewed (*Table 4.1*).

Main author	Topic
T.A. Tomalia	Starburst dendrimers: synthesis and properties[1].
G.R. Newkome	Concepts, synthesis and perspectives[2].
M.R. Bryce	Redox-active dendrimers[3].
O.A.Matthews	Synthesis, architecture and applications[4].
M. Fisher	From design to Application[5].
Bosman, A.W.	Structure, physical properties and applications[6].
G.R. Newkome	Metellodendrimers[7].
A. Adronov	Light-harvesting dendrimers[8].
K. Inoue	Functional dendrimers, hyperbranched and star polymers[9].
S. Hecht	Dendritic encapsulation of function[10].

Table 4.1 Recent reviews on specific aspects of dendrimers.

Redox-active dendrimers comprising organomettalic groups (metallodendrimers) or redox-active molecules at the centre or on the periphery, are excellent candidates for use in practical applications such as new organic semiconductors, electron transfer mediators, new materials for energy conversion, new sensors and mimic molecules of biological redox processes.

4.1.1 Metallodendrimers.

The three dimensional structure of dendrimers can influence the microenvironment around the electroactive centre and hence studies are focused on both the dendritic wedge effect on the electroactive core and the redox behaviour of multiple electroactive sites on the higher generation dendrimer surfaces. Recently, Majoral et al.[11] studied the incorporation of ferrocene units at the core (**83-87**), within branches (**88**), and on the periphery (**89**) of phosphorous-containing dendrimers. A marked dendritic effect has been observed for this class of compounds. For **83-87** (*Scheme 4.1*), the ferrocenyl core is insulated as the generation is increased leading to almost electrochemically inactive molecules for **86** and **87** (comprising 32 and 64 CHO end groups, respectively).
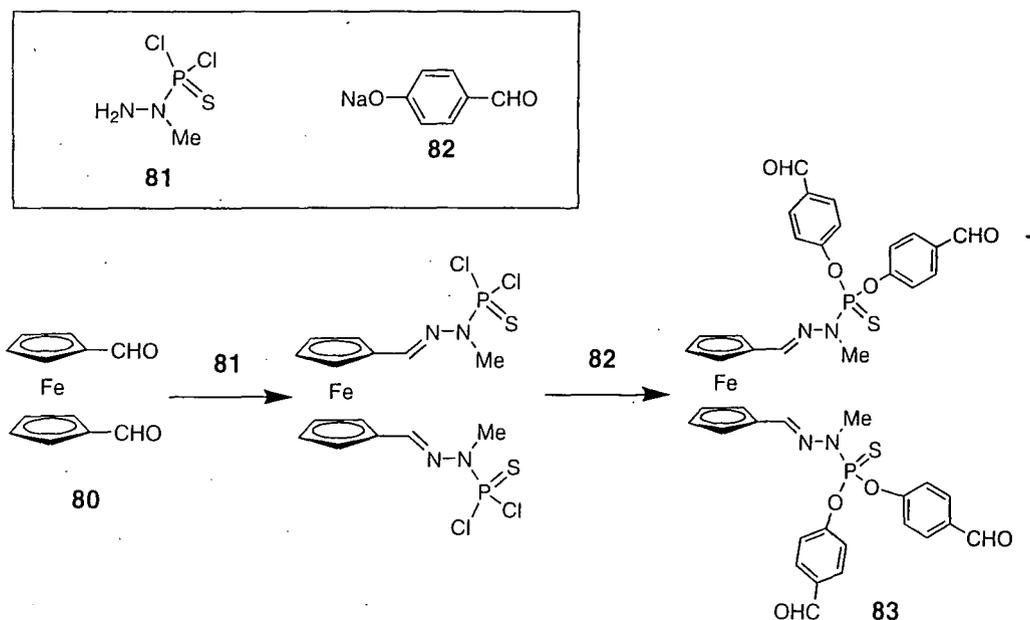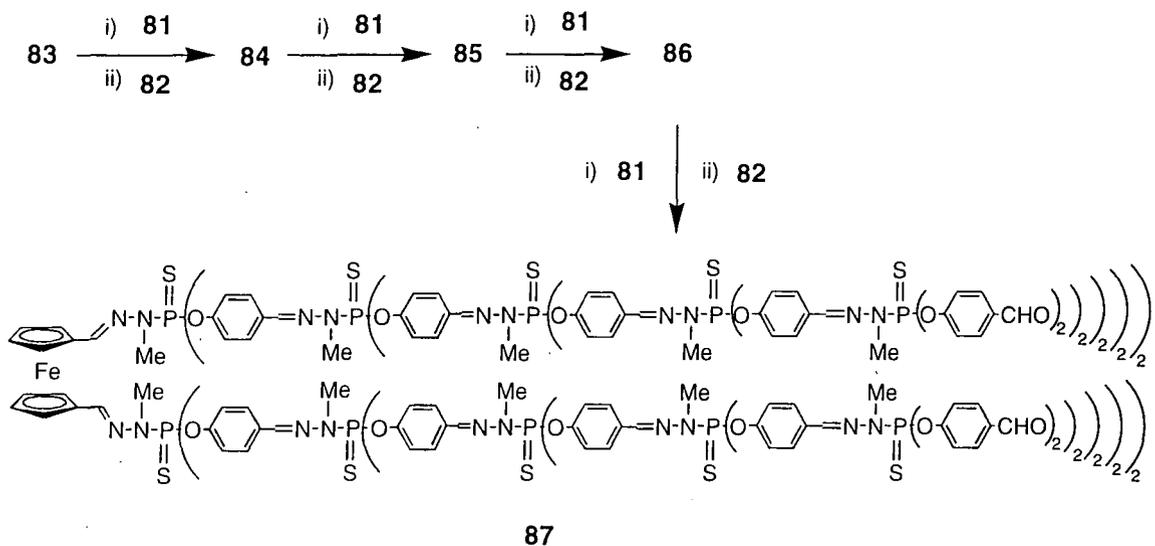
Scheme 4.1 Synthesis of phosphorous containing dendrimers **83-87** comprising a ferrocenyl core.

Dendrimer **88** having three consecutive ferrocene layers within the branches displays two sequential redox processes. Both inner layers are oxidised at the same potential, the outer layer needed a higher potential for oxidation due to the presence of the electron-withdrawing formyl groups ($E_1^{1/2} = 0.66$ V, $E_2^{1/2} = 0.80$ V *vs.* SCE in THF/acetone 2:1 v/v). This behaviour indicates that electronic effects have a greater importance than the localisation upon the oxidation process.
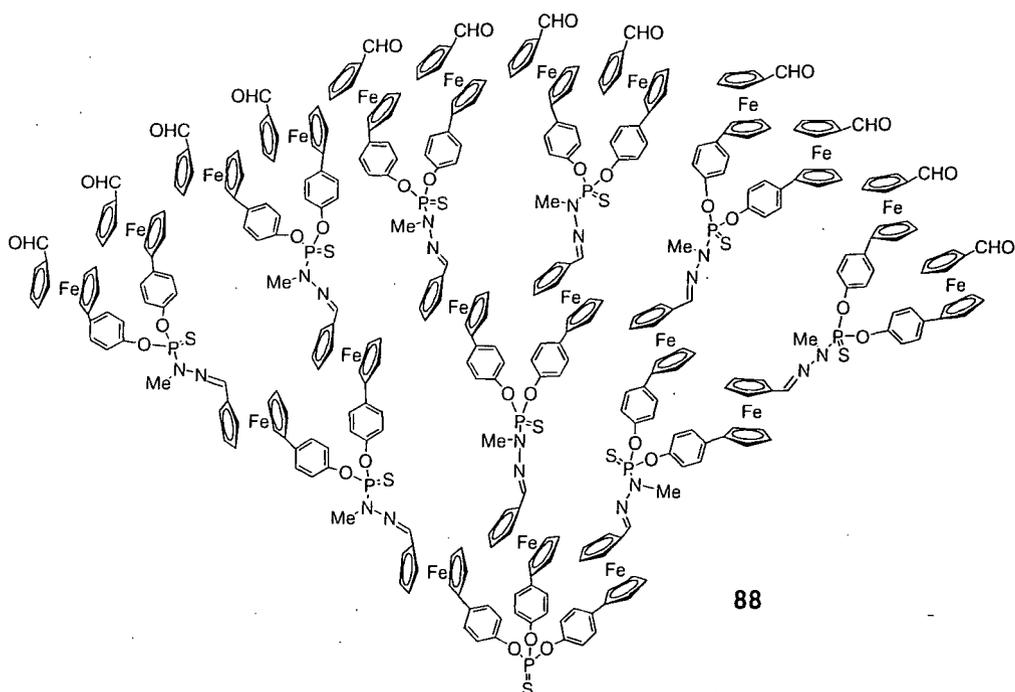
Finally, the largest dendritic ferrocenyl derivative **89** comprising theoretically 1536 ferrocenyl groups on its periphery has been studied by cyclic voltammetry and displays one oxidation wave corresponding to the oxidation of all the ferrocenyl units at the same potential (theoretical number of transferred electrons 1532, consistent for a such large molecule which can easily be adsorbed at the surface of the electrode and therefore modify the measurement of transferred electrons).

89
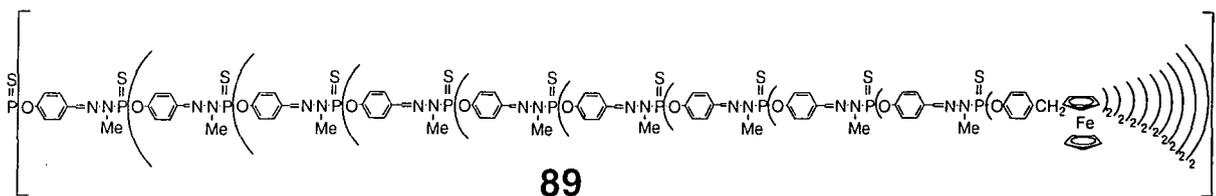
The multiferrocenium derivatives obtained from exhaustive electrolysis of **89**, which deposit onto the Pt electrode surface, formed conducting films. Cuadrado *et al.*[12] studied the immobilisation of silicon based ferrocenyl dendrimer such as compounds **90-93** on electrode surfaces and obtained successfully modified electrodes which were used as amperometric biosensors.[13]

90 n = 0

91 n = 2

92 n = 0

93 n = 2
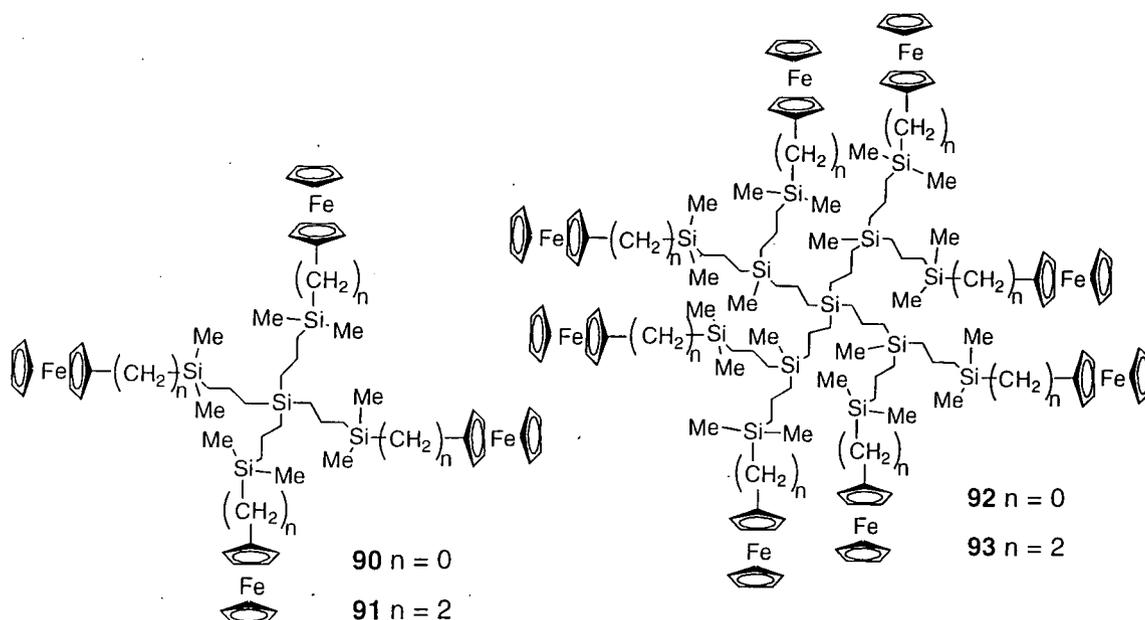
Ferrocenyl dendrimers **90-93** act in this process as electron mediating species in dendrimer/glucose-oxidase/carbon paste electrodes. Cyclic voltammograms of these carbon paste electrodes showed that the addition of glucose leads to the enhancement of the oxidation current and decrease of the cathodic peak indicative of a the enzyme-dependent catalytic reduction of the ferricinium cations (*Figure 4.2*).

(a)   (b)
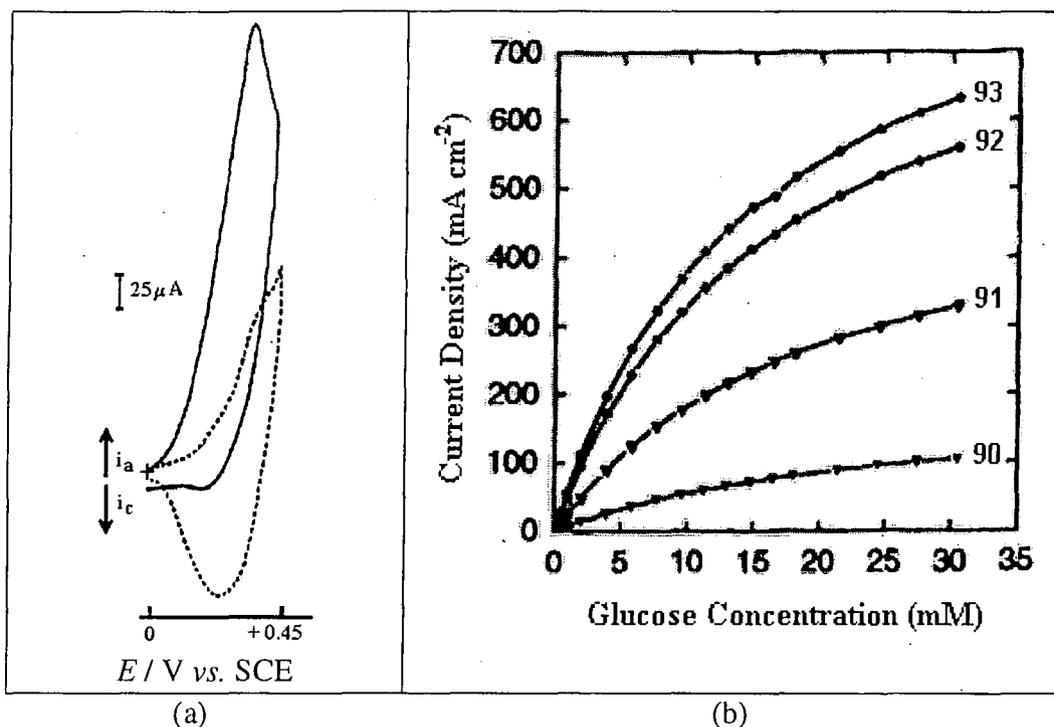
Figure 4.2 Cyclic voltammograms for dendrimer **93**/glucose oxidase/carbon paste electrode with no glucose present (----) and with 0.1 M glucose (——) (a), Variation of the steady-state current of the dendrimer/glucose oxidase/carbon paste electrodes with glucose concentration for dendrimers **90-93** (b)

For their high redox stability, ferrocenyl dendrimers can also be considered as molecular batteries, electron sponges or electron reservoirs, which might find applications in molecular-electronic devices.[14,15]

Among the more studied redox systems incorporated in dendritic structures, metalloporphyrin dendrimers such as compounds **94-96** have been designed in attempts to mimic the properties of heme proteins and chlorophylls.[16,17]

94	R =	$HN-\overset{O}{\underset{O}{\overset{|}{C}}}\overset{CO_2CH_3}{\underset{CO_2CH_3}{\overset{CO_2CH_3}{}}}$	M = Zn
95	R =	$O\frown O\frown O\frown O\text{-}CH_3$	M = Zn
96	R =	$O\frown O\frown O\frown O\text{-}CH_3$	M = FeCl
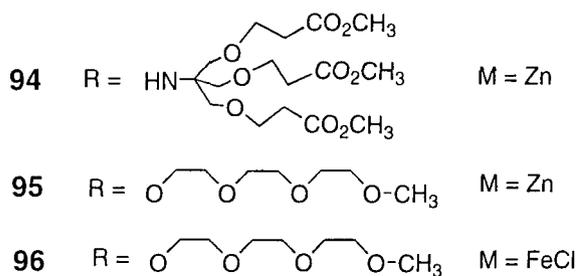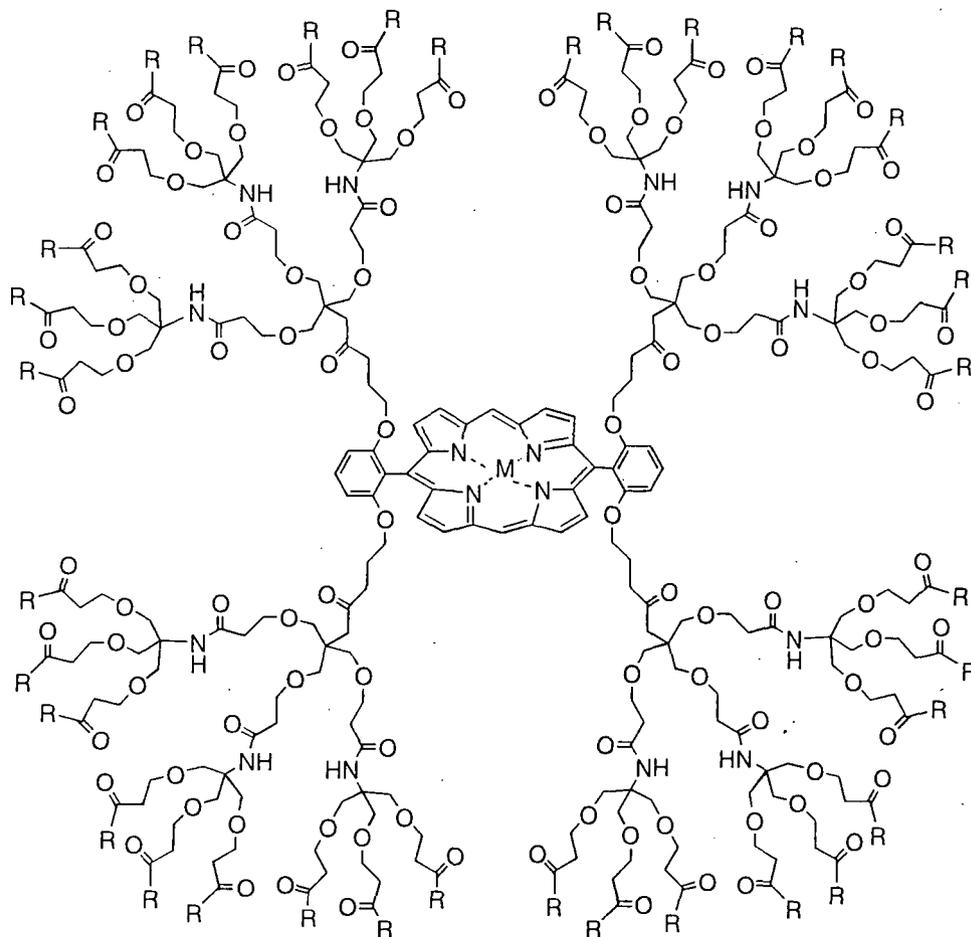
Dendrimers **94-96** are water-soluble compounds and model studies suggest their use as mimic to heme-containing proteins such as cytochrome *c* (*Figure 4.3*).
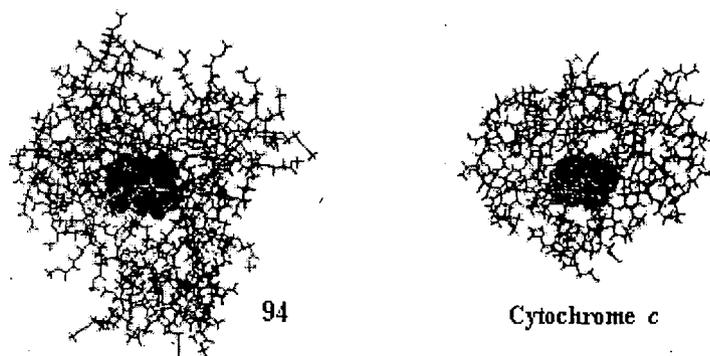
Figure 4.3 Computer-generated model of the dendritic zinc porphyrin **94** and X-ray crystal structure of cytochrome *c* (bonita).

Electrochemical studies on dendritic Zn or Fe porphyrins such as **94-96** are very dependent on generation, in particular, the polarity of the pendant arms strongly influences the redox potential of electrochemical reactions at the porphyrin core. For dendrimer **96**, the potential of the Fe^{2+}/Fe^{3+} couple in water was raised by *ca.* 300 mV compare to lower generation systems. This is consistent with the dense packing of higher generation preventing solvation of the core, which destabilises the Fe^{3+} state. This observation is similar to the electron transfer proteins such as cytochrome *c*, for which the oxidation potential of the Fe^{2+}/Fe^{3+} couple in aqueous solution is raised of 300-400 mV compare to similar heme proteins which lack of hydrophobic peptide shell.

Porphyrin dendrimers have also been studied for the mimicry of natural oxidation catalysts, in particular heme-based oxygenases. Manganese porphyrins carrying oxidatively robust poly(phenyl ester) dendrons such as compound **97** were reported by Moore *et al.*[18,19] and were found to catalyse the shape-selective epoxidation of alkenes when iodosobenzene was used as the oxidizing agent (*Figure 4.4*). The shape-selectivity of the epoxidation is due to the structure of the dendrimer, which has been studied by molecular modelling showing that the top access is completely blocked but the side-access to the putative metal oxo intermediate is available with an entrance opening of 7 Å (*Figure 4. 5*).
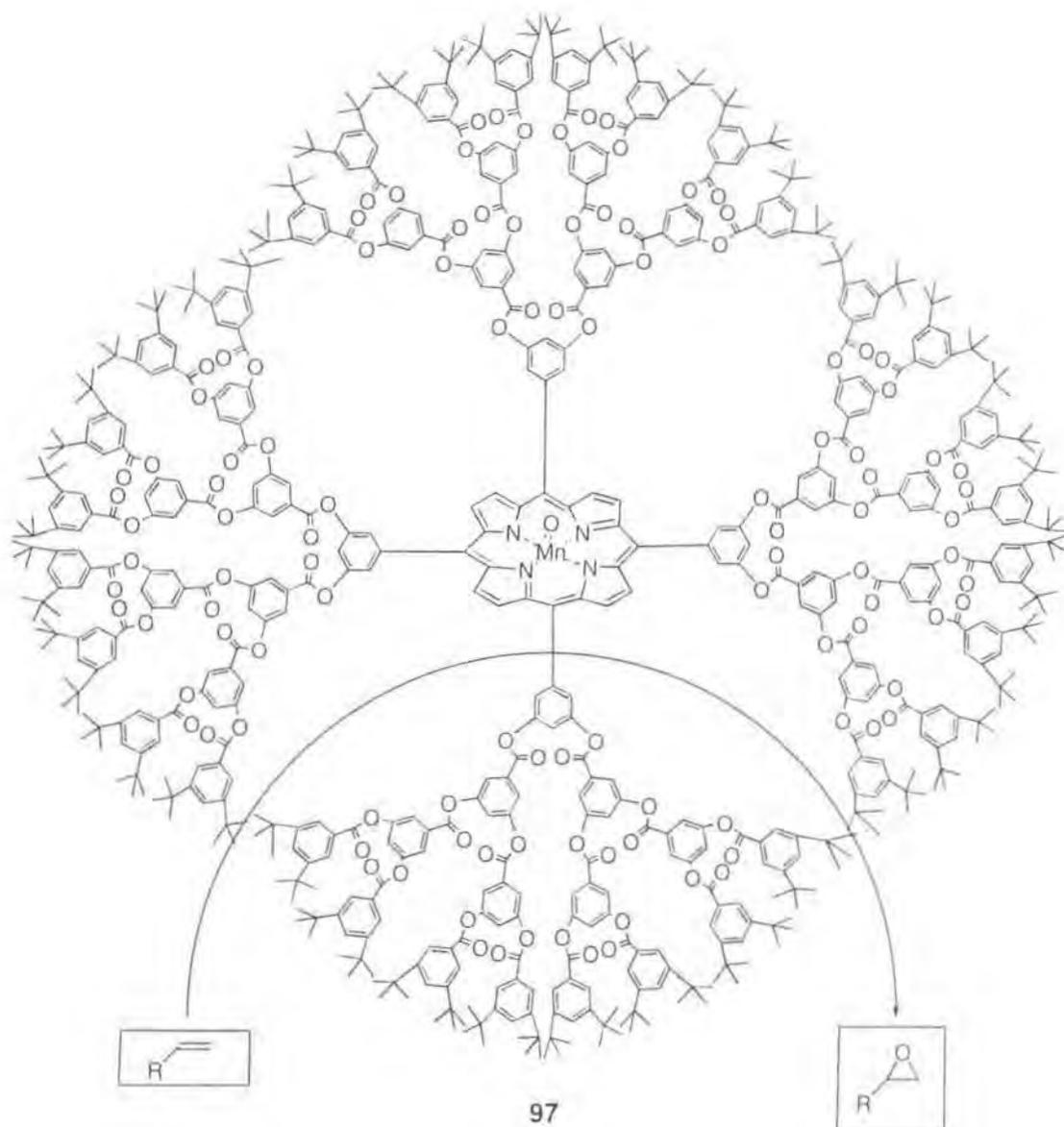
Figure 4.4 Shape-selective olefin epoxidation using dendrimer **97** with a manganese (III) porphyrin core as catalyst.
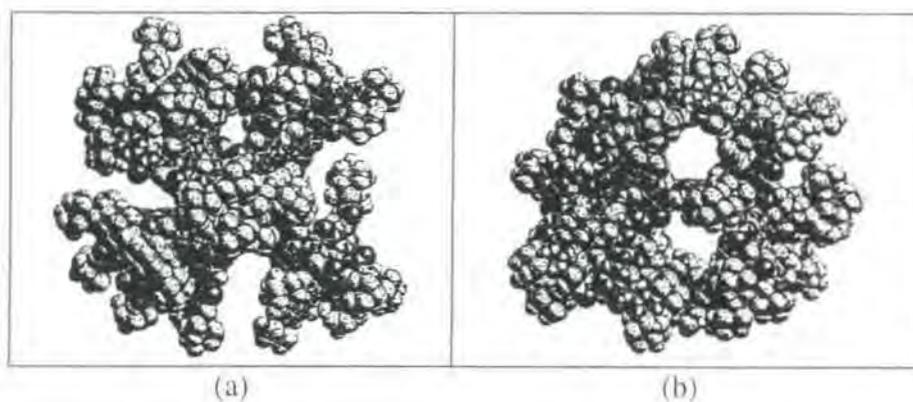
Figure 4.5. Molecular models of **97**. Top view (a), showing the sterically crowded top access, and side view (b) showing the pocket of 7 Å.

Other metallic redox active moieties have been incorporated into dendritic structures, on their periphery or inside their framework such as ruthenium(II)bis(terpyridiyl) complex[20], metal(bipyridyl)[21,22] and iron-sulfur cluster[23] in the search for new applications such as described previously for ferrocenyl and metalloporphyrins dendrimers.

4.1.2 Tetrathiafulvalene Dendritic Structures.

The first dendrimers incorporating tetrathiafulvalene units (**98-101**) were synthesised using a convergent strategy based on a repetitive coupling/deprotection sequence using 4-(hydroxymethyl)-TTF as the starting monomer.[24,25]
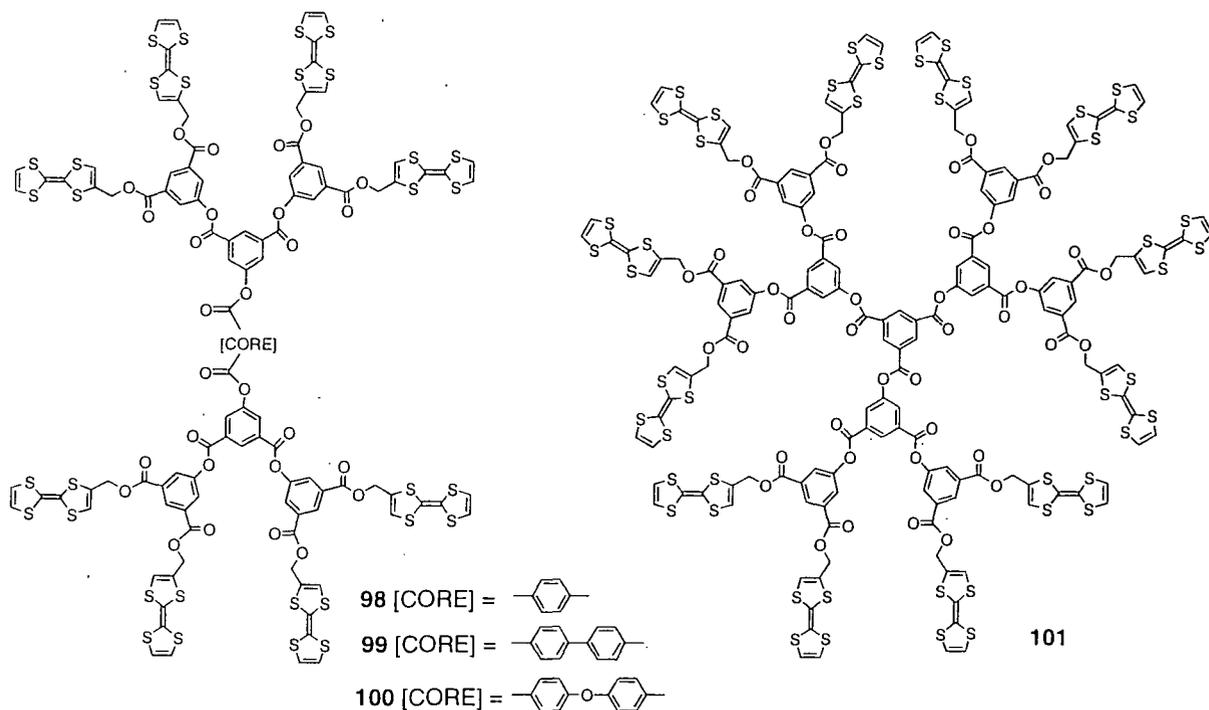
Several problems emerged as a result. These dendrimers have limited solubility in most organic solvents and higher generation dendrimers must be kept a low temperature to prevent decomposition due to instability.

Other dendrimers containing a lipophilic linker such as **102**, which comprises 21 TTF units, were synthesised in order to improve the solubility and increase the flexibility of the macrostructure, which should facilitate interactions between the TTF units.[26,27]

102
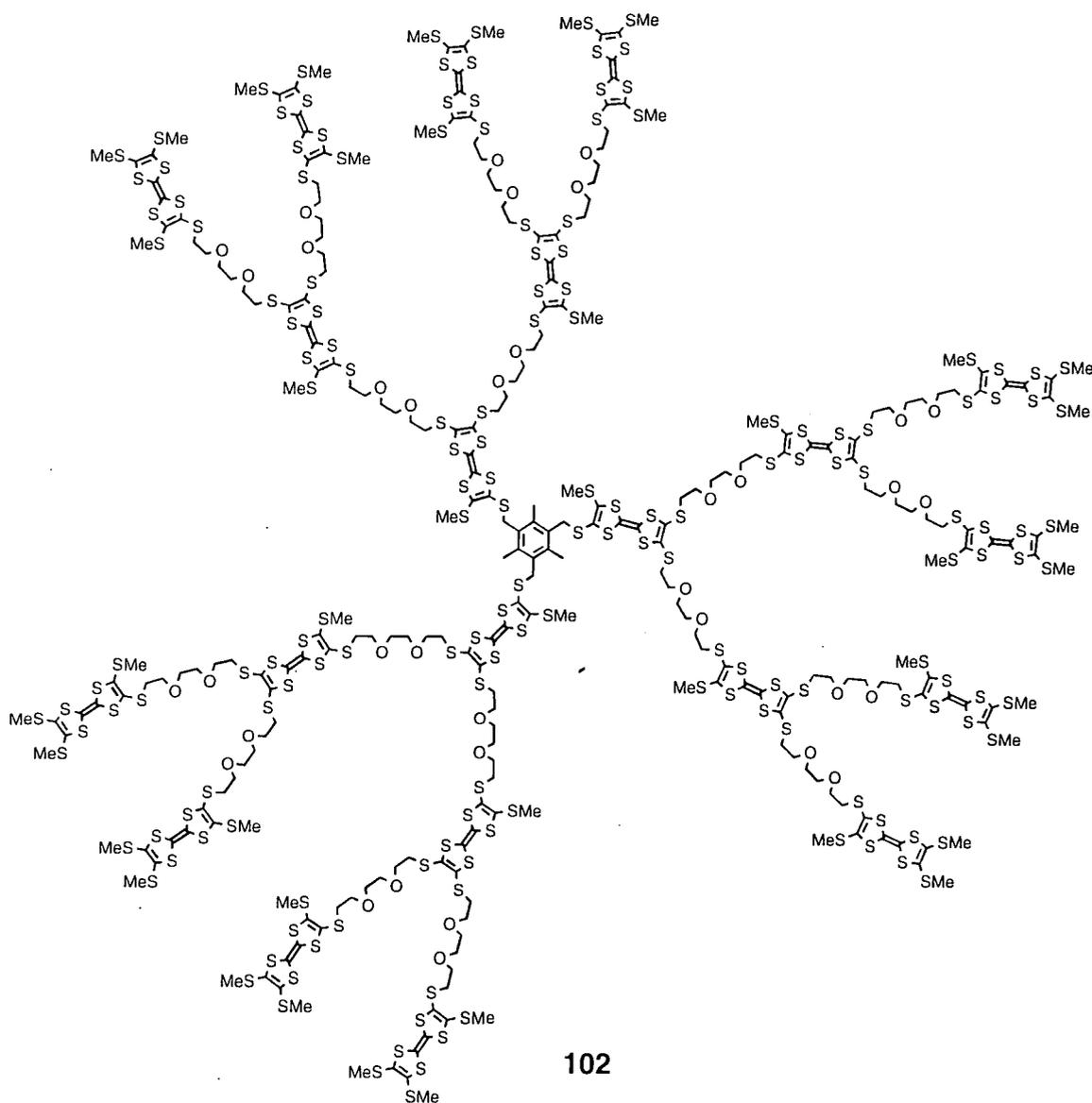
All of these dendrimers exhibit two redox couples corresponding to the TTF cation radical and TTF dication species. All the TTF units are independent, no interference was observed during the oxidation. As the number of TTF units increases, the first and second redox waves tend to broaden and sharpen, respectively, probably due to the adsorption or precipitation on the Pt electrode. Dendrimers **98-101** form charge transfer complexes with iodine, analysed by UV-Vis spectroscopy showing two absorption bands in the 516-590 nm and 810-836 nm regions assignable to isolated TTF cation radicals and cation radical dimers, respectively. The absorption in the lower energy band decreased with increasing dilution, indicating that the dimers form intermolecularly and the oxidised dendrimers self-associate in solution. For dendrimer **102**, a spectroelectrochemistry study upon oxidation at 0.7 V showed the two absorption bands of isolated (non-interacting) TTF cation radical (425 nm), and interacting TTF cation radical dimers (800 nm). Even at very low concentration, both bands are always present, indicating of their intramolecular nature, which is a consequence of the flexibility of the oxyethylene chains.

In a search for optoelectonic properties, compounds containing a phthalocyanine core surrounding by TTF units[28] such as compound **103** and dendrimers comprising anthraquinone and TTF units,[29] *e.g* compound **104** have been successfully synthesised.

103 R = n-C$_6$H$_{13}$

104
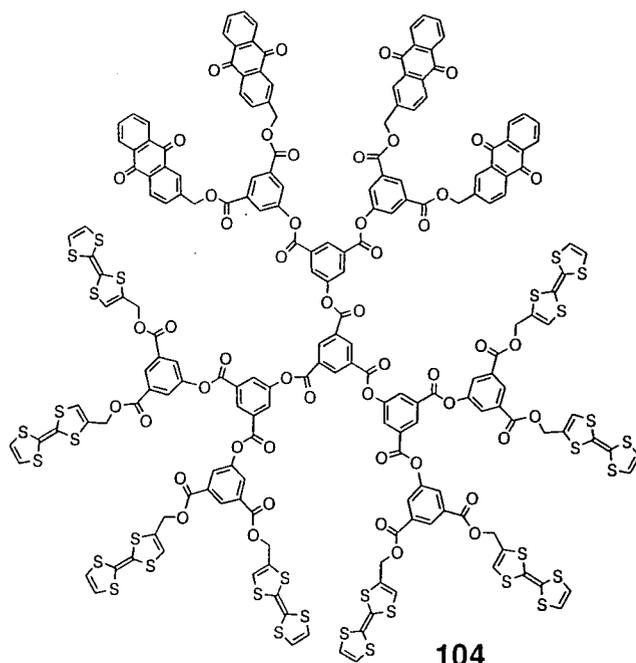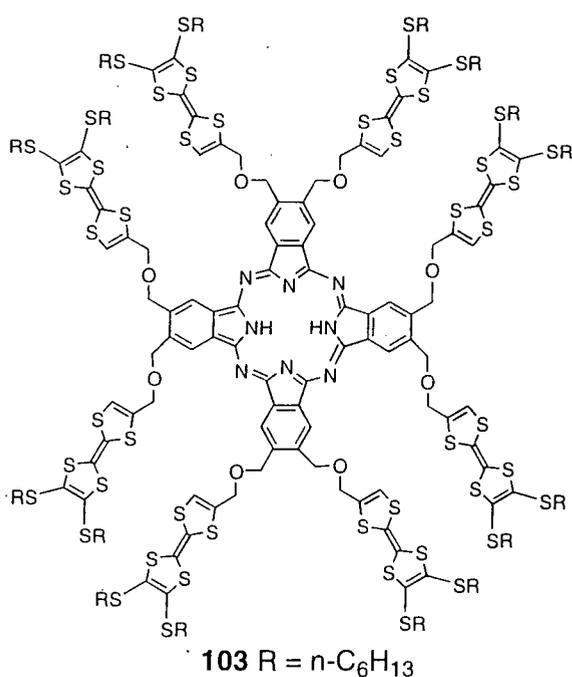
Compound **103**, in which both phthalocyanine and TTF units are liable to self-assemble by face-to face π-π stacking, displays supramolecular aggregations depending on the solvent properties. Quenching of the fluorescence in dendrimer **103** is ascribed to rapid intramolecular electron transfer between the excited singlet state of the phthalocyanine core and a peripheral neutral TTF unit acting as an electron donor group.

Dendrimer **104** comprising 8 TTF units (π-donors) and 4 anthraquinone units (π-acceptors) exhibits clean amphoteric redox behaviour with reversible charged states switching between **104^{+16}**, **104^{+8}**, **104**, **104^{-4}**, and **104^{-8}** and intramolecular charge transfer interaction have been observed by UV-Vis spectroscopy.

Other dendrimers containing redox active organic moieties such as bipyridiium[30], fullerenes[31], naphthalene diimides[32], phenothiazines[33] have been synthesised, all presenting specific properties due to their unique structures.

4.2.1 Preliminary Studies of oligomers.

We first evaluated the possibility of forming dendrimers comprising anthracenediylidene derivatives units at peripheral sites, by synthesising dimer **105** and trimer **106** by reaction of **47** with 1,4-benzenedicarbonyl chloride and 1,3,5-benzene tricarbonyl chloride, respectively (*Scheme 4.2*).
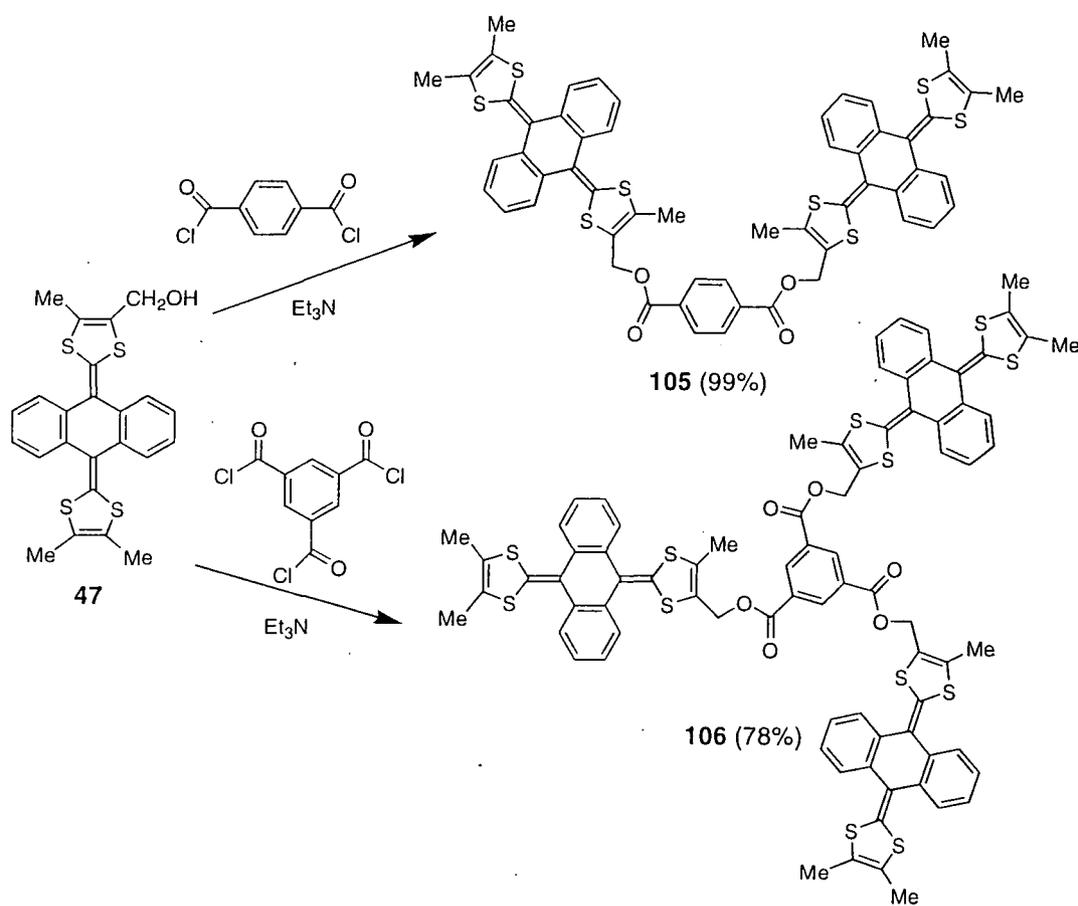
Scheme 4.2 Synthesis of diemr **105** and trimer **106**.

The only previous multi anthracene-TTF derivatives reported in the literature are structurally very different, linked by an oxygen atom bridge between the anthracene units synthesised directly from the corresponding bis (anthraquinone) precursor.[35]

Probably due to mixture of conformers, since each anthracene-TTF unit adopts two possible conformations (*Cf. Chapter Two*), crystals of dimer **105** and trimer **106** have not been obtained.

Electrochemical data for the dimer **105** and the trimer **106** are consistent with each donor unit acting independently. Dimer **105** displays a four-electron wave related to the formation of the tetracation species, whilst trimer **106** displays a six-electron wave corresponding to the formation of the hexacation species. A comparison with benzyl ester derivative **52** reveals that the oxidation potential are not significantly changed within the series, although it seams that it becomes slightly harder to oxidise in the sequence monomer (**52**), dimer (**105**) amd trimer (**106**) (*Table 4.2*)
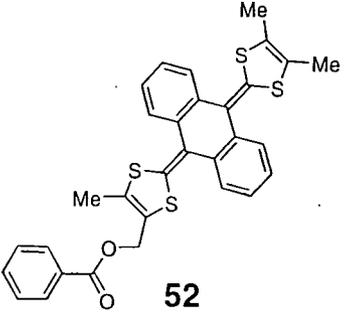
Compound	E^{Ox}_{pa} / V	E^{Ox}_{pc} / V	ΔE / V	
52	0.45 (2e)	0.21	0.24	
105	0.47 (4e)	0.12	0.35	
106	0.49 (6e)	0.19	0.30	

Table 4.2 Cyclic voltammetric data. $\Delta E = E^{Ox}_{pa} - E^{Ox}_{pc}$

E^{Ox}_{pa} is the oxidation peak potential on the first anodic scan;

E^{Ox}_{pc} is the coupled reduction peak potential on the cathodic scan.

[Experimental conditions: Dichloromethane, Pt electrode, versus Ag/AgCl, electrolyte $Bu_4N^+ClO_4^-$ (0.1M), 20°C, scan rate 100 mV s^{-1}.]

Trimer **106** can be considered as a generation zero dendrimer, therefore these preliminary results on oligomers of anthracenediylidene derivatives pave the way for the incorporation of this π-system into dendritic structures, which should possess well-defined redox behaviour.

4.2.2 Polyester dendrimers.

The first dendrimer containing anthracene-TTF units was obtained following Miller's methodology by reacting **47** with the silyl-protected diacid chloride **107**,[34] using triethylamine as base in dichloromethane to afford the first dendron wedge **108** (97% yield) comprising two units of anthracene-TTF. Deprotection of **108** by tetra-n-butylammonium fluoride (TBAF) afforded the dendron wedge **109** almost quantitatively. By analogy with the synthesis of trimer **106**, dendrimer **110** comprising six anthracene-TTF units was obtained by reacting **109** with 1,3,5-benzenetricarbonyl chloride (*Scheme 4.3*).

108 (97%) R = SiMe$_2$Bu^t

109 (99%) R = H

) TBAF
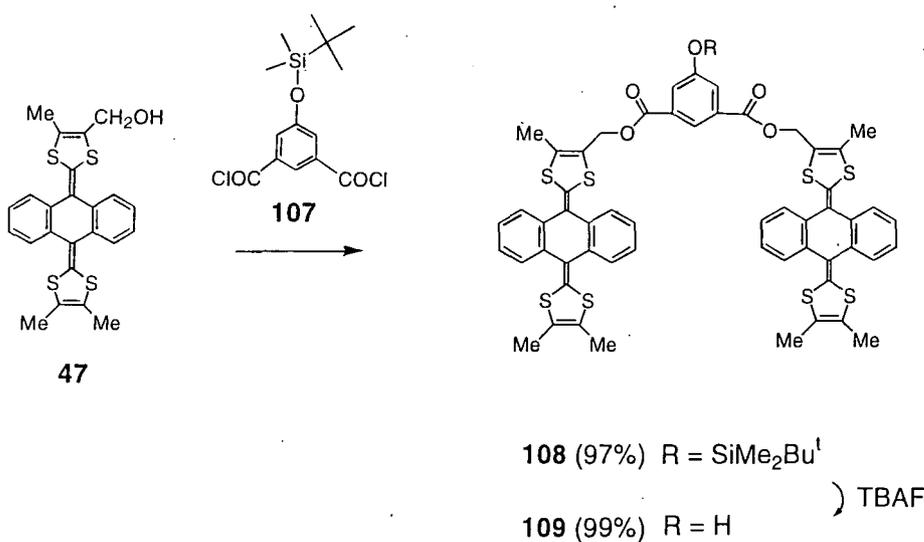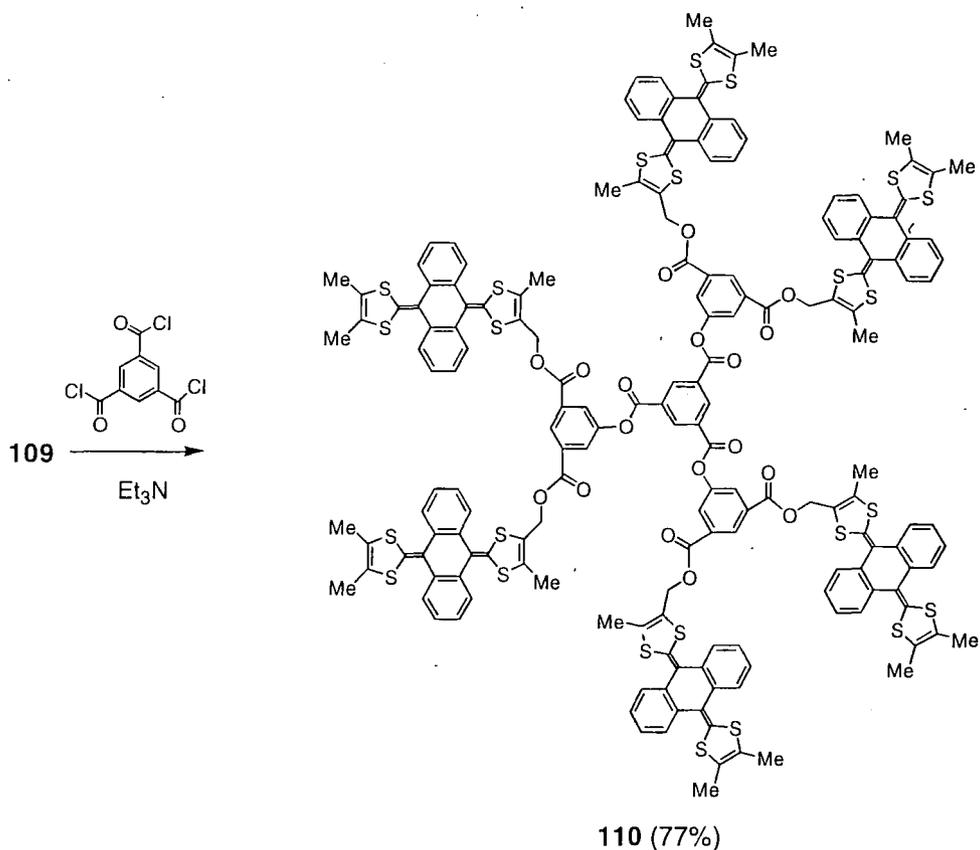
Scheme 4.3 Synthesis of dendrimer **110** comprising 6 anthracene TTF units and ester linkages.

Similarly to the synthesis of the first dendron wedge **108, 109** reacted with the silyl-protected diacid chloride **107** afforded dendron wedge **111** (72% yield) comprising 4 units of anthracene-TTF. However, repeated attempts to deprotect **111** unexpectedly led to the fragmentation of the molecule and essentially quantitative conversion back to the dendron wedge **109** (*Scheme 4.4*). Therefore, we were unable to synthesis higher generation analogues of dendrimer **110** by this strategy.
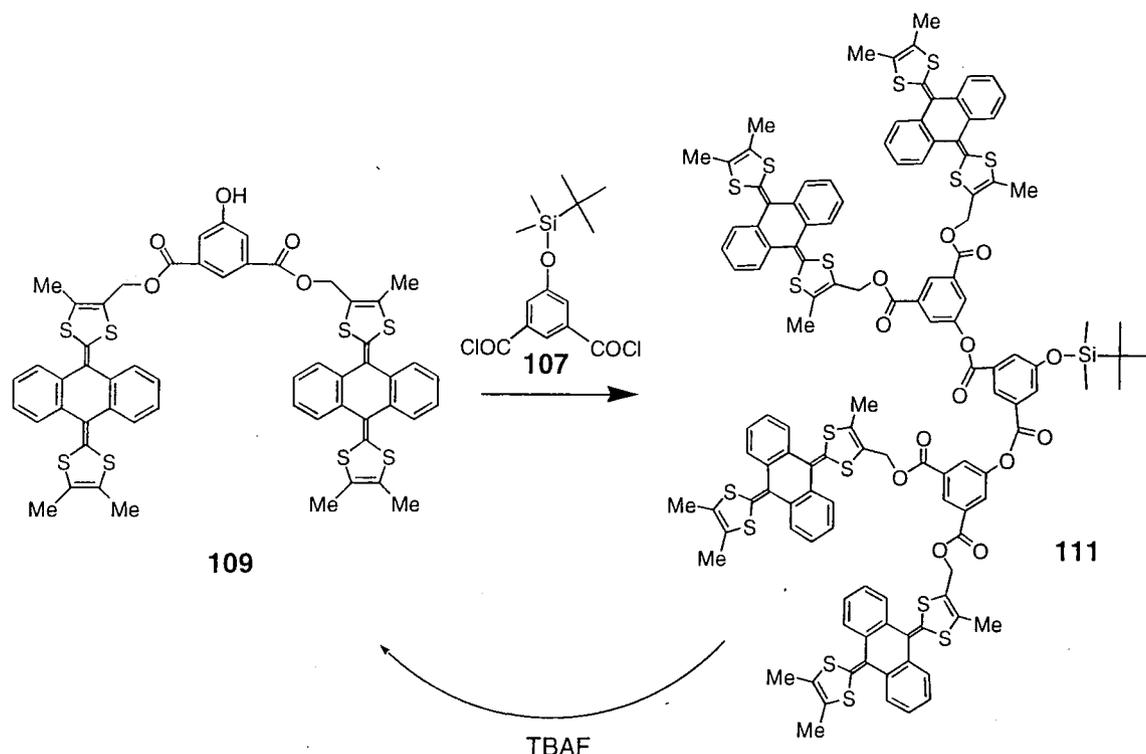
Scheme 4.4 Synthesis of dendron wedge **111** comprising 4 units of anthracene-TTF.

To circumvent this problem, we decided to incorporate more robust ether linkages into the dendritic scaffold, using the convergent strategy developed by Fréchet for poly(arylether) systems.[36]

4.2.3 Polyether dendrimers.

The monohydroxymethyl anthracene-TTF derivative **47** was converted into the chloromethyl derivative **112** (95% yield) by treatment with triphenylphosphine in carbon tetrachloride. Compound **112** is easily decomposed in presence of acidic media and for this reason dichloromethane must be avoided during the purification by chromatography on silica gel, for which ethyl acetate appeared to be the best solvent. Two-fold reaction of **112** with 3,5-dihydroxybenzyl alcohol (**113**), using potassium carbonate as base, afforded the dendron wedge **114** in only 28% yield. The disappointing yield for this reaction is due

to the heterogeneous mixture and poor reactivity of the chloromethyl derivative **112**. The

dendron wedge **114** was converted into dendrimer **115** (57%) by direct analogy with the

preparation of dendrimer **110** (*Scheme 4.5*).
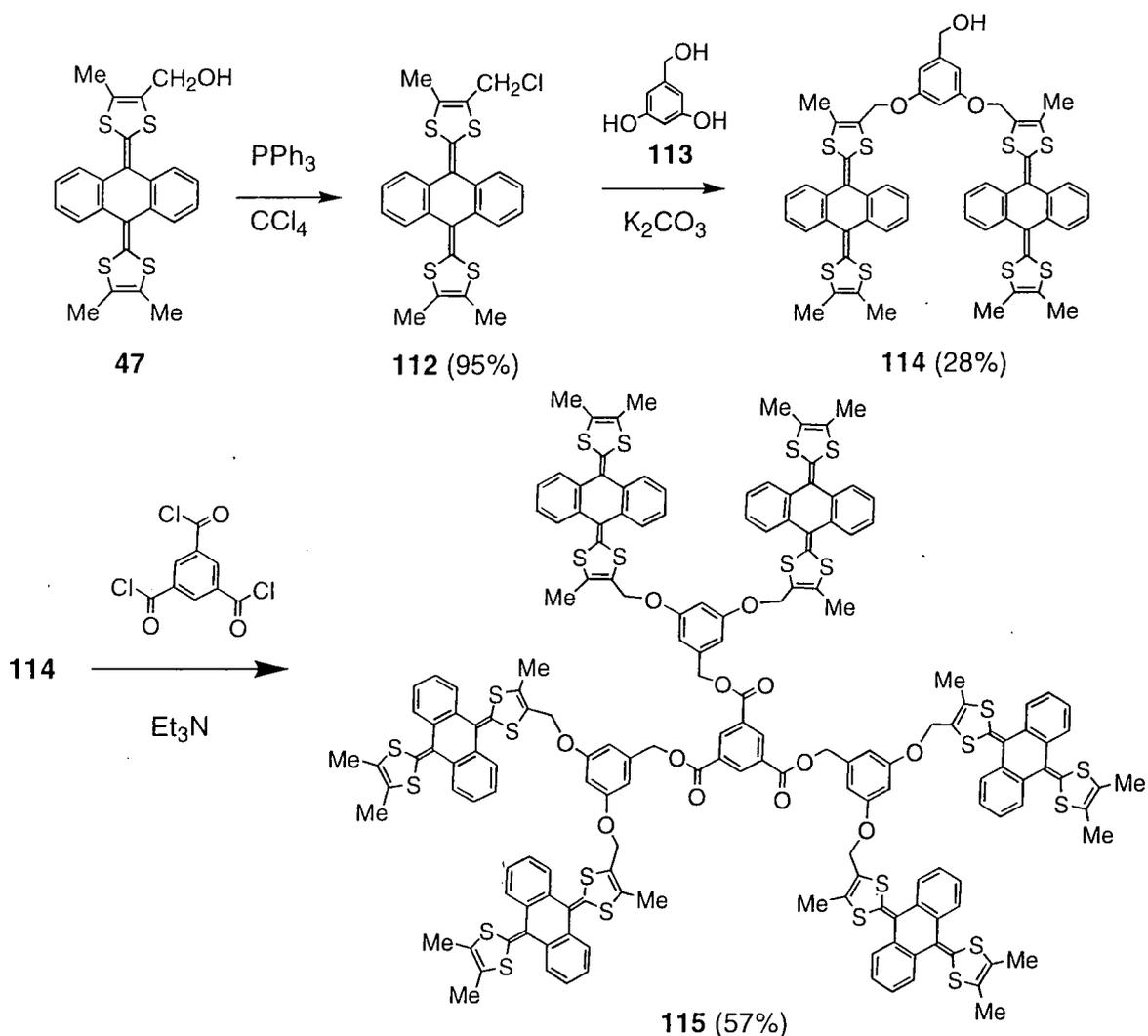
Scheme 4.5 Synthesis of dendrimer **115** comprising 6 anthracene TTF units and ether
linkages.

Reaction of dendron wedge **114** with the silyl-protected diacid chloride **107**

afforded dendron wedge **116** (65%). Unlike **111** (*Scheme 4.4*), dendron wedge **116** was

cleanly deprotected using tetra-n-butylammonium fluoride (TBAF) to yield the

corresponding alcohol derivative **117** (70% yield). Three fold esterification of **117** with

1,3,5-benzenetricarbonyl chloride gave the dendrimer **118** (54% yield) (*Scheme 4.6*).
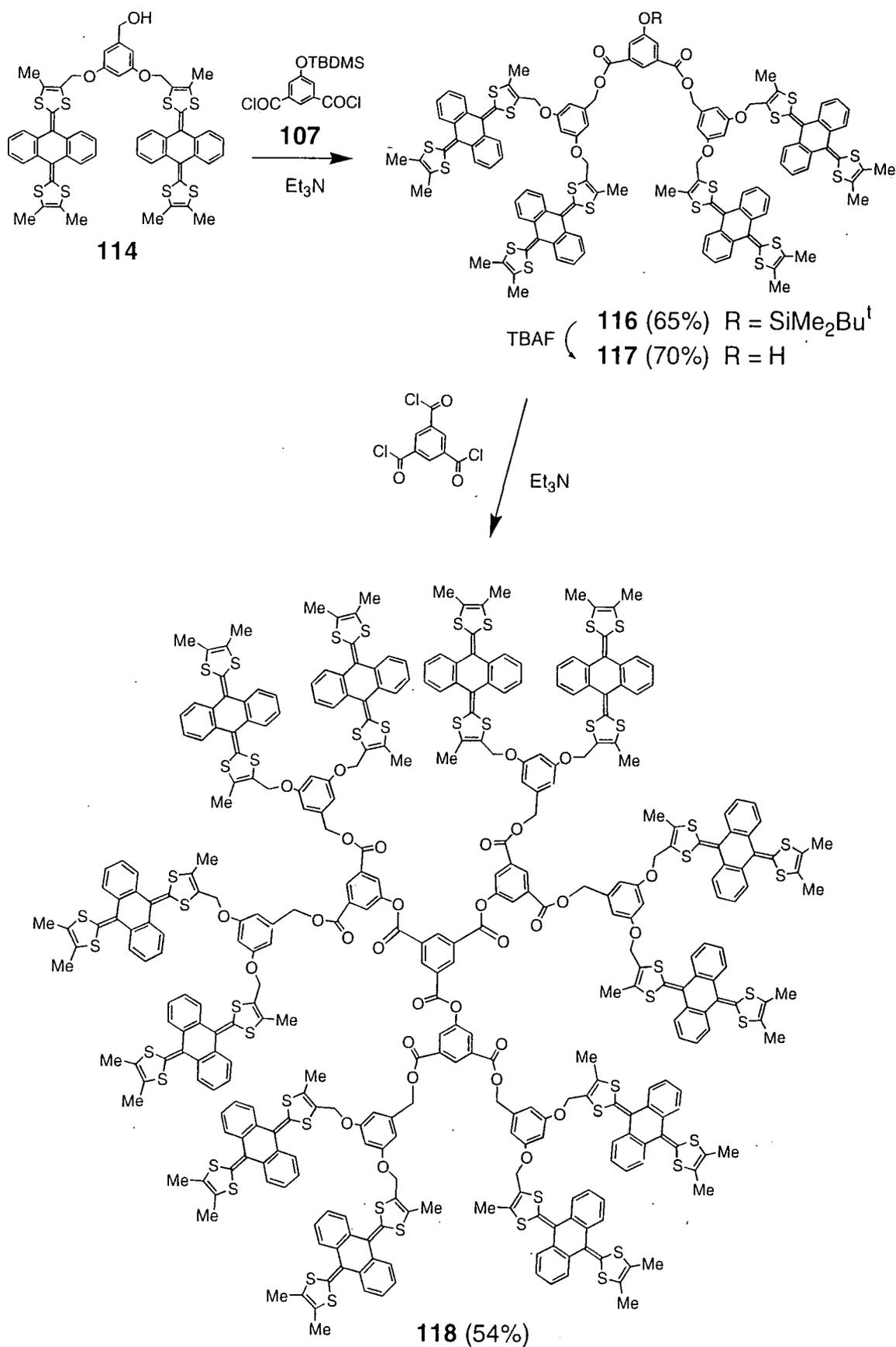
Scheme 4.6 Synthesis of dendrimer **118** comprising 12 anthracene TTF units and ether linkages.

Evidence for the synthesis of dendrimers **110**, **115** and **118** was first obtained by [1]H

NMR spectra. Unlike for dendrimer **110** and **115** where the two methyl groups (Me$_1$, Me$_2$)

display different chemical shift (*Figure 4.6*); for dendrimer **118**, they are no longer

differentiable (*Figure 4.7*). This observation could be a result of intramolecular

interactions inside dendrimer **118**, which place the two methyl groups in a more analogous

environment for which the nuclear magnetic properties are more similar.
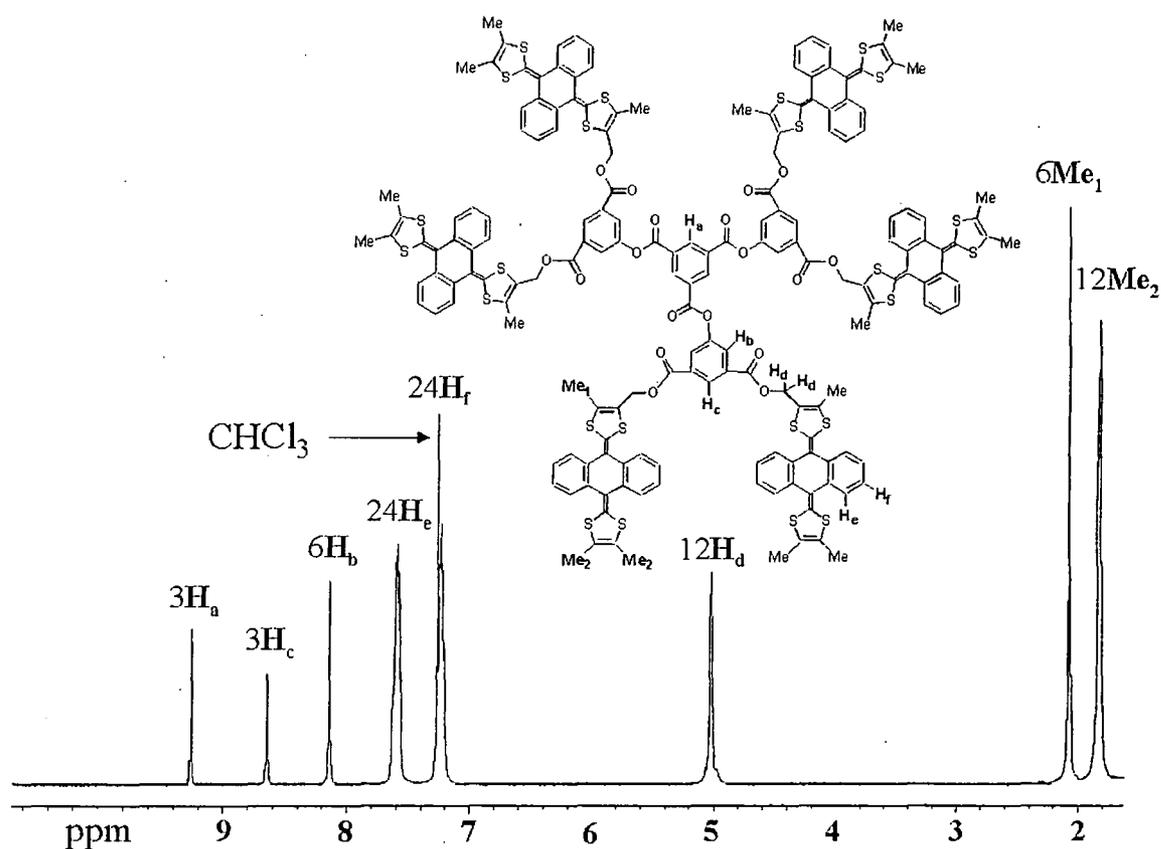
Figure 4.6 ^{1}H NMR of dendrimer **110** in CDCl$_3$.
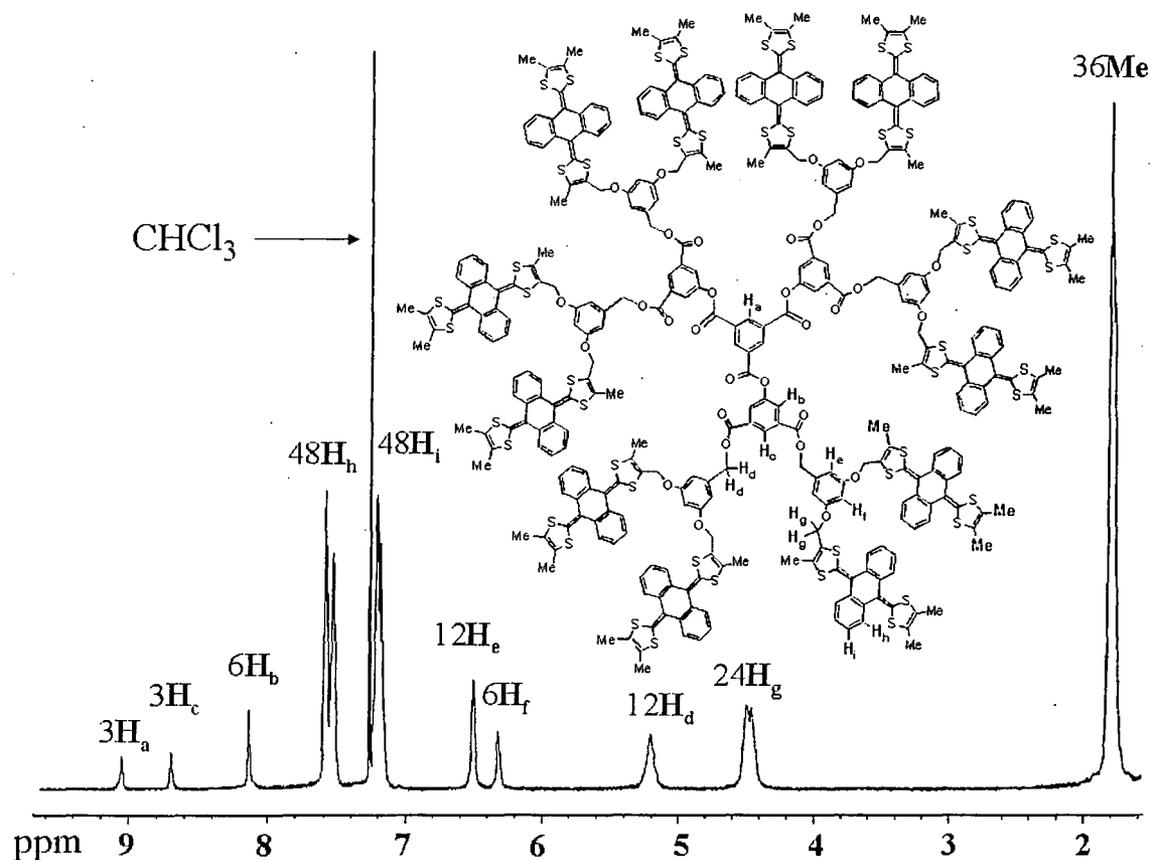
Figure 4.7 ^{1}H NMR of dendrimer **118** in CDCl$_3$.

4.2.4 Electrochemical Studies.

Solution electrochemical data, obtained by cyclic voltammetry were performed in two different solvents (THF and Dichloromethane/Acetonitrile (2:1, v/v)), to compare the effect of solubility on the electrochemical behaviour of the dendrimers. A comparison of the model compound **52** (benzyl ester anthracene-TTF derivative) with the dendritic molecules **106, 110, 115** and **118** reveals some interesting trends (*Table 4.3*).

The benzoyl ester **52** shows the typical quasi-reversible two-electron redox wave from neutral to dication species observed for anthracene-TTF derivatives (*See Chapter One*).

104

Compound	THF			DCM/Acetonitrile (2:1 v/v)		
	E^{Ox}_{pa} / V	E^{Ox}_{pc} / V	ΔE / V	E^{Ox}_{pa} / V	E^{Ox}_{pc} / V	ΔE / V
52	0.60 (2e)	0.18	0.42	0.46 (2e)	0.16	0.30
106	0.62 (6e)	0.16	0.46	n.d.	n.d	n.d
110	0.66 (12e)	-0.13	0.79	0.51 (12e)	0.11	0.40
115	0.64 (12e)	0.02	0.62	0.54 (12e)	0.08	0.46
118	0.61 (24e)	-0.54	1.15	not soluble		

Table 4.3 Cyclic voltammetric data. (n.d. Non determined) $\Delta E = E^{Ox}_{pa} - E^{Ox}_{pc}$

E^{Ox}_{pa} is the oxidation peak potential on the first anodic scan;

E^{Ox}_{pc} is the coupled reduction peak potential on the cathodic scan.

[Experimental conditions: Pt electrode, versus Ag/AgCl, electrolyte $Bu_4N^+PF_6^-$ (0.1M), 20°C, scan rate 100 mV s^{-1}.]

The oxidation potential (E^{ox}_{pa}) is almost identical for all the compounds [ca. 600 mV in THF and 500 mV in DCM/AcN (2:1 v/v)]. All anthracene-bis(dithiole) units are independent and oxidised at the same time. A broadening of the oxidation peak can be noticed as the generation is increasing. This feature has already been reported with certain other dendrimers containing redox moieties at the periphery.[3]

A striking feature of these data is the as the generation increases there is a decrease in the reversibility of the redox wave in THF leading to a complete electrochemical irreversibility for **118** (ΔE = 1150 mV) (*Figure 4.8*).
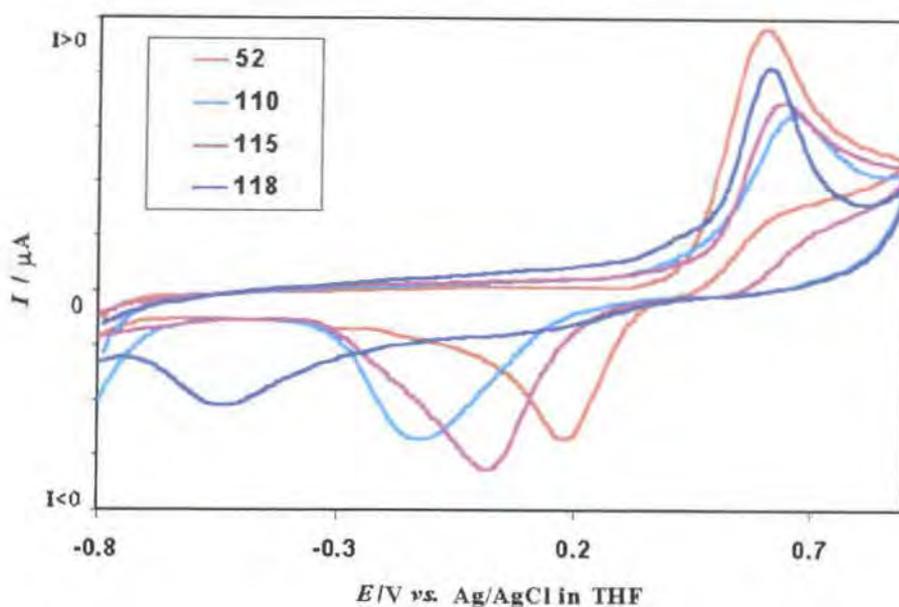
Figure 4.8 Cyclic voltammograms of dendrimers **110**, **115**, **118** and benzyl ester derivative **52** in THF (under the conditions stated in *Table 4.3*).

However, in a mixture of DCM/AcN where the charged species are more soluble, this irreversibility is less pronounced (*Figure 4.9*).
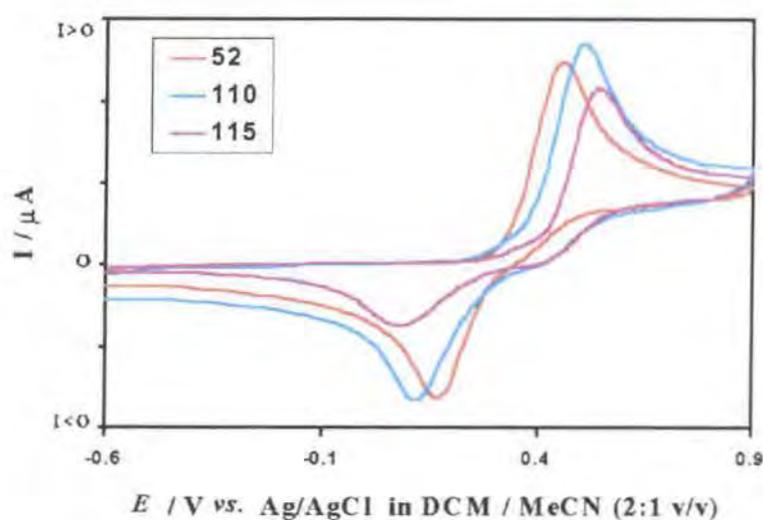
Figure 4.9 Cyclic voltammograms of dendrimers **110**, **115**, **118** and benzyl ester derivative **52** in Dichloromethane/Acetonitrile (2:1 v/v) (under the conditions stated in *Table 4.3*).

This difference of reversibility in the two solvent systems studied is consistent with a precipitation of the charged species occurring on the surface of the Pt electrode in THF, which does not take place in DCM/MeCN. This is confirmed by the electrode being completely blocked after few scans around E^{ox}_{pa} for **110** and **118** in THF and the observation of deposition on the surface of the electrode. However the non-aligned stacking prevents their use as modified electrodes, cf. the ferrocenyl dendrimers reported recently by Astruc et al.[14] and Cuadrado et al.[12] which are useful in this regard. Consequently, the decrease of reversibility for **110** and **115** in DCM/MeCN (ΔE increased by 100 mV and 160 mV, respectively) can be attributed to the dramatic change of conformation which must occur on reduction of the oxidised form of **10**$^{12+}$ and **15**$^{12+}$ back to their neutral form. This represents an interesting dendritic effect on the solution redox chemistry.

4.2.5 Chemical oxidation vs. Electrochemical oxidation.

Addition of iodine to a dichloromethane solution of dendrimers **110,115** and **118** gave red-purple precipitates of the iodide salts of **110**$^{n+}$, **115**$^{n+}$ and **118**$^{n+}$. These precipitates could be reduced back to the neutral species by adding sodium hydrosulfite and heating the mixture. The ^{1}H NMR spectra recorded before oxidation and after reduction were identical, showing that the chemical redox processes in these dendrimers are reversible without any significant decomposition of the oxidised species. Evidence of complete oxidation to **110**$^{12+}$ was provided by ^{1}H NMR data in dry DMF (*Figure 4.10*) in which both the neutral and the oxidised species are soluble: in particular, the methyl and CH$_2$ protons (Me$_1$, Me$_2$ and H$_d$) shifted downfield from δ 2.19, 1.88 and 5.23 ppm to δ

3.36, 3.10 and 6.28 ppm, respectively, consistent with each unit being oxidised to the bis(1,3-dithiolium) cation, as shown previously in monomeric derivatives (Cf. Chapter Three). No paramagnetic broadening of the NMR spectra were observed, confirming that no cation radical species derived from **110** were present.
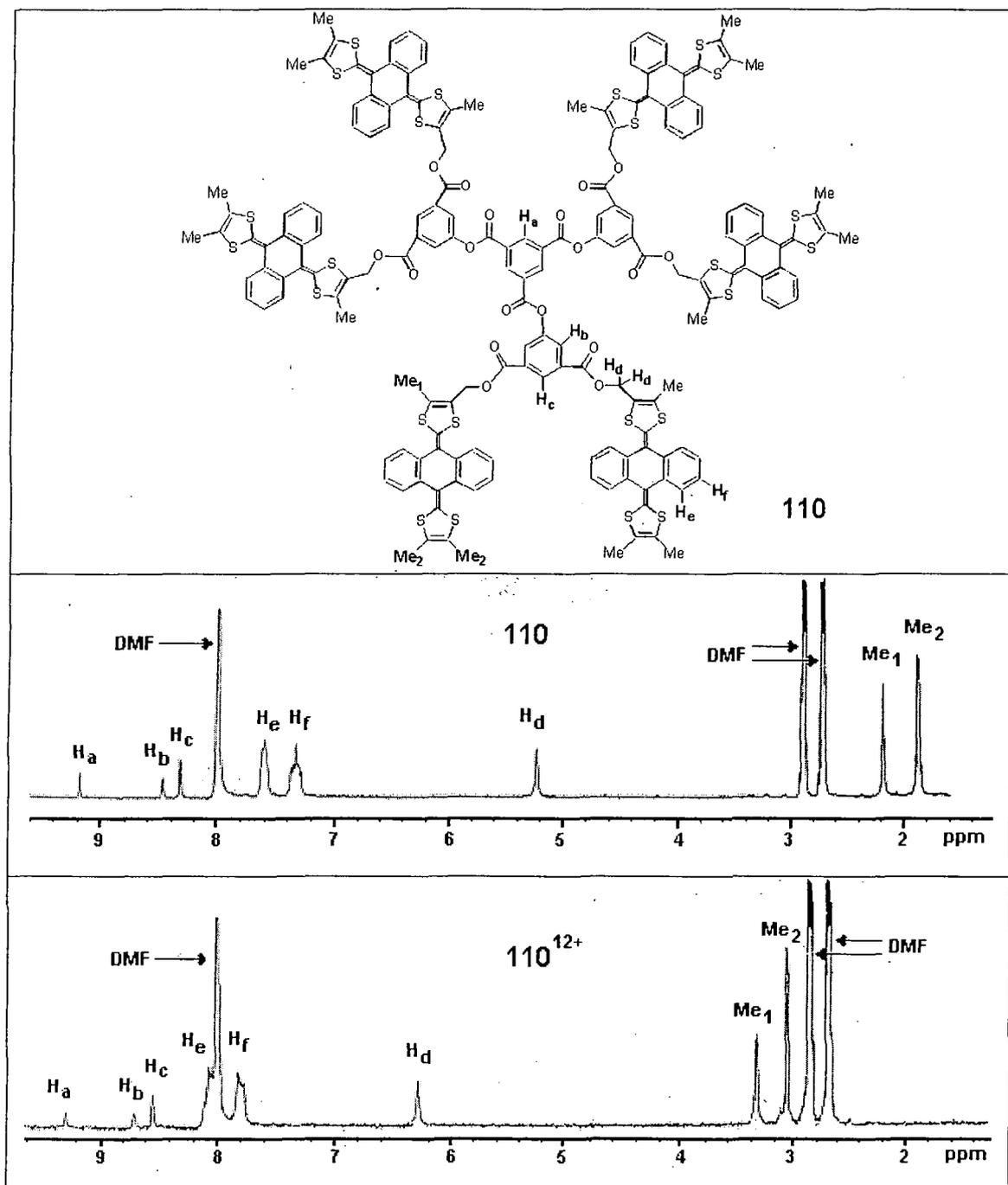
Figure 4.10 ^{1}H NMR spectra in d$_7$-DMF of dendrimers **110** and **110**$^{12+}$ (obtained by adding iodine into the NMR tube).

4.2.6 UV-Vis Spectroscopy.

UV-VIS spectra of dendrimers **110**, **115** and **118** were obtained in dichloromethane solutions. The benzoyl ester **52** was employed as a model compound, which shows the two characteristic absorption bands at λ_{max}= 368nm and λ_{max}= 436 nm for anthracene-bis(ditiole).[37] UV-VIS spectra of compound **52** were recorded for a range of concentration varying from C to 20xC (where C = 6.31×10^{-6} M). The absorbance at λ_{max}= 368 nm and λ_{max}= 436 nm is a linear function of the concentration (*Figure 4.11*).

(a) (b)
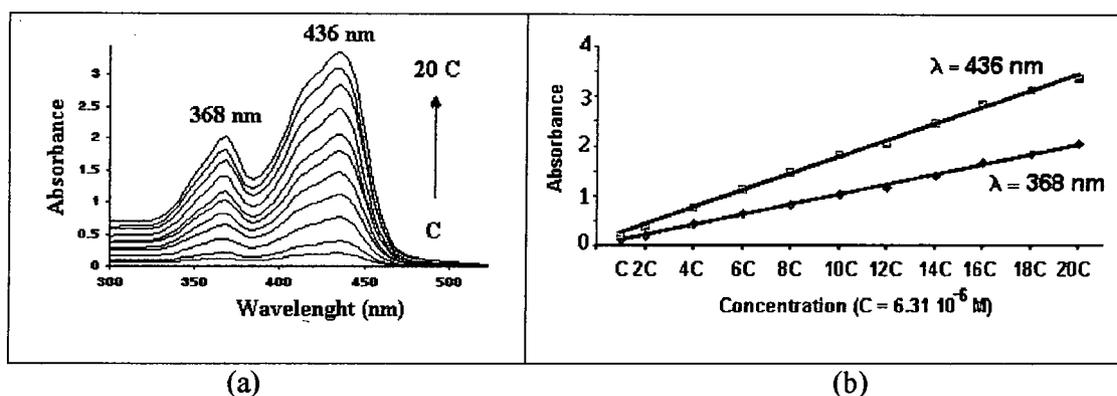
Figure 4.11 UV-Vis spectra of **52** at varying concentrations C to 20C (a), linear variation of absorbance as a function of the concentration of compound **52** for the two wavelenght of maximum of absorbance: λ = 368 nm and λ = 436 nm (b) with C = 6.31×10^{-6} M.

UV-VIS spectra of dendrimers **110**, **115** and **118** were recorded at the same concentration C= 6.31×10^{-6} M. The spectra obtained for **110** and **115** (curves II and III respectively) are equivalent to a 6xC spectrum of **52**, and for **118** (curve I), equivalent to a 12xC spectrum of **52** (*Figure 4.12*). Consequently, the extinction coefficient of each dendrimer corresponds to the extinction coefficient of one chromophore unit multiplied by

the number of units in the dendrimer. This confirms that each chromophore unit is acting independently, with no dendritic effect observed in the optical spectra. Therefore, this spectroscopic technique could also be used to quantify the number of units present for a new dendrimer.

(a)   (b)
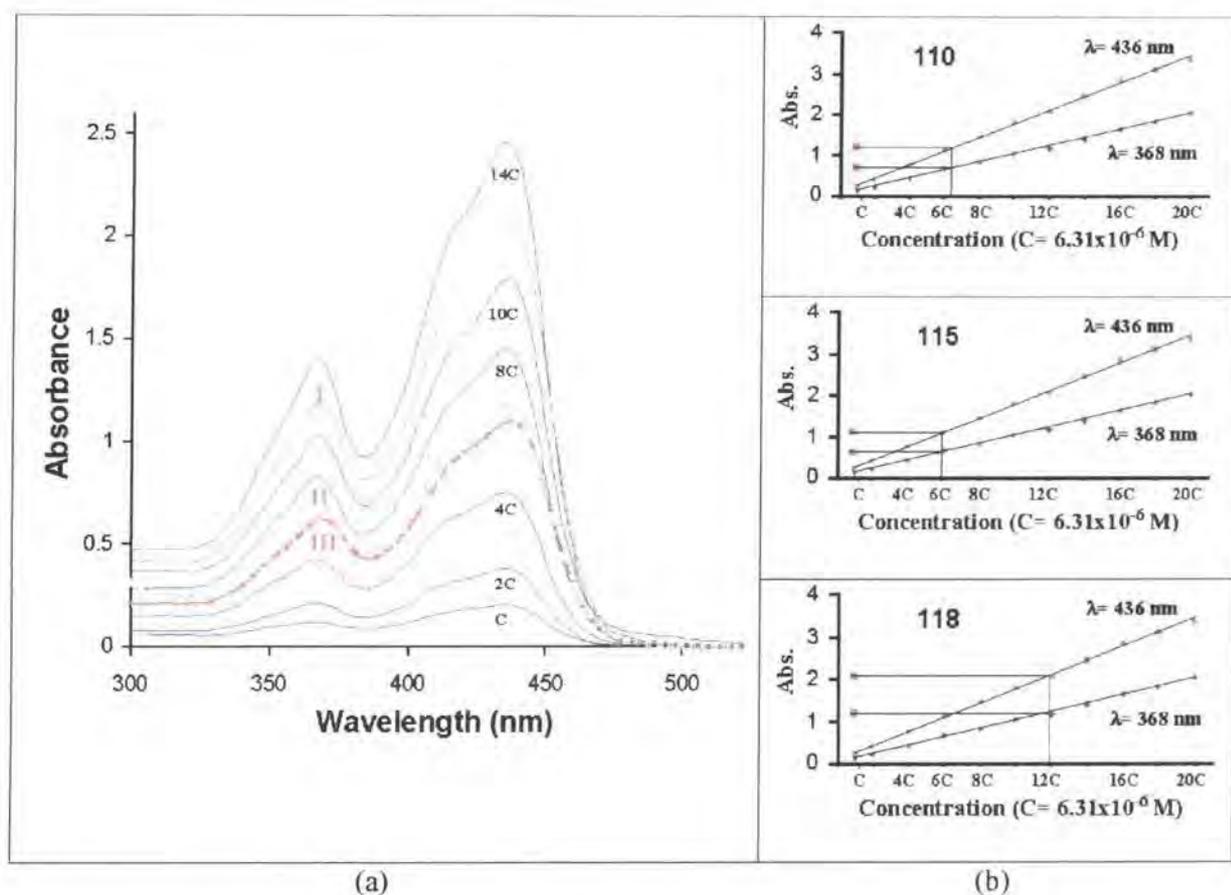
Figure 4.12 UV-Vis spectra of **52** (at varying concentration C to 20 C, blue curves), dendrimers **110** (concentration C, red curve II), dendrimer **115** (concentration C, red curve III) and dendrimer **118** (concentration C, red curve I); C = 6.31×10^{-6} M in dichloromethane (a). Correlation of the maxima of absorption for dendrimers **110**, **115** and **118** at concentration C (red points) to the linear variation of absorbance as a function of the concentration of compound **52** (b).

4.2.7 Modelling Studies.

In order to visualise the change in conformation occurring during oxidation, molecular modelling studies were performed on dendrimers **110, 118** and their oxidised form **110**$^{12+}$ and **118**$^{24+}$ by molecular mechanics.

In the precedent Chapter, we performed the energy minimisation of the anthracene-bis(dithiole) unit in the neutral state with the dihydroxymethyl derivatives (*E*) and (*Z*) **76** (*See also Appendix Two*), showing the most favourable saddle-shape conformation which is in agreement with X-ray crystal structures[37-39] and theoretical calculations[40] reported in the literature for monomeric derivatives.

Energy minimisation of the core was then performed before the addition of the energy-minimised units at its periphery. Geometry optimisation of the dendrimers **110** was then calculated. The energy-minimised conformation of **110**$^{12+}$ was obtained by setting to the energy-minimised conformation of **110** (*Figure 4.13*), a positive charge on the C(2) atom of each dithiole ring (i.e. 12 positive charges in total). The structure obtained for **10**$^{12+}$ (*Figure 4.14*) shows that each unit adopts the characteristic dicationic shape wherein the anthracene moiety is planar with the two dithiole units perpendicular to it, which is in accord with theoretical calculations and X-ray crystal structures (*Cf. Chapter One*). It also complies with a maximum space expansion between the units arisen from Coulombic repulsion between the positively charged dithiole rings. It should be noted that for the neutral form of dendrimer **110** other unsymmetrical local minima of comparable energy can be reached where π−π interactions between the units occur. On the contrary, starting from different non-optimised geometries of **110**$^{12+}$, only one converged form was

observed, in which all the charged units are as far as possible one of each other. The presented structure of **110** (2 views) is therefore shown to help visualise the neutral structure and allow a good comparison between the shape of the neutral and oxidised forms of the dendrimer. The main feature of these structures is the average molecular diameter of their spherical shape, which is of 40 Å for **110** and 46 Å for **110**[12+]. This is representative of the compact form of **110** imposed by the saddle-shape conformation of the units, compared to the more extended form of **110**[12+] imposed by the Coulombic repulsion.

(a)   (b)
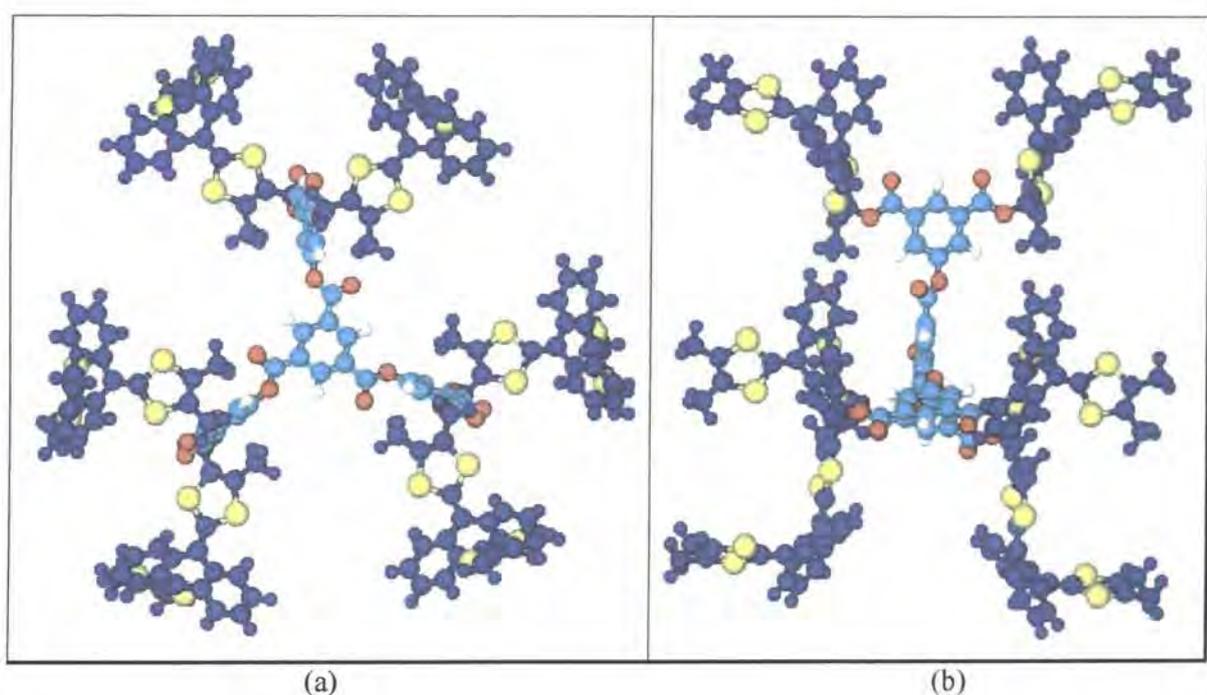
Figure 4.13 Molecular model of dendrimer **110**: perpendicular to the plane of the core benzene ring (a) and along the plane of this ring (b). Colour code: 9,10-bis(1,3-dithiole-2-ylidene)-9,10-dihydroanthracene system (dark blue); sulfur (yellow); oxygen (red); remaining carbon scaffold (light blue).
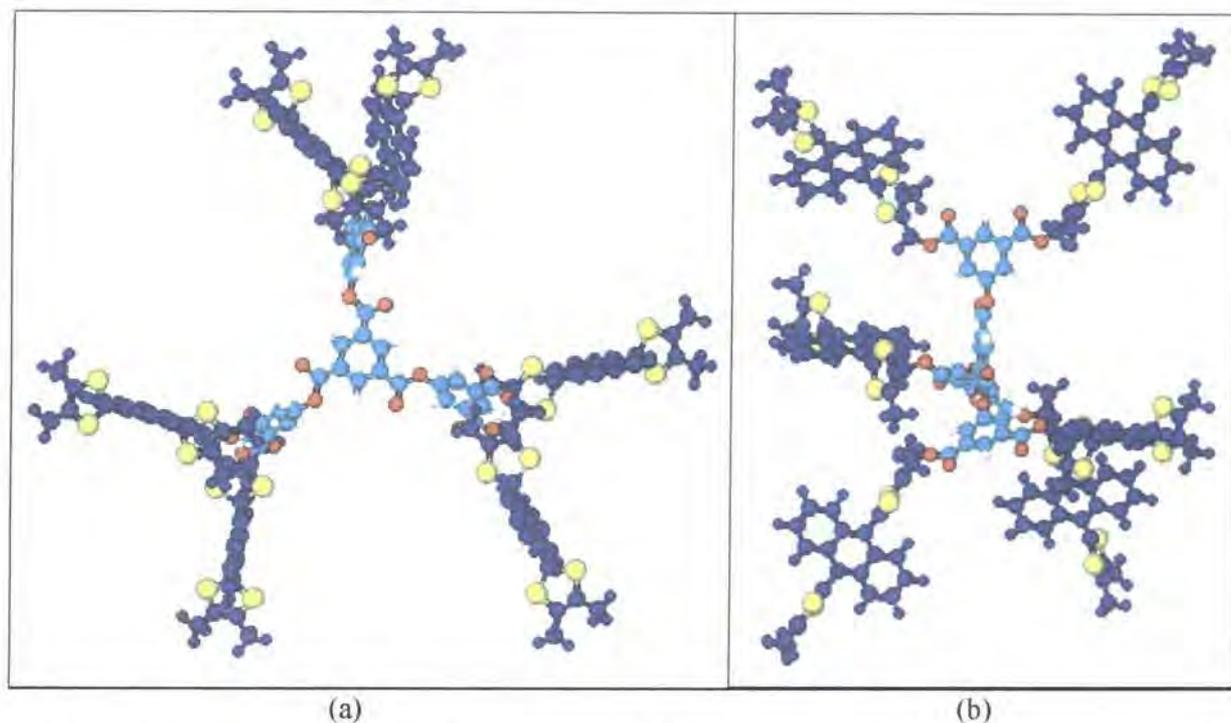
Figure 4.14 Molecular model of dendrimer **110**$^{12+}$
(views and colour codes as for *Figure 4.13*)

Modelling studies of dendrimer 118, were performed similarly to the calculations performed for dendrimer **110**. The proximity of the 12 units of dendrimer **118** leads to π-π interactions between the units and consequently to several converged unsymmetrical structures, but also to a symmetrical one of lowest energy (*Figure 4.15*). The energy-minimised structure of **118**$^{24+}$ was obtained by setting a positive charge on each c(2) atom of each dithiole ring (i.e 24 positive charges in total), and like for **110**$^{12+}$, only one converged structure of **118**$^{24+}$ (*Figure 4.16*) was obtained due to Coulombic repulsion, placing the charged units with the maximum space expansion. The structural differences between the neutral and the oxidised forms of dendrimer 118 are even more pronounced especially due to the π-π interactions occurring inside the dendritic structure. Consequently, dendrimer **118** presents a cylindrical shape (*ca.* 52 Å x 30 Å) and its oxidised form the expected spherical shape with an average molecular diameter of 61 Å.
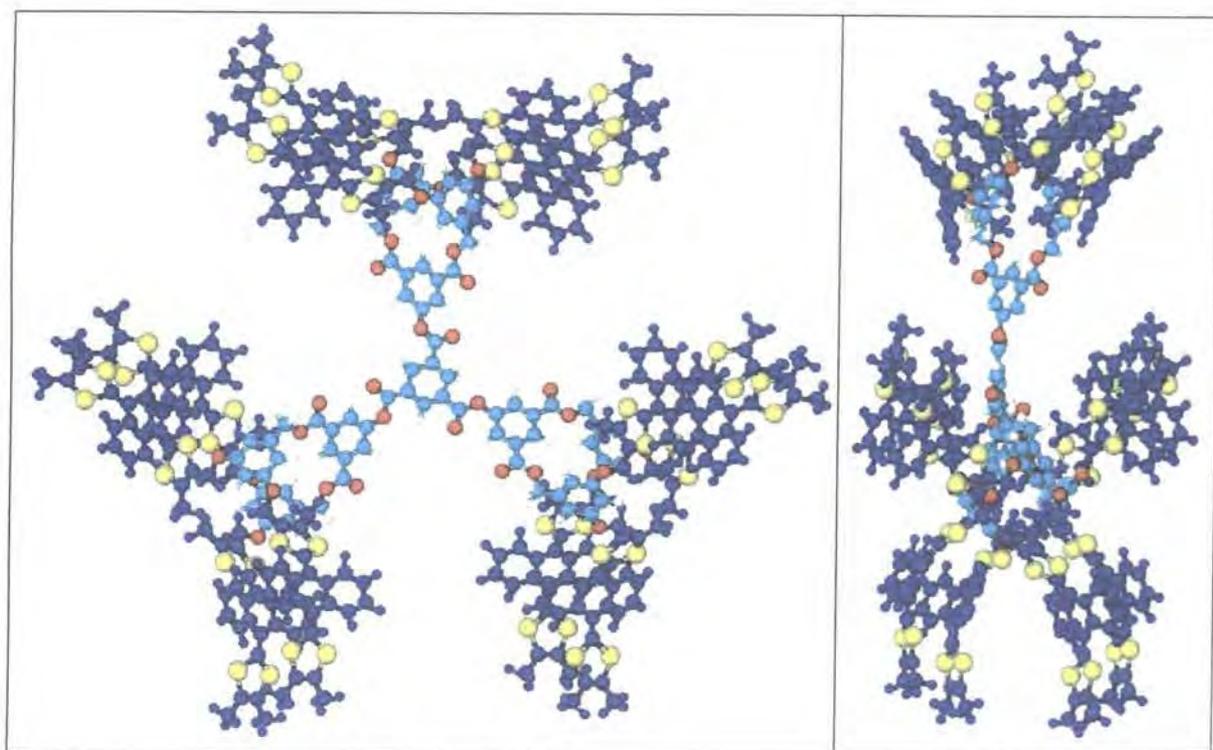
Figure 4.15 Molecular model of dendrimer **118**.
(views and colour codes as for *Figure 4.13*)
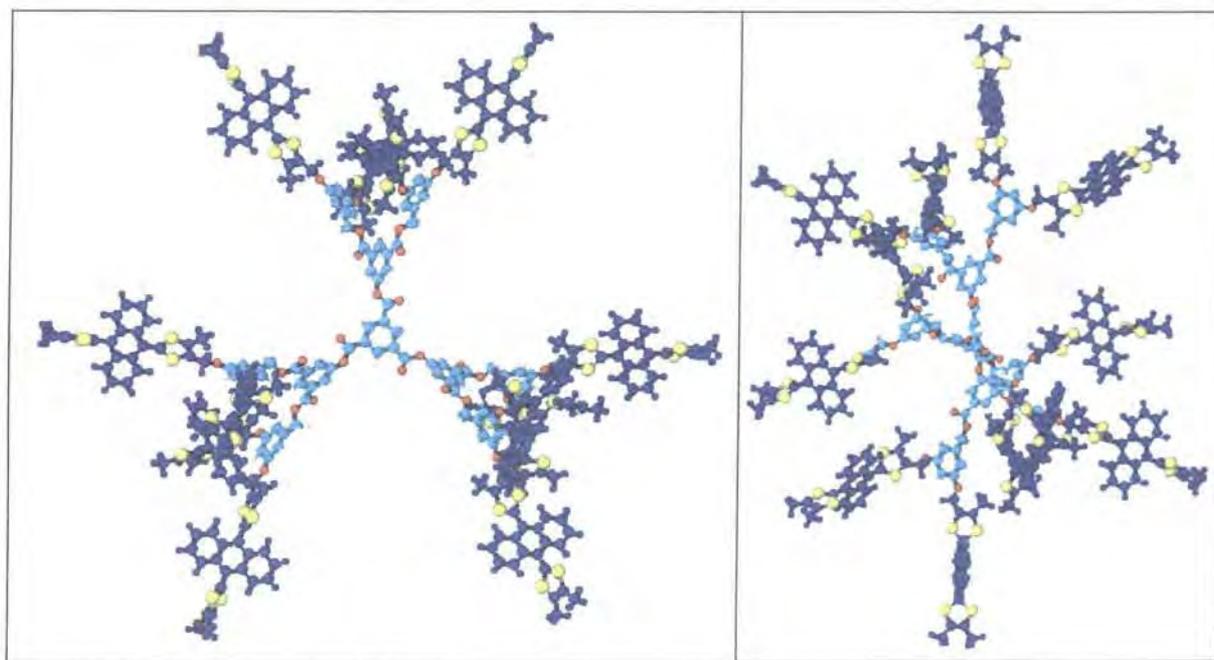
Figure 4.16 Molecular model of dendrimer **118^{24+}**.
(views and colour codes as for *Figure 4.13*)

4.3 Conclusion.

We have successfully synthesised and extensively characterised the first dendrimers to incorporate the anthracene-bis(dithiole) system, with 3, 6 and 12 of these redox units at the periphery using a convergent methodology with aryl ester and aryl ether units in the branches, joined to a 1,3,5-benzene triester core. These macromolecules possess well-defined redox activity, and the two-electron oxidation of each of the redox units affords species with high charge:molecular weight ratio. The structural properties of the anthracenediylidene derivatives, which undergo a dramatic change of conformation upon oxidation impart to these dendrimers unique properties. 1H NMR studies of dendrimer **118** suggest intramolecular interactions inside the dendritic structure between the units, which have been supported by molecular models. These interactions bestow to the dendrimer a more compact structure, which upon oxidation, due to Coulombic repulsion undergoes a global change of conformation simultaneously to the change of conformation of each unit. Consequently, the cavities inside the neutral and oxidised forms are completely different which opens the door to host-guest properties, which can be forecast for this class of nanoparticles. Charged organic nanoparticles of this type are also relevant to the miniaturisation of electronic materials.[41] The dendritic wedges synthesised during the course of this work, which possess reactive alcohol substituents, are available in synthetically useful quantities and should be amenable to other synthetic transformations to yield dendronised polymers or new systems which undergo multi-electron charge-transfer processes.

4.4 References.

(1)   Tomalia, D. A.; Naylor, A. M.; Goddard III, W. A. *Angew. Chem., Int. Ed. Engl.* **1990**, *29*, 138-175.

(2)   Newkome, G. R.; Moorefield, C. N.; Vögtle, F. *Dendritic molecules: concepts, synthesis, perspectives.*; VCH: Weinheim, 1996.

(3)   Bryce, M. R.; Devonport, W. *Advances in Dendritic Macromolecules* **1996**, *3*, 115-149.

(4)   Matthews, O. A.; Shipway, A. N.; Stoddart, J. F. *Prog. Polym. Sci.* **1998**, *23*, 1-56.

(5)   Fisher, M.; Vögtle, F. *Angew. Chem., Int. Ed. Engl.* **1999**, *38*, 884-905.

(6)   Bosman, A. W.; Janssen, H. M.; Meijer, E. W. *Chem. Rev.* **1999**, *99*, 1665-1688.

(7)   Newkome, G. R.; He, E.; Moorefield, C. N. *Chem. Rev.* **1999**, *99*, 1689-1746.

(8)   Adronov, A.; Fréchet, J. M. J. *Chem. Commun.* **2000**, 1701-1710.

(9)   Inoue, K. *Prog. Polym. Sci.* **2000**, *25*, 453-571.

(10)   Hecht, S.; Fréchet, J. M. J. *Angew. Chem., Int. Ed. Engl.* **2001**, *40*, 74-91.

(11)   Turrin, C. O.; Chiffre, J.; de Montauzon, D.; Daran, J.-C.; Caminade, A.-M.; Manoury, E.; Balavoine, G.; Majoral, J.-P. *Macromolecules* **2000**, *33*, 7328-7336.

(12)   Casado, C. M.; Cuadrado, I.; Morán, M.; Alonso, B.; Garciá, B.; Gonzáles, B.; Losada, J. *Coord. Chem. Rev.* **1998**, *185-186*, 53-79.

(13)   Losada, J.; Cuadrado, I.; Morán, M.; Casado, C. M.; Alonso, B.; Barranco, M. *Anal. Chim. Acta* **1997**, *338*, 191-198.

(14)   Nlate, S.; Ruiz, J.; Sartor, V.; Navarro, R.; Blais, J.-C.; Astruc, D. *Chem. Eur. J.* **2000**, *6*, 2544-2553.

(15)   Astruc, D. *Acc. Chem. Res.* **2000**, *33*, 287-298.

(16)   Dandliker, P. J.; Diederich, F.; Gross, M.; Knobler, C. B.; Louati, A.; Sanford, E. M. *Angew. Chem., Int. Ed. Engl.* **1994**, *33*, 1739-1742.

(17)   Dandliker, P. J.; Diederich, F.; Gisselbrecht, J. P.; Louati, A.; Gross, M. *Angew. Chem., Int. Ed. Engl.* **1995**, *34*, 2725-2728.

(18)   Bhyrappa, P.; Young, J. K.; Moore, J. S.; Suslick, K. S. *J. Am. Chem. Soc.* **1996**, *118*, 5708-5711.

(19)   Bhyrappa, P.; Young, J. K.; Moore, J. S.; Suslick, K. S. *J. Mol. Catal. A* **1996**, *113*, 109-116.

(20)   Kimura, M.; Shiba, T.; Muto, T.; Hanabusa, K.; Shirai, H. *Chem. Commun.* **2000**, 11-12.

(21)   Serroni, S.; Juris, A.; Venturi, M.; Campagna, S.; Resino, I. R.; Denti, G.; Credi, A.; Balzani, V. *J. Mater. Chem.* **1997**, *7*, 1227-1236.

(22)   Newkome, G. R.; Patri, A. K.; Godínez, L. A. *Chem. Eur. J.* **1999**, *5*, 1445-1451.

(23)   Gorman, C. B.; Smith, J. C.; Hager, M. W.; Parkhurst, B. L.; Sierzputowska-Gracz, H.; Habey, C. A. *J. Am. Chem. Soc.* **1999**, *121*, 9958-9966.

(24)   Devonport, W.; Bryce, M. R.; Marshallsay, G. J.; Moore, A. J.; Goldenberg, L. M. *J. Mater. Chem.* **1998**, *8*, 1361-1372.

(25)   Bryce, M. R.; Devonport, W. *Synth. Met.* **1996**, *76*, 305-307.

(26)   Christensen, C. A.; Goldenberg, L. M.; Bryce, M. R.; Becker, J. *J. Chem. Soc. Chem. Commun.* **1998**, 509-510.

(27)   Christensen, C. A.; Bryce, M. R.; Becher, J. *Synthesis* **2000**, *12*, 1695-1704.

(28)   Bryce, M. R.; Devonport, W.; Goldenberg, L. M.; Wang, C. *Chem. Commun.* **1998**, 945-951.

(29)   Bryce, M. R.; De Miguel, P.; Devonport, W. *J. Chem. Soc. Chem. Commun.* **1998**, 2565-2566.

(30)   Toba, R.; Quintela, J. M.; Peinador, C.; Román, E.; Kaifer, A. E. *Chem. Commun.* **2001**, 857-858.

(31)   Camps, X.; Dietel, E.; Hirsch, A.; Pyo, S.; Echegoyen, L.; Hackbarth, S.; Röder, B. *Chem. Eur. J.* **1999**, *5*, 2362-2373.

(32)   Tabakovic, I.; Miller, L. L.; Duan, R. G.; Tully, D. C.; Tomalia, D. A. *Chem. Mater.* **1997**, *9*, 736-745.

(33)   Christensen, J. B.; Nielsen, M. F.; J.A.E.H., v. H.; Baars, M. W. P. L.; Janssen, R. A. J.; Meijer, E. W. *Eur. J. Org. Chem.* **2001**, 2123-2128.

(34)   Miller, T. M.; Kwock, E. W.; Neeman, T. X. *Macromolecules* **1992**, *25*, 3143-3148.

(35)   Martín, N.; Perez, I.; Sanchez, L.; Seoane, C. *J. Org. Chem.* **1997**, *62*, 870-877.

(36)   Hawker, C.; Fréchet, J. M. J. *J. Chem. Soc. Chem. Commun.* **1990**, 1011-1013.

(37)   Jones, A. E.; Christensen, C. A.; Perepichka, D. F.; Batsanov, A. S.; Beeby, A.; Low, P. J.; Bryce, M. R.; Parker, A. W. *Chem. Eur. J.* **2001**, *5*, 973-978.

(38)   Bryce, M. R.; Moore, A. J.; Hasan, M.; Ashwell, G. J.; Fraser, A. T.; Clegg, W.; Hursthouse, M. B.; Karaulov, A. I. *Angew. Chem., Int. Ed. Engl.* **1990**, *29*, 1450-1452.

(39)   Bryce, M. R.; Finn, T.; Moore, A.; Batsanov, A. S.; Howard, J. A. K. *Eur. J. Org. Chem.* **2000**, 51-60.

(40)   Martín, N.; Sánchez, L.; Seoane, C.; Ortí, E.; Viruela, P. M.; Viruela, R. *J. Org. Chem.* **1998**, *63*, 1268-1279.

(41)   Simon, U. *Adv. Mater.* **1998**, *10*, 1487-1492.

Chapter Five

Experimental Details.

5.1 General Equipments and Procedures.

^{1}H and ^{13}C NMR spectra were obtained on Oxford 200, Varian Unity 300 and Varian VXR 400S spectrometers operating at 199.992 (^{1}H) and 50.293 (^{13}C), 299.908 (^{1}H) and 75.420 (^{13}C), and 400.0 (^{1}H) and 100.6 (^{13}C) MHz, respectively.

Mass spectra were recorded on a Micromass Autospec spectrometer operating at 70 eV.

MALDI TOF mass spectra were obtained on a Kratos IV instrument in the reflection mode, operating with irradiation from a nitrogen laser at 337 nm. The matrix was 2,5-dihydroxybenzoic acid, and spectra were averaged over 100 pulses whilst scanning across the sample: peak half-widths were between 6-10 amus.

Infra-red spectra were recorded using KBr disks on a Perkin Elmer 1600 FTIR, spectrometer operated from a Grams Analyst 1600.

Electronic absorption spectra were obtained using a Perkin Elmer II UV-vis spectrophotometer operating with 1 mL quartz cells.

Melting points were obtained on a Philip Harris melting point apparatus and are uncorrected.

Cyclic voltammetric data were measured with iR compensation using a BAS CV50 electrochemical analyser. The experiments were carried out with 3 mL of a *ca.* 10^{-4} M solution of the compound in dichloromethane containing 0.1M tetrabutylammonium perchlorate as the electrolyte, at scan rate 100 mV s^{-1} (unless specified otherwise). The oxidation potentials were measured *versus* a platinum wire quasi-reference electrode and corrected *versus* decamethylferrocene/decamethylferrocenium$^+$ by adding decamethylferrocene to the studied solution after the experiment, and referenced *versus* Ag/AgCl.

Structures were modelled and optimised in the gas phase and without consideration of the counter ions using the MM+ program Hyperchem 5.0: Hyperchem, Inc., 1115 NW 4th Street, Gainesville, FL 32601 (USA) (See Appendix Two).

Column chromatography was carried out using Merck silica gel (70-230 mesh) and solvents were distilled prior to use in column chromatography.

All reactions were performed under an inert atmosphere of nitrogen in pre-dried glassware.

5.2 Experimental Procedures for Chapter Two.

10-(4,5-Dimethyl-1,3-dithiol-2-ylidene)- 9,10-dihydro-9-(4-hydroxymethyl-5-methyl-1,3-dithiol-2-ylidene)anthracene (47):
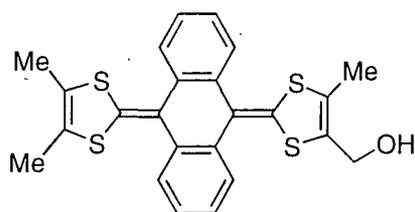
47

To a stirred solution of 9-(4-methyloxycarbonyl-5-methyl-1,3-dithiol-2-ylidene)-10-(4',5'-dimethyl-1',3'-dithiol-2'-ylidene)-9,10-dihydroanthracene **26**[1] (3.00 g , 6.25 mmol) in dry THF under N_2 at 0°C was added dropwise lithium aluminium hydride (1.00 g, 26.38 mmol) and the resultant mixture was stirred for 1 h at 0°C and 2 h at room temperature. After adding dropwise wet sodium sulphate (in excess), the reaction mixture was stirred for 1 h, during which time the solution changed from green to orange. The reaction mixture was filtered through Celite. After evaporation, the residue was chromatographed on a silica column eluting with dichloromethane to afford **47** (2.55 g,

90%). Recrystallisation, if required, may be achieved by dissolution in dichloromethane and addition of hexane. M.p. >250 °C. ^{1}H NMR (DMSO-d$_6$): δ = 7.56-7.54 (m, 4H) 7.34-7.30 (m, 4H) 4.20 (dd, J_{AB}= 13 Hz, 2H) 1.95 (s, 3H) 1.92 (s, 6H). IR (KBr): ν = 3400 (*br.*), 1514, 1512, 1452, 1446, 755, 644 cm^{-1}. UV/Vis (CH$_2$Cl$_2$): λ_{max} (logε) 368 (4.03), 436 (4.30) nm. MS (EI): m/z (%) 452 (100) [M$^+$]. C$_{24}$H$_{20}$OS$_4$ (452.7): calcd. C 63.68, H 4.45; found C 63.39, H 4.50.

9-(4-5-Dimethyl-1,3-dithiol-2-ylidene)-9,10-dihydro-10-(4-methoxycarbonyl-1,3-dithiol-2-ylidene)anthracene (49)
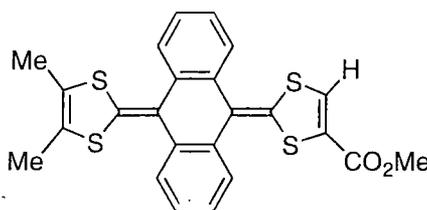
49

To a stirred solution of **48**^{2} (0.5 g, 1.22 mmol) in dry THF (30 mL), under N$_2$, at $-$78°C was added lithium diisopropylamide monotetrahydrofuran (*ca.* 1.5 M in cyclohexane, 0.9 ml, 1.35 mmol). The reaction mixture was stirred at $-$78°C during 2 h. Methyl chloroformate (0.18 ml, 2.44 mmol) was then added and the mixture was stirred and left to warm to 20°C overnight. Solvents were removed in vacuo and the residue was purified by chromatography on silica gel with DCM/Hexane (1:1 v/v) as eluent to afford **49** (0.19 g, 40%) as an orange solid, separated from unchanged **48** and traces of **50**. M.p. 180-182 °C. ^{1}H NMR (CDCl$_3$): δ (ppm) = 7.7-7.5 (m, 4H), 7.4-7.2 (m, 4H+1H), 3.79 (s, 3H), 1.93 (s, 6H). IR (KBr): ν = 1712, 1564, 1517, 1457, 1445, 1251, 1056, 754, 674, 643 cm^{-1}. UV/Vis (CH$_2$Cl$_2$): λ_{max} (logε) 360 (4.08), 428 (4.31) nm. MS (EI): m/z (%) 466 (100) [M$^+$]. C$_{24}$H$_{18}$O$_2$S$_4$ (466.7): calcd. C 61.77, H 3.89; found C 62.07, H 4.09.

10-[4,5-Di(methoxycarbonyl)-1,3-dithiol-2-ylidene]-9-(4-5-dimethyl-1,3-dithiol-2-ylidene)-9,10-dihydroanthracene (50)
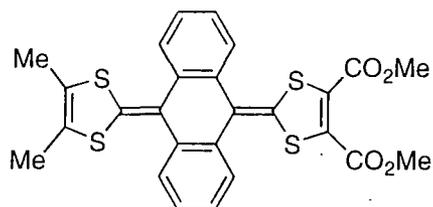
50

To a stirred solution of **48**[2] (210 mg, 0.51 mmol) in dry THF (15 mL), under N_2, at –78°C was added lithium bis(trimethylsilyl)amide (*ca.* 1.06 M in THF, 2 ml, 2.04 mmol). The reaction mixture was stirred at –78 °C during 2 h. Methyl chloroformate (0.16 mL, 2.04 mmol) was then added. Workup and purification as described above for **49**, gave **50** (0.26 g, 96%) as an orange-red solid. M.p. >250 °C. ^{1}H NMR (CDCl$_3$): δ (ppm) = 7.7-7.6 (m, 2H), 7.5-7.4 (m, 2H), 7.3-7.2 (m, 4H), 3.81 (s, 6H), 1.93 (s, 6H). IR (KBr): ν = 1739, 1718, 1583, 1512, 1454, 1444, 1259, 755, 675, 644 cm^{-1}. UV/Vis (CH$_2$Cl$_2$): λ$_{max}$ (logε) 356 (4.19), 428 (4.40) nm. MS (EI): m/z (%) 524 (40) [M$^+$]. C$_{26}$H$_{20}$O$_4$S$_4$ (524.7): calcd. C 59.52, H 3.84; found C 59.26, H 3.79.

10-[4,5-Di(hydroxymethyl)-1,3-dithiol-2-ylidene]-9-(4-5-dimethyl-1,3-dithiol-2-ylidene)-9-10-dihydroanthracene (51)
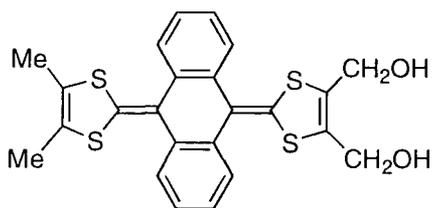
51

Following the same procedure as for compound **47**, compound **50** (200 mg, 0.38 mmol) and lithium aluminium hydride (0.11 g, 3 mmol) afforded **51** (180 mg, 95%) as a orange solid. Recrystallisation from dichloromethane/methanol gave purple prisms

suitable for X-Ray analysis. M.p. >250 °C. ^{1}H NMR (DMSO-d$_6$): δ (ppm) = 7.6-7.5 (m,

4H) 7.4-7.3 (m, 4H), 5.42 (t, $J_{OH,H}$ = 5.5Hz, 2H), 4.27 (dd, J_{AB} = 13.5 Hz, $J_{H, OH}$ = 5.5 Hz,

2H), 4.19 (dd, J_{AB} = 13.5 Hz, $J_{H, OH}$ = 5.5 Hz, 2H), 1.93 (s, 6H). IR (KBr): ν = 3400 (br.),

1519, 1443, 1279, 755, 675, 644 cm^{-1}. UV/Vis (CH$_2$Cl$_2$): λ$_{max}$ (logε) 364 (4.14), 432 (4.40)

nm. MS (EI): m/z (%) 468 (49) [M$^+$], 450 (100). C$_{24}$H$_{20}$O$_2$S$_4$ (468.7): calcd. (+ 0.5mol of

H$_2$O) C 60.34, H 4.43; found C 60.22, H 4.26.

10-(4,5-Dimethyl-1,3-dithiol-2-ylidene)-9,10-dihydro-9-(5-methyl-4-phenyl carbonyloxymethyl-1,3-dithiol-2-ylidene)anthracene (52)
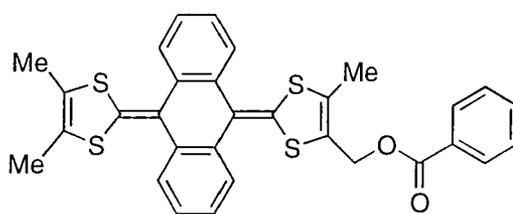
52

To a stirred solution of alcohol **47** (100 mg, 0.22 mmol) in dry dichloromethane (10

mL) under N$_2$ at room temperature was added benzoyl chloride (26 µl, 0.22 mmol) and

triethylamine (61µL, 0.44 mmol). The resultant mixture was stirred during 2 h. After

evaporation, the residue was chromatographed on silica eluting with dichloromethane to

give **52** as an orange powder (122 mg, 99%). An orange prism suitable for X-ray structural

analysis was obtained by recrystallisation from dichloromethane. M.p. 228-231 °C. ^{1}H

NMR (CDCl$_3$): δ (ppm) = 8.0 (dd, J = 7 Hz, J = 1 Hz, 2H) 7.6 (m, 4H) 7.55 (tt, J = 7.5 Hz,

J = 1 Hz, 1H) 7.4 (dd, J = 7 Hz, J = 7.5 Hz, 2H) 7.2 (m, 4H) 5.04 (d, J_{AB} = 13 Hz, 1H) 5.01

(d, J_{AB} = 13 Hz, 1H) 2.11 (s, 3H) 1.92 (s, 6H). IR (KBr): ν = 1724, 1512, 1456, 1444,

1262, 754, 709 cm^{-1}. UV/Vis (CH$_2$Cl$_2$): λ$_{max}$ (logε) 368 (4.15), 436 (4.41) nm. MS (EI):

m/z (%) 556 (48) [M$^+$], 436 (100). C$_{31}$H$_{24}$O$_2$S$_4$ (556.8): calcd. C 66.65; H 4.21; found C

66.87; H 4.34.

10-(4,5-Dimethyl-1,3-dithiol-2-ylidene)-9,10-dihydro-9-(5-methyl-4-(2-naphthyl) carbonyloxymethyl-1,3-dithiol-2-ylidene)anthracene (53)
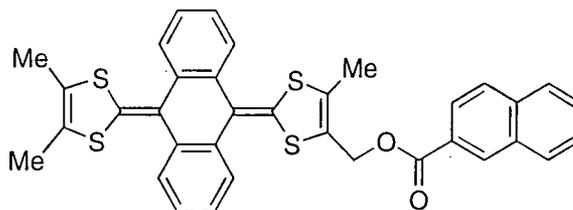
53

Following the same procedure as for compound **52**, alcohol **47** (52 mg, 0.11 mmol), 2-naphthaloyl chloride (22 mg, 0.11 mmol) and triethylamine (32 μL, 0.22 mmol) in dichloromethane (10 mL) were stirred during 2h, under N_2, at room temperature. After evaporation and chromatography (dichloromethane as eluent), recrystallisation from dichloromethane/hexane gave **53** (47 mg, 67%) as orange prisms suitable for X-ray analysis. Mp: 176-178 °C. ^{1}H NMR (CDCl$_3$): δ (ppm) = 8.60 (s, 1H) 8.0-7.7 (m, 4H) 7.6-7.3 (m, 6H) 7.2 (m, 4H) 5.07 (d, J_{AB} = 13 Hz, 1H) 5.03 (d, J_{AB} = 13 Hz, 1H) 2.12 (s, 3H) 1.87 (s, 6H). IR (KBr): 1716, 1523 1456 1444 1279 1192 777 755 cm^{-1}. UV/Vis (CH$_2$Cl$_2$): λ_{max} (logε) 368 (4.09), 436 (4.35) nm. MS (EI): m/z (%) 606 (87) [M$^+$], 127 (100). $C_{35}H_{26}O_2S_4$ calcd. (+ 1 mole of CH$_2$Cl$_2$) C 62.50, H 4.08; found C 62.33, H 3.98.

9-(4-(2-Anthraquinoyl)-carbonyloxymethyl-5-methyl-1,3-dithiol-2-ylidene)-9,10-dihydro-10-(4,5-dimethyl-1,3-dithiol-2-ylidene)anthracene (54)
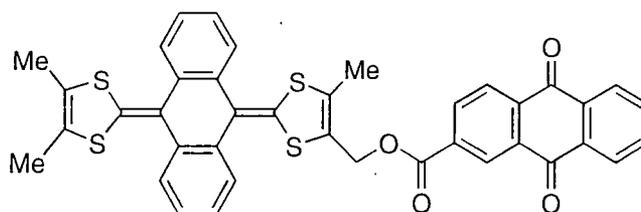
54

Following the same procedure as for compound **52**, alcohol **47** (300 mg, 0.66 mmol), anthraquinone-2-carbonyl chloride (180 mg, 0.66 mmol) and triethylamine (192 µL, 1.32 mmol) in dichloromethane (30 mL) were stirred during 2h, under N_2, at room temperature. After evaporation and chromatography (dichloromethane as eluent), recrystallisation from dichloromethane/hexane gave **54** (430 mg, 96%) as a black-green crystalline powder. Mp: 216-218 °C. ^{1}H NMR (CDCl$_3$): δ (ppm) = 8.95 (s, 1H) 8.4-8.2 (m, 4H) 7.9-7.8 (m, 2H) 7.6-7.5 (m, 4H) 7.3-7.2 (m, 4H) 5.1 (s, 2H) 2.15 (s, 3H) 1.90 (s, 6H). IR (KBr): 1727, 1677 1594 1516 1443 1268 1237 755 705 cm^{-1}. UV/Vis (CH$_2$Cl$_2$): λ_{max} (logε) 368 (4.07), 436 (4.31) nm. MS (EI): m/z (%) 686 (100) [M$^+$]. C$_{39}$H$_{26}$O$_4$S$_4$ (686.89) HRMS: 686.0782 (calcd. 686.0714)

5.3 Experimental Procedures for Chapter Three.

(E, Z)-9,10-Bis(4-methyl-1,3-dithiol-2-ylidene)-9,10-dihydroanthracene (**74**).
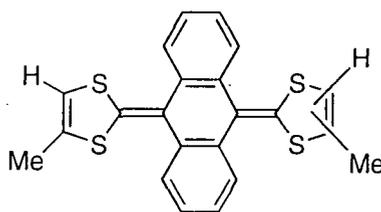
74 (E/Z)

Compound **73**[1] (5.11 g, 22.3 mmol) was dissolved in dry tetrahydrofuran (100 mL), under N_2, at -78°C and a solution of lithium diisopropylamide 1.5M (16.4 mL, 24.6 mmol) was added dropwise. The mixture was stirred at –78°C during 1 h then anthraquinone (2.32 g, 11 mmol) was added and the mixture was left to warm at room temperature overnight. After evaporation of solvent, the crude residue was chromatographed on a silica column

(eluent: dichloromethane/hexanes (1:1 v/v)) to afford **74** (3.34 g, 73%) as a yellow solid. (The coproduct of the reaction is the monoWittig adduct which can be easily separated from **74** during chromatography). M.p. 239-240 °C. ^{1}H NMR (CDCl$_3$): δ (ppm) = 7.70-7.64 (m, 4H) 7.30-7.23 (m, 4H) 5.82 (dd, J = 1.5 Hz, 2H) 2.05 (dd, J = 1.5 Hz, 6H). IR (KBr): ν = 1518, 1455, 1441, 1279, 755, 642 cm^{-1}. UV/Vis (CH$_2$Cl$_2$): λ_{max} (logε) 368 (4.05), 432 (4.29) nm. MS (EI): m/z (%) 408 (100) [M$^+$]. C$_{22}$H$_{16}$S$_4$ (408.63) calcd. C 64.66, H 3.95; found C 64.83; H 4.02.

(E,Z)-9,10-Bis[(4-methyloxycarbonyl-5-methyl)-1,3-dithiol-2-ylidene]-9,10-dihydroanthracene (75a).
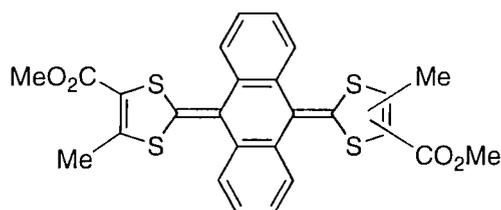
75a (E/Z)

To a stirred solution of **74** (3 g, 73.5 mmol) in dry tetrahydrofuran (250 mL), under N$_2$, at - 78°C was added dropwise a solution of lithium diisopropylamide 1.5M (10.8 mL, 162 mmol). The mixture was stirred at −78 °C during 2 h then methylchloroformate (3.42 mL, 440 mmol) was added. The mixture was left to warm at room temperature overnight. After evaporation of solvent in vacuo, the residue was chromatographed on a silica column (eluent dichloromethane/hexanes (1:3, then 1:1 v/v)) to afford **75a** (2.36 g, 61%) as a yellow solid. (The coproducts of the reaction are the monoester **75b** and the unchanged **74** which can be easily separated from **75a** during chromatography). M.p. 152-154 °C. ^{1}H NMR (CDCl$_3$): δ (ppm) = 7.63-7.55 (m, 4H) 7.33-7.25 (m, 4H) 3.77 (s, 6H) 2.38 (s, 6H). IR (KBr): ν = 1716, 1696, 1585, 1523, 1445, 1432, 1292, 1241, 1062, 755, 644 cm^{-1}.

UV/Vis (CH$_2$Cl$_2$): λ_{max} (logϵ) 356 (4.04), 420 (4.26) nm. MS (EI): m/z (%) 524 (100) [M$^+$].

C$_{26}$H$_{20}$O$_4$S$_4$ (524.70) calcd. C 59.52; H 3.84; found C 59.14; H 3.87.

(E,Z)-9-(4-Methyl-1,3-dithiol-2-ylidene)-10-[(4-methyloxycarbonyl-5-methyl)-1,3-dithiol-2-ylidene]-9,10-dihydroanthracene (75b).
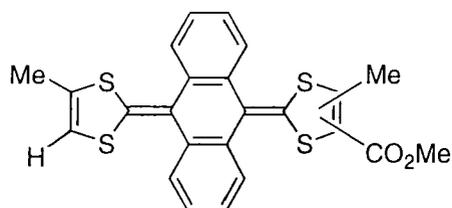
75b (E/Z)

Compound **75b** was obtained as a side product of the preceding reaction and isolated during chromatography on silica gel (See experimental procedure for compound **75a**). M.p. 171-174 °C. ^{1}H NMR (CDCl$_3$): δ (ppm) = 7.7-7.5 (m, 4H), 7.4-7.2 (m, 4H), 5.85 (s, 1H), 3.77 (s, 3H), 2.37 (s, 3H) 2.05 (s, 3H). IR (KBr): ν = 1712, 1565, 1515, 1457, 1445, 1249, 1053, 754, 643 cm^{-1}. UV/Vis (CH$_2$Cl$_2$): λ_{max} (logϵ) 360 (4.05), 428 (4.33) nm. MS (EI): m/z (%) 466 (100) [M$^+$]. C$_{24}$H$_{18}$O$_2$S$_4$ (466.66): calcd. C 61.77, H 3.89; found C 62.04, H 3.92.

(E, Z)-9,10-Bis[(4-hydroxymethyl-5-methyl)-1,3-dithiol-2-ylidene]-9,10-dihydro anthracene (76).
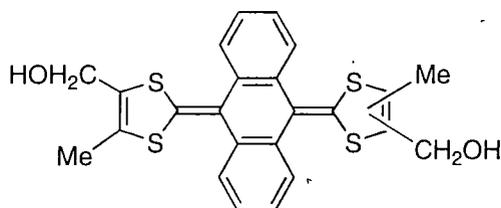
76 (E/Z)

Following the same procedure as for compound **47**, **76** was obtained by reduction of **75a** (2.0 g, 3.8mmol), in dry THF (200 mL) and lithium aluminium hydride (1.15 g, 30.4 mmol). The chromatography was achieved using ethyl acetate as eluent, to afford **76** (1.45 g, 82%). M.p >250 °C. ^{1}H NMR (CDCl$_3$): δ (ppm) = 7.64-7.57 (m, 4H) 7.31-7.28 (m, 4H) 4.38 (s, 4H) 2.00 (s, 6H). IR (KBr): ν = 3407 (*br.*), 1513, 1457, 1445, 1283, 997, 756, 675, 645 cm^{-1}. UV/Vis (CH$_2$Cl$_2$): λ_{max} (logε) 368 (4.09), 432 (4.31) nm. MS (EI): m/z (%). 468 (100) [M$^+$]. C$_{24}$H$_{20}$O$_2$S$_4$ (468.68): calcd C, 61.50; H, 4.30; found C, 61.82; H, 4.60.

Benzyl cyclophane (78a)
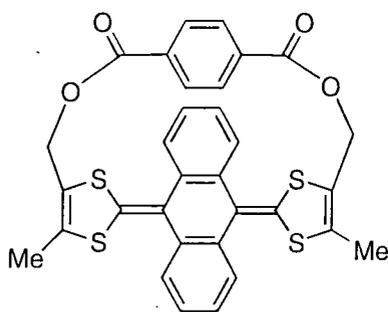
78a

To a solution of **76** (300 mg, 0.64 mmol), in dry dichloromethane (300 mL), were added 1,4-benzenedicarbonyl chloride (130 mg, 0.64 mmol) and triethylamine (0.36 mL, 2.56 mmol) and the mixture was stirred at 20°C for 2 h. After evaporation in vacuo, the residue was chromatographed on silica with dichloromethane as eluent to give **78a** as a yellow solid. Recrystallisation from dichloromethane/hexanes afforded **78a** (42 mg, 11%). Mp. *ca.* 250 °C (decomp.). ^{1}H NMR (CDCl$_3$): δ (ppm) = 7.88 (s, 4H) 7.60-7.59 (m, 2H) 7.38-7.36 (m, 2H) 7.34-7.32 (m, 2 H) 7.26-7.2 (m, 2H) 5.70 (d, 2H, J = 13 Hz, H$_a$) 4.43 (d, 2H, J = 13 Hz, H$_b$) 2.05 (s, 6H). IR (KBr): ν = 1725, 1528, 1457, 1446, 1261, 1055, 756, 644 cm^{-1}. UV/Vis (CH$_2$Cl$_2$): λ_{max} (logε) 356 (4.17), 420 (4.41) nm. MS (EI): m/z (%) 598 (100) [M$^+$]. C$_{32}$H$_{22}$O$_4$S$_4$ (598.78) calcd C, 64.19; H, 3.70; found C, 63.90; H, 3.94.

Thienyl cyclophane (78b)

78b
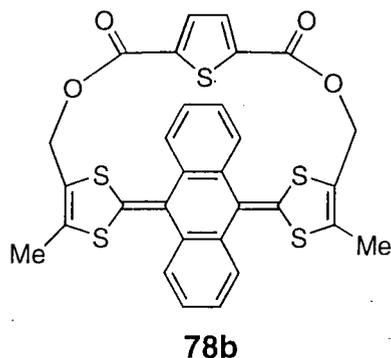
Following the same procedure as for compound **78a**, **78b** was obtained by double esterification of **76** (300 mg, 0.64 mmol), in dry dichloromethane (300 mL) with 1,3-thiophenedicarbonyl chloride (134 mg, 0.64 mmol) and triethylamine (0.36 mL, 2.56 mmol). The chromatography was achieved using dichloromethane as eluent. Recrystallisation was achieved by dissolving **78b** in dichloromethane and adding hexanes to afford **78b** (32 mg, 8%) as yellow crystals. Mp. *ca.* 200 °C (decomp.). ^{1}H NMR (CDCl$_3$): δ (ppm) = 7.65 (s, 2H) 7.53-7.49 (m, 2H) 7.37-7.28 (m, 6H) 5.12 (d, 2H, *J* = 13 Hz, Ha) 4.61 (d, 2H, *J* = 13 Hz, Hb) 2.06 (s, 6H). IR (KBr): ν = 1719, 1528, 1457, 1446, 1236, 1091, 756, 646 cm^{-1}. UV/Vis (CH$_2$Cl$_2$): λ_{max} (logε) 356 (4.17), 420 (4.41) nm. MS (EI): m/z (%) 604 (100) [M$^+$]. C$_{30}$H$_{20}$O$_4$S$_5$ (604.81) HRMS: 604.00487 (calcd. 686.00497).

Ferrocenyl cyclophane (78c)

78c
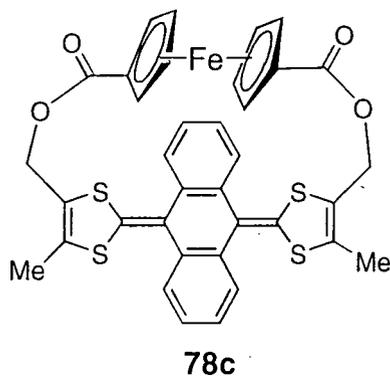
Following the same procedure as for compound **78a**, **78c** was obtained by double esterification of **76** (300 mg, 0.64 mmol), in dry dichloromethane (300 mL) with 1,1'-ferrocenedicarbonyl chloride[3] (184 mg, 0.64 mmol) and triethylamine (0.36 mL, 2.56 mmol). The chromatography was achieved using dichloromethane as eluent, and recrystallisation was achieved from dichloromethane/hexanes to afford **78c** (62 mg, 14%) as yellow crystals. Mp. *ca.* 230 °C (decomp.). ^{1}H NMR (CDCl$_3$): δ (ppm) = 7.50-7.48 (m, 2H) 7.39-7.37 (m, 4H) 7.29-7.27 (m, 2H) 4.87 (d, J = 13 Hz, 2 H) 4.74-4.72 (m, 4H) 4.71 (d, *J* = 13 Hz, 2H) 4.60-4.58 (m, 2H) 4.34-4.28 (m, 4H) 2.07 (s, 6H). IR (KBr): ν = 1713, 1458, 1272, 1183, 1144, 1, 752 cm^{-1}. UV/Vis (CH$_2$Cl$_2$): λ$_{max}$ (logε) 356 (4.13), 420 (4.28) nm. MS (EI): m/z (%) 706 (21) [M$^+$]. C$_{36}$H$_{26}$FeO$_4$S$_4$ HRMS: 706.01316 (calcd. 706.01305).

Oxobisphenyl cyclophane (78d)

78d
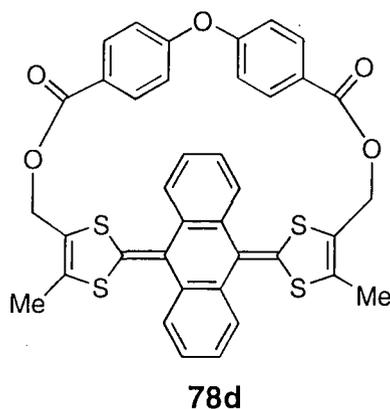
Following the same procedure as for compound **78a**, **78d** was obtained by double esterification of **76** (300 mg, 0.64 mmol), in dry dichloromethane (300 mL) with 4,4'-oxybis(carbonyl chloride) (190 mg, 0.64 mmol) and triethylamine (0.36 mL, 2.56 mmol). The chromatography was achieved using dichloromethane as eluent, and recrystallisation was achieved from dichloromethane/hexanes to afford **78d** (66 mg, 15%) as yellow crystals. M.p. 194-196 °C. ^{1}H NMR (CDCl$_3$): δ (ppm) = 7.9 (d, J = 7 Hz, 4H) 7.66-7.62

(m, 4H) 7.29-7.26 (m, 4H) 6.86 (d, J = 7 Hz, 4H) 5.37 (d, J = 13 Hz, 2 H) 4.65 (d, J= 13 Hz, 4H) 2.12 (s, 6H). IR (KBr): ν = 1720, 1593, 1518, 1497, 1457, 1444, 1260, 1217, 1091, 1068, 755, 735, 644 cm^{-1}. UV/Vis (CH$_2$Cl$_2$): λ_{max} (logε) 368 (4.10), 440 (4.38) nm. C$_{38}$H$_{26}$O$_5$S$_4$ (690.87) HRMS: 690.07300 (calcd. 690.07307).

5.4 Experimental Procedures for Chapter Four.

Dimer 105.
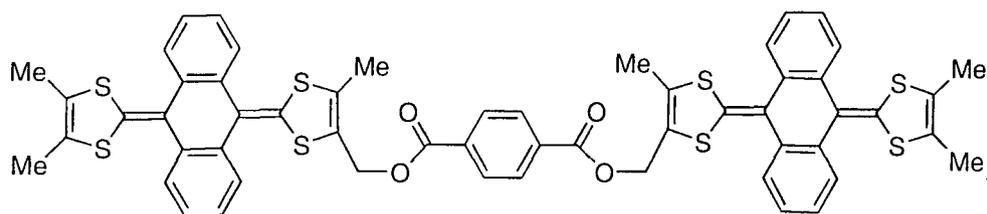
105

To a stirred solution of alcohol **47** (55 mg, 0.12 mmol) in dry dichloromethane (10 mL) under N$_2$ at room temperature was added terephthaloyl chloride (12.4 mg, 0.06 mmol) and triethylamine (34 µl, 0.24 mmol). The resultant mixture was stirred during 2 h. After evaporation, the residue was chromatographed on silica eluting with dichloromethane to give **105** as an orange powder (122 mg, 99%). Mp: 250 °C (darkening at 220°C). ^{1}H NMR (CDCl$_3$): δ (ppm) = 8.02 (s, 4H) 7.5 (m, 8H) 7.2 (m, 8H) 4.96 (d, J_{AB} = 13 Hz, 2H), 4.92 (d, J_{AB} = 13 Hz, 2H) 2.03 (s, 6H) 1.82 (s, 12H). IR (KBr): ν = 1721, 1520, 1455, 1444, 1261, 1242, 1096, 755, 644 cm^{-1}. UV/Vis (CH$_2$Cl$_2$): λ_{max} (logε) 368 (4.12), 436 (4.31) nm. MS (MALDI-TOF): M$^+$ = 1035. C$_{56}$H$_{42}$O$_4$S$_8$ (1035.46) calcd. C 64.96, H 4.09; found C 65.13, H 4.35.

Trimer 106

106
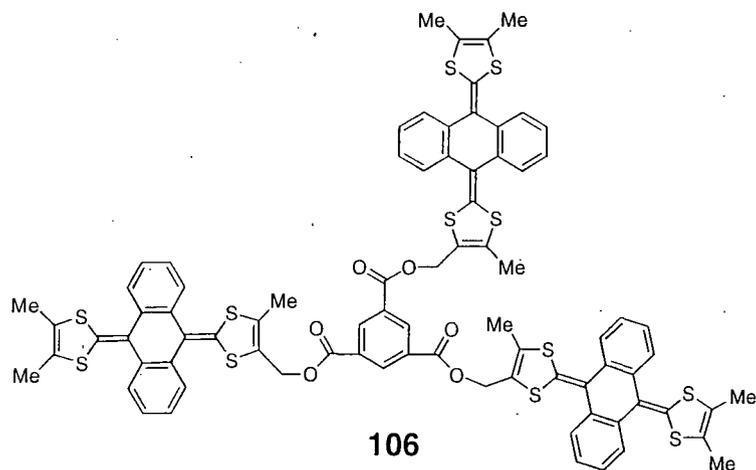
Following the same procedure as for compound **105**, **106** was obtained by triple esterification of **47** (80 mg, 0.18 mmol), in dry dichloromethane (30 mL) with 1,3,5-benzenetricarbonyl trichloride (15.6 mg, 0.06 mmol) and triethylamine (49 μL, 0.36 mmol). The chromatography was achieved using dichloromethane as eluent to afford **106** (70 mg, 78%) as an orange solid. Mp>250 °C. ^{1}H NMR (CDCl$_3$): δ (ppm) = 8.77 (s, 3H) 7.5 (m, 12H) 7.2 (m, 12H) 4.96 (m, 6H) 2.02 (s, 9H) 1.79 (s, 18H). IR (KBr): ν = 1734, 1444, 1223, 755, 644 cm^{-1}. UV/Vis (CH$_2$Cl$_2$): λ_{max} (logε) 368 (4.05), 436 (4.31) nm. MS (MALDI-TOF): M$^+$ = 1514. C$_{81}$H$_{60}$O$_6$S$_{12}$ (1514.13) calcd. (with 1 mol. of CH$_2$Cl$_2$) C 61.59, H 3.91; found C 61.77, H 3.92.

133

Dendron wedge 108.

108
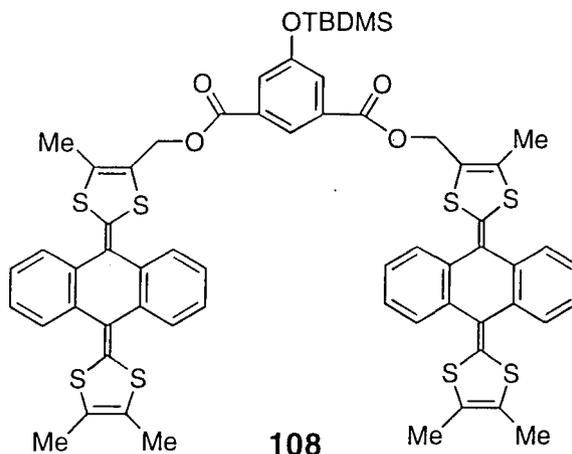
To a stirred solution of alcohol **47** (800 mg, 1.77 mmol) in dry dichloromethane under N_2 at room temperature was added dichloride **107**[4] (320 mg, 0.885 mmol) and triethylamine (0.5 mL, 3.54 mmol). The resultant mixture was stirred overnight. After evaporation of the solvents in vacuo, the residue was purified by chromatography on silica gel eluting with dichloromethane to afford the **108** (1.00 g, 97%) as an orange solid. Mp: 213-215 °C, ^{1}H NMR (CDCl$_3$): δ (ppm) = 8.26 (s, 1H) 7.6 (m, 10H) 7.2 (m, 8H) 5.01 (s, 4H) 2.09 (s, 6H) 1.88 (s, 12H) 0.98 (s, 9H) 0.20 (s, 6H). IR (KBr): ν = 1727, 1521, 1445, 1219, 755, 675, 644 cm^{-1}. UV/Vis (CH$_2$Cl$_2$): λ_{max} (lgε) 368 (4.33), 436 (4.58). MS (MALDI-TOF): M+ = 1164. C$_{62}$H$_{56}$O$_5$S$_8$Si (1164.17): calcd. C 63.88, H 4.84; found C 63.76, H 5.01.

Dendron wedge 119.

109

134
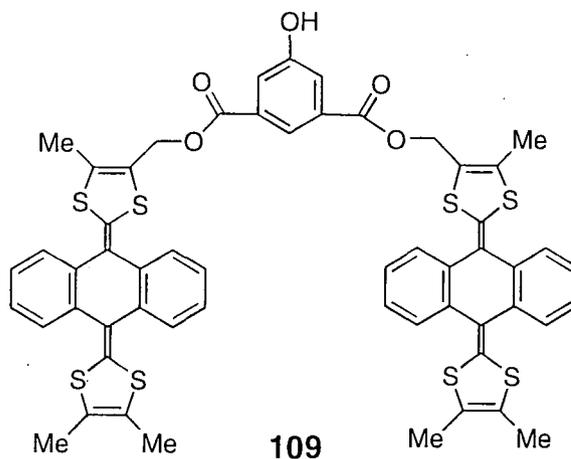
To a stirred solution of **108** (200 mg, 0.17 mmol) in dry THF under N_2 at room temperature was added tetrabutylammonium fluoride (1M in THF, 0.17 mL, 0.17 mmol). The resultant mixture was stirred during 1 h. The solvents were removed by evaporation in vacuo and the residue was purified by chromatography on silica gel with dichloromethane containing 2 % of methanol as eluent, to afford **109** (178 mg, 99%) as an orange solid. Mp>250 °C. ^{1}H NMR (CDCl$_3$): δ (ppm) = 8.24 (s, 1H) 7.6 (m, 10H) 7.2 (m, 8H) 5.01 (s, 4H) 2.09 (s, 6H) 1.89 (s, 12H). IR (KBr): ν = 3500 (br.), 1727, 1521, 1445, 1219, 755, 675, 645 cm^{-1}. UV/Vis (CH$_2$Cl$_2$): λ_{max} (lgε) 368 (4.39), 436 (4.63). MS (MALDI-TOF): M+ = 1050. C$_{56}$H$_{42}$O$_5$S$_8$, (1051.46): calcd. C 63.97, H 4.03; found C 63.72, H 4.04.

Dendrimer 110.

110

135
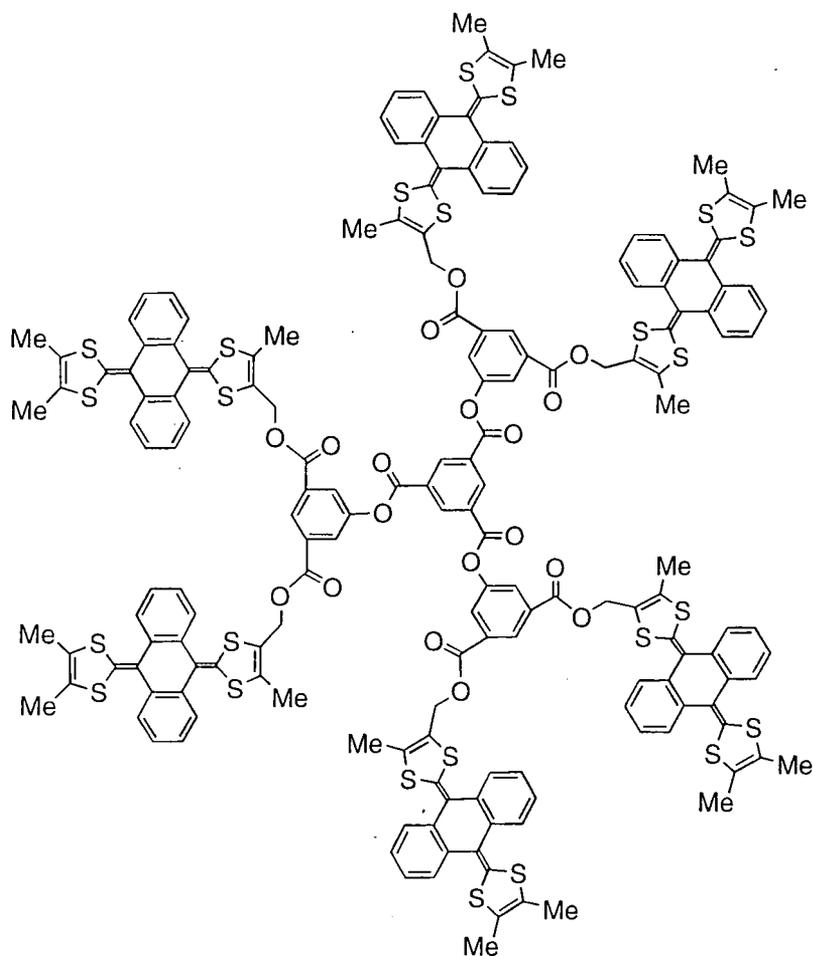
By analogy with the preparation of **108**, alcohol **109** (100 mg, 0.1 mmol), 1,3,5-benzenetricarbonyl trichloride (8.4 mg, 0.033 mmol) and triethylamine (26 µl, 0.2 mmol) in dry dichloromethane (20 mL) were stirred under N_2 at room temperature. Chromatography on silica gel eluting with dichloromethane afforded dendrimer **110** (81 mg, 77%) as an orange solid. Mp>250 °C. ^{1}H NMR (CDCl$_3$): δ (ppm) = 9.26 (s, 3H) 8.64 (s, 3H) 8.14 (s, 6H) 7.6 (m, 24H) 7.2 (m, 24H) 5.03 (s, 12H) 2.08 (s, 18H) 1.83 (s, 36H). IR (KBr): ν = 1729, 1520, 1444, 1213, 754, 675, 644 cm^{-1}. UV/Vis (CH$_2$Cl$_2$): λ_{max} (lgε) 368 (5.03), 436 (5.27). MS (MALDI-TOF): M+ = 3308. C$_{177}$H$_{126}$O$_{18}$S$_{24}$, (3310.47): calcd. C 64.22, H 3.84; found C 63.81, H 4.05.

Dendron wedge 111.

111
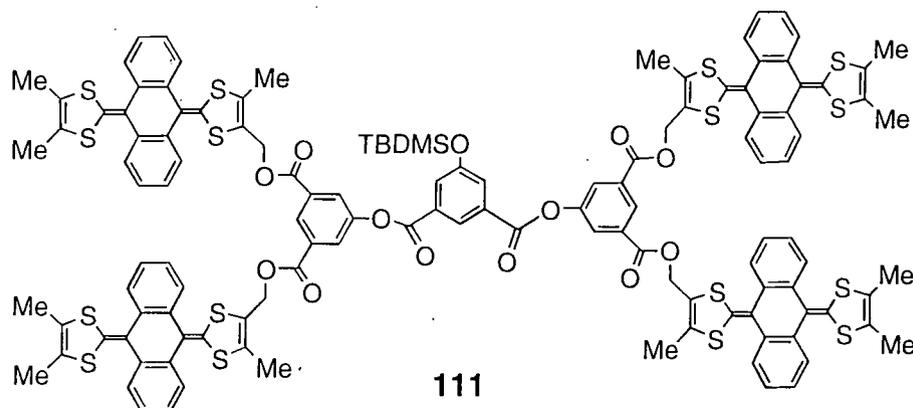
Following the same procedure as for compound **108**, alcohol **109** (550 mg, 0.52 mmol), dichloride **107** (100 mg, 0.26 mmol) and triethylamine (0.14 ml, 1.04 mmol) afforded **111** (450 mg, 72%) as an orange solid. Mp 230°C (black powder above 200°C). ^{1}H NMR (CDCl$_3$): δ (ppm) = 8.62 (m, 3H) 8.11 (d, J= 1 Hz, 4H) 7.89 (d, J= 1 Hz, 4H) 7.6 (m, 16H) 7.2 (m, 16H) 5.02 (s, 8H) 2.09 (s, 12H) 1.85 (s, 24H) 1.03 (s, 9H) 0.29 (s, 6H). UV/Vis (CH$_2$Cl$_2$): λ_{max} (lgε) 368 (4.85), 436 (5.12). IR (KBr): ν = 1728, 1519, 1444, 1215, 756, 675, 644 cm^{-1}. MS (MALDI-TOF): M+ = 2362. C$_{126}$H$_{100}$O$_{13}$S$_{16}$Si (2363.28).

10-(4,5-Dimethyl-1,3-dithiol-2-ylidene)-9,10-dihydroxy-9-(4-chloromethyl-5-methyl-1,3-dithiol-2-ylidene)anthracene (112).
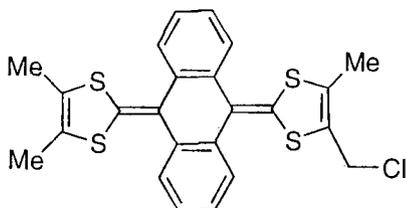
112

To a stirred solution of alcohol **47** (2000 mg, 4.4 mmol) in dry acetonitrile (50 mL) was added triphenylphosphine (1.25 g, 4.8 mmol) and carbontetrachloride (20 mL). The reaction was carried out at reflux, following by TLC until completion after *ca.* 1h in which time the colour changed from orange to dark brown. The reaction mixture was filtered through a plug of silica gel, eluting with ethyl acetate and concentrated in vacuo. Flash chromatography of the residue on silica gel eluting with ethyl acetate/hexane (1:2) afforded compound **112** (2 g, 95%) as an orange solid.

Note: this compound is easily decomposed on silica and especially in solvents like dichloromethane, and also in acid conditions. Mp decomp. to black powder at 225 °C. ^{1}H NMR (CDCl$_3$): δ (ppm) = 7.66-7.59 (m, 4H) 7.29-7.25 (m, 4H) 4.27 (s, 2H) 2.03 (s, 3H) 1.93 (s, 6H). UV/Vis (EtOAc): λ_{max} (lgε) 364 (4.24), 428 (4.49). IR (KBr): ν = 1512, 1456, 1445, 755, 675, 644 cm^{-1}. C$_{24}$H$_{19}$ClS$_4$ (471.12): calcd. C 61.18, H 4.06; found C 61.26, H 4.13.

Dendron wedge 114.
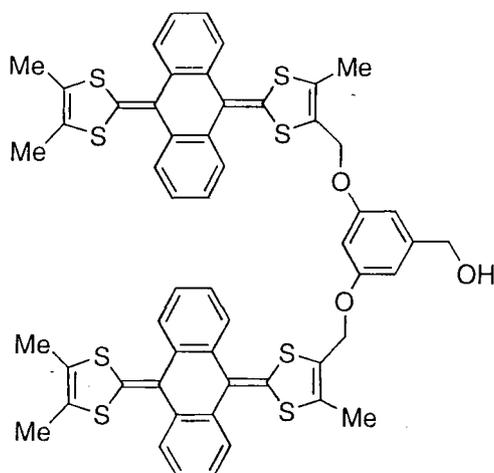
114

To a stirred solution of chloride **112** (2 g, 4.2 mmol) in dry THF (50 mL) was added

3,5-dihydroxybenzyl alcohol (298 mg, 2.1 mmol), K_2CO_3 (640 mg, 4.2 mmol) and 18-

crown-6 (112 mg, 0.4 mmol). The resulting mixture was heated at reflux under N_2 and

vigorously stirred for 24h. Solvents were evaporated in vacuo. Water (100 mL) was added

to the residue and the crude product extracted with chloroform (3x50 mL). Combined

organic layers were dried over $MgSO_4$ and evaporated to dryness. The residue was

chromatographed on a silica gel column (eluent: dichloromethane) to afford **14** (600 mg,

28%) as an orange solid. Mp ca. 240°C. ^1H NMR ($CDCl_3$): δ (ppm) = 7.65-7.61 (m, 8H)

7.28-7.23 (m, 8H) 6.56 (s, 2H) 6.42 (s, 1H) 4.64 (s, 4H) 4.61 (s, 2H) 1.98 (s, 6H) 1.90 (s,

12H). IR (KBr): ν = 3450 (br.) 1595, 1520, 1456, 1444, 1281, 1144, 755, 675, 644 cm^{-1}.

UV/Vis (CH_2Cl_2): λ_{max} (lgε) 368 (4.56), 436 (4.80). MS (MALDI-TOF): M+ = 1009.

$C_{55}H_{44}O_3S_8$ (1009.5): calcd. (+ 0.5 mol of H_2O) C 64.86, H 4.45; found C 64.77, H 4.35.

Dendrimer 115.

115
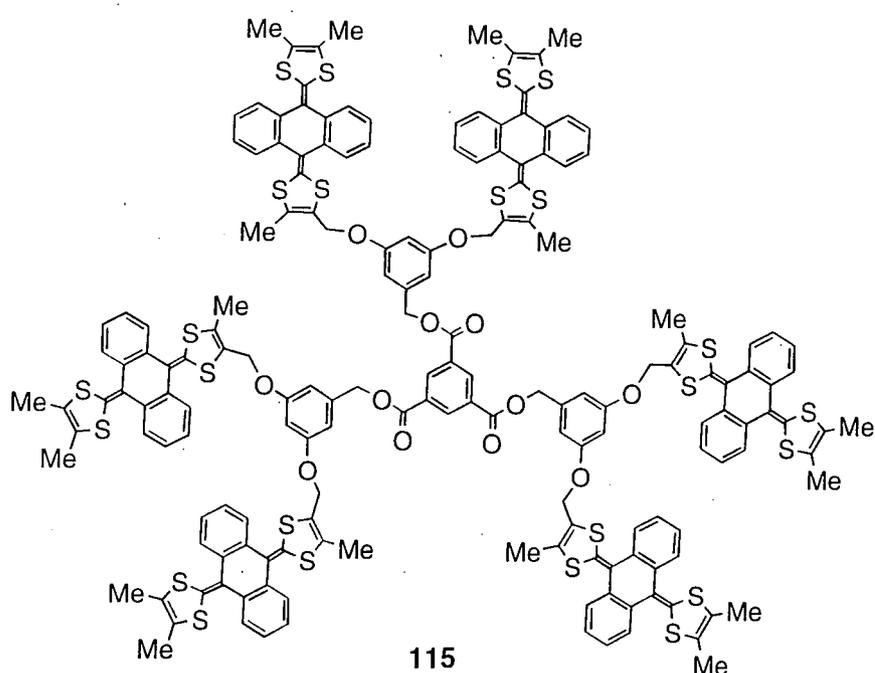
By analogy with the preparation of **108**, alcohol **114** (100 mg, 0.1 mmol), 1,3,5-benzenetricarbonyl trichloride (8.4 mg, 0.03 mmol) and triethylamine (26 μl, 0.2 mmol) in dry dichloromethane (10 mL) were stirred under N_2 at room temperature. Chromatography on silica gel eluting with dichloromethane afforded dendrimer **115** (60 mg, 57%) as an orange solid. Mp 242-245 °C. ^{1}H NMR (CDCl$_3$): δ (ppm) = 8.92 (s, 3H) 7.62-7.54 (m, 24H) 7.26-7.21 (m, 24H) 6.52 (s, 6H) 6.37 (s, 3H) 5.22 (s, 6H) 4.51 (s, 12H) 1.84 (bs, 54H). UV/Vis (CH$_2$Cl$_2$): λ_{max} (lgϵ) 368 (4.99), 436 (5.24). MS (MALDI-TOF): M+ = 3184. C$_{174}$H$_{132}$O$_{12}$S$_{24}$ (3184.49): calcd. C 65.63, H 4.18; found C 65.42, H 4.03.

Dendron wedge 116.

116
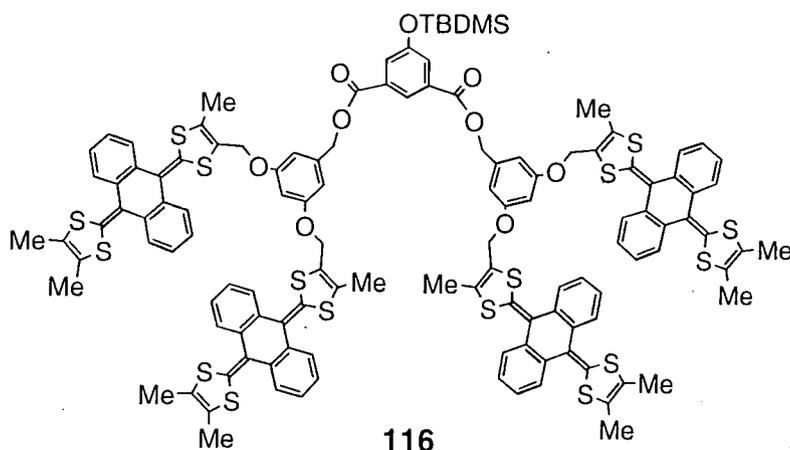
Following the same procedure as for compound **108**, alcohol **114** (300 mg, 0.3 mmol), dichloride **6** (54 mg, 0.15 mmol) and triethylamine (80 μL, 0.6 mmol) afforded **116** (220 mg, 65%) as an orange solid. Mp 243-246 °C. ^{1}H NMR (CDCl$_3$): δ (ppm) = 8.34 (bs, 1H) 7.73 (s, 2H) 7.65-7.54 (m, 16H) 7.29-7.22 (m, 16H) 6.54 (bs, 4H) 6.37 (bs, 2H) 5.20 (bs, 4H) 4.51 (bs, 8H) 1.84 (bs, 36H) 0.99 (s, 9H) 0.23 (s, 6H). IR (KBr): ν =1725, 1595, 1520, 1444, 1216, 1144, 754, 675, 644 cm^{-1}. UV/Vis (CH$_2$Cl$_2$): λ$_{max}$ (lgε) 368 (4.81), 436 (5.03). MS (MALDI-TOF): M+ = 2278. C$_{124}$H$_{104}$O$_9$S$_{16}$Si (2279.3): calcd. C 65.34, H 4.60; found C 65.43, H 4.73.

Dendron wedge 117.
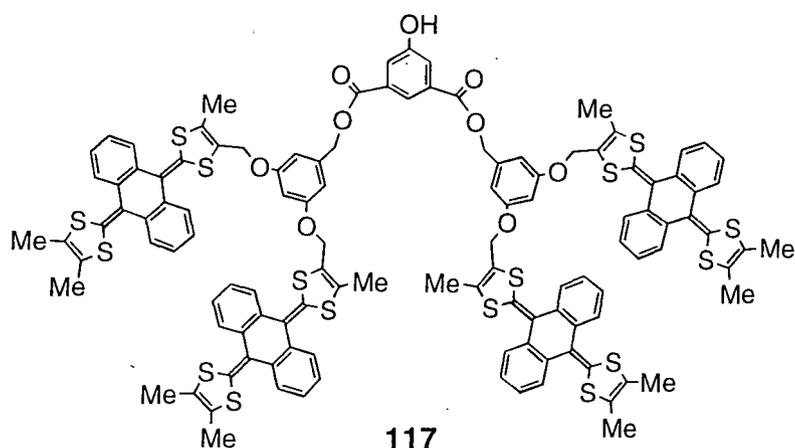
Following the same procedure as for compound **109**, dendron **116** (200 mg, 0.09 mmol) was dissolved in dry THF. Tetrabutylammonium fluoride (1M in THF, 0.09 mL, 0.09 mmol) was added and the resultant mixture was stirred during 1 h. The solvents were removed by evaporation in vacuo and the residue was purified by chromatography on silica gel with dichloromethane as eluent, to afford **117** (133 mg, 70%) as an orange solid mp decomp. to black powder at 245 °C. ^{1}H NMR (CDCl$_3$): δ (ppm) = 8.3 (bs, 1H) 7.71 (s, 2H) 7.65-7.54 (m, 16H) 7.27-7.17 (m, 16H) 6.52 (bs, 4H) 6.37 (bs, 2H) 5.20 (bs, 4H) 4.52 (bs, 8H) 1.84 (bs, 36H). IR (KBr): ν =3450 (br.), 1726, 1596, 1520, 1445, 1222, 1146, 755, 675, 644 cm^{-1}. UV/Vis (CH$_2$Cl$_2$): λ$_{max}$ (lgε) 368 (4.85), 436 (5.09). MS (MALDI-TOF): M+ = 2164. C$_{118}$H$_{90}$O$_9$S$_{16}$ (2165.0): calcd. (+ 2 mol of H$_2$O) C 64.39, H 4.30; found C 64.15, H 4.23.

Dendrimer 118.

118
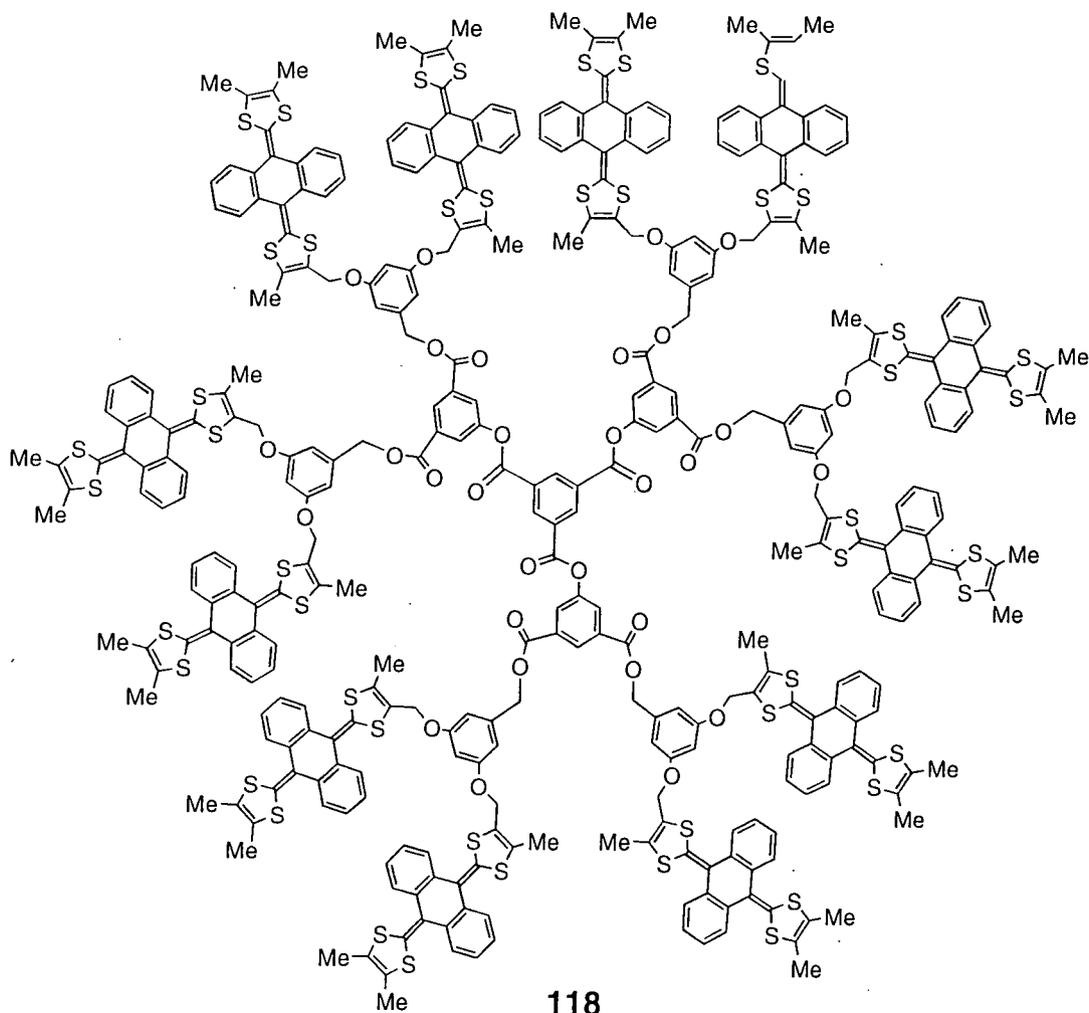
By analogy with the preparation of **108**, alcohol **117** (130 mg, 0.06 mmol), 1,3,5-benzenetricarbonyl trichloride (5.3 mg, 0.02 mmol) and triethylamine (16 μl, 0.12 mmol) in dry dichloromethane (10 mL) were stirred under N_2 at room temperature. Chromatography on silica gel eluting with dichloromethane afforded dendrimer **18** (72 mg, 54%) as an orange solid. Mp decomp. to black powder at 240 °C. ^{1}H NMR (CDCl$_3$): δ (ppm) = 9.05 (s, 3H) 8.69 (s, 3H) 8.14 (s, 6H) 7.59-7.46 (m, 48H) 7.28-7.18 (m, 48H) 6.51 (s, 12H) 6.33 (s, 6H) 5.22 (bs, 12H) 4.50 (m, 24H) 1.82-1.79 (bs, 108H). IR (KBr): ν = 1731, 1596, 1520, 1444, 1222, 1146, 753, 675, 644 cm^{-1}. UV/Vis (CH$_2$Cl$_2$): λ$_{max}$ (lgε) 368 (5.27), 436 (5.51). MS (MALDI-TOF): M+ = 6648. C$_{363}$H$_{270}$O$_{30}$S$_{48}$ (6651.2): calcd. C 65.55, H 4.09; found C 65.37, H 4.23.

5.5 References.

(1)   Bryce, M. R.; Finn, T.; Moore, A.; Batsanov, A. S.; Howard, J. A. K. *Eur. J. Org. Chem.* **2000**, 51-60.

(2)   Moore, A. J.; Bryce, M. R. *J. Chem. Soc. Perkin Trans. 1* **1991**, 157-168.

(3)   Medina, J. C.; Gay, I.; Chen, Z.; Echegoyen, L.; Gokel, G. W. *J. Am. Chem. Soc.* **1991**, *113*, 365-366.

(4)   Miller, T. M.; Kwock, E. W.; Neeman, T. X. *Macromolecules* **1992**, *25*, 3143-3148.

Appendix One

Dynamic NMR Studies.

Determination

of the Activation Enthalpy $\Delta H^{\ddagger}$

and the Activation Entropy $\Delta S^{\ddagger}$.

^{1}H NMR studies performed on **47**, showed a difference in chemical shift for the two protons **H$_a$** and **H$_b$** in α-position of the hydroxyl group (*Figure 2.3*), observed at 20 °C in d$_6$-DMSO, giving a four-line AB system (J$_{AB}$ = *ca.* 13 Hz). This four-line AB system is coalescing into a singlet with increasing of temperature, consistent with the increase of interconversion between the two forms A and B. The rate exchange corresponding to this interconversion can be studied by looking at the variation of the chemical shift of protons H$_a$ and H$_b$ for a range of temperature until coalescence. Simulations of the process have been performed by Dr Paul Hazendonk, currently working in the Solid State NMR department of the University of Durham, and gave accurate values of rate exchange for each studied temperature (*Table A1.1*).
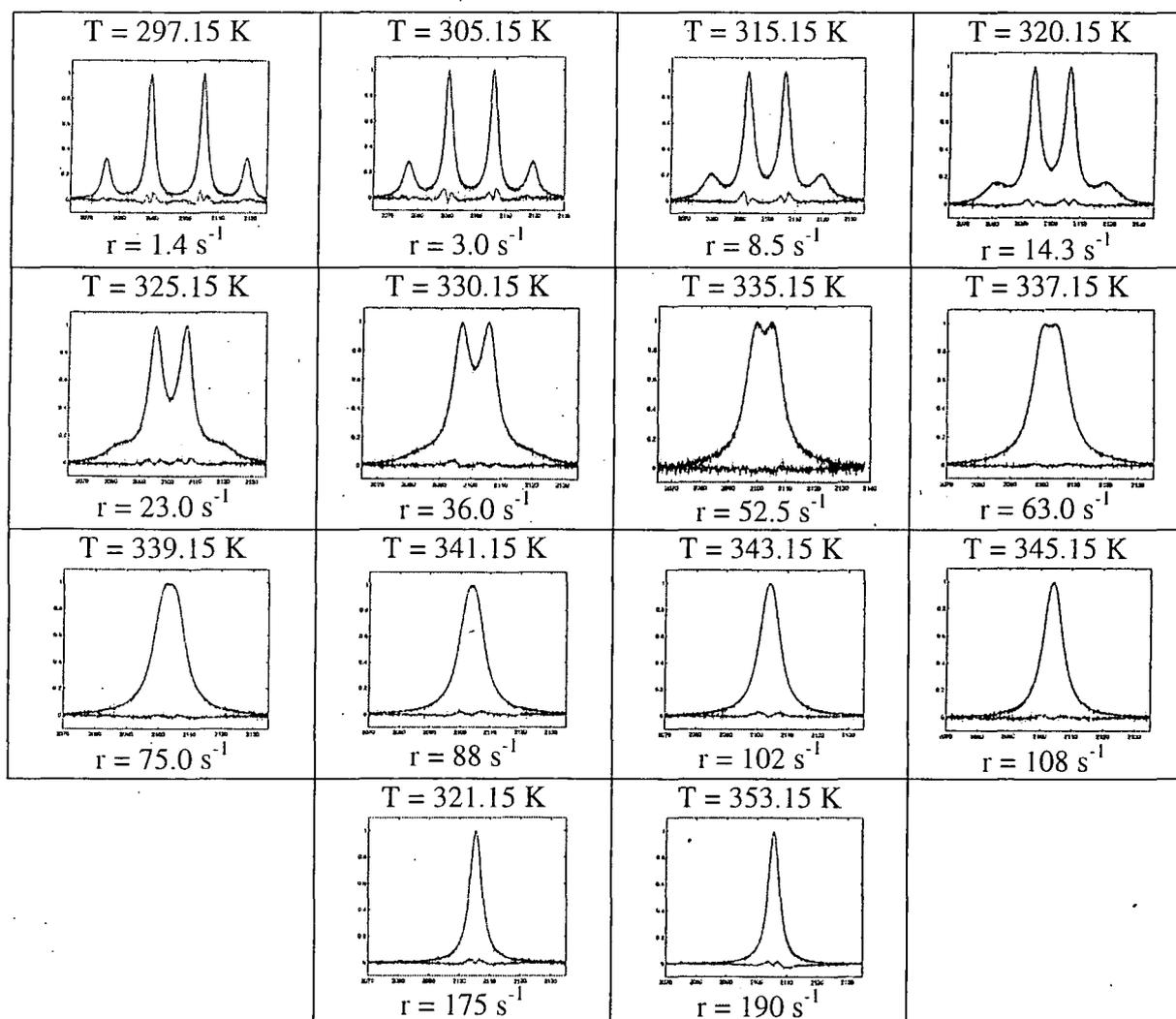
Table A1.1 Calculated rate exchange for the interconversion process.

The Eyring equation is linking directly this rate exchange to the activation energy, E_a, of the system.

$$r = \frac{k_b T}{h} \exp\left(\frac{-E_a}{RT}\right) \quad (1)$$

r is the rate exchange, k_b is the Boltzmann constant, h is the Plank constant, R is the ideal gas constant and T is the temperature (h = $6.62 \ 10^{-34}$ J s and K_b = $1.38 \ 10^{-23}$ J K^{-1}).

The activation energy can be decomposed in activation enthalpy of and activation entropy:

$$E_a = \Delta H^{\ddagger} - T\Delta S^{\ddagger} \quad (2)$$

Thus, the Eyring equation can be written:

$$\ln\left(\frac{r}{T}\right) = \ln\left(\frac{k_b}{h}\right) + \frac{\Delta S^{\ddagger}}{R} - \frac{\Delta H^{\ddagger}}{RT} \quad (3)$$

Consequently, when ln (r/T) is plotted as a function of 1/T, the slope of the obtained linear variation is $-\Delta H^{\ddagger}/R$ and the intercept obtained by extrapolating to 1/T = 0 is ln(k_b/h) + $\Delta S^{\ddagger}/R$ (*Figure A1.1*). However, there can be large extrapolation errors due to small errors in the slope. To minimise extrapolation error, it is essential to have data over as large a temperature range as possible. Unfortunately for this interconversion process studied, the melting temperature of d_6-DMSO (in which the separation of the AB system is the wider) , the coalescence temperature and the boiling temperature of d_6-DMSO are limiting the number of experiments in our case between T = 24 °C and T = 80 °C, and, the error obtained in $\Delta S^{\ddagger}$ is too large for reliable interpretation .

Eyring Plot

$$\ln(r/T) = -9052.9/T + 25.146$$
$$R^2 = 0.9982$$
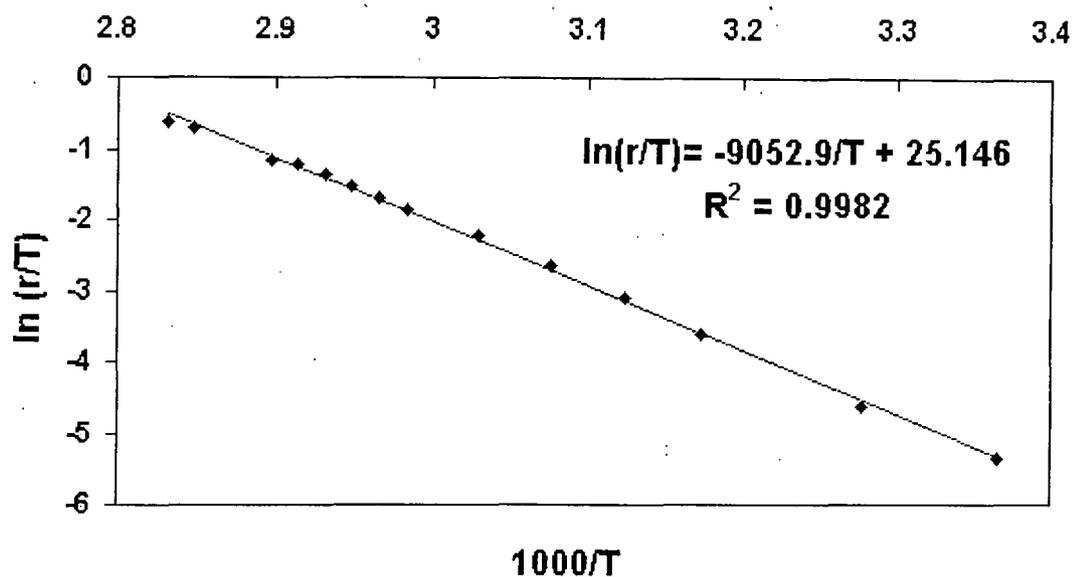
Figure A1.1 Eyring plot relative to the interconversion process.

Using Eyring equation and the linear equation obtained by the Eyring plot (*Figure A1.1*), the activation enthalpy $\Delta H^{\ddagger}$ is found to be equal to 75.3 kJ mol^{-1} and the activation entropy $\Delta S^{\ddagger}$ equal to 11.5 J mol-1 K^{-1} with standard deviations of 0.9 kJ mol^{-1} and 8.4 J mol^{-1} K^{-1} respectively, which is not reliable for the activation entropy as we discuss previously.

Appendix Two

Molecular Modelling Studies.

A 2.1 Software and Calculation Procedures.

All structures studied were modelled and optimised in the gas phase and without consideration of the counter ions using Hyperchem 5.02: Hyperchem, Inc., 1115 NW 4th Street, Gainesville, FL 32601 (USA). For compounds **77c** and **78c** only (ferrocenyl diacid chloride and ferrocenyl bridge), Hyperchem 6.0 was used, the PM3 method having being configured for transition metals as un update of Hyperchem 5.02.

For all the diacid chlorides (**77a-f**) and the anthracenediylidene derivatives studied (**(E) 76** , **(Z) 76**, **78a-d** and their dicationic oxided species), the optimisation was performed by semi-empirical calculations using the PM3 method. These calculations solve the Schrödinger equation, with certain approximations, to describe the electron properties of atoms and molecules.

For the dendritic molecules, the optimisation was performed by molecular mechanics calculations using the MM+ method. The total number of orbitals for these molecules was too high to use semi-empirical calculations. Molecular mechanical calculations treat atoms as Newtonian particles interacting through a potential energy function. Potential energy depends on bond lengths, bond angles, torsion angles, and nonbonded interactions (van der Waals forces, electrostatic interactions, and hydrogen bonds).

In all cases, the same algorithm was used (Polak-Ribiere), which attempts to lower the energy of a molecular system by adjusting its geometry. The same final condition of convergence was also used (RMS gradient of 0.001 kcal/Åmol).

A 2.2 Diacid chloride derivatives.

Terephthaloyl chloride (**77a**) and Thiophene dicarbonyl chloride (**77b**)
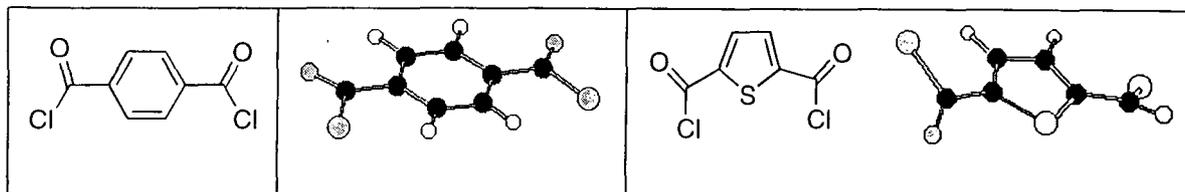
Ferrocenyl dicarbonyl dichloride (**77c**) and oxybis(carbonyl chloride) (**77d**):
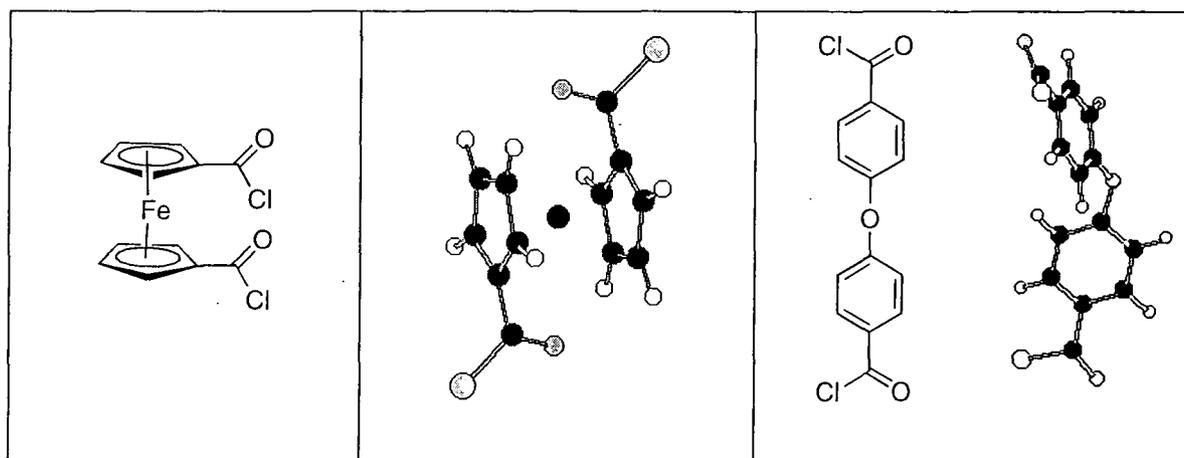
77e and 77f
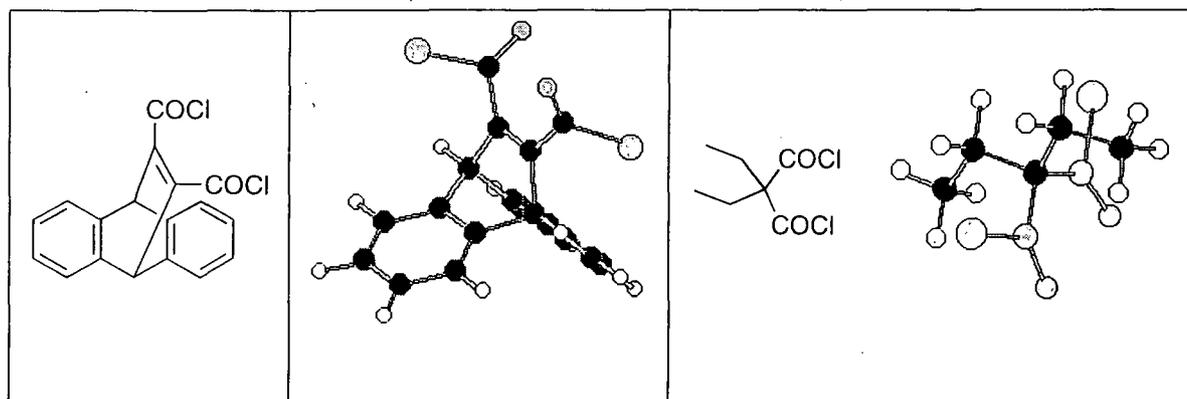
A 2.3 Anthracenediylidene derivatives.

Calculations were performed on the neutral forms of (*E*)76 and (*Z*)76 to compare the intramolecular distance between the two oxygen atoms in an attempt to explain the selectivity of the cyclisation reaction (Chapter Three).

9,10-bis[(4-hydroxymethyl-5-methyl)-1,3-dithiol-2-ylidene]-9,10-dihydroanthracene
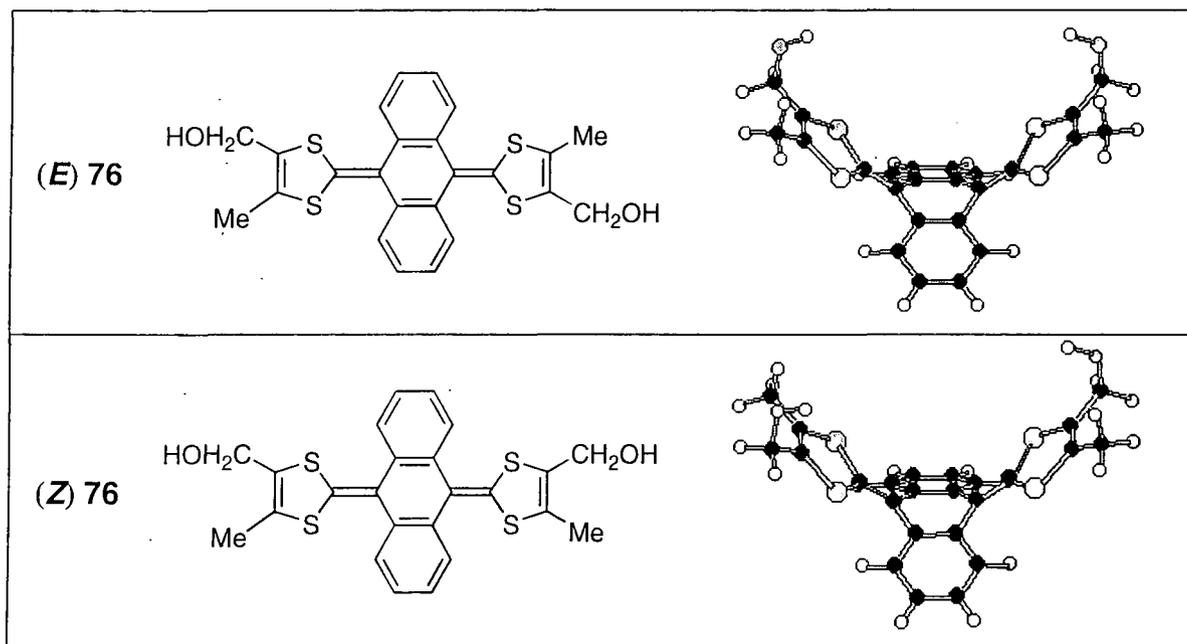
Modelling studies of the dication species can be performed by semi-empirical calculations adding a global charge of +2 on the molecule. On the converged structure, the charges are then distributed mainly on the sulfur atoms of the dithiolium rings.
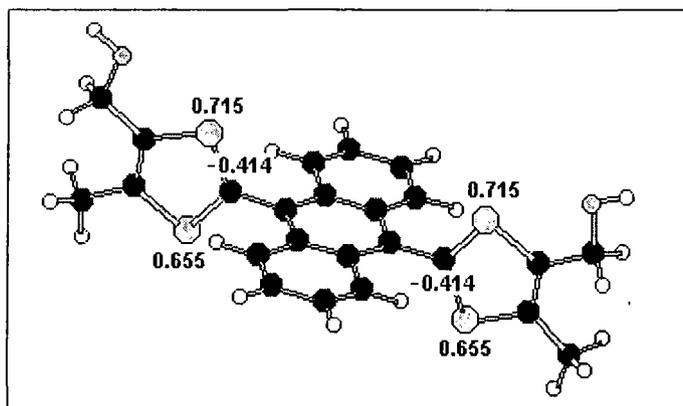
All the bridged derivative (**78a-d**) and their corresponding oxidised form have been studied following the same procedure as for **76**.

A 2.4 Dendrimers.

Modelling studies performed on dendrimers **110**, were realised by adding to the energy-minimised conformation of the core (*Figure A2.1*), the energy-minimised conformation of the units (*Figure A2.2*) at its periphery. The resulting structure was then energy-minimised by molecular mechanics using the MM+ method. Depending on the starting positions of the units around the core (attached angles), several converged structures have been obtained, most of them asymmetric, presenting π-π interactions between the units. The presented structure of **110** (*See Chapter Four*) was obtained with a final energy comparable to the other asymmetric structures.
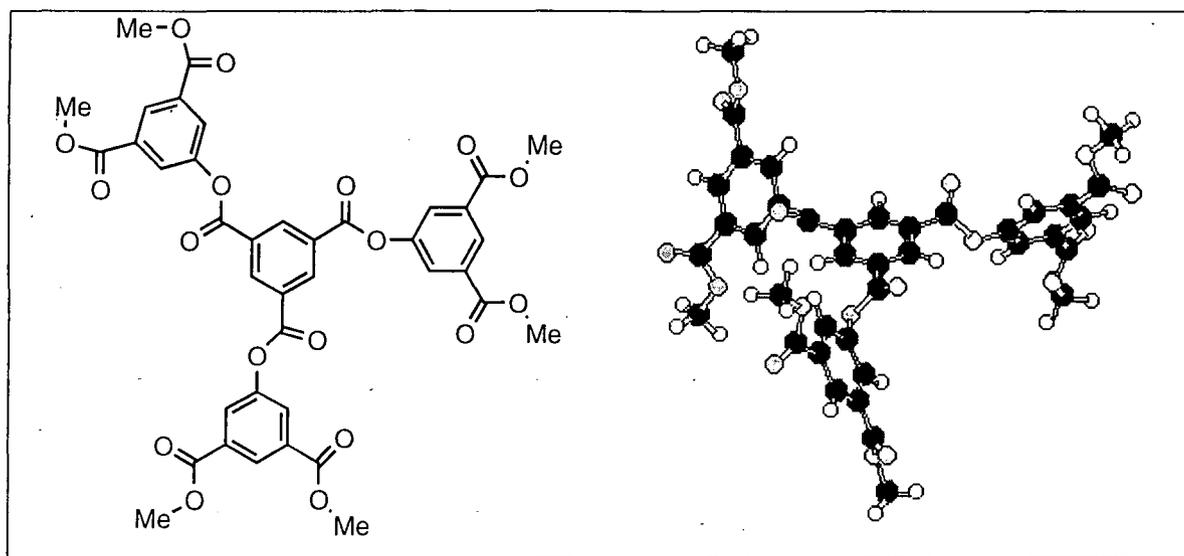
Figure A2.1. Energy minimised conformation of the core obtained by semi-empirical calculations (PM3 method)
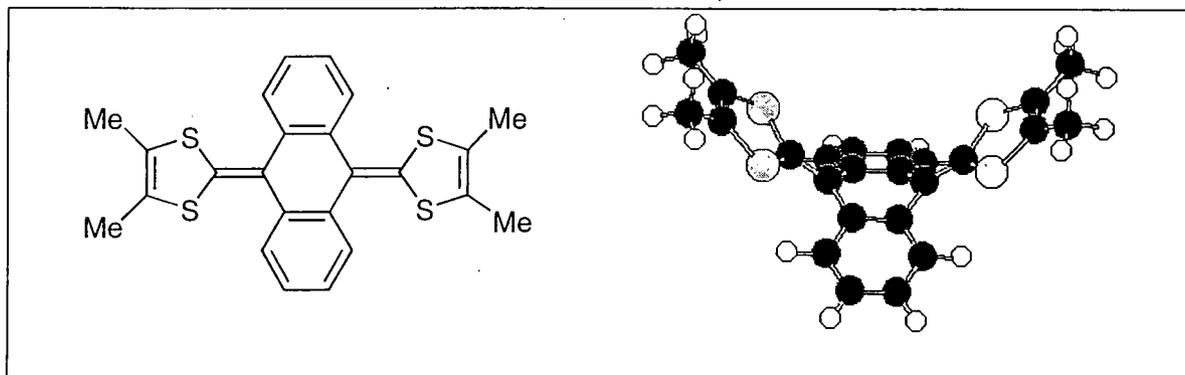
Figure A2.2. Energy minimised conformation of the unit obtained by semi-empirical calculations (PM3 method).

For dendrimer **118**, the starting structure was obtained by adding to the energy-minimised conformation of the core, the energy-minimised conformation of dimer **119** (*Figure A2.3*). The energy of the presented structure (*see chapter Four*) was the lowest observed for the obtained conformations on an average number of 10 different starting structures (by varying the attached angles between the core and the dimer).
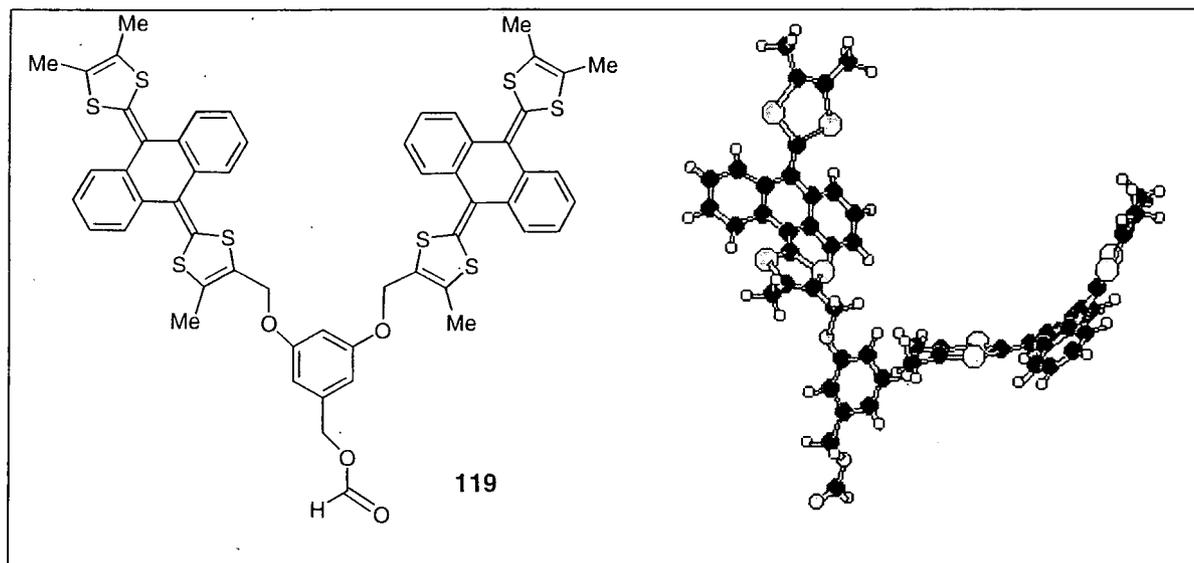
Figure A2.3. Energy minimised conformation of **119** obtained by Molecular mechanics calculations (MM+ method).

For the oxidised forms **110**$^{12+}$ and **118**$^{24+}$, only one converged structure was obtained for each dendrimer due to Coulombic repulsion which forces the cationic units to be placed as far as possible from each other with, therefore, the maximum space expansion between them. The calculations were performed using partial atomic charges to calculate non-bonded electrostatic interactions.

For other reported work on modelling studies of dendritic molecules using Hyperchem 5.0, see also:

- Camps, X.; Dietel, E.; Hirsch, A.; Pyo, S.; Echegoyen, L.; Hackbarth, S.; Röder, B. *Chem. Eur. J.* **1999**, *5*, 2362-2373.
- Heinen, S. and Walden, L. *Angew. Chem. Int. Ed.* **2000**, 39, 806-809.

Appendix Three

X-Ray Crystallographic Data.

Index
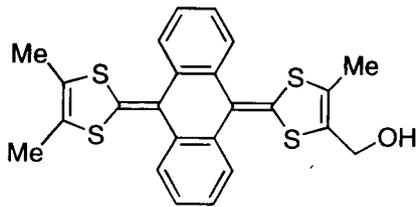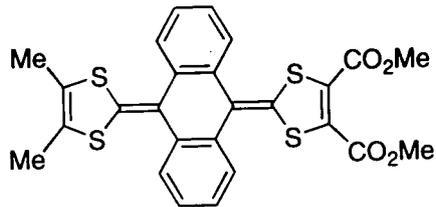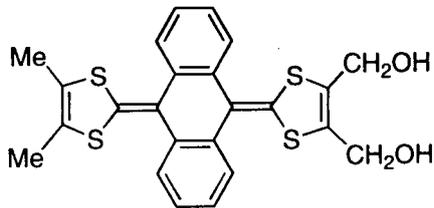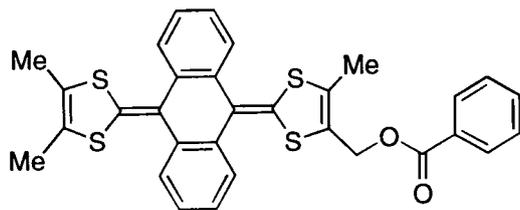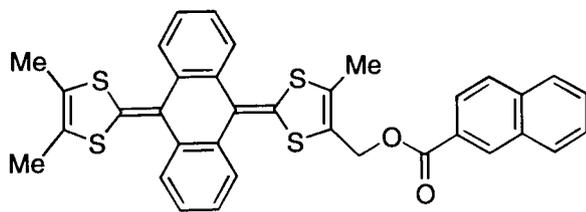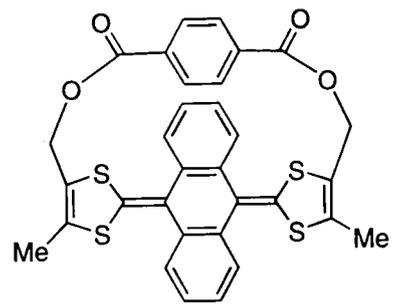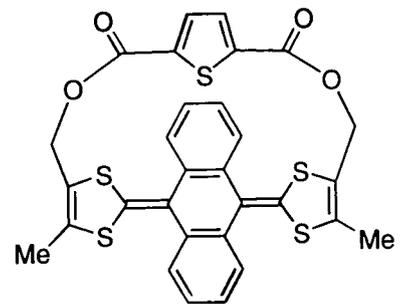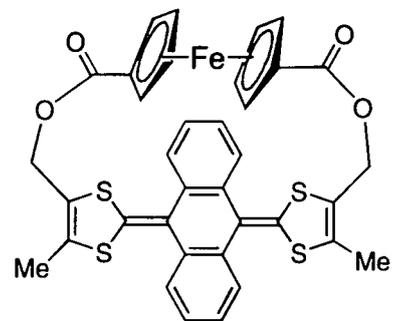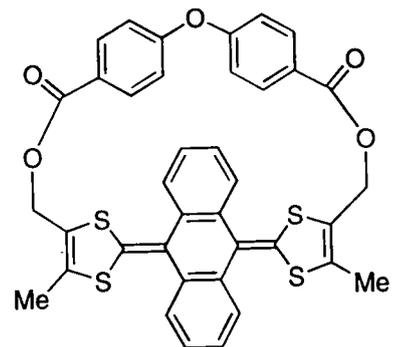
10-(4,5-Dimethyl-1,3-dithiol-2-ylidene)- 9,10-dihydro-9-(4-hydroxymethyl-5-methyl-1,3-dithiol-2-ylidene)anthracene (47):
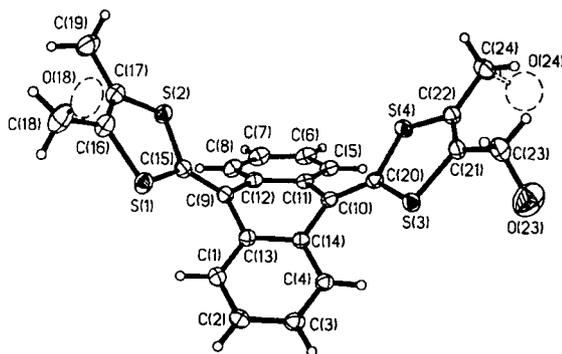
Table 1. Crystal data and structure refinement

Identification code	
Empirical formula	C24 H20 O S4
Formula weight	452.64
Temperature	120(2) K
Wavelength	0.71073 Å
Crystal system	Monoclinic
Space group	$P2_1/n$ (No. 14)
Unit cell dimensions	$a = 11.036(3)$ Å $\alpha = 90°$
	$b = 12.871(4)$ Å $\beta = 101.48(1)°$
	$c = 15.266(5)$ Å $\gamma = 90°$
Volume	2125(1) Å^3
Z	4
Density (calculated)	1.415 g/cm^3
Absorption coefficient	0.461 mm^{-1}
F(000)	944
Crystal size	0.35 × 0.4 × 0.5 mm^3
θ range for data collection	2.09 to 29.00°.
Index ranges	$-15 \leq h \leq 15, -17 \leq k \leq 17, -20 \leq l \leq 20$
Reflections collected	25707
Independent reflections	5612 [R(int) = 0.0234]
Reflections with I > 2σ(I)	4694
Completeness to θ = 29.00°	99.6 %
Absorption correction	Semi-empirical from equivalents
Max. and min. transmission	0.8622 and 0.7523
Refinement method	Full-matrix least-squares on F^2
Data / restraints / parameters	5612 / 0 / 291
Largest final shift/e.s.d. ratio	0.002
Goodness-of-fit on F^2	1.038
Final R indices [I > 2σ(I)]	R1 = 0.0343, wR2 = 0.0922
R indices (all data)	R1 = 0.0435, wR2 = 0.0987
Largest diff. peak and hole	0.546 and -0.322 e.Å^{-3}

Table 2. Atomic coordinates (×10⁵) and equivalent isotropic displacement parameters (Å² ×10⁴) U(eq) is defined as one third of the trace of the orthogonalized Uij tensor.

	x	y	z	U(eq)
S(1)	31615(4)	7889(3)	15634(3)	261(1)
S(2)	55242(4)	11746(3)	27816(3)	259(1)
S(3)	32263(3)	58628(3)	3116(3)	231(1)
S(4)	56142(3)	60106(3)	15397(3)	243(1)
C(1)	13991(14)	25812(12)	17585(11)	250(3)
C(2)	3334(14)	30334(13)	12598(11)	267(3)
C(3)	3653(14)	40583(13)	9822(11)	250(3)
C(4)	14591(13)	46290(12)	12008(10)	213(3)
C(5)	52785(14)	51359(12)	33441(11)	236(3)
C(6)	59332(15)	48259(14)	41753(11)	285(3)
C(7)	58384(16)	38097(14)	44648(11)	298(3)
C(8)	51079(15)	30976(13)	39085(10)	262(3)
C(9)	36731(13)	26620(12)	24545(9)	210(3)
C(10)	37455(13)	47410(11)	19027(10)	195(3)
C(11)	45306(13)	44345(12)	27716(10)	201(3)
C(12)	44664(13)	33907(12)	30585(10)	216(3)
C(13)	25141(13)	31262(12)	19540(9)	201(3)
C(14)	25522(13)	41779(11)	16723(10)	192(3)
C(15)	40415(14)	16729(12)	23125(10)	220(3)
C(16)	43285(16)	-1461(13)	15876(12)	301(3)
C(17)	54092(16)	285(13)	21430(12)	296(3)
C(18)	39770(20)	-10663(16)	9835(15)	446(5)
O(18)	40300(50)	-7410(40)	810(30)	681(13)
C(19)	65342(18)	-6624(16)	23134(16)	427(5)
C(20)	41209(13)	54491(11)	13443(10)	203(3)
C(21)	44226(14)	64999(12)	-861(11)	239(3)
C(22)	55174(14)	65603(12)	4731(11)	241(3)
C(23)	40783(16)	69526(14)	-10081(11)	307(3)
O(23)	30460(40)	76070(30)	-11050(20)	654(10)
C(24)	66784(16)	70784(14)	3187(12)	323(4)
O(24)	65200(300)	81500(200)	5500(200)	1080(80)

Table 3. Bond lengths [Å] and angles [°]

S(1)-C(16)	1.7576(18)	C(9)-C(15)	1.367(2)
S(1)-C(15)	1.7615(16)	C(9)-C(12)	1.475(2)
S(2)-C(17)	1.7587(18)	C(9)-C(13)	1.4792(19)
S(2)-C(15)	1.7706(16)	C(10)-C(20)	1.367(2)
S(3)-C(21)	1.7616(16)	C(10)-C(14)	1.483(2)
S(3)-C(20)	1.7675(15)	C(10)-C(11)	1.486(2)
S(4)-C(22)	1.7590(17)	C(11)-C(12)	1.419(2)
S(4)-C(20)	1.7696(15)	C(13)-C(14)	1.423(2)
C(1)-C(2)	1.395(2)	C(16)-C(17)	1.338(2)
C(1)-C(13)	1.396(2)	C(16)-C(18)	1.504(3)
C(2)-C(3)	1.388(2)	C(17)-C(19)	1.507(2)
C(3)-C(4)	1.396(2)	C(18)-O(18)	1.453(5)
C(4)-C(14)	1.402(2)	C(21)-C(22)	1.336(2)
C(5)-C(6)	1.388(2)	C(21)-C(23)	1.501(2)
C(5)-C(11)	1.405(2)	C(22)-C(24)	1.504(2)
C(6)-C(7)	1.391(3)	C(23)-O(23)	1.401(4)
C(7)-C(8)	1.392(2)	C(24)-O(24)	1.44(3)
C(8)-C(12)	1.401(2)		

C(16)-S(1)-C(15)	96.99(8)	C(20)-C(10)-C(14)	122.88(13)
C(17)-S(2)-C(15)	96.93(8)	C(20)-C(10)-C(11)	122.57(13)
C(21)-S(3)-C(20)	97.11(8)	C(14)-C(10)-C(11)	114.48(13)
C(22)-S(4)-C(20)	97.20(7)	C(5)-C(11)-C(12)	118.41(13)
C(2)-C(1)-C(13)	121.24(14)	C(5)-C(11)-C(10)	123.42(14)
C(3)-C(2)-C(1)	119.56(14)	C(12)-C(11)-C(10)	118.08(13)
C(2)-C(3)-C(4)	120.03(14)	C(8)-C(12)-C(11)	119.59(14)
C(3)-C(4)-C(14)	121.32(14)	C(8)-C(12)-C(9)	122.39(14)
C(6)-C(5)-C(11)	121.23(15)	C(11)-C(12)-C(9)	117.97(13)
C(5)-C(6)-C(7)	120.16(15)	C(1)-C(13)-C(14)	119.41(13)
C(6)-C(7)-C(8)	119.74(15)	C(1)-C(13)-C(9)	122.83(14)
C(7)-C(8)-C(12)	120.82(16)	C(14)-C(13)-C(9)	117.76(13)
C(15)-C(9)-C(12)	122.22(13)	C(4)-C(14)-C(13)	118.36(13)
C(15)-C(9)-C(13)	123.25(13)	C(4)-C(14)-C(10)	123.52(13)
C(12)-C(9)-C(13)	114.25(13)	C(13)-C(14)-C(10)	118.12(12)
C(9)-C(15)-S(1)	124.16(11)	C(10)-C(20)-S(4)	123.68(11)
C(9)-C(15)-S(2)	123.6(12)	S(3)-C(20)-S(4)	111.31(8)
S(1)-C(15)-S(2)	111.98(9)	C(22)-C(21)-C(23)	127.22(15)
C(17)-C(16)-C(18)	127.58(16)	C(22)-C(21)-S(3)	116.83(12)
C(17)-C(16)-S(1)	117.09(13)	C(23)-C(21)-S(3)	115.90(12)
C(18)-C(16)-S(1)	115.33(14)	C(21)-C(22)-C(24)	128.02(15)
C(16)-C(17)-C(19)	127.61(17)	C(21)-C(22)-S(4)	116.67(12)
C(16)-C(17)-S(2)	116.69(13)	C(24)-C(22)-S(4)	115.27(12)
C(19)-C(17)-S(2)	115.66(14)	O(23)-C(23)-C(21)	112.4(2)
O(18)-C(18)-C(16)	107.5(2)	O(24)-C(24)-C(22)	103.6(12)
C(10)-C(20)-S(3)	124.90(11)		

10-[4,5-Di(methoxycarbonyl)-1,3-dithiol-2-ylidene]-9-(4-5-dimethyl-1,3-dithiol-2-ylidene)-9,10-dihydroanthracene (50)
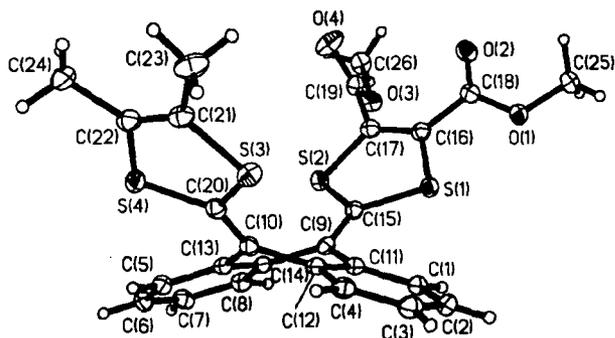
Table 1. Crystal data and structure refinement

Identification code	
Empirical formula	$C_{26} H_{20} O_4 S_4$
Formula weight	524.66
Temperature	120(2) K
Wavelength	0.71073 Å
Crystal system	Triclinic
Space group	P $\bar{1}$
Unit cell dimensions	a = 9.828(1) Å α= 104.70(1)°
	b = 10.459(1) Å β= 91.88(1)°
	c = 12.635(1) Å γ = 108.47(1)°
Volume	1182.4(2) Å^3
Z	2
Density (calculated)	1.474 g/cm^3
Absorption coefficient	0.435 mm^{-1}
F(000)	544
Crystal size	0.44 × 0.28 × 0.07 mm^3
θ range for data collection	1.6 to 27.5°.
Index ranges	$-12 \leq h \leq 12, -13 \leq k \leq 13, -16 \leq l \leq 16$
Reflections collected	8536
Independent reflections	5326 [R(int) = 0.0248]
Reflections with I>2σ(I)	4317
Completeness to θ = 27.5°	97.9 %
Absorption correction	Integration
Max. and min. transmission	0.9721 and 0.8560
Refinement method	Full-matrix least-squares on F^2
Data / restraints / parameters	5326 / 0 / 387
Largest final shift/e.s.d. ratio	0.002
Goodness-of-fit on F^2	1.012
Final R indices [I>2σ(I)]	R$_1$ = 0.0330, wR$_2$ = 0.0782
R indices (all data)	R$_1$ = 0.0461, wR$_2$ = 0.0837
Largest diff. peak and hole	0.313 and -0.286 e.Å^{-3}

Table 2. Atomic coordinates (×10⁴) and equivalent isotropic displacement parameters (Å² · 10⁴)

U(eq) is defined as one third of the trace of the orthogonalized U_{ij} tensor.

	x	y	z	U(eq)
S(1)	4046.9(4)	6153.9(4)	4663.6(4)	180(1)
S(2)	5702.0(4)	5530.1(4)	2808.1(3)	192(1)
S(3)	-1850.3(5)	3418.0(5)	954.9(4)	212(1)
S(4)	-173.2(5)	2599.0(5)	-792.7(3)	218(1)
O(1)	5227(1)	8832(1)	6207(1)	230(3)
O(2)	6749(1)	10008(1)	5198(1)	249(3)
O(3)	8715(1)	8492(1)	3813(1)	227(3)
O(4)	7269(2)	8884(2)	2600(1)	361(3)
C(1)	1378(2)	3591(2)	4451(1)	196(3)
C(2)	15(2)	3249(2)	4803(2)	233(4)
C(3)	-1212(2)	2664(2)	4030(2)	230(4)
C(4)	-1075(2)	2438(2)	2912(2)	196(3)
C(5)	1805(2)	1223(2)	67(1)	185(3)
C(6)	3052(2)	884(2)	-155(2)	208(4)
C(7)	4272(2)	1474(2)	614(2)	208(4)
C(8)	4253(2)	2407(2)	1615(2)	198(3)
C(9)	2960(2)	3756(2)	2907(1)	160(3)
C(10)	483(2)	2575(2)	1354(1)	165(3)
C(11)	1537(2)	3392(2)	3331(1)	165(3)
C(12)	285(2)	2806(2)	2538(1)	163(3)
C(13)	1766(2)	2169(2)	1060(1)	158(3)
C(14)	3023(2)	2775(2)	1850(1)	160(3)
C(15)	4080(2)	4950(2)	3405(1)	166(3)
C(16)	5500(2)	7546(2)	4486(1)	181(3)
C(17)	6232(2)	7269(2)	3625(1)	190(3)
C(18)	5901(2)	8939(2)	5314(1)	193(3)
C(19)	7454(2)	8325(2)	3285(1)	207(4)
C(20)	5585(2)	10122(2)	7105(2)	283(4)
C(21)	9958(2)	9543(2)	3574(2)	258(4)
C(22)	-399(2)	2797(2)	612(1)	171(3)
C(23)	-2189(2)	3761(2)	-309(2)	215(4)
C(24)	-1421(2)	3387(2)	-1107(2)	216(4)
C(25)	-3337(2)	4425(2)	-349(2)	300(4)
C(26)	-1494(2)	3536(2)	-2258(2)	280(4)

Table 3. Bond lengths [Å] and angles [°]

S(1)-C(16)	1.755(2)	C(7)-H(7)	0.97(2)
S(1)-C(15)	1.769(2)	C(8)-C(14)	1.399(2)
S(2)-C(17)	1.748(2)	C(8)-H(8)	0.98(2)
S(2)-C(15)	1.782(2)	C(9)-C(15)	1.361(2)
S(3)-C(23)	1.767(2)	C(9)-C(14)	1.480(2)
S(3)-C(22)	1.770(2)	C(9)-C(11)	1.484(2)
S(4)-C(22)	1.763(2)	C(10)-C(22)	1.366(2)
S(4)-C(24)	1.765(2)	C(10)-C(13)	1.482(2)
O(1)-C(18)	1.338(2)	C(10)-C(12)	1.484(2)
O(1)-C(20)	1.458(2)	C(11)-C(12)	1.422(2)
O(2)-C(18)	1.211(2)	C(13)-C(14)	1.423(2)
O(3)-C(19)	1.327(2)	C(16)-C(17)	1.345(2)
O(3)-C(21)	1.460(2)	C(16)-C(18)	1.486(2)
O(4)-C(19)	1.198(2)	C(17)-C(19)	1.510(2)
C(1)-C(2)	1.391(3)	C(20)-H(201)	0.96(2)
C(1)-C(11)	1.399(2)	C(20)-H(202)	0.94(3)
C(1)-H(1)	0.97(2)	C(20)-H(203)	0.98(2)
C(2)-C(3)	1.390(3)	C(21)-H(211)	0.94(2)
C(2)-H(2)	0.92(2)	C(21)-H(212)	0.94(2)
C(3)-C(4)	1.390(3)	C(21)-H(213)	0.96(3)
C(3)-H(3)	0.92(2)	C(23)-C(24)	1.333(3)
C(4)-C(12)	1.403(2)	C(23)-C(25)	1.506(2)
C(4)-H(4)	0.97(2)	C(24)-C(26)	1.503(3)
C(5)-C(13)	1.397(2)	C(25)-H(251)	0.96(3)
C(5)-C(6)	1.398(2)	C(25)-H(252)	0.95(3)
C(5)-H(5)	0.95(2)	C(25)-H(253)	0.99(3)
C(6)-C(7)	1.383(3)	C(26)-H(261)	0.93(3)
C(6)-H(6)	0.95(2)	C(26)-H(262)	0.95(2)
C(7)-C(8)	1.393(2)	C(26)-H(263)	0.95(3)
C(16)-S(1)-C(15)	95.24(8)	C(18)-O(1)-C(20)	115.79(14)
C(17)-S(2)-C(15)	95.26(8)	C(19)-O(3)-C(21)	114.97(14)
C(23)-S(3)-C(22)	97.36(8)	C(2)-C(1)-C(11)	121.04(17)
C(22)-S(4)-C(24)	97.50(8)	C(2)-C(1)-H(1)	118.7(12)
C(11)-C(1)-H(1)	120.3(13)	C(14)-C(13)-C(10)	117.46(14)
C(3)-C(2)-C(1)	119.73(17)	C(8)-C(14)-C(13)	119.45(15)
C(3)-C(2)-H(2)	121.0(13)	C(8)-C(14)-C(9)	122.51(15)
C(1)-C(2)-H(2)	119.2(13)	C(13)-C(14)-C(9)	118.03(14)
C(4)-C(3)-C(2)	120.05(17)	C(9)-C(15)-S(1)	124.06(13)
C(4)-C(3)-H(3)	120.9(13)	C(9)-C(15)-S(2)	123.35(13)
C(2)-C(3)-H(3)	118.9(13)	S(1)-C(15)-S(2)	112.47(9)
C(3)-C(4)-C(12)	121.31(17)	C(17)-C(16)-C(18)	123.57(16)
C(3)-C(4)-H(4)	119.0(12)	C(17)-C(16)-S(1)	117.54(13)
C(12)-C(4)-H(4)	119.7(12)	C(18)-C(16)-S(1)	118.83(13)
C(13)-C(5)-C(6)	121.?8(16)	C(16)-C(17)-C(19)	126.06(16)
C(13)-C(5)-H(5)	119.2(12)	C(16)-C(17)-S(2)	117.06(13)
C(6)-C(5)-H(5)	119.7(12)	C(19)-C(17)-S(2)	116.87(13)
C(7)-C(6)-C(5)	120.30(16)	O(2)-C(18)-O(1)	125.34(16)
C(7)-C(6)-H(6)	117.8(12)	O(2)-C(18)-C(16)	124.10(16)
C(5)-C(6)-H(6)	121.9(12)	O(1)-C(18)-C(16)	110.54(14)
C(6)-C(7)-C(8)	119.73(16)	O(4)-C(19)-O(3)	126.27(17)
C(6)-C(7)-H(7)	120.3(11)	O(4)-C(19)-C(17)	122.70(16)
C(8)-C(7)-H(7)	120.0(11)	O(3)-C(19)-C(17)	110.99(14)
C(7)-C(8)-C(14)	120.96(16)	O(1)-C(20)-H(201)	109.5(14)
C(7)-C(8)-H(8)	120.1(11)	O(1)-C(20)-H(202)	106.6(15)
C(14)-C(8)-H(8)	118.9(11)	H(201)-C(20)-H(202)	104.7(19)
C(15)-C(9)-C(14)	122.58(15)	O(1)-C(20)-H(203)	109.9(12)
C(15)-C(9)-C(11)	122.71(15)	H(201)-C(20)-H(203)	112.7(19)
C(14)-C(9)-C(11)	114.53(14)	H(202)-C(20)-H(203)	113.1(19)
C(22)-C(10)-C(13)	123.02(15)	O(3)-C(21)-H(211)	112.0(14)
C(22)-C(10)-C(12)	122.60(15)	O(3)-C(21)-H(212)	104.5(13)
C(13)-C(10)-C(12)	114.28(14)	H(211)-C(21)-H(212)	109.8(19)
C(1)-C(11)-C(12)	119.43(16)	O(3)-C(21)-H(213)	109.7(14)
C(1)-C(11)-C(9)	123.54(15)	H(211)-C(21)-H(213)	108(2)
C(12)-C(11)-C(9)	117.02(14)	H(212)-C(21)-H(213)	113.4(19)
C(4)-C(12)-C(11)	118.41(15)	C(10)-C(22)-S(4)	124.42(13)
C(4)-C(12)-C(10)	123.17(15)	C(10)-C(22)-S(3)	124.25(13)
C(11)-C(12)-C(10)	118.40(14)	S(4)-C(22)-S(3)	111.23(9)
C(5)-C(13)-C(14)	118.55(15)	C(24)-C(23)-C(25)	128.25(17)
C(5)-C(13)-C(10)	123.99(15)	C(24)-C(23)-S(3)	116.55(13)
C(25)-C(23)-S(3)	115.19(14)	H(251)-C(25)-H(253)	112(2)
C(23)-C(24)-C(26)	128.03(17)	H(252)-C(25)-H(253)	110(2)
C(23)-C(24)-S(4)	116.69(13)	C(24)-C(26)-H(261)	109.5(17)
C(26)-C(24)-S(4)	115.28(14)	C(24)-C(26)-H(262)	112.1(14)
C(23)-C(25)-H(251)	111.2(16)	H(261)-C(26)-H(262)	114(2)
C(23)-C(25)-H(252)	110.3(19)	C(24)-C(26)-H(263)	112.9(15)
H(251)-C(25)-H(252)	101(2)	H(261)-C(26)-H(263)	103(2)
C(23)-C(25)-H(253)	112.5(16)	H(262)-C(26)-H(263)	106(2)

10-[4,5-Di(hydroxymethyl)-1,3-dithiol-2-ylidene]-9-(4-5-dimethyl-1,3-dithiol-2-ylidene)-9-10-dihydroanthracene (51)
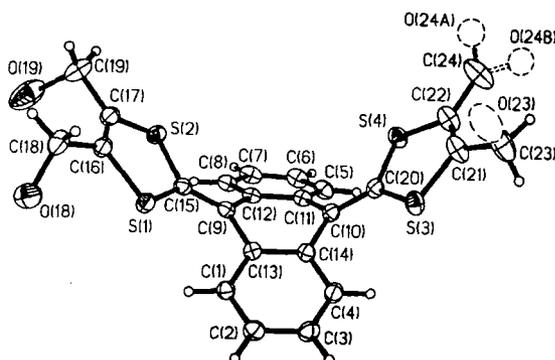
Table 1. Crystal data and structure refinement

Identification code	
Empirical formula	C24 H20 O2 S4
Formula weight	468.64
Temperature	120(2) K
Wavelength	0.71073 Å
Crystal system	Monoclinic
Space group	$P2_1/n$ (No. 14)
Unit cell dimensions	$a = 11.193(3)$ Å $\alpha = 90°$
	$b = 12.803(4)$ Å $\beta = 102.48(1)°$
	$c = 15.343(5)$ Å $\gamma = 90°$
Volume	2147(1) Å^3
Z	4
Density (calculated)	1.450 g/cm^3
Absorption coefficient	0.462 mm^{-1}
F(000)	976
Crystal size	0.26 × 0.22 × 0.20 mm^3
θ range for data collection	2.06 to 29.00°.
Index ranges	$-15 \leq h \leq 15, -17 \leq k \leq 17, -20 \leq l \leq 20$
Reflections collected	26077
Independent reflections	5686 [R(int) = 0.0436]
Reflections with I > 2σ(I)	4203
Completeness to θ = 29.00°	99.6 %
Absorption correction	None
Max. and min. transmission	0.9132 and 0.8892
Refinement method	Full-matrix least-squares on F^2
Data / restraints / parameters	5686 / 0 / 288
Largest final shift/e.s.d. ratio	0.003
Goodness-of-fit on F^2	1.039
Final R indices [I > 2σ(I)]	R$_1$ = 0.0398, wR$_2$ = 0.1051
R indices (all data)	R$_1$ = 0.0607, wR$_2$ = 0.1145
Largest diff. peak and hole	0.430 and -0.531 e.Å^{-3}

Table 2. Atomic coordinates (× 10³) and equivalent isotropic displacement parameters (Å² ×10⁴)
U(eq) is defined as one third of the trace of the orthogonalized Uij tensor.

	x	y	z	U(eq)
S(1)	32260(4)	58531(4)	2689(3)	256(1)
S(2)	55993(4)	60228(4)	15132(4)	278(1)
S(3)	31456(5)	7735(4)	15892(3)	295(1)
S(4)	54940(5)	11685(4)	28149(4)	296(1)
C(1)	14862(16)	46418(15)	11636(12)	228(4)
C(2)	4003(18)	40682(16)	9476(13)	277(4)
C(3)	3702(18)	30450(16)	12292(14)	294(4)
C(4)	14265(17)	25915(15)	17341(13)	273(4)
C(5)	51143(18)	31322(16)	39017(13)	286(4)
C(6)	58412(19)	38526(17)	44525(14)	321(4)
C(7)	59274(18)	48703(17)	41572(13)	304(4)
C(8)	52777(17)	51678(15)	33185(13)	255(4)
C(9)	37550(16)	47556(14)	18722(12)	205(4)
C(10)	36815(16)	26744(14)	24455(12)	222(4)
C(11)	44731(16)	34143(15)	30461(12)	229(4)
C(12)	45365(16)	44581(15)	27479(12)	218(4)
C(13)	25708(16)	41906(14)	16399(12)	207(4)
C(14)	25316(16)	31394(15)	19324(12)	216(4)
C(15)	41232(16)	54579(14)	13087(12)	221(4)
C(16)	43947(18)	65044(15)	-1192(13)	263(4)
C(17)	54782(18)	65746(15)	4463(14)	280(4)
C(18)	40290(20)	69780(17)	-10377(14)	330(5)
C(19)	65960(20)	71480(20)	3071(16)	417(6)
C(20)	40317(17)	16748(14)	23230(13)	239(4)
C(21)	42820(20)	-1829(17)	16420(15)	378(5)
C(22)	53630(20)	-21(17)	22001(15)	380(5)
C(23)	38970(30)	-11210(20)	10572(18)	532(7)
C(24)	64680(30)	-6930(20)	24120(20)	603(8)
O(18)*	29000(30)	75970(30)	-11440(20)	423(8)
O(19)*	62950(40)	83330(30)	4010(30)	757(14)
O(23)*	38640(40)	-9200(30)	1920(30)	654(12)
O(24A)‡	71490(60)	-6700(50)	19470(40)	527(15) ↳
O(24B)‡	65150(80)	-16040(70)	22860(60)	510(20) ↳

*Occupancy 0.5

†Occupancy 0.3

‡Occupancy 0.2

↳U(iso)

Table 3. Bond lengths [Å] and angles [°]

S(1)-C(16)	1.760(2)	C(9)-C(13)	1.484(2)
S(1)-C(15)	1.766(2)	C(9)-C(12)	1.486(3)
S(2)-C(17)	1.761(2)	C(10)-C(20)	1.363(3)
S(2)-C(15)	1.7684(19)	C(10)-C(11)	1.476(3)
S(3)-C(21)	1.755(2)	C(10)-C(14)	1.481(2)
S(3)-C(20)	1.761(2)	C(11)-C(12)	1.419(3)
S(4)-C(22)	1.760(2)	C(13)-C(14)	1.422(3)
S(4)-C(20)	1.7706(19)	C(16)-C(17)	1.333(3)
C(1)-C(2)	1.397(3)	C(16)-C(18)	1.507(3)
C(1)-C(13)	1.399(3)	C(17)-C(19)	1.505(3)
C(2)-C(3)	1.382(3)	C(18)-O(18)	1.471(4)
C(3)-C(4)	1.393(3)	C(19)-O(19)	1.567(5)
C(4)-C(14)	1.397(3)	C(21)-C(22)	1.342(3)
C(5)-C(6)	1.389(3)	C(21)-C(23)	1.506(3)
C(5)-C(11)	1.401(3)	C(22)-C(24)	1.498(3)
C(6)-C(7)	1.390(3)	C(23)-O(23)	1.345(5)
C(7)-C(8)	1.388(3)	C(24)-O(24A)	1.152(7)
C(8)-C(12)	1.402(3)	C(24)-O(24B)	1.185(10)
C(9)-C(15)	1.371(3)		
C(16)-S(1)-C(15)	97.03(9)	C(13)-C(9)-C(12)	114.39(15)
C(17)-S(2)-C(15)	96.77(9)	C(20)-C(10)-C(11)	122.47(17)
C(21)-S(3)-C(20)	97.19(10)	C(20)-C(10)-C(14)	123.15(17)
C(22)-S(4)-C(20)	96.94(10)	C(11)-C(10)-C(14)	114.16(16)
C(2)-C(1)-C(13)	121.26(17)	C(5)-C(11)-C(12)	119.59(17)
C(3)-C(2)-C(1)	120.18(18)	C(5)-C(11)-C(10)	122.44(18)
C(2)-C(3)-C(4)	119.60(18)	C(12)-C(11)-C(10)	117.92(16)
C(3)-C(4)-C(14)	121.14(18)	C(8)-C(12)-C(11)	118.22(17)
C(6)-C(5)-C(11)	120.9(2)	C(8)-C(12)-C(9)	123.48(17)
C(5)-C(6)-C(7)	119.80(19)	C(11)-C(12)-C(9)	118.18(16)
C(8)-C(7)-C(6)	120.03(19)	C(1)-C(13)-C(14)	118.23(16)
C(7)-C(8)-C(12)	121.45(19)	C(1)-C(13)-C(9)	123.58(16)
C(15)-C(9)-C(13)	122.87(16)	C(14)-C(13)-C(9)	118.18(16)
C(15)-C(9)-C(12)	122.68(16)	C(4)-C(14)-C(13)	119.51(16)
C(4)-C(14)-C(10)	122.74(17)	C(10)-C(20)-S(3)	124.36(15)
C(13)-C(14)-C(10)	117.75(16)	C(10)-C(20)-S(4)	123.48(15)
C(9)-C(15)-S(1)	124.61(14)	S(3)-C(20)-S(4)	111.94(11)
C(9)-C(15)-S(2)	123.58(14)	C(22)-C(21)-C(23)	128.4(2)
S(1)-C(15)-S(2)	111.73(10)	C(22)-C(21)-S(3)	116.96(17)
C(17)-C(16)-C(18)	127.33(18)	C(23)-C(21)-S(3)	114.67(18)
C(17)-C(16)-S(1)	116.74(15)	C(21)-C(22)-C(24)	128.6(2)
C(18)-C(16)-S(1)	115.82(15)	C(21)-C(22)-S(4)	116.63(17)
C(16)-C(17)-C(19)	127.4(2)	C(24)-C(22)-S(4)	114.66(19)
C(16)-C(17)-S(2)	117.03(15)	O(23)-C(23)-C(21)	112.3(3)
C(19)-C(17)-S(2)	115.35(16)	O(24A)-C(24)-O(24B)	82.2(6)
O(18)-C(18)-C(16)	111.92(19)	O(24A)-C(24)-C(22)	118.5(4)
C(17)-C(19)-O(19)	104.9(2)	O(24B)-C(24)-C(22)	127.6(5)

10-(4,5-Dimethyl-1,3-dithiol-2-ylidene)-9,10-dihydro-9-(5-methyl-4-phenyl carbonyloxymethyl-1,3-dithiol-2-ylidene)anthracene (52)
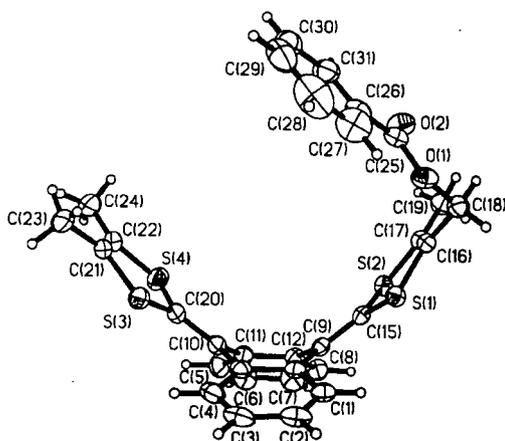
Table 1. Crystal data and structure refinement

Identification code	
Empirical formula	C31 H24 O2 S4
Formula weight	556.74
Temperature	150(2) K
Wavelength	0.71073 Å
Crystal system	Monoclinic
Space group	$P2_1/n$ (No. 14)
Unit cell dimensions	$a = 15.803(6)$ Å $\alpha = 90°$
	$b = 10.258(4)$ Å $\beta = 113.94(2)°$
	$c = 18.149(7)$ Å $\gamma = 90°$
Volume	2689.0(18) Å^3
Z	4
Density (calculated)	1.375 g/cm^3
Absorption coefficient	0.381 mm^{-1}
F(000)	1160
Crystal size	0.40 x 0.40 x 0.24 mm^3
θ range for data collection	1.45 to 29.00°.
Index ranges	$-21 \leq h \leq 21, -13 \leq k \leq 13, -24 \leq l \leq 24$
Reflections collected	26639
Independent reflections	7069 [R(int) = 0.0295]
Reflections with I > 2σ(I)	5320
Completeness to θ = 29.00°	98.9 %
Absorption correction	Semi-empirical from equivalents
Max. and min. transmission	0.9447 and 0.6991
Refinement method	Full-matrix least-squares on F^2
Data / restraints / parameters	7069 / 0 / 357
Largest final shift/e.s.d. ratio	0.004
Goodness-of-fit on F^2	1.010
Final R indices [I > 2σ(I)]	R1 = 0.0396, wR2 = 0.0936
R indices (all data)	R1 = 0.0607, wR2 = 0.1045
Largest diff. peak and hole	0.528 and -0.423 e.Å^{-3}

Table 2. Atomic coordinates (×10⁵) and equivalent isotropic displacement parameters (Å² ×10⁴)
U(eq) is defined as one third of the trace of the orthogonalized Uij tensor.

	x	y	z	U(eq)
S(1)	18149(3)	39208(4)	61132(2)	266(1)
S(2)	8819(3)	55815(4)	47005(3)	273(1)
S(3)	49976(3)	27004(5)	47305(4)	416(1)
S(4)	39939(4)	45834(6)	34761(3)	421(1)
O(1)	29037(10)	58571(12)	75801(8)	350(3)
O(2)	30072(10)	78031(13)	70506(9)	394(3)
C(1)	22251(13)	12695(17)	54944(10)	307(4)
C(2)	28018(15)	1872(18)	57688(12)	386(4)
C(3)	34699(15)	-570(19)	54769(12)	412(5)
C(4)	35738(13)	7673(18)	49132(12)	362(4)
C(5)	19675(14)	34810(20)	26336(12)	402(5)
C(6)	10877(16)	38590(20)	21060(12)	455(5)
C(7)	3981(15)	40480(20)	23813(12)	414(5)
C(8)	5912(13)	38739(18)	31938(11)	329(4)
C(9)	17185(11)	32645(16)	46029(10)	240(3)
C(10)	30836(12)	28051(18)	40396(11)	289(4)
C(11)	21765(12)	32941(18)	34545(11)	297(4)
C(12)	14746(12)	35064(17)	37355(10)	264(3)
C(13)	23192(11)	21161(16)	49280(10)	260(3)
C(14)	30088(12)	18689(17)	46309(11)	289(4)
C(15)	14795(11)	41052(16)	50670(10)	239(3)
C(16)	15927(12)	55534(17)	62926(11)	275(3)
C(17)	11570(12)	63034(17)	56455(11)	277(3)
C(18)	19019(14)	59272(19)	71613(11)	344(4)
C(19)	8514(14)	76987(19)	56249(13)	379(4)
C(20)	39048(13)	32584(19)	40629(11)	326(4)
C(21)	56625(14)	38940(20)	45070(15)	457(6)
C(22)	52042(15)	47510(20)	39401(15)	446(5)
C(23)	66970(15)	37990(20)	49800(20)	627(8)
C(24)	56014(18)	58650(30)	36386(17)	589(7)
C(25)	33809(13)	68625(17)	74490(10)	310(4)
C(26)	44003(14)	66754(19)	78500(11)	357(4)
C(27)	47951(19)	56020(30)	83273(15)	581(6)
C(28)	57620(20)	54930(40)	86796(17)	792(10)
C(29)	63100(19)	64170(30)	85638(16)	674(8)
C(30)	59241(17)	74810(30)	80935(17)	607(7)
C(31)	49640(15)	76080(20)	77296(14)	456(5)

Table 3. Bond lengths [Å] and angles [°]

S(1)-C(15)	1.7621(18)	C(9)-C(15)	1.362(2)
S(1)-C(16)	1.7684(19)	C(9)-C(13)	1.477(2)
S(2)-C(17)	1.7532(19)	C(9)-C(12)	1.482(2)
S(2)-C(15)	1.7657(18)	C(10)-C(20)	1.363(3)
S(3)-C(20)	1.755(2)	C(10)-C(14)	1.480(3)
S(3)-C(21)	1.764(2)	C(10)-C(11)	1.483(3)
S(4)-C(22)	1.758(2)	C(11)-C(12)	1.413(2)
S(4)-C(20)	1.767(2)	C(13)-C(14)	1.421(2)
O(1)-C(25)	1.354(2)	C(16)-C(17)	1.338(3)
O(1)-C(18)	1.454(2)	C(16)-C(18)	1.494(3)
O(2)-C(25)	1.207(2)	C(17)-C(19)	1.506(3)
C(1)-C(2)	1.394(3)	C(21)-C(22)	1.324(3)
C(1)-C(13)	1.399(2)	C(21)-C(23)	1.510(3)
C(2)-C(3)	1.383(3)	C(22)-C(24)	1.509(3)
C(3)-C(4)	1.387(3)	C(25)-C(26)	1.487(3)
C(4)-C(14)	1.402(3)	C(26)-C(27)	1.383(3)
C(5)-C(6)	1.386(3)	C(26)-C(31)	1.384(3)
C(5)-C(11)	1.402(3)	C(27)-C(28)	1.401(4)
C(6)-C(7)	1.384(3)	C(28)-C(29)	1.357(5)
C(7)-C(8)	1.391(3)	C(29)-C(30)	1.367(4)
C(8)-C(12)	1.394(2)	C(30)-C(31)	1.394(3)
C(15)-S(1)-C(16)	95.82(8)	C(7)-C(8)-C(12)	120.57(18)
C(17)-S(2)-C(15)	96.39(8)	C(15)-C(9)-C(13)	123.54(15)
C(20)-S(3)-C(21)	97.24(11)	C(15)-C(9)-C(12)	122.23(15)
C(22)-S(4)-C(20)	97.12(11)	C(13)-C(9)-C(12)	113.94(14)
C(25)-O(1)-C(18)	115.87(14)	C(20)-C(10)-C(14)	123.64(17)
C(2)-C(1)-C(13)	120.53(18)	C(20)-C(10)-C(11)	122.58(18)
C(3)-C(2)-C(1)	119.84(19)	C(14)-C(10)-C(11)	113.60(15)
C(2)-C(3)-C(4)	120.62(18)	C(5)-C(11)-C(12)	118.78(17)
C(3)-C(4)-C(14)	120.85(19)	C(5)-C(11)-C(10)	123.33(16)
C(6)-C(5)-C(11)	120.68(18)	C(12)-C(11)-C(10)	117.77(16)
C(7)-C(6)-C(5)	120.38(18)	C(8)-C(12)-C(11)	119.68(16)
C(6)-C(7)-C(8)	119.90(19)	C(8)-C(12)-C(9)	123.28(16)
C(11)-C(12)-C(9)	116.98(15)	S(3)-C(20)-S(4)	111.73(10)
C(11)-C(13)-C(14)	119.64(16)	C(22)-C(21)-C(23)	127.5(2)
C(1)-C(13)-C(9)	123.09(16)	C(22)-C(21)-S(3)	116.79(16)
C(14)-C(13)-C(9)	117.27(15)	C(23)-C(21)-S(3)	115.7(2)
C(4)-C(14)-C(13)	118.55(17)	C(21)-C(22)-C(24)	127.5(2)
C(4)-C(14)-C(10)	124.17(17)	C(21)-C(22)-S(4)	116.93(17)
C(13)-C(14)-C(10)	117.29(16)	C(24)-C(22)-S(4)	115.6(2)
C(9)-C(15)-S(1)	124.12(13)	O(2)-C(25)-O(1)	122.84(18)
C(9)-C(15)-S(2)	123.39(13)	O(2)-C(25)-C(26)	124.48(18)
S(1)-C(15)-S(2)	112.28(9)	O(1)-C(25)-C(26)	112.68(16)
C(17)-C(16)-C(18)	127.48(17)	C(27)-C(26)-C(31)	119.6(2)
C(17)-C(16)-S(1)	116.95(14)	C(27)-C(26)-C(25)	122.2(2)
C(18)-C(16)-S(1)	115.57(13)	C(31)-C(26)-C(25)	118.19(18)
C(16)-C(17)-C(19)	127.87(17)	C(26)-C(27)-C(28)	118.7(3)
C(16)-C(17)-S(2)	116.81(14)	C(29)-C(28)-C(27)	121.4(3)
C(19)-C(17)-S(2)	115.30(13)	C(28)-C(29)-C(30)	120.2(3)
O(1)-C(18)-C(16)	111.01(15)	C(29)-C(30)-C(31)	119.7(3)
C(10)-C(20)-S(3)	124.61(16)	C(26)-C(31)-C(30)	120.5(2)
C(10)-C(20)-S(4)	123.46(15)		

10-(4,5-Dimethyl-1,3-dithiol-2-ylidene)-9,10-dihydro-9-(5-methyl-4-(2-naphthyl)

carbonyloxymethyl-1,3-dithiol-2-ylidene)anthracene (53)
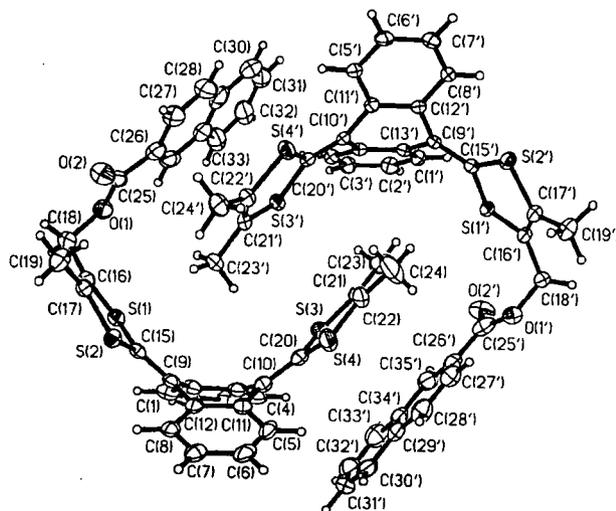
Table 1. Crystal data and structure refinement

Identification code	
Empirical formula	C35 H26 O2 S4,C H2 Cl2
Formula weight	691.72
Temperature	100(2) K
Wavelength	0.71073 Å
Crystal system	Monoclinic
Space group	$P2_1/n$ (No. 14)
Unit cell dimensions	$a = 13.842(5)$ Å $\alpha= 90°$
	$b = 26.390(10)$ Å $\beta= 110.04(1)°$
	$c = 19.064(7)$ Å $\gamma= 90°$
Volume	6542(4) Å^3
Z	8
Density (calculated)	1.405 g/cm^3
Absorption coefficient	0.487 mm^{-1}
F(000)	2864
Crystal size	$0.45 \times 0.35 \times 0.16$ mm^3
θ range for data collection	1.37 to 27.50°.
Index ranges	$-17 \leq h \leq 17, -28 \leq k \leq 34, -24 \leq l \leq 24$
Reflections collected	46854
Independent reflections	15004 [R(int) = 0.0454]
Reflections with I>2σ(I)	10911
Completeness to θ = 27.50°	99.9 %
Absorption correction	Integration
Max. and min. transmission	0.9299 and 0.8203
Refinement method	Full-matrix least-squares on F^2
Data / restraints / parameters	15004 / 0 / 809
Largest final shift/e.s.d. ratio	0.010
Goodness-of-fit on F^2	1.049
Final R indices [I>2σ(I)]	R1 = 0.0882, wR2 = 0.2179
R indices (all data)	R1 = 0.1195, wR2 = 0.2411
Largest diff. peak and hole	1.361 and -1.201 e.Å^{-3}

Table 2. Atomic coordinates (×10⁴) and equivalent isotropic displacement parameters (Å² ×10⁴) U(eq) is defined as one third of the trace of the orthogonalized Uij tensor.

	x	y	z	U(eq)
S(1)	6338(1)	2897(1)	2170(1)	268(2)
S(2)	7686(1)	2932(1)	3735(1)	264(2)
S(3)	6221(1)	5265(1)	1961(1)	570(5)
S(4)	7349(2)	5282(1)	3567(1)	583(5)
O(1)	4070(3)	2658(1)	2311(2)	408(9)
O(2)	4126(3)	2681(2)	3514(3)	518(10)
C(1)	7445(4)	3534(2)	1275(3)	356(11)
C(2)	7191(4)	3775(3)	587(3)	483(15)
C(3)	7155(5)	4300(3)	549(3)	542(17)
C(4)	7371(4)	4583(3)	1193(4)	493(16)
C(5)	9438(4)	4676(2)	3811(3)	397(13)
C(6)	10205(4)	4431(2)	4373(3)	388(12)
C(7)	10266(4)	3909(2)	4395(3)	322(10)
C(8)	9543(3)	3626(2)	3842(3)	274(9)
C(9)	7937(3)	3583(2)	2683(3)	254(9)
C(10)	7855(4)	4625(2)	2618(3)	368(12)
C(11)	8685(4)	4396(2)	3249(3)	323(10)
C(12)	8745(3)	3861(2)	3277(3)	275(9)
C(13)	7651(3)	3819(2)	1932(3)	300(10)
C(14)	7627(4)	4349(2)	1895(3)	363(12)
C(15)	7417(3)	3186(2)	2832(2)	228(8)
C(16)	5930(4)	2561(2)	2825(3)	273(9)
C(17)	6550(4)	2576(2)	3537(3)	282(9)
C(18)	4918(4)	2293(2)	2514(3)	325(10)
C(19)	6408(4)	2328(2)	4201(3)	386(12)
C(20)	7264(4)	5015(2)	2699(4)	459(14)
C(21)	5690(5)	5635(2)	2506(6)	680(20)
C(22)	6199(6)	5637(2)	324(6)	700(20)
C(23)	4722(5)	5912(2)	2069(7)	900(30)
C(24)	5922(9)	5926(3)	3837(7)	1090(40)
C(25)	3778(4)	2824(2)	2899(4)	405(13)
C(26)	2938(4)	3227(2)	2637(4)	432(13)
C(27)	2524(5)	3411(2)	3171(4)	519(15)
C(28)	1718(5)	3750(2)	2954(4)	552(16)
C(29)	1319(4)	3907(2)	2207(4)	475(14)
C(30)	418(5)	4259(3)	1964(5)	640(20)
C(31)	31(4)	4404(2)	1235(4)	506(15)
C(32)	502(4)	4231(2)	729(4)	571(18)
C(33)	1340(5)	3909(2)	944(4)	548(17)
C(34)	1731(5)	3742(2)	1674(4)	469(14)
C(35)	2584(4)	3379(2)	1924(3)	418(13)
S(1')	3584(1)	7125(1)	2446(1)	257(2)
S(2')	3596(1)	7146(1)	3984(1)	284(2)
S(3')	3891(1)	4656(1)	2651(1)	269(2)
S(4')	3823(1)	4677(1)	4164(1)	286(3)
O(1')	6151(3)	7420(2)	2865(2)	449(9)
O(2')	5366(3)	7206(2)	1670(2)	525(11)
C(1')	1907(3)	6352(2)	1569(3)	259(9)
C(2')	1671(4)	6065(2)	922(3)	295(10)
C(3')	1760(4)	5538(2)	969(3)	293(10)
C(4')	2088(3)	5301(2)	1661(2)	245(9)
C(5')	2037(3)	5369(2)	4162(2)	242(9)
C(6')	1699(4)	5643(2)	4659(3)	286(10)
C(7')	1633(4)	6168(2)	4616(3)	281(9)
C(8')	1903(3)	6420(2)	4071(2)	238(9)
C(9')	2557(3)	6406(2)	2980(2)	199(8)
C(10')	2693(3)	5351(2)	3075(2)	202(8)
C(11')	2329(3)	5618(2)	3617(2)	211(8)
C(12')	2257(3)	6155(2)	3571(2)	203(8)
C(13')	2266(3)	6118(2)	2274(2)	209(8)
C(14')	2355(3)	5585(2)	2320(2)	208(8)
C(15')	3128(3)	6838(2)	3106(2)	217(8)
C(16')	4541(3)	7495(2)	3094(3)	283(10)
C(17')	4551(4)	7504(2)	3796(3)	301(10)
C(18')	5285(4)	7762(2)	2808(3)	359(11)
C(19')	5279(4)	7789(2)	4462(3)	426(13)
C(20')	3346(3)	4948(2)	3261(2)	220(8)
C(21')	4807(4)	4283(2)	3325(3)	297(10)
C(22')	4768(4)	4288(2)	4014(3)	305(10)
C(23')	5516(4)	3982(2)	3037(3)	394(12)
C(24')	5409(4)	3981(2)	4679(3)	422(13)
C(25')	6075(4)	7167(2)	2265(3)	420(13)
C(26')	6976(4)	6807(2)	2374(3)	334(11)
C(27')	7685(5)	6715(2)	3083(3)	438(13)
C(28')	8527(5)	6400(2)	3182(3)	457(13)
C(29')	8671(4)	6179(2)	2549(3)	377(12)
C(30')	9541(4)	5864(2)	2614(4)	440(14)
C(31')	9644(4)	5666(2)	1976(4)	514(16)
C(32')	8935(6)	5761(3)	1282(4)	576(17)
C(33')	8113(5)	6053(3)	1204(4)	523(15)
C(34')	7951(4)	6268(2)	1821(3)	383(12)
C(35')	7087(4)	6589(2)	1758(3)	432(13)
Cl(1A)	-113(2)	2749(1)	5441(1)	642(6)
Cl(2A)	1651(2)	2631(1)	4978(2)	883(8)
C(01A)	549(8)	2333(4)	5061(6)	660(20)
Cl(1B)	2084(12)	2166(6)	4606(9)	840(40)
Cl(2B)	2803(14)	3203(7)	4913(10)	960(50)
C(01B)	165(2)	2631(1)	4978(2)	883(8)
Cl(2C)	-410(17)	2734(8)	5355(12)	630(50)
Cl(3)	-846(3)	1447(1)	5624(2)	604(8)
Cl(4)	-1422(3)	409(1)	5657(2)	644(9)
Cl(5)	-588(7)	-459(3)	5083(5)	498(18)
Cl(6)	-417(4)	725(2)	4708(3)	540(12)
Cl(7)	-1294(7)	671(4)	5861(5)	620(20)
Cl(8)	-1064(9)	1942(5)	5478(7)	590(30)
Cl(9)	-861(13)	397(6)	5295(10)	500(40)
C(02A)	-294(11)	791(5)	5757(8)	820(30)
C(02B)	-563(11)	1374(6)	5388(8)	230(30)

Table 3. Bond lengths [Å] and angles [°].

S(1)-C(15)	1.764(4)	C(22)-C(24)	1.523(12)
S(1)-C(16)	1.775(5)	C(25)-C(26)	1.528(8)
S(2)-C(17)	1.757(5)	C(26)-C(35)	1.337(9)
S(2)-C(15)	1.765(4)	C(26)-C(27)	1.415(8)
S(3)-C(21)	1.760(8)	C(27)-C(28)	1.378(9)
S(3)-C(20)	1.763(7)	C(28)-C(29)	1.401(9)
S(4)-C(20)	1.764(7)	C(29)-C(34)	1.395(9)
S(4)-C(22)	1.766(8)	C(29)-C(30)	1.496(10)
O(1)-C(25)	1.387(7)	C(30)-C(31)	1.362(10)
O(1)-C(18)	1.465(6)	C(31)-C(32)	1.411(10)
O(2)-C(25)	1.167(7)	C(32)-C(33)	1.382(8)
C(1)-C(2)	1.391(7)	C(33)-C(34)	1.380(10)
C(1)-C(13)	1.403(7)	C(34)-C(35)	1.469(9)
C(2)-C(3)	1.387(10)	S(1')-C(15')	1.761(4)
C(3)-C(4)	1.380(10)	S(1')-C(16')	1.766(5)
C(4)-C(14)	1.404(8)	S(2')-C(17')	1.758(5)
C(5)-C(6)	1.383(8)	S(2')-C(15')	1.772(4)
C(5)-C(11)	1.420(8)	S(3')-C(21')	1.765(5)
C(6)-C(7)	1.381(8)	S(3')-C(20')	1.765(4)
C(7)-C(8)	1.395(7)	S(4')-C(22')	1.763(5)
C(8)-C(12)	1.397(7)	S(4')-C(20')	1.769(4)
C(9)-C(15)	1.356(6)	O(1')-C(25')	1.298(7)
C(9)-C(12)	1.483(6)	O(1')-C(18')	1.473(6)
C(9)-C(13)	1.485(6)	O(2')-C(25')	1.223(7)
C(10)-C(20)	1.356(7)	C(1')-C(2')	1.388(7)
C(10)-C(11)	1.479(8)	C(1')-C(13')	1.406(7)
C(10)-C(14)	1.493(8)	C(2')-C(3')	1.397(7)
C(11)-C(12)	1.414(7)	C(3')-C(4')	1.387(7)
C(13)-C(14)	1.402(7)	C(4')-C(14')	1.401(6)
C(16)-C(17)	1.334(7)	C(5')-C(6')	1.394(6)
C(16)-C(18)	1.498(7)	C(5')-C(11')	1.402(6)
C(17)-C(19)	1.496(7)	C(6')-C(7')	1.389(7)
C(21)-C(22)	1.335(12)	C(7')-C(8')	1.389(6)
C(21)-C(23)	1.502(10)	C(8')-C(12')	1.400(6)
C(9')-C(15')	1.362(6)	C(25')-C(26')	1.524(8)
C(9')-C(13')	1.476(6)	C(26')-C(35')	1.363(8)
C(9')-C(12')	1.482(6)	C(26')-C(27')	1.392(8)
C(10')-C(20')	1.360(6)	C(27')-C(28')	1.390(9)
C(10')-C(11')	1.475(6)	C(28')-C(29')	1.415(8)
C(10')-C(14')	1.487(6)	C(29')-C(34')	1.424(8)
C(11')-C(12')	1.421(6)	C(29')-C(30')	1.432(8)
C(13')-C(14')	1.412(6)	C(30')-C(31')	1.376(9)
C(16')-C(17')	1.333(7)	C(31')-C(32')	1.372(10)
C(16')-C(18')	1.496(6)	C(32')-C(33')	1.340(10)
C(17')-C(19')	1.522(7)	C(33')-C(34')	1.392(9)
C(21')-C(22')	1.331(7)	C(34')-C(35')	1.437(8)
C(21')-C(23')	1.506(6)	Cl(1A)-C(01A)	1.740(10)
C(22')-C(24')	1.509(7)	Cl(2A)-C(01A)	1.769(10)

C(10)-C(20)-S(4)	124.2(5)	C(6')-C(5')-C(11')	120.6(4)
S(3)-C(20)-S(4)	111.8(3)	C(7')-C(6')-C(5')	120.5(4)
C(22)-C(21)-C(23)	129.0(8)	C(8')-C(7')-C(6')	119.6(4)
C(22)-C(21)-S(3)	116.4(5)	C(7')-C(8')-C(12')	121.1(4)
C(23)-C(21)-S(3)	114.6(8)	C(15')-C(9')-C(13')	123.5(4)
C(21)-C(22)-C(24)	127.4(8)	C(15')-C(9')-C(12')	122.4(4)
C(21)-C(22)-S(4)	117.1(6)	C(13')-C(9')-C(12')	113.9(4)
C(24)-C(22)-S(4)	115.5(8)	C(20')-C(10')-C(11')	123.1(4)
O(2)-C(25)-O(1)	125.3(5)	C(20')-C(10')-C(14')	122.6(4)
O(2)-C(25)-C(26)	124.0(5)	C(11')-C(10')-C(14')	114.1(4)
O(1)-C(25)-C(26)	110.8(5)	C(5')-C(11')-C(12')	118.8(4)
C(35)-C(26)-C(27)	122.0(6)	C(5')-C(11')-C(10')	123.4(4)
C(35)-C(26)-C(25)	120.9(5)	C(12')-C(11')-C(10')	117.8(4)
C(27)-C(26)-C(25)	117.0(6)	C(8')-C(12')-C(11')	119.4(4)
C(28)-C(27)-C(26)	119.5(6)	C(8')-C(12')-C(9')	123.2(4)
C(27)-C(28)-C(29)	119.6(6)	C(11')-C(12')-C(9')	117.4(4)
C(34)-C(29)-C(28)	122.1(6)	C(1')-C(13')-C(14')	119.5(4)
C(34)-C(29)-C(30)	118.3(6)	C(1')-C(13')-C(9')	122.9(4)
C(28)-C(29)-C(30)	119.7(6)	C(14')-C(13')-C(9')	117.6(4)
C(31)-C(30)-C(29)	119.0(7)	C(4')-C(14')-C(13')	119.1(4)
C(30)-C(31)-C(32)	119.7(6)	C(4')-C(14')-C(10')	123.0(4)
C(33)-C(32)-C(31)	122.2(7)	C(13')-C(14')-C(10')	117.9(4)
C(34)-C(33)-C(32)	119.7(7)	C(9')-C(15')-S(1')	124.2(3)
C(33)-C(34)-C(29)	121.2(6)	C(9')-C(15')-S(2')	123.6(3)
C(33)-C(34)-C(35)	122.1(6)	S(1')-C(15')-S(2')	111.9(2)
C(29)-C(34)-C(35)	116.7(6)	C(17')-C(16')-C(18')	125.9(4)
C(26)-C(35)-C(34)	120.0(5)	C(17')-C(16')-S(1')	117.4(3)
C(15')-S(1')-C(16')	96.0(2)	C(18')-C(16')-S(1')	116.7(4)
C(17')-S(2')-C(15')	96.4(2)	C(16')-C(17')-C(19')	128.4(4)
C(21')-S(3')-C(20')	97.3(2)	C(16')-C(17')-S(2')	116.4(4)
C(22')-S(4')-C(20')	97.3(2)	C(19')-C(17')-S(2')	115.1(4)
C(25')-O(1')-C(18')	115.6(5)	O(1')-C(18')-C(16')	109.3(4)
C(2')-C(1')-C(13')	120.5(4)	C(10')-C(20')-S(3')	124.3(3)
C(1')-C(2')-C(3')	119.9(4)	C(10')-C(20')-S(4')	124.2(3)
C(4')-C(3')-C(2')	120.1(4)	S(3')-C(20')-S(4')	111.3(2)
C(3')-C(4')-C(14')	120.8(4)	C(22')-C(21')-C(23')	128.0(5)
C(22')-C(21')-S(3')	116.8(4)	C(27')-C(28')-C(29')	119.2(6)
C(23')-C(21')-S(3')	115.1(4)	C(28')-C(29')-C(34')	120.5(5)
C(21')-C(22')-C(24')	127.8(5)	C(28')-C(29')-C(30')	121.7(6)
C(21')-C(22')-S(4')	116.6(4)	C(34')-C(29')-C(30')	117.8(5)
C(24')-C(22')-S(4')	115.6(4)	C(31')-C(30')-C(29')	118.9(5)
O(2')-C(25')-O(1')	124.8(6)	C(32')-C(31')-C(30')	121.7(6)
O(2')-C(25')-C(26')	122.5(6)	C(33')-C(32')-C(31')	120.8(6)
O(1')-C(25')-C(26')	112.7(5)	C(32')-C(33')-C(34')	121.1(6)
C(35')-C(26')-C(27')	120.8(5)	C(33')-C(34')-C(29')	119.7(5)
C(35')-C(26')-C(25')	118.3(5)	C(33')-C(34')-C(35')	122.7(6)
C(27')-C(26')-C(25')	120.9(5)	C(29')-C(34')-C(35')	117.6(5)
C(28')-C(27')-C(26')	121.0(6)	C(26')-C(35')-C(34')	120.9(5)

C(15)-S(1)-C(16)	96.2(2)	C(5)-C(11)-C(10)	124.4(5)
C(17)-S(2)-C(15)	96.9(2)	C(8)-C(12)-C(11)	119.5(4)
C(21)-S(3)-C(20)	97.5(4)	C(8)-C(12)-C(9)	124.1(4)
C(20)-S(4)-C(22)	96.9(4)	C(11)-C(12)-C(9)	116.4(4)
C(25)-O(1)-C(18)	115.0(4)	C(14)-C(13)-C(1)	119.7(5)
C(2)-C(1)-C(13)	120.4(6)	C(14)-C(13)-C(9)	117.4(5)
C(3)-C(2)-C(1)	119.9(6)	C(1)-C(13)-C(9)	122.8(5)
C(4)-C(3)-C(2)	120.1(5)	C(13)-C(14)-C(4)	118.7(6)
C(3)-C(4)-C(14)	121.2(6)	C(13)-C(14)-C(10)	116.5(4)
C(6)-C(5)-C(11)	120.9(5)	C(4)-C(14)-C(10)	124.7(5)
C(7)-C(6)-C(5)	120.7(5)	C(9)-C(15)-S(1)	124.4(3)
C(6)-C(7)-C(8)	119.4(5)	C(9)-C(15)-S(2)	123.3(3)
C(7)-C(8)-C(12)	121.2(5)	S(1)-C(15)-S(2)	112.2(2)
C(15)-C(9)-C(12)	122.5(4)	C(17)-C(16)-C(18)	127.2(4)
C(15)-C(9)-C(13)	122.7(4)	C(17)-C(16)-S(1)	116.9(4)
C(12)-C(9)-C(13)	114.3(4)	C(18)-C(16)-S(1)	115.9(3)
C(20)-C(10)-C(11)	123.3(5)	C(16)-C(17)-C(19)	128.5(5)
C(20)-C(10)-C(14)	122.0(5)	C(16)-C(17)-S(2)	116.7(4)
C(11)-C(10)-C(14)	114.2(4)	C(19)-C(17)-S(2)	114.7(4)
C(12)-C(11)-C(15)	118.2(5)	O(1)-C(18)-C(16)	110.5(4)
C(12)-C(11)-C(10)	117.3(5)	C(10)-C(20)-S(3)	123.6(5)

167

Benzyl cyclophane (78a)
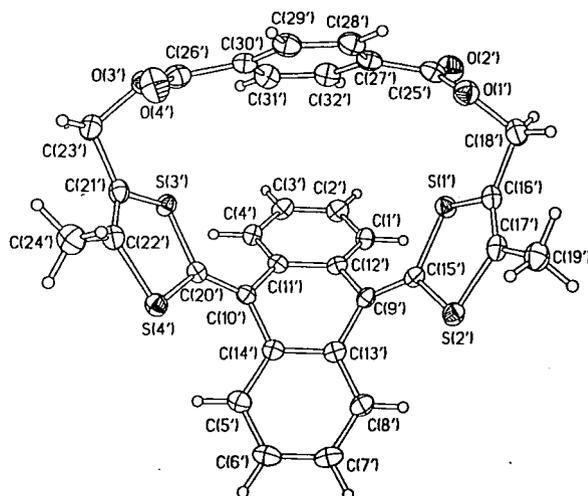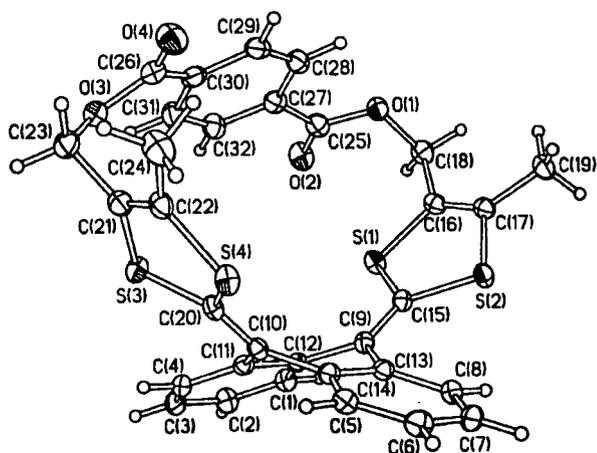
Table 1. Crystal data and structure refinement

Identification code	
Empirical formula	$C_{32}H_{22}O_4S_4$
Formula weight	598.74
Temperature	100(2) K
Wavelength	0.71073 Å
Crystal system	Monoclinic
Space group	$P2_1/c$ (No. 14)
Unit cell dimensions	a = 19.957(4) Å α= 90°
	b = 18.278(4) Å β= 111.15(1)°
	c = 16.306(3) Å γ = 90°
Volume	5547(2) Å³
Z	8
Density (calculated)	1.434 g/cm³
Absorption coefficient	0.381 mm⁻¹
F(000)	2480
Crystal size	0.45 × 0.22 × 0.10 mm³
θ range for data collection	1.0 to 29.0°.
Index ranges	-27 ≤ h ≤ 26, -24 ≤ k ≤ 24, -21 ≤ l ≤ 22
Reflections collected	67857
Independent reflections	14676 [R(int) = 0.068]
Reflections with I>2σ(I)	9818
Completeness to θ = 29.0°	99.5 %
Absorption correction	Semi-empirical from equivalents
Max. and min. transmission	0.962 and 0.719
Refinement method	Full-matrix least-squares on F²
Data / restraints / parameters	14676 / 0 / 729
Largest final shift/e.s.d. ratio	0.001
Goodness-of-fit on F²	1.008
Final R indices [I>2σ(I)]	R_1 = 0.0451, wR_2 = 0.0946
R indices (all data)	R_1 = 0.0866, wR_2 = 0.1103
Largest diff. peak and hole	0.476 and -0.386 e.Å⁻³

168

Table 2. Atomic coordinates (×10⁴) and equivalent isotropic displacement parameters (Å² ×10⁴) U(eq) is defined as one third of the trace of the orthogonalized U_{ij} tensor.

	x	y	z	U(eq)
S(1)	4383(1)	3116(1)	9405(1)	209(1)
S(2)	3918(1)	4579(1)	9690(1)	216(1)
S(3)	5102(1)	4030(1)	6072(1)	203(1)
S(4)	4734(1)	5565(1)	6188(1)	211(1)
O(1)	6042(1)	3168(1)	10827(1)	244(4)
O(2)	5824(1)	2098(1)	10079(1)	296(4)
O(3)	6741(1)	3918(1)	6923(1)	245(4)
O(4)	7142(1)	4898(1)	7812(1)	349(4)
C(1)	3427(1)	2717(1)	7464(1)	203(5)
C(2)	3399(1)	2197(1)	6827(2)	236(5)
C(3)	3587(1)	2389(1)	6118(2)	222(5)
C(4)	3790(1)	3103(1)	6031(2)	197(5)
C(5)	3282(1)	5613(1)	6456(1)	199(5)
C(6)	2894(1)	6086(1)	6785(2)	230(5)
C(7)	2726(1)	5882(1)	7508(2)	235(5)
C(8)	2949(1)	5210(1)	7907(1)	198(5)
C(9)	3631(1)	4021(1)	8018(1)	167(4)
C(10)	3965(1)	4425(1)	6559(1)	167(4)
C(11)	3807(1)	3642(1)	6651(1)	169(4)
C(12)	3630(1)	3438(1)	7385(1)	165(4)
C(13)	3356(1)	4734(1)	7599(1)	172(4)
C(14)	3528(1)	4940(1)	6859(1)	170(4)
C(15)	3912(1)	3914(1)	8903(1)	172(4)
C(16)	4812(1)	3512(1)	10461(1)	199(5)
C(17)	4597(1)	4177(1)	10591(1)	199(5)
C(18)	5424(1)	3081(1)	11092(2)	241(5)
C(19)	4831(1)	4627(1)	11419(2)	251(5)
C(20)	4507(1)	4644(1)	6295(1)	182(4)
C(21)	5759(1)	4686(1)	6108(1)	210(5)
C(22)	5595(1)	5390(1)	6164(1)	216(5)
C(23)	6475(1)	4392(1)	6153(2)	247(5)
C(24)	6061(2)	6046(1)	6211(2)	323(6)
C(25)	6082(1)	2704(1)	10199(2)	241(5)
C(26)	6949(1)	4269(1)	7703(2)	255(5)
C(27)	6439(1)	3059(1)	9636(2)	221(5)
C(28)	6731(1)	3760(1)	9821(2)	232(5)
C(29)	6937(1)	4128(1)	9209(2)	233(5)
C(30)	6854(1)	3799(1)	8404(2)	231(5)
C(31)	6597(1)	3081(1)	8241(2)	257(5)
C(32)	6389(1)	2715(1)	8853(2)	262(5)
S(1')	1066(1)	6567(1)	5221(1)	254(1)
S(2')	1242(1)	5014(1)	5679(1)	251(1)
S(3')	177(1)	5878(1)	1081(1)	235(1)
S(4')	218(1)	4319(1)	1491(1)	241(1)
O(1')	-578(1)	6809(1)	5098(1)	311(4)
O(2')	-59(1)	7823(1)	4786(1)	355(4)
O(3')	-1386(1)	6379(1)	507(1)	˙283(4)
O(4')	-2051(1)	5579(1)	945(1)	389(5)
C(1')	1974(1)	6883(1)	4080(2)	243(5)
C(2')	2011(1)	7430(1)	3502(2)	281(5)
C(3')	1795(1)	7288(1)	2608(2)	262(5)
C(4')	1545(1)	6595(1)	2292(2)	230(5)
C(5')	1706(1)	4017(1)	2902(2)	252(5)
C(6')	2017(1)	3467(1)	3508(2)	299(6)
C(7')	2212(1)	3602(1)	4397(2)	292(6)
C(8')	2116(1)	4296(1)	4691(2)	258(5)
C(9')	1641(1)	5595(1)	4351(1)	211(5)
C(10')	1219(1)	5300(1)	2558(2)	203(5)
C(11')	1490(1)	6044(1)	2857(2)	199(5)
C(12')	1707(1)	6192(1)	3770(2)	206(5)
C(13')	1790(1)	4854(1)	4093(2)	215(5)
C(14')	1572(1)	4707(1)	3181(2)	205(5)
C(15')	1381(1)	5712(1)	5007(2)	214(5)
C(16')	552(1)	6214(1)	5824(2)	264(5)
C(17')	640(1)	5503(1)	6040(2)	261(5)
C(18')	11(1)	6726(2)	5951(2)	316(6)
C(19')	293(1)	5061(2)	6560(2)	320(6)
C(20')	637(1)	5180(1)	1813(2)	206(5)
C(21')	-613(1)	5370(1)	540(2)	239(5)
C(22')	-597(1)	4657(1)	734(2)	256(5)
C(23')	-1235(1)	5816(1)	-40(2)	277(5)
C(24')	-1190(1)	4105(1)	381(2)	339(6)
C(25')	-472(1)	7315(1)	4550(2)	289(5)
C(26')	-1680(1)	6123(1)	1081(2)	284(5)
C(27')	-881(1)	7121(1)	3609(2)	269(5)
C(28')	-1512(1)	6712(1)	3358(2)	296(6)
C(29')	-1795(1)	6428(1)	2510(2)	290(5)
C(30')	-1452(1)	6551(1)	1915(2)	257(5)
C(31')	-838(1)	6995(1)	2159(2)	297(6)
C(32')	-559(1)	7279(1)	3002(2)	298(6)

Table 3. Bond lengths [Å] and angles [°].

Bond	Length	Bond	Length
S(1)-C(15)	1.768(2)	C(17)-C(19)	1.504(3)
S(1)-C(16)	1.776(2)	C(21)-C(22)	1.339(3)
S(2)-C(17)	1.760(2)	C(21)-C(23)	1.504(3)
S(2)-C(15)	1.765(2)	C(22)-C(24)	1.501(3)
S(3)-C(21)	1.761(2)	C(25)-C(27)	1.497(3)
S(3)-C(20)	1.765(2)	C(26)-C(30)	1.495(3)
S(4)-C(22)	1.762(2)	C(27)-C(32)	1.394(3)
S(4)-C(20)	1.768(2)	C(27)-C(28)	1.395(3)
O(1)-C(25)	1.356(3)	C(28)-C(29)	1.383(3)
O(1)-C(18)	1.454(3)	C(29)-C(30)	1.398(3)
O(2)-C(25)	1.207(3)	C(30)-C(31)	1.399(3)
O(3)-C(26)	1.349(3)	C(31)-C(32)	1.383(3)
O(3)-C(23)	1.459(3)	S(1')-C(15')	1.766(2)
O(4)-C(26)	1.207(3)	S(1')-C(16')	1.777(3)
C(1)-C(2)	1.394(3)	S(2')-C(17')	1.759(3)
C(1)-C(12)	1.398(3)	S(2')-C(15')	1.768(2)
C(2)-C(3)	1.383(3)	S(3')-C(20')	1.762(2)
C(3)-C(4)	1.390(3)	S(3')-C(21')	1.768(2)
C(4)-C(11)	1.402(3)	S(4')-C(22')	1.761(2)
C(5)-C(6)	1.391(3)	S(4')-C(20')	1.769(2)
C(5)-C(14)	1.399(3)	O(1')-C(25')	1.354(3)
C(6)-C(7)	1.388(3)	O(1')-C(18')	1.469(3)
C(7)-C(8)	1.386(3)	O(2')-C(25')	1.208(3)
C(8)-C(13)	1.401(3)	O(3')-C(26')	1.354(3)
C(9)-C(15)	1.360(3)	O(3')-C(23')	1.462(3)
C(9)-C(13)	1.482(3)	O(4')-C(26')	1.212(3)
C(9)-C(12)	1.483(3)	C(1')-C(12')	1.393(3)
C(10)-C(20)	1.361(3)	C(1')-C(2')	1.394(3)
C(10)-C(14)	1.481(3)	C(2')-C(3')	1.386(3)
C(10)-C(11)	1.484(3)	C(3')-C(4')	1.390(3)
C(11)-C(12)	1.415(3)	C(4')-C(11')	1.396(3)
C(13)-C(14)	1.419(3)	C(5')-C(6')	1.390(3)
C(16)-C(17)	1.331(3)	C(5')-C(14')	1.399(3)
C(16)-C(18)	1.505(3)	C(6')-C(7')	1.381(4)
C(7')-C(8')	1.394(3)	C(17')-C(19')	1.510(3)
C(8')-C(13')	1.399(3)	C(21')-C(22')	1.339(3)
C(9')-C(15')	1.363(3)	C(21')-C(23')	1.501(3)
C(9')-C(13')	1.481(3)	C(22')-C(24')	1.502(3)
C(9')-C(12')	1.483(3)	C(25')-C(27')	1.498(4)
C(10')-C(20')	1.362(3)	C(26')-C(30')	1.490(4)
C(10')-C(11')	1.478(3)	C(27')-C(32')	1.392(4)
C(10')-C(14')	1.478(3)	C(27')-C(28')	1.394(4)
C(11')-C(12')	1.418(3)	C(28')-C(29')	1.391(4)
C(13')-C(14')	1.417(3)	C(29')-C(30')	1.393(4)
C(16')-C(17')	1.341(3)	C(30')-C(31')	1.403(3)
C(16')-C(18')	1.498(4)	C(31')-C(32')	1.385(4)

Angle	°	Angle	°
C(15)-S(1)-C(16)	95.91(10)	C(1)-C(12)-C(11)	119.7(2)
C(17)-S(2)-C(15)	96.90(11)	C(1)-C(12)-C(9)	122.8(2)
C(21)-S(3)-C(20)	96.25(11)	C(11)-C(12)-C(9)	117.49(19)
C(22)-S(4)-C(20)	96.72(11)	C(8)-C(13)-C(14)	119.3(2)
C(25)-O(1)-C(18)	116.30(18)	C(8)-C(13)-C(9)	123.2(2)
C(26)-O(3)-C(23)	114.98(18)	C(14)-C(13)-C(9)	117.47(19)
C(2)-C(1)-C(12)	120.6(2)	C(5)-C(14)-C(13)	118.8(2)
C(3)-C(2)-C(1)	120.0(2)	C(5)-C(14)-C(10)	123.6(2)
C(2)-C(3)-C(4)	120.0(2)	C(13)-C(14)-C(10)	117.66(18)
C(3)-C(4)-C(11)	121.2(2)	C(9)-C(15)-S(2)	124.35(17)
C(6)-C(5)-C(14)	121.1(2)	C(9)-C(15)-S(1)	123.87(17)
C(7)-C(6)-C(5)	119.9(2)	S(2)-C(15)-S(1)	111.59(12)
C(8)-C(7)-C(6)	120.2(2)	C(17)-C(16)-C(18)	126.8(2)
C(7)-C(8)-C(13)	120.7(2)	C(17)-C(16)-S(1)	117.09(17)
C(15)-C(9)-C(13)	123.89(19)	C(18)-C(16)-S(1)	115.93(17)
C(15)-C(9)-C(12)	122.09(19)	C(16)-C(17)-C(19)	129.0(2)
C(13)-C(9)-C(12)	113.84(18)	C(16)-C(17)-S(2)	116.37(17)
C(20)-C(10)-C(14)	123.16(19)	C(19)-C(17)-S(2)	114.62(17)
C(20)-C(10)-C(11)	122.5(2)	O(1)-C(18)-C(16)	107.79(18)
C(14)-C(10)-C(11)	114.10(19)	C(10)-C(20)-S(3)	123.34(17)
C(4)-C(11)-C(12)	118.5(2)	C(10)-C(20)-S(4)	124.95(17)
C(4)-C(11)-C(10)	123.7(2)	S(3)-C(20)-S(4)	111.63(12)
C(12)-C(11)-C(10)	117.75(19)	C(22)-C(21)-C(23)	126.3(2)

Angle	°	Angle	°
C(22)-C(21)-S(3)	117.37(18)	C(15')-C(9')-C(13')	122.6(2)
C(23)-C(21)-S(3)	116.13(17)	C(15')-C(9')-C(12')	122.2(2)
C(21)-C(22)-C(24)	127.5(2)	C(13')-C(9')-C(12')	114.7(2)
C(21)-C(22)-S(4)	116.06(17)	C(20')-C(10')-C(11')	122.4(2)
C(24)-C(22)-S(4)	116.46(18)	C(20')-C(10')-C(14')	122.3(2)
O(3)-C(23)-C(21)	107.41(18)	C(11')-C(10')-C(14')	114.9(2)
O(2)-C(25)-O(1)	124.0(2)	C(4')-C(11')-C(12')	119.2(2)
O(2)-C(25)-C(27)	124.7(2)	C(4')-C(11')-C(10')	123.5(2)
O(1)-C(25)-C(27)	111.2(2)	C(12')-C(11')-C(10')	117.3(2)
O(4)-C(26)-O(3)	124.4(2)	C(1')-C(12')-C(11')	119.1(2)
O(4)-C(26)-C(30)	123.8(2)	C(1')-C(12')-C(9')	123.1(2)
O(3)-C(26)-C(30)	111.6(2)	C(11')-C(12')-C(9')	117.8(2)
C(32)-C(27)-C(28)	119.9(2)	C(8')-C(13')-C(14')	118.9(2)
C(32)-C(27)-C(25)	118.3(2)	C(8')-C(13')-C(9')	124.1(2)
C(28)-C(27)-C(25)	121.3(2)	C(14')-C(13')-C(9')	117.0(2)
C(29)-C(28)-C(27)	120.1(2)	C(5')-C(14')-C(13')	119.3(2)
C(28)-C(29)-C(30)	120.2(2)	C(5')-C(14')-C(10')	122.6(2)
C(29)-C(30)-C(31)	119.5(2)	C(13')-C(14')-C(10')	118.2(2)
C(29)-C(30)-C(26)	117.8(2)	C(9')-C(15')-S(1')	123.92(18)
C(31)-C(30)-C(26)	122.1(2)	C(9')-C(15')-S(2')	124.21(18)
C(32)-C(31)-C(30)	120.1(2)	S(1')-C(15')-S(2')	111.64(13)
C(31)-C(32)-C(27)	120.1(2)	C(17')-C(16')-C(18')	127.0(2)
C(15')-S(1')-C(16')	96.09(11)	C(17')-C(16')-S(1')	116.72(19)
C(17')-S(2')-C(15')	96.86(12)	C(18')-C(16')-S(1')	115.96(19)
C(20')-S(3')-C(21')	96.32(11)	C(16')-C(17')-C(19')	128.5(2)
C(22')-S(4')-C(20')	96.57(11)	C(16')-C(17')-S(2')	116.43(19)
C(25')-O(1')-C(18')	115.7(2)	C(19')-C(17')-S(2')	115.04(18)
C(26')-O(3')-C(23')	114.51(19)	O(1')-C(18')-C(16')	107.7(2)
C(12')-C(1')-C(2')	120.7(2)	C(10')-C(20')-S(3')	123.70(17)
C(3')-C(2')-C(1')	120.3(2)	C(10')-C(20')-S(4')	124.62(18)
C(2')-C(3')-C(4')	119.7(2)	S(3')-C(20')-S(4')	111.59(12)
C(3')-C(4')-C(11')	121.0(2)	C(22')-C(21')-C(23')	128.5(2)
C(6')-C(5')-C(14')	120.7(2)	C(22')-C(21')-S(3')	116.88(18)
C(7')-C(6')-C(5')	120.1(2)	C(23')-C(21')-S(3')	114.54(17)
C(6')-C(7')-C(8')	120.1(2)	C(21')-C(22')-C(24')	127.9(2)
C(7')-C(8')-C(13')	120.8(2)	C(21')-C(22')-S(4')	116.35(18)
C(24')-C(22')-S(4')	115.74(18)	C(32')-C(27')-C(25')	117.2(2)
O(3')-C(23')-C(21')	107.61(18)	C(28')-C(27')-C(25')	122.0(2)
O(2')-C(25')-O(1')	124.4(2)	C(29')-C(28')-C(27')	119.4(2)
O(2')-C(25')-C(27')	124.4(2)	C(28')-C(29')-C(30')	120.5(2)
O(1')-C(25')-C(27')	110.9(2)	C(29')-C(30')-C(31')	119.6(2)
O(4')-C(26')-O(3')	123.0(2)	C(29')-C(30')-C(26')	119.1(2)
O(4')-C(26')-C(30')	124.2(2)	C(31')-C(30')-C(26')	120.7(2)
O(3')-C(26')-C(30')	112.6(2)	C(32')-C(31')-C(30')	119.7(2)
C(32')-C(27')-C(28')	120.2(2)	C(31')-C(32')-C(27')	120.3(2)

Thienyl cyclophane (78b)

Table 1. Crystal data and structure refinement

Identification code	
Empirical formula	$C_{30}H_{20}O_4S_5 \cdot CH_2Cl_2$
Formula weight	689.69
Temperature	123(2) K
Wavelength	0.71073 Å
Crystal system	Monoclinic
Space group	$P2_1/c$ (No. 14)
Unit cell dimensions	$a = 11.407(5)$ Å $\quad \alpha = 90°$
	$b = 17.160(8)$ Å $\quad \beta = 99.83(2)°$
	$c = 15.607(7)$ Å $\quad \gamma = 90°$
Volume	3010(2) Å^3
Z	4
Density (calculated)	1.522 g/cm^3
Absorption coefficient	0.600 mm^{-1}
F(000)	1416
Crystal size	0.48 x 0.03 x 0.02 mm^3
θ range for data collection	1.78 to 25.00°.
Index ranges	$-13 \leq h \leq 11, -20 \leq k \leq 20, -17 \leq l \leq 18$
Reflections collected	18028
Independent reflections	5302 [R(int) = 0.1508]
Reflections with $I > 2\sigma(I)$	2901
Completeness to θ = 25.00°	100.0 %
Absorption correction	None
Max. and min. transmission	0.9881 and 0.7616
Refinement method	Full-matrix least-squares on F^2
Data / restraints / parameters	5302 / 6 / 398
Largest final shift/e.s.d. ratio	0.011
Goodness-of-fit on F^2	1.009
Final R indices [$I > 2\sigma(I)$]	$R_1 = 0.0716$, $wR_2 = 0.1255$
R indices (all data)	$R_1 = 0.1506$, $wR_2 = 0.1523$
Largest diff. peak and hole	0.615 and -0.437 e.Å^{-3}

171

Table 2. Atomic coordinates (× 10⁴) and equivalent isotropic displacement parameters (Å² × 10⁴). U(eq) is defined as one third of the trace of the orthogonalized U_{ij} tensor.

	x	y	z	U(eq)
S(1)	7763(1)	6273(1)	2233(1)	253(4)
S(2)	5268(1)	5983(1)	1505(1)	263(4)
S(3)	6724(1)	6610(1)	5929(1)	246(4)
S(4)	4216(1)	6236(1)	5348(1)	223(4)
S(5)	8550(1)	4545(1)	4681(1)	221(4)
O(1)	8532(3)	4544(2)	2901(2)	249(10)
O(2)	10092(4)	3743(3)	2808(3)	324(11)
O(3)	7729(3)	4883(2)	6199(2)	280(10)
O(4)	9067(3)	4254(2)	7195(3)	301(11)
C(1)	7874(5)	7874(3)	3227(4)	260(15)
C(2)	8631(6)	8263(4)	3864(4)	324(16)
C(3)	8352(6)	8328(4)	4691(4)	380(18)
C(4)	7318(6)	8003(4)	4879(4)	324(17)
C(5)	3241(5)	7383(4)	3806(4)	292(16)
C(6)	2350(6)	7474(4)	3101(4)	318(16)
C(7)	2614(6)	7472(4)	2270(4)	348(17)
C(8)	3771(5)	7357(4)	2138(4)	298(16)
C(9)	5948(5)	7116(3)	2748(4)	198(14)
C(10)	5436(5)	7222(3)	4421(4)	221(14)
C(11)	6546(5)	7607(3)	4243(4)	256(15)
C(12)	6802(5)	7539(3)	3399(4)	251(15)
C(13)	4686(5)	7258(3)	2841(4)	243(14)
C(14)	4418(5)	7279(3)	3689(4)	237(14)
C(15)	6271(5)	6564(3)	2219(4)	231(14)
C(16)	7393(6)	5321(3)	1829(4)	254(15)
C(17)	6245(5)	5182(4)	1499(4)	269(15)
C(18)	8374(5)	4746(4)	1980(4)	267(15)
C(19)	5685(6)	4424(4)	1182(4)	357(17)
C(20)	5445(5)	6784(3)	5131(3)	207(14)
C(21)	6193(5)	5746(3)	6330(4)	217(14)
C(22)	5036(5)	5567(3)	6066(3)	194(13)
C(23)	7119(5)	5233(4)	6846(4)	233(15)
C(24)	4374(5)	4856(3)	6297(4)	254(15)
C(25)	9423(5)	4066(3)	3230(4)	209(14)
C(26)	8662(5)	4411(4)	6442(4)	242(14)
C(27)	9463(5)	3973(3)	4168(4)	215(14)
C(28)	10174(5)	3503(4)	4756(4)	279(15)
C(29)	9978(5)	3599(3)	5612(4)	256(15)
C(30)	9121(5)	4144(3)	5671(4)	195(13)
Cl(1A)*	2515(4)	5071(2)	571(3)	626(12)
Cl(2A)*	1489(4)	6641(3)	193(3)	470(13)
C(0A)*	1933(12)	5919(7)	1004(8)	330(40)
Cl(1B)*	433(3)	5165(2)	462(3)	494(10)
Cl(2B)*	2101(5)	6353(4)	173(3)	648(16)
C(0B)*	1822(12)	5561(9)	842(9)	460(40)

* Occupancy 50%.

Table 3. Bond lengths [Å] and angles [°]

S(1)-C(15)	1.771(6)	C(8)-C(13)	1.389(8)
S(1)-C(16)	1.776(6)	C(9)-C(15)	1.348(8)
S(2)-C(15)	1.763(6)	C(9)-C(12)	1.473(8)
S(2)-C(17)	1.770(6)	C(9)-C(13)	1.492(8)
S(3)-C(21)	1.757(6)	C(10)-C(20)	1.338(8)
S(3)-C(20)	1.774(6)	C(10)-C(14)	1.487(8)
S(4)-C(22)	1.757(6)	C(10)-C(11)	1.496(8)
S(4)-C(20)	1.768(6)	C(11)-C(12)	1.402(8)
S(5)-C(30)	1.714(6)	C(13)-C(14)	1.408(8)
S(5)-C(27)	1.724(6)	C(16)-C(17)	1.344(8)
O(1)-C(25)	1.338(7)	C(16)-C(18)	1.481(8)
O(1)-C(18)	1.460(6)	C(17)-C(19)	1.496(8)
O(2)-C(25)	1.222(6)	C(21)-C(22)	1.349(7)
O(3)-C(26)	1.340(7)	C(21)-C(23)	1.500(8)
O(3)-C(23)	1.451(6)	C(23)-C(24)	1.511(8)
O(4)-C(26)	1.218(7)	C(25)-C(27)	1.466(8)
C(1)-C(2)	1.374(8)	C(26)-C(30)	1.465(8)
C(1)-C(12)	1.417(8)	C(27)-C(28)	1.377(8)
C(2)-C(3)	1.387(8)	C(28)-C(29)	1.402(8)
C(3)-C(4)	1.381(8)	C(29)-C(30)	1.368(8)
C(4)-C(11)	1.387(8)	Cl(1A)-C(0A)	1.779(11)
C(5)-C(6)	1.374(8)	Cl(2A)-C(0A)	1.781(10)
C(5)-C(14)	1.398(8)	Cl(1B)...Cl(1B)#1	1.701(8)
C(6)-C(7)	1.380(8)	Cl(1B)-C(0B)	1.733(11)
C(7)-C(8)	1.385(8)	Cl(2B)-C(0B)	1.776(11)

C(15)-S(1)-C(16)	94.9(3)	C(1)-C(2)-C(3)	119.8(6)
C(15)-S(2)-C(17)	95.8(3)	C(4)-C(3)-C(2)	120.3(6)
C(21)-S(3)-C(20)	95.7(3)	C(3)-C(4)-C(11)	120.5(6)
C(22)-S(4)-C(20)	96.7(3)	C(6)-C(5)-C(14)	120.3(6)
C(30)-S(5)-C(27)	91.4(3)	C(5)-C(6)-C(7)	120.2(6)
C(25)-O(1)-C(18)	118.7(4)	C(6)-C(7)-C(8)	120.5(6)
C(26)-O(3)-C(23)	120.3(4)	C(7)-C(8)-C(13)	120.4(6)
C(2)-C(1)-C(12)	121.0(6)	C(15)-C(9)-C(12)	123.4(5)
C(15)-C(9)-C(13)	122.9(5)	C(10)-C(20)-S(4)	124.3(5)
C(12)-C(9)-C(13)	112.8(5)	C(10)-C(20)-S(3)	124.4(5)
C(20)-C(10)-C(14)	124.7(5)	S(4)-C(20)-S(3)	111.1(3)
C(20)-C(10)-C(11)	121.0(5)	C(22)-C(21)-C(23)	126.4(5)
C(14)-C(10)-C(11)	113.7(5)	C(22)-C(21)-S(3)	117.5(5)
C(4)-C(11)-C(12)	120.3(5)	C(23)-C(21)-S(3)	115.6(4)
C(4)-C(11)-C(10)	122.5(5)	C(21)-C(22)-C(24)	127.8(5)
C(12)-C(11)-C(10)	117.2(5)	C(21)-C(22)-S(4)	115.6(4)
C(11)-C(12)-C(1)	118.0(6)	C(24)-C(22)-S(4)	116.5(4)
C(11)-C(12)-C(9)	118.0(5)	O(3)-C(23)-C(21)	104.3(4)
C(1)-C(12)-C(9)	124.0(5)	O(2)-C(25)-O(1)	125.1(5)
C(8)-C(13)-C(14)	119.0(6)	O(2)-C(25)-C(27)	125.0(5)
C(8)-C(13)-C(9)	123.4(5)	O(1)-C(25)-C(27)	109.9(5)
C(14)-C(13)-C(9)	117.6(5)	O(4)-C(26)-O(3)	124.0(5)
C(5)-C(14)-C(13)	119.6(6)	O(4)-C(26)-C(30)	126.5(6)
C(5)-C(14)-C(10)	123.3(5)	O(3)-C(26)-C(30)	109.5(5)
C(13)-C(14)-C(10)	117.0(5)	C(28)-C(27)-C(25)	130.1(5)
C(9)-C(15)-S(2)	124.7(5)	C(28)-C(27)-S(5)	110.9(4)
C(9)-C(15)-S(1)	123.6(5)	C(25)-C(27)-S(5)	119.0(4)
S(2)-C(15)-S(1)	111.5(3)	C(27)-C(28)-C(29)	113.3(5)
C(17)-C(16)-C(18)	127.1(6)	C(30)-C(29)-C(28)	112.1(5)
C(17)-C(16)-S(1)	117.1(5)	C(29)-C(30)-C(26)	128.9(5)
C(18)-C(16)-S(1)	115.4(5)	C(29)-C(30)-S(5)	112.3(4)
C(16)-C(17)-C(19)	127.8(6)	C(26)-C(30)-S(5)	118.8(4)
C(16)-C(17)-S(2)	115.7(5)	Cl(1A)-C(0A)-Cl(2A)	112.2(7)
C(19)-C(17)-S(2)	116.4(5)	Cl(1B)-C(0B)-Cl(2B)	110.1(7)
O(1)-C(18)-C(16)	106.1(4)		

Symmetry transformations used to generate equivalent atoms: #1 -x,-y+1,-z

Ferrocenyl cyclophane (78c)

Table 1. Crystal data and structure refinement

Identification code	
Empirical formula	$C_{36}H_{26}FeO_4S_4$
Formula weight	706.66
Temperature	123(2) K
Wavelength	0.71073 Å
Crystal system	Monoclinic
Space group	$P2_1/n$
Unit cell dimensions	$a = 14.739(3)$ Å $\quad \alpha = 90°$
	$b = 16.152(3)$ Å $\quad \beta = 94.94(1)°$
	$c = 26.187(9)$ Å $\quad \gamma = 90°$
Volume	6211(3) Å^3
Z	8
Density (calculated)	1.511 g/cm^3
Absorption coefficient	0.796 mm^{-1}
F(000)	2912
Crystal size	$0.42 \times 0.14 \times 0.06$ mm^3
θ range for data collection	1.53 to 25.00°.
Index ranges	$-17 \le h \le 17, -19 \le k \le 19, -27 \le l \le 31$
Reflections collected	36823
Independent reflections	10934 [R(int) = 0.0629]
Reflections with I > 2σ(I)	8145
Completeness to θ = 25.00°	100.0 %
Absorption correction	Integration
Max. and min. transmission	0.9590 and 0.8707
Refinement method	Full-matrix least-squares on F^2
Data / restraints / parameters	10934 / 4 / 846
Largest final shift/e.s.d. ratio	0.015
Goodness-of-fit on F^2	1.052
Final R indices [I > 2σ(I)]	$R_1 = 0.0494$, $wR_2 = 0.0947$
R indices (all data)	$R_1 = 0.0769$, $wR_2 = 0.1051$
Largest diff. peak and hole	0.535 and -0.626 e.Å^{-3}

Disorder: Fe(2), O(5), O(6), O(7), O(8), C(61) to C(72) with their hydrogens are disordered over 2 positions, with occupancies 86.1(2)% (unprimed) and 13.9(2)% (primed), Cp-rings in the minor positions were refined as rigid bodies with equal U(iso) for 5 carbon atoms.

173

Table 2. Atomic coordinates (×10⁴) and equivalent isotropic displacement parameters (Å² ×10⁴) U(eq) is defined as one third of the trace of the orthogonalized Uij tensor.

	x	y	z	U(eq)
Fe(1)	8801.4(3)	3974.4(3)	707.4(2)	175(1)
S(1)	5416.5(6)	3229.2(6)	-654.7(3)	194(2)
S(2)	3782.7(6)	4173.8(6)	-476.3(3)	192(2)
S(3)	6206.1(6)	2295.6(6)	1567.3(3)	198(2)
S(4)	4566.4(6)	3007.3(6)	1946.6(3)	211(2)
O(1)	6964(2)	4328(2)	-364(1)	240(6)
O(2)	8265(2)	4585(2)	-726(1)	285(6)
O(3)	7686(2)	3739(2)	1909(1)	212(6)
O(4)	9107(2)	3212(2)	2069(1)	266(6)
C(1)	5180(2)	1467(2)	-268(1)	197(8)
C(2)	5766(2)	818(2)	-130(1)	224(8)
C(3)	5935(3)	593(2)	381(1)	222(9)
C(4)	5528(2)	1037(2)	752(1)	193(8)
C(5)	2903(2)	2600(2)	1173(1)	239(9)
C(6)	2077(2)	2945(3)	1005(2)	259(9)
C(7)	1911(3)	3188(2)	498(2)	264(9)
C(8)	2575(2)	3071(2)	158(1)	210(8)
C(9)	4179(2)	2649(2)	-11(1)	162(8)
C(10)	4527(2)	2204(2)	1008(1)	155(8)
C(11)	3602(2)	2505(2)	844(1)	184(8)
C(12)	3424(2)	2741(2)	322(1)	168(8)
C(13)	4780(2)	1927(2)	103(1)	161(8)
C(14)	4963(2)	1708(2)	623(1)	156(8)
C(15)	4395(2)	3242(2)	-350(1)	174(8)
C(16)	5472(2)	4323(2)	-723(1)	175(8)
C(17)	4724(2)	4757(2)	-656(1)	181(8)
C(18)	6404(2)	4643(2)	-804(1)	212(8)
C(19)	4563(3)	5671(2)	-722(1)	234(9)
C(20)	5012(2)	2446(2)	1447(1)	174(8)
C(21)	6362(2)	2992(2)	2087(1)	195(8)
C(22)	5615(2)	3310(2)	2266(1)	194(8)
C(23)	7327(2)	3174(2)	2274(1)	219(8)
C(24)	5540(3)	3866(2)	2719(1)	231(9)
C(25)	7858(2)	4244(2)	-402(1)	191(8)
C(26)	8256(2)	3670(2)	-10(1)	187(8)
C(27)	9193(3)	3423(2)	63(1)	225(9)
C(28)	9284(3)	2861(2)	479(2)	253(9)
C(29)	8417(3)	2761(2)	668(2)	239(9)
C(30)	7778(3)	3247(2)	369(1)	207(8)
C(31)	8828(2)	4295(2)	1457(1)	212(8)
C(32)	8224(3)	4830(2)	1154(1)	210(8)
C(33)	8736(3)	5242(2)	795(2)	256(9)
C(34)	9656(3)	4965(2)	874(2)	266(9)
C(35)	9718(3)	4382(2)	1278(1)	238(9)
C(36)	8581(2)	3694(2)	1842(1)	195(8)
Fe(2)	2081.8(5)	4217.6(5)	3030.5(3)	227(2)
Fe(2')	2058(5)	4557(4)	3007(3)	340(20)
S(5)	5475.4(7)	2576.7(7)	4126.2(4)	286(2)
S(6)	6819.7(7)	2071.6(6)	3433.7(4)	253(2)
S(7)	5513.2(9)	6111.0(7)	3481.8(4)	374(3)
S(8)	6837.9(8)	5799.8(7)	2732.4(4)	339(3)
O(5)	3659(2)	2600(2)	3547(1)	300(8)
O(6)	2289(2)	1998(2)	3596(2)	362(9)
O(7)	3660(2)	5754(2)	2595(1)	319(8)
O(8)	2304(3)	6416(3)	2607(1)	381(9)
O(5')	3552(10)	2598(9)	3261(7)	110(40)
O(6')	2107(13)	2171(11)	3341(8)	230(50)
O(7')	3816(15)	5969(14)	3064(8)	530(70)
O(8')	2598(12)	6744(11)	2698(6)	130(40)
C(37)	6440(3)	3931(3)	4867(1)	255(9)
C(38)	6165(3)	4555(3)	5183(2)	318(10)
C(39)	6180(3)	5368(3)	5025(2)	351(11)
C(40)	6458(3)	5563(3)	4547(2)	301(10)
C(41)	8452(3)	4843(3)	3252(1)	276(10)
C(42)	9114(3)	4293(3)	3118(2)	331(11)
C(43)	9131(3)	3489(3)	3293(2)	328(11)
C(44)	8483(2)	3219(3)	3609(1)	247(9)
C(45)	7021(2)	3490(2)	4025(1)	192(8)
C(46)	7023(3)	5112(2)	3707(1)	223(9)
C(47)	7783(2)	4581(2)	3562(1)	217(9)
C(48)	7800(2)	3750(2)	3739(1)	199(8)
C(49)	6717(2)	4119(2)	4384(1)	191(8)
C(50)	6713(3)	4946(2)	4222(1)	228(9)
C(51)	6541(3)	2797(2)	3902(1)	205(8)
C(52)	5076(3)	1987(2)	3582(2)	273(9)
C(53)	5693(3)	1745(2)	3267(2)	262(9)
C(54)	4075(3)	1820(3)	3519(2)	346(10)
C(55)	55´6(3)	1223(3)	2799(2)	342(11)
C(56)	6553(3)	5628(2)	3364(2)	280(9)
C(57)	5141(3)	6284(2)	2832(2)	332(11)
C(58)	5744(3)	6138(3)	2491(2)	345(11)
C(59)	4171(3)	6534(3)	2711(2)	418(12)
C(60)	5597(4)	6180(3)	1917(2)	511(15)
C(61)	2749(3)	2612(3)	3587(2)	261(11)
C(62)	2437(3)	3465(3)	3640(2)	274(11)
C(63)	1498(3)	3706(3)	3636(2)	342(13)
C(64)	1466(4)	4571(4)	3666(2)	406(15)
C(65)	2371(4)	4886(4)	3690(2)	370(13)
C(66)	2977(4)	4204(3)	3671(2)	321(12)
C(67)	2348(3)	4968(3)	2442(2)	251(11)
C(68)	2849(3)	4210(3)	2419(2)	250(11)
C(69)	2219(3)	3548(3)	2372(2)	283(11)
C(70)	1328(3)	3876(4)	2366(2)	297(12)
C(71)	1400(3)	4747(4)	2406(2)	354(13)
C(72)	2733(3)	5787(3)	2552(2)	295(11)
C(61')	2607(16)	2678(16)	3144(10)	290(70)
C(62')	2280(15)	3353(12)	2789(9)	320(40)
C(63')	1360(13)	3569(14)	2643(10)	320(40)
C(64')	1360(15)	4271(16)	2316(11)	320(40)
C(65')	2280(18)	4488(14)	2260(10)	320(40)
C(66')	2849(12)	3921(16)	2553(11)	320(40)
C(72')	2942(17)	6221(17)	2972(10)	320(70)
C(67')	2502(12)	5621(12)	3296(8)	270(30)
C(68')	2906(11)	4964(13)	3596(9)	270(30)
C(69')	2199(16)	4525(12)	3814(9)	270(30)
C(70')	1359(12)	4910(14)	3648(10)	270(30)
C(71')	1546(12)	5587(12)	3328(8)	270(30)

174

Table 3. Bond lengths [Å] and angles [°]

Fe(1)-C(31)	2.027(4)	C(9)-C(15)	1.363(5)
Fe(1)-C(35)	2.035(4)	C(9)-C(13)	1.478(5)
Fe(1)-C(27)	2.036(4)	C(9)-C(12)	1.480(5)
Fe(1)-C(26)	2.039(4)	C(10)-C(20)	1.359(5)
Fe(1)-C(29)	2.040(4)	C(10)-C(11)	1.476(5)
Fe(1)-C(28)	2.043(4)	C(10)-C(14)	1.477(5)
Fe(1)-C(32)	2.043(4)	C(11)-C(12)	1.419(5)
Fe(1)-C(30)	2.053(4)	C(13)-C(14)	1.411(5)
Fe(1)-C(34)	2.060(4)	C(16)-C(17)	1.331(5)
Fe(1)-C(33)	2.063(4)	C(16)-C(18)	1.501(5)
S(1)-C(15)	1.764(4)	C(17)-C(19)	1.503(5)
S(1)-C(16)	1.778(4)	C(21)-C(22)	1.335(5)
S(2)-C(15)	1.771(4)	C(21)-C(23)	1.493(5)
S(2)-C(17)	1.774(4)	C(22)-C(24)	1.499(5)
S(3)-C(21)	1.766(4)	C(25)-C(26)	1.468(5)
S(3)-C(20)	1.777(4)	C(26)-C(30)	1.437(5)
S(4)-C(22)	1.763(4)	C(26)-C(27)	1.435(5)
S(4)-C(20)	1.764(4)	C(27)-C(28)	1.415(5)
O(1)-C(25)	1.337(4)	C(28)-C(29)	1.420(5)
O(1)-C(18)	1.450(4)	C(29)-C(30)	1.411(5)
O(2)-C(25)	1.212(4)	C(31)-C(32)	1.431(5)
O(3)-C(36)	1.347(4)	C(31)-C(35)	1.437(5)
O(3)-C(23)	1.454(4)	C(31)-C(36)	1.467(5)
O(4)-C(36)	1.217(4)	C(32)-C(33)	1.420(5)
C(1)-C(2)	1.387(5)	C(33)-C(34)	1.426(5)
C(1)-C(13)	1.394(5)	C(34)-C(35)	1.414(5)
C(2)-C(3)	1.387(5)	Fe(2)-C(67)	2.025(5)
C(3)-C(4)	1.384(5)	Fe(2)-C(71)	2.033(5)
C(4)-C(14)	1.391(5)	Fe(2)-C(62)	2.038(5)
C(5)-C(6)	1.377(5)	Fe(2)-C(68)	2.039(5)
C(5)-C(11)	1.407(5)	Fe(2)-C(63)	2.043(5)
C(6)-C(7)	1.384(5)	Fe(2)-C(66)	2.043(5)
C(7)-C(8)	1.393(5)	Fe(2)-C(64)	2.045(5)
C(8)-C(12)	1.393(5)	Fe(2)-C(65)	2.050(5)
Fe(2)-C(70)	2.058(5)	C(40)-C(50)	1.383(5)
Fe(2)-C(69)	2.060(5)	C(41)-C(42)	1.388(6)
Fe(2')-C(67')	1.97(2)	C(41)-C(47)	1.396(5)
Fe(2')-C(68')	2.01(2)	C(42)-C(43)	1.376(6)
Fe(2')-C(65')	2.01(3)	C(43)-C(44)	1.387(5)
Fe(2')-C(66')	2.02(3)	C(44)-C(48)	1.388(5)
Fe(2')-C(71')	2.04(2)	C(45)-C(51)	1.349(5)
Fe(2')-C(64')	2.05(3)	C(45)-C(49)	1.480(5)
Fe(2')-C(62')	2.06(2)	C(45)-C(48)	1.484(5)
Fe(2')-C(63')	2.08(2)	C(46)-C(56)	1.369(5)
Fe(2')-C(69')	2.11(2)	C(46)-C(50)	1.486(5)
Fe(2')-C(70')	2.12(2)	C(46)-C(47)	1.485(5)
S(5)-C(51)	1.760(4)	C(47)-C(48)	1.419(5)
S(5)-C(52)	1.773(4)	C(49)-C(50)	1.402(5)
S(6)-C(53)	1.762(4)	C(52)-C(53)	1.336(6)
S(6)-C(51)	1.769(4)	C(52)-C(54)	1.496(6)
S(7)-C(57)	1.764(4)	C(53)-C(55)	1.488(6)
S(7)-C(56)	1.770(4)	C(57)-C(58)	1.333(6)
S(8)-C(56)	1.764(4)	C(57)-C(59)	1.494(6)
S(8)-C(58)	1.767(5)	C(58)-C(60)	1.503(6)
O(5)-C(61)	1.354(5)	C(61)-C(62)	1.463(7)
O(5)-C(54)	1.406(5)	C(62)-C(66)	1.433(7)
O(6)-C(61)	1.203(6)	C(62)-C(63)	1.437(6)
O(7)-C(72)	1.362(6)	C(63)-C(64)	1.399(8)
O(7)-C(59)	1.486(6)	C(64)-C(65)	1.424(8)
O(8)-C(72)	1.213(6)	C(65)-C(66)	1.422(7)
O(5')-C(61')	1.41(3)	C(67)-C(68)	1.433(7)
O(5')-C(54)	1.594(15)	C(67)-C(71)	1.437(6)
O(6')-C(61')	1.24(3)	C(67)-C(72)	1.458(7)
O(7')-C(72')	1.35(3)	C(68)-C(69)	1.416(7)
O(7')-C(59)	1.429(18)	C(69)-C(70)	1.415(7)
O(8')-C(72')	1.19(2)	C(70)-C(71)	1.415(8)
C(37)-C(38)	1.386(6)	C(61')-C(62')	1.49(3)
C(37)-C(49)	1.395(5)	C(62')-C(63')	1.4200
C(38)-C(39)	1.378(6)	C(62')-C(66')	1.4200
C(39)-C(40)	1.385(6)	C(63')-C(64')	1.4200
C(64')-C(65')	1.4200	C(67')-C(68')	1.4200
C(65')-C(66')	1.4200	C(68')-C(69')	1.4200
C(72')-C(67')	1.47(3)	C(69')-C(70')	1.4200
C(67')-C(71')	1.4200	C(70')-C(71')	1.4200

C(15)-S(1)-C(16)	94.70(17)	C(13)-C(14)-C(10)	117.7(3)
C(15)-S(2)-C(17)	95.91(17)	C(9)-C(15)-S(1)	122.9(3)
C(21)-S(3)-C(20)	96.36(17)	C(9)-C(15)-S(2)	125.2(3)
C(22)-S(4)-C(20)	97.29(17)	S(1)-C(15)-S(2)	111.5(2)
C(25)-O(1)-C(18)	118.2(3)	C(17)-C(16)-C(18)	128.0(3)
C(36)-O(3)-C(23)	117.9(3)	C(17)-C(16)-S(1)	117.7(3)
C(2)-C(1)-C(13)	120.8(3)	C(18)-C(16)-S(1)	114.0(3)
C(1)-C(2)-C(3)	120.4(3)	C(16)-C(17)-C(19)	128.9(3)
C(4)-C(3)-C(2)	119.2(3)	C(16)-C(17)-S(2)	115.5(3)
C(3)-C(4)-C(14)	121.4(3)	C(19)-C(17)-S(2)	115.6(3)
C(6)-C(5)-C(11)	121.5(3)	O(1)-C(18)-C(16)	103.4(3)
C(5)-C(6)-C(7)	120.0(3)	C(10)-C(20)-S(4)	124.9(3)
C(6)-C(7)-C(8)	119.9(4)	C(10)-C(20)-S(3)	123.5(3)
C(12)-C(8)-C(7)	121.1(3)	S(4)-C(20)-S(3)	111.43(19)
C(15)-C(9)-C(13)	121.1(3)	C(22)-C(21)-C(23)	126.9(3)
C(15)-C(9)-C(12)	122.9(3)	C(22)-C(21)-S(3)	117.3(3)
C(13)-C(9)-C(12)	115.4(3)	C(23)-C(21)-S(3)	115.8(3)
C(20)-C(10)-C(11)	123.9(3)	C(21)-C(22)-C(24)	128.9(3)
C(20)-C(10)-C(14)	120.3(3)	C(21)-C(22)-S(4)	116.3(3)
C(11)-C(10)-C(14)	115.2(3)	C(24)-C(22)-S(4)	114.8(3)
C(5)-C(11)-C(12)	118.4(3)	O(3)-C(23)-C(21)	107.3(3)
C(5)-C(11)-C(10)	124.3(3)	O(2)-C(25)-O(1)	123.8(3)
C(12)-C(11)-C(10)	117.3(3)	O(2)-C(25)-C(26)	125.9(3)
C(8)-C(12)-C(11)	119.1(3)	O(1)-C(25)-C(26)	110.3(3)
C(8)-C(12)-C(9)	123.9(3)	C(30)-C(26)-C(27)	107.4(3)
C(11)-C(12)-C(9)	117.0(3)	C(30)-C(26)-C(25)	126.4(3)
C(1)-C(13)-C(14)	118.9(3)	C(27)-C(26)-C(25)	126.2(3)
C(1)-C(13)-C(9)	124.2(3)	C(28)-C(27)-C(26)	107.9(3)
C(14)-C(13)-C(9)	116.9(3)	C(27)-C(28)-C(29)	108.3(3)
C(4)-C(14)-C(13)	119.3(3)	C(30)-C(29)-C(28)	108.7(3)
C(4)-C(14)-C(10)	123.0(3)	C(29)-C(30)-C(26)	107.7(3)
C(32)-C(31)-C(35)	107.5(3)	C(44)-C(48)-C(45)	123.9(3)
C(32)-C(31)-C(36)	126.9(3)	C(47)-C(48)-C(45)	116.1(3)
C(35)-C(31)-C(36)	125.2(3)	C(37)-C(49)-C(50)	119.2(3)
C(33)-C(32)-C(31)	108.0(3)	C(37)-C(49)-C(45)	123.7(3)
C(32)-C(33)-C(34)	108.0(3)	C(50)-C(49)-C(45)	117.1(3)
C(35)-C(34)-C(33)	108.5(3)	C(40)-C(50)-C(49)	119.7(3)
C(34)-C(35)-C(31)	107.9(3)	C(40)-C(50)-C(46)	123.4(4)
O(4)-C(36)-O(3)	124.1(3)	C(49)-C(50)-C(46)	116.9(3)
O(4)-C(36)-C(31)	124.9(3)	C(45)-C(51)-S(5)	123.5(3)
O(3)-C(36)-C(31)	111.0(3)	C(45)-C(51)-S(6)	124.6(3)
C(51)-S(5)-C(52)	94.80(18)	S(5)-C(51)-S(6)	111.4(2)
C(53)-S(6)-C(51)	95.72(19)	C(53)-C(52)-C(54)	126.6(4)
C(57)-S(7)-C(56)	96.0(2)	C(53)-C(52)-S(5)	117.2(3)
C(56)-S(8)-C(58)	95.7(2)	C(54)-C(52)-S(5)	116.2(3)
C(61)-O(5)-C(54)	117.1(4)	C(52)-C(53)-C(55)	128.0(4)
C(72)-O(7)-C(59)	118.1(4)	C(52)-C(53)-S(6)	115.9(3)
C(61')-O(5')-C(54)	126.7(15)	C(55)-C(53)-S(6)	116.1(3)
C(72')-O(7')-C(59)	95.1(16)	O(5)-C(54)-C(52)	105.2(3)
C(38)-C(37)-C(49)	120.4(4)	O(5)-C(54)-O(5')	28.2(6)
C(39)-C(38)-C(37)	120.1(4)	C(52)-C(54)-O(5')	109.9(6)
C(38)-C(39)-C(40)	120.0(4)	C(46)-C(56)-S(8)	124.2(3)
C(50)-C(40)-C(39)	120.6(4)	C(46)-C(56)-S(7)	123.5(3)
C(42)-C(41)-C(47)	120.1(4)	S(8)-C(56)-S(7)	111.9(2)
C(43)-C(42)-C(41)	120.8(4)	C(58)-C(57)-C(59)	125.9(4)
C(42)-C(43)-C(44)	120.1(4)	C(58)-C(57)-S(7)	116.6(3)
C(43)-C(44)-C(48)	120.2(4)	C(59)-C(57)-S(7)	117.4(3)
C(51)-C(45)-C(49)	122.8(3)	C(57)-C(58)-C(60)	128.0(4)
C(51)-C(45)-C(48)	121.8(3)	C(57)-C(58)-S(8)	117.1(3)
C(49)-C(45)-C(48)	114.6(3)	C(60)-C(58)-S(8)	114.8(4)
C(56)-C(46)-C(50)	121.8(4)	O(7')-C(59)-O(7)	52.0(10)
C(56)-C(46)-C(47)	122.3(3)	O(7')-C(59)-C(57)	95.0(9)
C(50)-C(46)-C(47)	115.2(3)	O(7)-C(59)-C(57)	105.8(3)
C(41)-C(47)-C(48)	118.9(4)	O(6)-C(61)-O(5)	123.5(4)
C(41)-C(47)-C(46)	124.0(4)	O(6)-C(61)-C(62)	126.4(4)
C(48)-C(47)-C(46)	117.1(3)	O(5)-C(61)-C(62)	110.0(4)
C(44)-C(48)-C(47)	119.8(3)	C(66)-C(62)-C(63)	107.8(4)
C(66)-C(62)-C(61)	127.7(4)	O(5')-C(61')-C(62')	118(2)
C(63)-C(62)-C(61)	124.4(5)	C(63')-C(62')-C(66')	108.0
C(64)-C(63)-C(62)	107.9(5)	C(63')-C(62')-C(61')	126.8(18)
C(63)-C(64)-C(65)	108.8(5)	C(66')-C(62')-C(61')	125.1(18)
C(66)-C(65)-C(64)	108.1(5)	C(61')-C(62')-Fe(2')	124.7(19)
C(65)-C(66)-C(62)	107.4(5)	C(62')-C(63')-C(64')	108.0
C(68)-C(67)-C(71)	106.7(4)	C(65')-C(64')-C(63')	108.0
C(68)-C(67)-C(72)	126.2(4)	C(64')-C(65')-C(66')	108.0
C(71)-C(67)-C(72)	126.7(4)	C(65')-C(66')-C(62')	108.0
C(72)-C(67)-Fe(2)	119.4(3)	O(8')-C(72')-O(7')	132(2)
C(69)-C(68)-C(67)	108.2(4)	O(8')-C(72')-C(67')	129(2)
C(68)-C(69)-C(70)	108.7(4)	O(7')-C(72')-C(67')	99.2(18)
C(71)-C(70)-C(69)	107.9(4)	C(71')-C(67')-C(68')	108.0
C(70)-C(71)-C(67)	108.6(4)	C(71')-C(67')-C(72')	123.1(17)
O(8)-C(72)-O(7)	123.5(5)	C(68')-C(67')-C(72')	128.8(17)
O(8)-C(72)-C(67)	125.9(5)	C(69')-C(68')-C(67')	108.0
O(7)-C(72)-C(67)	110.6(4)	C(68')-C(69')-C(70')	108.0
O(6')-C(61')-O(5')	117(2)	C(71')-C(70')-C(69')	108.0
O(6')-C(61')-C(62')	125(2)	C(70')-C(71')-C(67')	108.0

Oxobisphenyl cyclophane (78d)
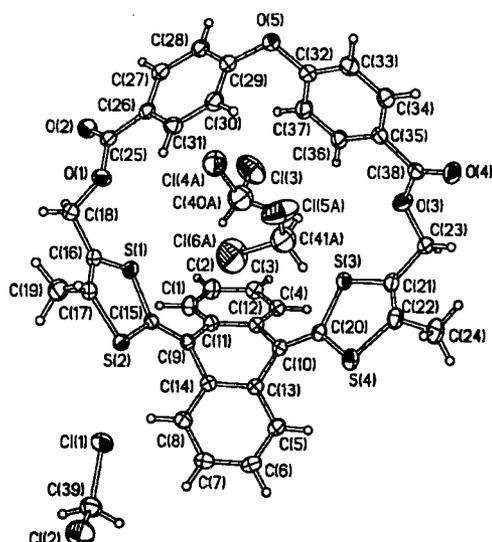
Table 1. Crystal data and structure refinement

Identification code	
Empirical formula	$C_{38}H_{26}O_5S_4 \cdot 3\ CH_2Cl_2$
Formula weight	945.61
Temperature	120(2) K
Wavelength	0.71073 Å
Crystal system	Triclinic
Space group	$P\overline{1}$ (No. 2)
Unit cell dimensions	$a = 11.535(3)$ Å $\quad \alpha = 72.46(1)°$
	$b = 13.215(3)$ Å $\quad \beta = 79.85(1)°$
	$c = 14.744(3)$ Å $\quad \gamma = 89.50(1)°$
Volume	2107.1(8) Å^3
Z	2
Density (calculated)	1.490 g/cm^3
Absorption coefficient	0.650 mm^{-1}
F(000)	968
Crystal size	$0.7 \times 0.4 \times 0.35$ mm^3
θ range for data collection	1.4 to 29.0°.
Index ranges	$-15 \leq h \leq 15,\ -18 \leq k \leq 17,\ -20 \leq l \leq 19$
Reflections collected	25443
Independent reflections	10988 [R(int) = 0.0184]
Reflections with I > 2σ(I)	9748
Completeness to θ = 29.0°	98.1 %
Absorption correction	Semi-empirical from equivalents
Max. and min. transmission	0.8015 and 0.7154
Refinement method	Full-matrix least-squares on F^2
Data / restraints / parameters	10988 / 6 / 536
Largest final shift/e.s.d. ratio	0.010
Goodness-of-fit on F^2	1.016
Final R indices [I > 2σ(I)]	$R_1 = 0.0507$, $wR_2 = 0.1278$
R indices (all data)	$R_1 = 0.0569$, $wR_2 = 0.1336$
Largest diff. peak and hole	1.484 and -0.955 e.Å^{-3}

176

Table 2. Atomic coordinates ($\times 10^5$) and equivalent isotropic displacement parameters ($\text{Å}^2 \times 10^4$) U(eq) is defined as one third of the trace of the orthogonalized U_{ij} tensor.

	x	y	z	U(eq)
S(1)	43035(5)	45506(5)	30930(4)	274(1)
S(2)	32075(4)	37678(4)	51410(4)	240(1)
S(3)	6382(5)	15722(4)	20094(4)	246(1)
S(4)	-7004(5)	8325(4)	39866(4)	277(1)
O(1)	67760(14)	31613(13)	32752(11)	294(3)
O(2)	79487(15)	40558(13)	18666(12)	333(4)
O(3)	15066(14)	-3278(13)	13518(15)	397(4)
O(4)	15914(15)	-21101(13)	17911(14)	365(4)
O(5)	69398(14)	-4501(14)	13119(14)	346(4)
C(1)	23140(20)	53132(17)	19496(16)	282(4)
C(2)	21550(20)	55670(18)	9932(16)	309(5)
C(3)	13990(20)	49295(17)	7335(15)	276(4)
C(4)	7929(18)	40481(16)	14358(14)	231(4)
C(5)	-10899(18)	27101(17)	47776(15)	256(4)
C(6)	-13163(18)	28852(18)	56822(16)	282(4)
C(7)	-5043(19)	34719(17)	59368(15)	266(4)
C(8)	5369(18)	38848(16)	52874(15)	232(4)
C(9)	2879(17)	28819(15)	31830(14)	199(3)
C(10)	18918(17)	41149(15)	36821(14)	205(3)
C(11)	17406(18)	44144(15)	26578(14)	219(4)
C(12)	9549(17)	37744(15)	24009(14)	208(4)
C(13)	-263(17)	30883(15)	41298(14)	210(4)
C(14)	7992(17)	36945(15)	43914(14)	202(3)
C(15)	29669(17)	41650(15)	39353(14)	215(4)
C(16)	52486(18)	40990(17)	39361(16)	259(4)
C(17)	47478(18)	37316(17)	48719(16)	252(4)
C(18)	65381(19)	41367(19)	35267(18)	312(5)
C(19)	53440(20)	32890(20)	57284(18)	335(5)
C(20)	655(17)	19196(15)	30649(14)	212(4)
C(21)	471(18)	2491(16)	24294(17)	267(4)
C(22)	-5556(19)	-900(16)	33352(17)	275(4)
C(23)	2450(20)	-3640(20)	17110(20)	351(5)
C(24)	-11900(20)	-11498(18)	38640(20)	363(5)
C(25)	74359(17)	32450(17)	24030(15)	237(4)
C(26)	74093(17)	22166(17)	21805(15)	229(4)
C(27)	79739(18)	21819(18)	12708(15)	259(4)
C(28)	78442(18)	12840(19)	9839(16)	281(4)
C(29)	71509(18)	4227(18)	16176(17)	284(4)
C(30)	66371(19)	4191(18)	25488(17)	298(4)
C(31)	67597(19)	13178(17)	28319(15)	265(4)
C(32)	57505(19)	-6234(18)	13104(17)	286(4)
C(33)	53330(20)	-16612(19)	14985(19)	332(5)
C(34)	41360(20)	-18532(18)	15364(18)	312(5)
C(35)	33693(18)	-10166(16)	13857(15)	242(4)
C(36)	38293(19)	269(17)	11475(17)	282(4)
C(37)	50150(20)	2249(18)	11064(18)	318(5)
C(38)	20782(18)	-12413(16)	15354(15)	243(4)
Cl(1)	18265(6)	31663(5)	75210(4)	396(1)
Cl(2)	7801(8)	26502(7)	95640(5)	553(2)
C(39)	7940(20)	35200(20)	83987(17)	357(5)
Cl(3)	41581(11)	40879(8)	-6798(7)	749(3)
Cl(4A)	51186(12)	29856(13)	10538(15)	603(4)
C(40A)	38740(40)	35300(40)	6170(40)	625(11)
Cl(4B)	45330(80)	29810(60)	12200(60)	810(20)
C(40B)	37250(100)	31210(90)	2960(80)	270(20)
Cl(5A)	36547(12)	-5741(10)	41941(13)	711(4)
Cl(6A)	32269(16)	16919(11)	36054(16)	946(5)
C(41A)	28720(40)	4770(40)	35640(30)	541(10)
Cl(5B)	37650(40)	15260(40)	41100(30)	282(8)
Cl(6B)	32620(100)	-4760(80)	37760(70)	700(20)
C(41B)	33200(200)	9080(120)	33260(160)	440(50)
Cl(5C)	39820(60)	11900(50)	44740(50)	523(13)
Cl(6C)	26900(70)	-1270(70)	36640(60)	611(16)
C(41C)	38750(160)	-1450(140)	43470(140)	300(40)

Table 3. Bond lengths [Å] and angles [°]

S(1)-C(16)	1.763(2)	C(13)-C(14)	1.423(3)
S(1)-C(15)	1.771(2)	C(16)-C(17)	1.339(3)
S(2)-C(17)	1.754(2)	C(16)-C(18)	1.499(3)
S(2)-C(15)	1.767(2)	C(17)-C(19)	1.504(3)
S(3)-C(21)	1.768(2)	C(21)-C(22)	1.336(3)
S(3)-C(20)	1.770(2)	C(21)-C(23)	1.502(3)
S(4)-C(22)	1.756(2)	C(22)-C(24)	1.504(3)
S(4)-C(20)	1.765(2)	C(25)-C(26)	1.493(3)
O(1)-C(25)	1.348(2)	C(26)-C(27)	1.398(3)
O(1)-C(18)	1.456(3)	C(26)-C(31)	1.403(3)
O(2)-C(25)	1.208(3)	C(27)-C(28)	1.392(3)
O(3)-C(38)	1.348(3)	C(28)-C(29)	1.385(3)
O(3)-C(23)	1.455(3)	C(29)-C(30)	1.395(3)
O(4)-C(38)	1.205(3)	C(30)-C(31)	1.388(3)
O(5)-C(32)	1.393(3)	C(32)-C(33)	1.388(3)
O(5)-C(29)	1.396(3)	C(32)-C(37)	1.392(3)
C(1)-C(2)	1.393(3)	C(33)-C(34)	1.394(3)
C(1)-C(11)	1.401(3)	C(34)-C(35)	1.400(3)
C(2)-C(3)	1.394(3)	C(35)-C(36)	1.401(3)
C(3)-C(4)	1.396(3)	C(35)-C(38)	1.486(3)
C(4)-C(12)	1.405(3)	C(36)-C(37)	1.382(3)
C(5)-C(6)	1.401(3)	Cl(1)-C(39)	1.767(2)
C(5)-C(13)	1.406(3)	Cl(2)-C(39)	1.753(3)
C(6)-C(7)	1.390(3)	Cl(3)-C(40B)	1.613(11)
C(7)-C(8)	1.396(3)	Cl(3)-C(40A)	1.800(5)
C(8)-C(14)	1.399(3)	Cl(4A)-C(40A)	1.739(5)
C(9)-C(20)	1.367(3)	Cl(4B)-C(40B)	1.746(13)
C(9)-C(12)	1.482(3)	Cl(5A)-C(41A)	1.762(5)
C(9)-C(13)	1.485(3)	Cl(6A)-C(41A)	1.682(6)
C(10)-C(15)	1.364(3)	Cl(5B)-C(41B)	1.748(15)
C(10)-C(14)	1.479(3)	Cl(6B)-C(41B)	1.745(15)
C(10)-C(11)	1.483(3)	Cl(5C)-C(41C)	1.837(15)
C(11)-C(12)	1.417(3)	Cl(6C)-C(41C)	1.931(14)
C(16)-S(1)-C(15)	96.31(10)		126.4(2)
C(17)-S(2)-C(15)	97.03(10)	C(17)-C(16)-C(18)	117.27(16)
C(21)-S(3)-C(20)	96.88(10)	C(17)-C(16)-S(1)	116.31(17)
C(22)-S(4)-C(20)	97.64(10)	C(18)-C(16)-S(1)	128.0(2)
C(25)-O(1)-C(18)	117.63(17)	C(16)-C(17)-C(19)	116.47(17)
C(38)-O(3)-C(23)	118.93(18)	C(16)-C(17)-S(2)	115.54(16)
C(32)-O(5)-C(29)	112.81(17)	C(19)-C(17)-S(2)	107.43(17)
C(2)-C(1)-C(11)	121.1(2)	O(1)-C(18)-C(16)	124.05(15)
C(1)-C(2)-C(3)	119.80(19)	C(9)-C(20)-S(4)	123.91(15)
C(2)-C(3)-C(4)	119.84(19)	C(9)-C(20)-S(3)	111.75(11)
C(3)-C(4)-C(12)	121.02(19)	S(4)-C(20)-S(3)	126.9(2)
C(6)-C(5)-C(13)	120.87(19)	C(22)-C(21)-C(23)	117.05(17)
C(7)-C(6)-C(5)	120.10(19)	C(22)-C(21)-S(3)	116.01(17)
C(6)-C(7)-C(8)	119.68(19)	C(23)-C(21)-S(3)	128.5(2)
C(7)-C(8)-C(14)	121.29(19)	C(21)-C(22)-C(24)	116.59(16)
C(20)-C(9)-C(12)	122.87(18)	C(21)-C(22)-S(4)	114.80(18)
C(20)-C(9)-C(13)	122.65(17)	C(24)-C(22)-S(4)	107.73(18)
C(12)-C(9)-C(13)	114.27(16)	O(3)-C(23)-C(21)	124.1(2)
C(15)-C(10)-C(14)	123.44(17)	O(2)-C(25)-O(1)	124.99(19)
C(15)-C(10)-C(11)	122.16(18)	O(2)-C(25)-C(26)	110.91(17)
C(14)-C(10)-C(11)	114.28(17)	O(1)-C(25)-C(26)	119.8(2)
C(1)-C(11)-C(12)	119.25(18)	C(27)-C(26)-C(31)	118.58(19)
C(1)-C(11)-C(10)	122.73(18)	C(27)-C(26)-C(25)	121.47(18)
C(12)-C(11)-C(10)	117.99(17)	C(31)-C(26)-C(25)	120.6(2)
C(4)-C(12)-C(11)	118.91(18)	C(28)-C(27)-C(26)	118.9(2)
C(4)-C(12)-C(9)	123.13(18)	C(29)-C(28)-C(27)	121.3(2)
C(11)-C(12)-C(9)	117.85(17)	C(28)-C(29)-C(30)	119.4(2)
C(5)-C(13)-C(14)	118.78(18)	C(28)-C(29)-O(5)	119.2(2)
C(5)-C(13)-C(9)	123.29(18)	C(30)-C(29)-O(5)	119.7(2)
C(14)-C(13)-C(9)	117.93(17)	C(31)-C(30)-C(29)	119.6(2)
C(8)-C(14)-C(13)	119.22(18)	C(30)-C(31)-C(26)	121.3(2)
C(8)-C(14)-C(10)	123.11(18)	C(33)-C(32)-C(37)	118.0(2)
C(13)-C(14)-C(10)	117.66(17)	C(33)-C(32)-O(5)	120.7(2)
C(10)-C(15)-S(2)	124.09(15)	C(37)-C(32)-O(5)	118.7(2)
C(10)-C(15)-S(1)	124.00(15)	C(32)-C(33)-C(34)	120.8(2)
S(2)-C(15)-S(1)	111.78(11)	C(33)-C(34)-C(35)	119.1(2)
C(34)-C(35)-C(38)	120.19(19)	C(34)-C(35)-C(36)	111.74(15)
C(36)-C(35)-C(38)	120.64(19)	Cl(2)-C(39)-Cl(1)	112.0(3)
C(37)-C(36)-C(35)	120.5(2)	Cl(4A)-C(40A)-Cl(3)	116.0(7)
C(36)-C(37)-C(32)	119.4(2)	Cl(3)-C(40B)-Cl(4B)	115.9(3)
O(4)-C(38)-O(3)	123.8(2)	Cl(6A)-C(41A)-Cl(5A)	113.1(12)
O(4)-C(38)-C(35)	125.8(2)	Cl(5B)-C(41B)-Cl(6B)	106.2(10)
O(3)-C(38)-C(35)	110.44(17)	Cl(6C)-C(41C)-Cl(5C)	

177

Oxobisphenyl cyclophane oxidised by Iodine (78d^{2+})
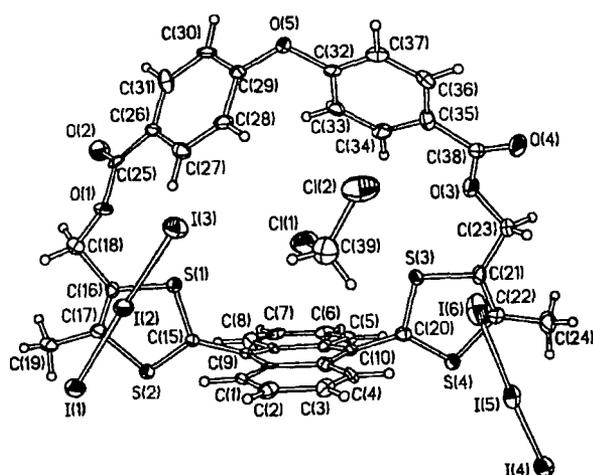
Table 1. Crystal data and structure refinement

Identification code	
Empirical formula	$C_{38}H_{26}O_5S_4{}^{2+}$ $(I_3^-)_2 \cdot 2.25\ CH_2Cl_2$
Formula weight	1643.31
Temperature	120(2) K
Wavelength	0.71073 Å
Crystal system	Monoclinic
Space group	$P2_1/c$ (No. 14)
Unit cell dimensions	$a = 15.486(5)$ Å $\alpha = 90°$
	$b = 23.259(7)$ Å $\beta = 117.35(1)°$
	$c = 15.957(5)$ Å $\gamma = 90°$
Volume	5105(3) Å^3
Z	4
Density (calculated)	2.138 g/cm^3
Absorption coefficient	4.090 mm^{-1}
F(000)	3082
Crystal size	$0.01 \times 0.17 \times 0.5$ mm^3
θ range for data collection	1.48 to 27.5°.
Index ranges	$-20 \leq h \leq 19, -30 \leq k \leq 30, -17 \leq l \leq 20$
Reflections collected	40267
Independent reflections	11710 [R(int) = 0.1125]
Reflections with $I > 2\sigma(I)$	7844
Completeness to $\theta = 27.50°$	99.9 %
Absorption correction	Integration
Max. and min. transmission	0.9592 and 0.2851
Refinement method	Full-matrix least-squares on F^2
Data / restraints / parameters	11710 / 0 / 555
Largest final shift/e.s.d. ratio	0.008
Goodness-of-fit on F^2	1.426
Final R indices [$I > 2\sigma(I)$]	$R_1 = 0.0658$, wR$_2 = 0.1004$
R indices (all data)	$R_1 = 0.1128$, wR$_2 = 0.1096$
Largest diff. peak and hole	1.420 and -1.133 e.Å^{-3}

In the DCM molecule Cl(3)C(40)Cl(4) the C atom is disordered between two positions, and Cl atoms between three positions each. DCM molecule Cl(5)C(41)Cl(5′) is located near an inversion centre, so that the two Cl atoms are related via this centre, and the C atom is disordered between 2 positions, related by this centre (the C site occupancies are 0.25, the Cl site 0.5).

Table 2. Atomic coordinates (×10⁴) and equivalent isotropic displacement parameters (Å² ×10³)
U(eq) is defined as one third of the trace of the orthogonalized Uij tensor.

	x	y	z	U(eq)
I(1)	7142.2(4)	4262.7(2)	7817.6(4)	24.5(1)
I(2)	6113.8(4)	3168.4(2)	7662.9(4)	21.6(1)
I(3)	5025.7(5)	2137.3(2)	7614.8(5)	30.1(2)
I(4)	-928.5(4)	4972.6(3)	991.4(4)	28.4(2)
I(5)	-330.1(4)	3960.5(3)	2215.2(4)	25.3(2)
I(6)	333.5(5)	2887.1(3)	3272.9(5)	38.0(2)
S(1)	6416.9(15)	3477.4(8)	5282.4(16)	18.6(5)
S(2)	6962.0(15)	4641.8(9)	5329.0(16)	19.1(5)
S(3)	2069.4(14)	3148.8(9)	2034.7(15)	18.1(5)
S(4)	1312.3(15)	4205.0(9)	1090.4(15)	19.5(5)
O(1)	7673(4)	2640(2)	6406(5)	24(2)
O(2)	8438(4)	2222(3)	5647(5)	29(2)
O(5)	4688(4)	637(2)	4356(4)	18(1)
O(3)	1347(4)	2121(3)	1230(5)	26(2)
O(4)	408(4)	1468(3)	1460(5)	36(2)
C(1)	4469(6)	4127(3)	5388(6)	18(2)
C(2)	3733(6)	4026(3)	5589(7)	22(2)
C(3)	2772(6)	3948(3)	4872(6)	19(2)
C(4)	2582(6)	3976(3)	3972(6)	18(2)
C(5)	3684(6)	4342(3)	1529(6)	20(2)
C(6)	4408(6)	4491(3)	1311(7)	20(2)
C(7)	5377(6)	4560(3)	2037(7)	20(2)
C(8)	5568(6)	4491(4)	2950(7)	22(2)
C(9)	5047(6)	4249(3)	4167(6)	18(2)
C(10)	3141(6)	4098(3)	2740(6)	14(2)
C(11)	3878(6)	4274(3)	2478(6)	15(2)
C(12)	4842(5)	4353(3)	3216(6)	13(2)
C(13)	4310(6)	4160(3)	4423(6)	13(2)
C(14)	3321(6)	4090(3)	3684(6)	16(2)
C(15)	6068(5)	4151(3)	4883(6)	13(2)
C(16)	7615(5)	3634(3)	5996(6)	15(2)
C(17)	7893(6)	4180(3)	6044(7)	20(2)
C(18)	8269(6)	3135(3)	6587(7)	25(2)
C(19)	8874(6)	4436(4)	6631(6)	35(3)
C(20)	2222(6)	3861(3)	2004(6)	16(2)
C(21)	988(6)	3098(4)	1017(6)	19(2)
C(22)	610(6)	3601(4)	563(6)	17(2)
C(23)	565(6)	2519(3)	775(7)	24(2)
C(24)	-321(6)	3674(4)	-332(7)	30(2)
C(25)	7790(6)	2209(3)	5867(7)	21(2)
C(26)	7029(6)	1770(3)	5593(6)	16(2)
C(27)	6182(6)	1846(4)	5722(6)	20(2)
C(28)	5424(6)	1470(3)	5331(6)	20(2)
C(29)	5483(6)	999(3)	4803(6)	15(2)
C(30)	6328(6)	897(3)	4726(6)	20(2)
C(31)	7089(6)	1286(4)	5122(6)	25(2)
C(32)	3843(6)	888(3)	3633(6)	19(2)
C(33)	3890(6)	1368(3)	3151(6)	22(2)
C(34)	3045(6)	1590(3)	2466(6)	20(2)
C(35)	2134(6)	1350(4)	2252(6)	22(2)
C(36)	2127(7)	849(4)	2706(7)	27(2)
C(37)	2976(6)	610(3)	3400(6)	20(2)
C(38)	1199(6)	1630(3)	1609(6)	21(2)
Cl(1)	3756(2)	2628(1)	4432(2)	44(1)
Cl(2)	2514(2)	1780(1)	4718(2)	56(1)
C(39)	3014(8)	2468(4)	5002(8)	42(3)
Cl(3A)	1915(4)	6906(3)	5851(4)	62(2)
Cl(4A)	1945(5)	5727(3)	6468(7)	85(2)
C(40A)	2270(13)	6455(8)	6849(15)	61(5)
Cl(3B)	2285(11)	6494(6)	6289(12)	57(3)
Cl(4B)	1468(9)	5307(6)	5936(10)	55(5)
C(40B)	1150(30)	6040(20)	5730(40)	51(12)
Cl(3C)	1640(40)	6520(20)	5810(50)	170(20)
Cl(4C)	2290(30)	5777(17)	7100(30)	108(14)
Cl(5)	778(7)	4613(3)	5128(6)	94(3)
C(41)	30(40)	4860(20)	5560(40)	55(13)

Table 3. Bond lengths [Å] and angles [°]

I(1)-I(2)	2.952(1)	C(10)-C(14)	1.400(12)
I(2)-I(3)	2.912(1)	C(10)-C(11)	1.444(12)
I(4)-I(5)	2.924(1)	C(10)-C(20)	1.474(11)
I(5)-I(6)	2.923(1)	C(11)-C(12)	1.426(10)
S(1)-C(15)	1.683(7)	C(13)-C(14)	1.449(11)
S(1)-C(16)	1.712(8)	C(16)-C(17)	1.330(11)
S(2)-C(15)	1.680(8)	C(16)-C(18)	1.544(11)
S(2)-C(17)	1.739(9)	C(17)-C(19)	1.495(11)
S(3)-C(20)	1.678(8)	C(21)-C(22)	1.359(12)
S(3)-C(21)	1.720(8)	C(21)-C(23)	1.469(11)
S(4)-C(20)	1.691(8)	C(22)-C(24)	1.502(12)
S(4)-C(22)	1.739(8)	C(25)-C(26)	1.466(11)
O(1)-C(25)	1.384(11)	C(26)-C(31)	1.381(12)
O(1)-C(18)	1.421(9)	C(26)-C(27)	1.429(12)
O(2)-C(25)	1.206(11)	C(27)-C(28)	1.363(11)
O(5)-C(29)	1.389(9)	C(28)-C(29)	1.411(11)
O(5)-C(32)	1.413(9)	C(29)-C(30)	1.389(13)
O(3)-C(38)	1.362(10)	C(30)-C(31)	1.387(11)
O(3)-C(23)	1.430(10)	C(32)-C(33)	1.378(12)
O(4)-C(38)	1.196(10)	C(32)-C(37)	1.378(12)
C(1)-C(2)	1.339(13)	C(33)-C(34)	1.364(11)
C(1)-C(13)	1.446(12)	C(34)-C(35)	1.406(12)
C(2)-C(3)	1.412(11)	C(35)-C(36)	1.374(13)
C(3)-C(4)	1.328(12)	C(35)-C(38)	1.486(12)
C(4)-C(14)	1.440(12)	C(36)-C(37)	1.387(12)
C(5)-C(6)	1.364(13)	Cl(1)-C(39)	1.800(12)
C(5)-C(11)	1.411(12)	Cl(2)-C(39)	1.744(11)
C(6)-C(7)	1.422(12)	Cl(3A)-C(40A)	1.77(2)
C(7)-C(8)	1.357(13)	Cl(4A)-C(40A)	1.79(2)
C(8)-C(12)	1.409(12)	Cl(3B)-C(40B)	1.88(5)
C(9)-C(13)	1.393(13)	Cl(4B)-C(40B)	1.77(5)
C(9)-C(12)	1.421(12)	Cl(5)-C(41)	1.70(6)
C(9)-C(15)	1.483(10)	Cl(5')-C(41)	1.74(5)
I(3)-I(2)-I(1)	174.76(3)	C(20)-S(4)-C(22)	97.1(4)
I(6)-I(5)-I(4)	173.06(3)	C(25)-O(1)-C(18)	117.1(7)
C(15)-S(1)-C(16)	96.6(4)	C(29)-O(5)-C(32)	116.0(6)
C(15)-S(2)-C(17)	97.5(4)	C(38)-O(3)-C(23)	119.5(7)
C(20)-S(3)-C(21)	97.4(4)	C(2)-C(1)-C(13)	121.2(8)
C(1)-C(2)-C(3)	121.6(9)	C(22)-C(21)-C(23)	128.2(7)
C(4)-C(3)-C(2)	119.8(8)	C(22)-C(21)-S(3)	116.0(6)
C(3)-C(4)-C(14)	122.7(8)	C(23)-C(21)-S(3)	115.7(6)
C(6)-C(5)-C(11)	120.5(8)	C(21)-C(22)-C(24)	126.5(8)
C(5)-C(6)-C(7)	120.3(9)	C(21)-C(22)-S(4)	114.6(6)
C(8)-C(7)-C(6)	119.3(8)	C(24)-C(22)-S(4)	118.9(6)
C(7)-C(8)-C(12)	122.7(8)	O(3)-C(23)-C(21)	106.8(6)
C(13)-C(9)-C(12)	121.8(7)	O(2)-C(25)-O(1)	121.8(8)
C(13)-C(9)-C(15)	118.6(8)	O(2)-C(25)-C(26)	126.4(9)
C(12)-C(9)-C(15)	119.0(8)	O(1)-C(25)-C(26)	111.8(8)
C(14)-C(10)-C(11)	121.5(7)	C(31)-C(26)-C(27)	118.4(8)
C(14)-C(10)-C(20)	119.7(8)	C(31)-C(26)-C(25)	118.9(8)
C(11)-C(10)-C(20)	118.5(8)	C(27)-C(26)-C(25)	122.5(8)
C(5)-C(11)-C(12)	119.9(8)	C(28)-C(27)-C(26)	120.6(8)
C(5)-C(11)-C(10)	122.4(7)	C(27)-C(28)-C(29)	119.6(8)
C(12)-C(11)-C(10)	117.7(8)	O(5)-C(29)-C(30)	120.0(7)
C(8)-C(12)-C(9)	122.9(8)	O(5)-C(29)-C(28)	119.5(7)
C(8)-C(12)-C(11)	117.3(8)	C(30)-C(29)-C(28)	120.5(7)
C(9)-C(12)-C(11)	119.6(8)	C(31)-C(30)-C(29)	119.1(8)
C(9)-C(13)-C(14)	118.7(8)	C(26)-C(31)-C(30)	121.6(9)
C(9)-C(13)-C(1)	124.0(8)	C(33)-C(32)-C(37)	121.6(8)
C(14)-C(13)-C(1)	117.4(8)	C(33)-C(32)-O(5)	121.7(7)
C(10)-C(14)-C(4)	123.5(7)	C(37)-C(32)-O(5)	116.6(7)
C(10)-C(14)-C(13)	119.1(8)	C(34)-C(33)-C(32)	118.5(8)
C(4)-C(14)-C(13)	117.3(8)	C(33)-C(34)-C(35)	122.1(8)
C(9)-C(15)-S(2)	126.9(6)	C(36)-C(35)-C(34)	117.3(8)
C(9)-C(15)-S(1)	118.6(5)	C(36)-C(35)-C(38)	119.7(8)
S(2)-C(15)-S(1)	114.4(4)	C(34)-C(35)-C(38)	122.9(8)
C(17)-C(16)-C(18)	125.3(7)	C(35)-C(36)-C(37)	121.8(8)
C(17)-C(16)-S(1)	117.7(6)	C(32)-C(37)-C(36)	118.5(8)
C(18)-C(16)-S(1)	116.9(6)	O(3)-C(38)-O(4)	122.9(7)
C(16)-C(17)-C(19)	128.7(8)	O(4)-C(38)-C(35)	125.7(8)
C(16)-C(17)-S(2)	113.7(6)	O(3)-C(38)-C(35)	111.4(7)
C(19)-C(17)-S(2)	117.5(6)	Cl(2)-C(39)-Cl(1)	111.6(6)
O(1)-C(18)-C(16)	107.7(6)	Cl(3A)-C(40A)-Cl(4A)	109.4(12)
C(10)-C(20)-S(3)	116.2(6)	C(40B)-Cl(4B)-Cl(5)	119.0(3)
C(10)-C(20)-S(4)	128.9(6)	Cl(4B)-C(40B)-Cl(3B)	110(3)
S(3)-C(20)-S(4)	114.8(5)	Cl(5)-C(41)-Cl(5')	114(3)

Symmetry transformations used to generate equivalent atoms (primed): -x,-y+1,-z+1